IMPACT OF GLYCEMIC THERAPY ON MYOCARDIAL SYMPATHETIC NERVOUS INTEGRITY AND LEFT VENTRICULAR FUNCTION IN INSULIN RESISTANT DIABETIC RATS:

Serial evaluation by [^{11}C]meta-hydroxyephedrine positron emission tomography

by

James Thackeray

uOttawa

L'Université canadienne
Canada's university

Department of Cellular and Molecular Medicine
Faculty of Graduate and Postdoctoral Studies
University of Ottawa

Thesis submitted to the Faculty of Graduate and Posdoctoral Studies as a partial fulfillment of the requirements for the PhD degree in Cellular and Molecular Medicine.

ABSTRACT

Diagnosis of diabetes mellitus, presence of hyperglycemia, and/or insulin resistance confer cardiovascular risk, particularly for diastolic dysfunction. Diabetes is associated with elevated myocardial norepinephrine (NE) content, enhanced sympathetic nervous system (SNS) activity, altered resting heart rate, and depressed heart rate variability. Positron emission tomography (PET) using the NE analogue [^{11}C]*meta*-hydroxyephedrine ([^{11}C]HED) provides an index of myocardial sympathetic neuronal integrity at the NE reuptake transporter (NET). The hypothesis of this project is that (i) hyperglycemia imparts heightened sympathetic tone and NE release, leading to abnormal sympathetic neuronal function in the hearts of diabetic rats, and (ii) these abnormalities may be reversed or prevented by treatments to normalize glycemia. Sprague Dawley rats were rendered insulin resistant by high fat feeding and diabetic by a single dose of streptozotocin (STZ). Diabetic rats were treated for 8 weeks with insulin, metformin or rosiglitazone, starting from either 1 week (prevention) or 8 weeks (reversal) after STZ administration. Sympathetic neuronal integrity was evaluated longitudinally by [^{11}C]HED PET. Echocardiography measures of systolic and diastolic function were completed at serial timepoints. Plasma NE levels were evaluated serially and expression of NET and β-adrenoceptors were tested at the terminal endpoints. Diabetic rats exhibited a 52-57% reduction of [^{11}C]HED standardized uptake value (SUV) at 8 weeks after STZ, with a parallel 2.5-fold elevation of plasma NE and a 17-20% reduction in cardiac NET expression. These findings were confirmed by *ex vivo* biodistribution studies. Transmitral pulse wave Doppler echocardiography established an extension of mitral valve deceleration time and elevated early to atrial velocity ratio, suggesting diastolic dysfunction. Subsequent treatment with insulin but not metformin restored glycemia, reduced plasma NE by 50%, normalized NET expression, and recovered [^{11}C]HED SUV towards non-diabetic age-matched control. Diastolic dysfunction in these

rats persisted. By contrast, early treatment with insulin, metformin, or rosiglitazone delayed the progression of diastolic dysfunction, but had no effect on elevated NE and reduced [^{11}C]HED SUV in diabetic rats, potentially owing to a latent decrease in blood glucose. In conclusion, diabetes is associated with heightened circulating and tissue NE levels which can be effectively reversed by lowering glycemia with insulin. Noninvasive interrogation of sympathetic neuronal integrity using [^{11}C]HED PET may have added value in the stratification of cardiovascular risk among diabetic patients and in determining the myocardial effects of glycemic therapy.

ACKNOWLEDGMENTS

The enormity and breadth of a doctoral research project necessitates the cooperation and confluence multiple researchers, technicians and students, without whose support many of the achievements presented in this thesis could not have been attained. To my supervisor Dr Jean DaSilva, I am thankful for the guidance and encouragement that have contributed to the development of my academi career. To my cosupervisor Dr Rob Beanlands, I am grateful for the knowledge and enthusiasm that have aided in the progression of the project and interpretation of findings.

To Stephanie Thorn, your organization, technical expertise, and friendship have contributed greatly to this work. Thank you for being my common sense when my own fails. To Miran Kenk, you made it a pleasure to come to the lab every da, providing assistance, (random) knowledge, and camaraderie. Thank you for providing perspective on everything – good and bad – over the last years. To Alex Gabor, our differential doctoral experiences gave us a lot to talk about. Thank you for the periodic stress relief and sanity checks.

The experiments in this thesis could not have been completed without the contributions of the radiochemistry laboratory, including Samantha Mason, Jeff Collins, Keegan Flowers, and Paul Coletta; the imaging physics group, including Ran Klein, Jennifer Renaud, Tyler Dumouchel, and Marc Lamoureux; imaging technicians Myra Kordos and Julia Lockwood; the many members of the PET Biotesting laboratory over the years; and the UOHI Animal Care and Veterinary Services staff. Thank you also to Drs Rob deKemp, Ross Milne, Kevin Burns, Jerry Radziuk, Kathy Ascah, Erik Suuronen, and Mary-Ellen Harper for providing input on the work and results.

To my family, your support over the years has been indispensible. Thank you.

Finally, I would like to acknowledge the funding support of the Heart and Stroke Foundation of Canada and the Ontario Graduate Scholarship in Science and Technology.

TABLE OF CONTENTS

LIST OF TABLES

LIST OF FIGURES

LIST OF ABBREVIATIONS

^{11}C	carbon-11
^{123}I	iodine-123
^{125}I	iodine-125
^{13}N	nitrogen-13
^{18}F	fluorine-18
^{64}Co	cobalt-64
^{82}Rb	rubidium-82
ADMIRE HF	AdreView Myocardial Imaging for Risk Evaluation in Heart Failure (clinical trial)
ADOPT	A Diabetes Outcome Progression Trial (clinical trial)
ADVANCE	Action in Diabetes and Vascular Disease (clinical trial)
Akt	protein kinase B
Al_2O_3	aluminum oxide
AMP	adenosine monophosphate
AMPK	AMP-activated protein kinase
ApoE	apolipoprotein E
ARIC	Atherosclerosis Risk in Communities (clinical trial)
ATP	adenosinetriphosphate
BH4	tetrahydrobiopterin
B_{max}	maximal binding
Ca^{2+}	calcium ion
cAMP	cyclic adenosine monophosphate
CIRKO	cardiac restricted insulin receptor knockout
CO_2	carbon dioxide
COMT	catechol-*O*-methyltransferase
CPT-1	carnitine palmitoyltransferase-1
CT	computed tomography (formerly computed axial tomography CAT)
db/db	leptin receptor knockout (mouse)
DIAD	Detection of Ischemia in Asymptomatic Diabetics (clinical trial)
dP/dt	change in pressure over time
DPP-IV	dipeptidyl peptidase-4
DREAM	Diabetes Reduction Assessment with ramipril and rosiglitazone
EF	ejection fraction
EKV	electrocardiogram-gated echocardiography acquisition
FAC	fractional area change
FAT/CD36	fatty acid translocase
FDG	fluorodeoxyglucose
FTHA	fluoro-6-thia-heptadecanoic acid
GAPDH	glyceraldehyde 3-phosphate dehydrogenase
G_i	inhibitory G protein
GLP-1	glucagon-like peptide-1
GLUT	glucose transporter
G_s	stimulatory G protein
HbA1c	glycosylated hemoglobin
HDL	high density lipoprotein
HED	hydroxyephedrine
HLB	hydrophilic lipophilic balanced (sorbent)

HPLC	high performance liquid chromatography
ip	intraperitoneal
IRS	insulin receptor substrate
iv	intravenous
K^+	potassium ion
K_{ATP}	potassium ATP channel
KCl	potassium chloride
k_i	dissociation constant of inhibitor
k_{mono}	monoexponential washout rate
LDL	low density lipoprotein
MAO	monoamine oxidase
MAX	maximal anion exchange (sorbent)
MCD	malonyl coA decarboxylase
MCX	maximal cation exchange (sorbent)
MeOH	methanol
MIBG	metaiodobenzylguanidine
mRNA	messenger ribonucleic acid
Na^+	sodium ion
NADH	nicotinamide adenine dinucleotide
NADPH	nicotinamide adenine dinucleotide phosphate
NE	norepinephrine
NEFA	non-esterified (free) fatty acid
NET	norepinephrine reuptake transporter (uptake-1)
NYHA	New York Heart Association
ob/ob	leptin knockout (mouse)
OLETF	Ostuka Long-Evans Tokushima Fatty rat
OSEM3D/MAP	ordered subset expectation maximization 3 dimensional maximum a posteriori
OVE26	overexpression calmodulin minigene under insulin II promoter (mouse)
PC12	pheochromocytoma cell line
PDK	pyruvate dehydrogenase kinase
PET	positron emission tomography
PI3K	phosphoinositide 3-kinase
PIP3	phosphoinositol (3,4,5)-trisphosphate
PKA	protein kinase A
PKC	protein kinase C
PPAR	peroxisome proliferator activated receptor
PROACTIVE	Prospective Pioglitazone Clincial Trial in Macrovascular Events (clinical trial)
RI	retention index
RSNA	renal sympathetic nerve activity
sc	subcutaneous
SERCA2A	sarco/endoplasmic reticulum calcium-ATPase 2A
SNARE	soluble N-ethylmaleimide-sensitive factor attachment protein receptor
SNS	sympathetic nervous system
SPECT	single photon emission computed tomography
STZ	streptozotocin
SUV	standardized uptake value

TAC	time-activity curve
TCA	tricarboxylic acid cycle, citric acid cycle, Krebs cycle
TUNEL	terminal deoxynucleotidyl transferase dUTP nick end labeling
UKPDS	United Kingdom Prospective Diabetes Study (clinical trial)
UV	ultraviolet (absorbance)
VMAT2	vesicular monoamine transporter 2
V_{max}	maximal velocity
WCX	weak cation exchange (sorbent)
ZDF	Zucker diabetic fatty rat

Chapter 1: Introduction

1.0 INTRODUCTION

1.1 Diabetes Mellitus

Diabetes mellitus is defined as a disorder of carbohydrate metabolism characterized by lack of cellular uptake and utilization of glucose, leading to excessive accumulation in the blood and accelerated disposal in urine. Fluctuation in carbohydrate metabolism affects the balance of fatty acid utilization, evoking a variety of metabolic adaptations. Prolonged diabetes is associated with a myriad of systemic complications including disturbances of the cardiovascular and nervous systems.

1.1.1 Glucose Metabolism

Metabolism of glucose is the primary source of adenosine triphosphate (ATP) in skeletal muscle. In the heart, glucose oxidation provides a secondary supply of ATP during periods of heavy cardiovascular demand. Dietary carbohydrates are broken down to simple sugars by digestive enzymes and are absorbed to the bloodstream. Cells actively transport glucose into cytoplasm via a specialized set of glucose transporters (GLUT). Cardiomyocytes express both GLUT1 which is the main transporter in basal metabolism and GLUT4 which is inducible by extrinsic stimuli, particularly insulin (Rosenblatt-Velin et al., 2004). Once inside the cell, glucose is converted to pyruvate by glycolysis, a series of reversible enzyme-catalysed steps with a net yield of 2 units of ATP and 2 units of the intermediate nicotinamide adenine dinucleotide (NADH) which are utilized in mitochondrial electron transport aerobic metabolism (Kolwicz and Tian, 2011). Pyruvate can be further converted to acetyl CoA by pyruvate dehydrogenase (Lydell et al., 2002), at which point it can enter the citric acid cycle (TCA) cycle, yielding an additional 2 units of ATP and intermediates for aerobic metabolism. These intermediates are utilized in mitochondrial electron transport proton gradient aerobic metabolism, ultimately generating a further 34 units of ATP (Fig 1.1).

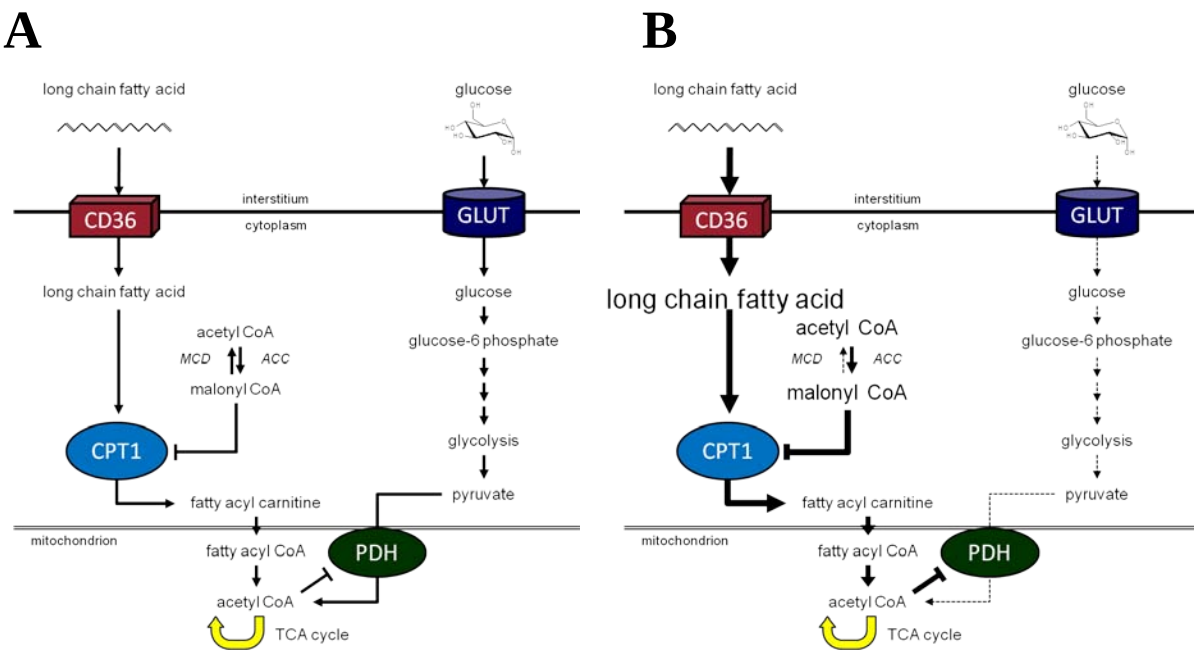

Figure 1.1 Cardiac metabolism of glucose and long chain fatty acids in healthy and diabetic heart. (**A**) In the healthy heart, long chain fatty acids are transported by fatty acid transporters (FAT/CD36, FABP, FATP) into the cardiomyocyte. Long chain fatty acids are converted to fatty acyl carnitine to facilitate entry into the mitochondrion by the rate limiting enzyme carnitine palmitoyl transferase 1 (CPT1). In the mitochondrion, fatty acyl carnitine is converted to fatty acyl CoA and further to acetyl CoA for entry into the citric acid (TCA) cycle. CPT1 is regulated by levels of malonyl CoA which is maintained in equilibrium with acetyl CoA by the enzymes acetyl CoA carboxylase (ACC) and malonyl CoA decarboxylase (MCD). Extracellular glucose is taken up by glucose transporters (GLUT) and converted to glucose-6-phosphate by hexokinase. The glycolosis pathway generates pyruvate which can be converted to acetyl CoA by pyruvate dehyrogenase (PDH) for entry into the TCA cycle. Acetyl CoA inhibits activity of PDH via the Randle cycle. (**B**) In diabetic heart, reduced capacity for glucose uptake necessitates greater energy demand from long chain fatty acids. Rising levels of acetyl CoA inhibit the conversion of pyruvate, further increasing dependence on fatty acids.

The primary stimulus for glucose uptake is provided by pancreatic beta cell secretion of insulin, controlled by an intrinsic sensing mechanism. As blood glucose levels rise, more is transported by pancreatic GLUT2 and the resulting production of ATP inhibits membrane bound K_{ATP} channels resulting in efflux of K^+ and influx of Ca^{2+} that stimulates insulin release from the beta-cell.

In myocytes, insulin binding to the transmembrane tyrosine kinase superfamily insulin receptor activates insulin receptor substrates 1 and 2 (IRS1/2) (Fasshauer et al., 2000; Kaburagi et al., 1997). IRS subsequently stimulates the p85 regulatory subunit of phosphatidylinositol-3-kinase (PI3K). Studies using the specific inhibitor wortmannin have demonstrated the integral involvement of PI3K in the translocation of GLUT4 to the sarcolemma in response to insulin (Cantley, 2002; Chan et al., 2010; Le Marchand-Brustel et al., 1995). The consequent cascade involves the activation of phosphatidylinositol-3,4,5-trisphosphate (PIP3) which in turn activates a series of protein kinases involved in GLUT4 translocation: Akt or protein kinase B type 2, protein kinase C λ/ζ (PKCλ/ζ), and 3-phosphoinositide-dependent protein kinase (PDK) (Bandyopadhyay et al., 1997; Cho et al., 2001; Luiken et al., 2009; Mora et al., 2005) (Fig 1.2).

Insulin signaling is complex, interacting with multiple cellular signaling cascades including human growth factor (Hemming et al., 2001; Jessen et al., 2005), endothelial growth factor (He et al., 2006), tumor necrosis factor (Nohara et al., 2011), and adrenoceptors (Morisco et al., 2005). Short term β-adrenoceptor stimulation has been shown to be required for GLUT4 translocation (Czech and Corvera, 1999; Morisco et al., 2005). Increased metabolic demand imposed by contraction has also been shown to stimulate GLUT4 translocation, mediated by AMP-activated protein kinase (AMPK) acting through a variety of second messenger pathways and culminating in the activation of PKC and PDK (Bertrand et al., 2006; Luiken et al., 2004; Steinbusch et al., 2011). There is evidence to suggest that both insulin and

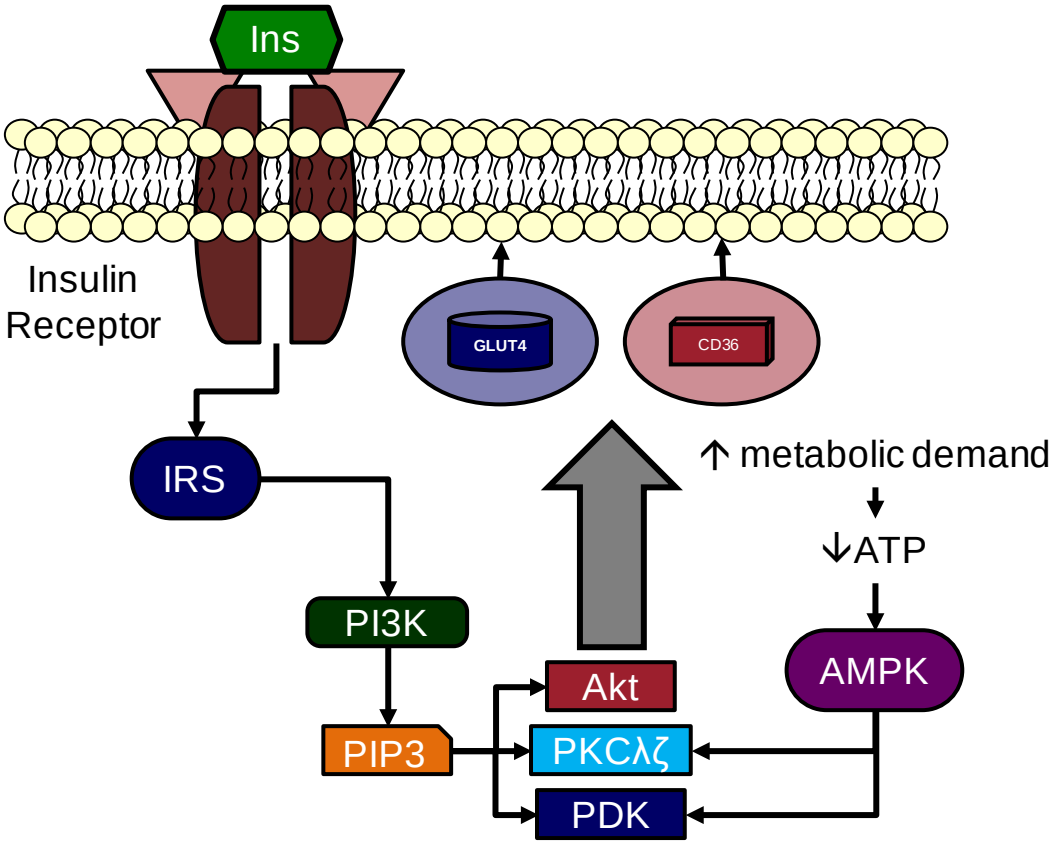

Figure 1.2 Insulin signaling in cardiomyocytes. Binding of insulin to the insulin receptor initiates autophosphorylation of the tyrosine kinase receptor and activation of the insulin receptor substrate 1 and 2 (IRS). Activated IRS stimulates phosphatidylinosidtide-3-kinase (PI3K) which in turn phosphorylates phosphatidylinositol-(3,4,5)-trisphosphate (PIP3). PIP3 then stimulates three protein kinases, protein kinase B (Akt), protein kinase C λ/ζ (PKCλζ) and 3-phosphotidylinositide-dependent D kinase (PDK). These proteins act independently to increase translocation of inducible glucose transporter-4 (GLUT4) from internalized vesicles to the membrane surface. Insulin signaling also elevates the expression of fatty acid transporter (CD36). In response to increased metabolic demand, rising cytosol levels of adenosine monophosphate (AMP) and dropping adenosine trisphosphate (ATP) are detected by AMP-activated protein kinase (AMPK) which can subsequently activate PKCλ/ζ and PDK to enhance GLUT4 translocation.

contraction-induced stimulation of GLUT4 sarcolemmal trafficking also influences the surface expression of the fatty acid translocase (FAT/CD36) (Luiken et al., 2003; Luiken et al., 2002) (Fig 1.2).

1.1.2 Epidemiology

Diabetes afflicts 5.5% of the Canadian population, with the vast majority (90-95%) of these cases non-insulin dependent type 2 diabetes (American Diabetes Association, 2006; Boyle et al., 2001). Over the period from 1994-1998, there was a steady rise in the prevalence of diabetes among Ontarians (Hux et al., 2002), which has been projected to continue. In 2000, approximately 1.4 million Canadians self-reported diabetes, a prevalence that is expected to rise to 2.4 million by 2016 (Ohinmaa et al., 2004). These trends are further supported by the World Health Organization, which anticipates that the worldwide prevalence of diabetes will rise from 2.8% in 2000 to 4.4% by 2030 (Wild et al., 2004). The financial burden of diabetes and its complications on the Canadian health care system is enormous, with an estimated annual cost of $6.7 billion, of which a third is directly attributable to cardiovascular costs. In Ontario alone, predicted healthcare costs for 2016 were $3.1 billion (Ohinmaa et al., 2004).

1.1.3 Type 1 and Type 2 Diabetes

Diabetes is classified as type 1 and type 2, of which the latter represents greater than 90% of total cases. Type 1 diabetes is characterized by a loss of pancreatic beta cell mass and insulin insufficiency. The reduction of pancreatic beta-cell function is believed to involve genetic susceptibility and autoimmunity (Cardell, 2006; Daneman, 2006; Tsai et al., 2006). By contrast, type 2 diabetes is characterized by insulin resistance and compensatory overproduction of insulin by pancreatic beta-cells, leading to eventual exhaustion, apoptosis, and partial loss of insulin secretion (Nugent et al., 2008; Saad et al., 1989; Stumvoll et al., 2005).

1.1.4 Insulin Resistance

An early indication of type 2 diabetes is the presence of hyperinsulinemia in an attempt to overcome insensitivity of insulin receptors to stimulation. The excessive levels of insulin lead to gradual desensitization of insulin receptors and downstream elements. Elevated fasting insulin levels are prognostic of the development of type 2 diabetes and the concomitance of multiple metabolic disorders (Haffner et al., 1992). Insulin resistance is frequently associated with obesity and the accumulation of non-esterified fatty acids in the blood. Multiple animal models of diabetes have been shown to exhibit reduced insulin sensitivity (Bruce et al., 2009; Kraegen et al., 1983; Leonard et al., 2005).

Development of insulin resistance relates to impaired GLUT4 translocation to the sarcolemma. High levels of fatty acids have been shown to dysregulate insulin receptor signaling at multiple sites within the signal cascade. Accumulation of fatty acid metabolites including ceramide and diacylglycerol inhibit the activity of PI3K, PKCζ and Akt (Hajduch et al., 2008). Diacylglycerol may also interfere with the phosphorylation of IRS1, inhibiting the activation of PI3K (Savage et al., 2005).

Basic research has linked insulin resistance to augmentation of concentrations of glucose and lipids in the blood. Drinking water administration of 10% D-glucose to Sprague Dawley rats resulted in insulin resistance as determined by homeostasis model assessment (El Midaoui et al., 2005). Over 4 weeks of feeding with a high fat diet (45% by kilocalorie), Wistar rats developed a 32% elevation in plasma non-esterifed fatty acid, associated with a significant increase in fatty acid oxidation and a marked 36% decrease in glucose infusion rate during hyperinsulinemic euglycemic clamp, reflecting impaired insulin sensitivity (Bruce et al., 2009). Skeletal muscle overexpression of carnitine palmitoyl transferase-1 (CPT1), the rate-limiting enzyme in transport of long-chain fatty acids to the mitochondria for fat oxidation,

has been shown to enhance lipid metabolism and improve glucose uptake in the presence of insulin (Bruce et al., 2009).

1.1.5 Insulin Signaling in the Heart

The interaction between insulin signaling, and particularly insulin resistance, and myocardial pathology has been demonstrated by studies using cardiac restricted insulin receptor knockout (CIRKO) mice. Insulin receptor signaling has been shown to play a pivotal role in myocardial development, as demonstrated by smaller hearts and lower cardiomyocyte surface area in CIRKO mice compared to wild type littermates (Belke et al., 2002). Moreover, CIRKO mice exhibit lower basal glucose uptake and an ablation of insulin- and IGF1-stimulated increases in glucose uptake by isolated cardiomyocytes (Belke et al., 2002). In the presence of a primary insult such as transverse aortic constriction, loss of insulin signaling augments ventricular deterioration, characterized by enhanced dilatation and interstitial collagen deposition (Hu et al., 2003). Subsequent studies demonstrated this anomaly was independent of coronary arterial blood flow abnormalities, with normal or heightened vasodilatory responsiveness of coronary vessels to acetylcholine or nitric oxide (Symons et al., 2011). Rather, the deterioration of ventricular function has been linked to metabolic abnormalities including reduced glucose oxidation (Bugger et al., 2012; Shimoni et al., 2004), impaired basal and insulin-induced fatty acid oxidation (Belke et al., 2002; Boudina et al., 2009; Bugger et al., 2012), and mitochondrial dysfunction (Boudina et al., 2009). Electrophysiology studies revealed a prolonged action potential in CIRKO mice compared to wild type littermates owing to a delay in the outward K^+ current and manifesting as bradycardia (Shimoni et al., 2004). Induction of diabetes by streptozotocin (STZ) reduced cardiac output dramatically in CIRKO diabetic mice compared to wild type diabetics, with a parallel increase in myocardial oxygen consumption and reduction of cardiac efficiency (Bugger et al., 2012). This maladaptation was attributed to reduced ATP synthesis from

pyruvate and palmitoyl carnitine and impaired mitochondrial function (Bugger et al., 2012). In addition, CIRKO mice display greater propensity for hypertrophy induced by the β-adrenoceptor agonist isoproterenol, characterized by ablation of left ventricular dP/dt increases, twofold elevation of collagen volume, higher augmentation of Akt phosphorylation, and increased apoptosis associated with a reduction of capillary density (McQueen et al., 2005). This finding underscores the interaction of insulin and adrenergic signaling in cardiomyocytes. Taken together, these findings indicate the involvement of insulin signaling in the maintenance of myocardial health in the presence and absence of hyperglycemia or overt diabetes.

1.1.6 Prevalence of Heart Disease in Diabetes

Interestingly, insulin resistance is also highly prevalent among heart failure patients, suggesting a link between diabetes and heart failure. Approximately 80% of diabetic mortality derives from heart disease or stroke (Chareonthaitawee et al., 2007; Kostis and Sanders, 2005; Swan et al., 1997). Presence of type 1 or type 2 diabetes confers a 2-4 fold increased risk of developing cardiovascular disease, manifesting as impaired left ventricular function and congestive heart failure (Goff et al., 2007; Kostis and Sanders, 2005; Mente et al., 2010; Stumvoll et al., 2005). An array of diabetic animal models has been shown to develop contractile dysfunction over time (Boudina and Abel, 2007).

Diabetics constitute a disproportionately high cohort in major heart failure clinical trials (25% vs 7% in the normal population), particularly among patients in New York Heart Association (NYHA) Functional Class III or IV heart failure (Kostis and Sanders, 2005). Swan and colleagues demonstrated an average reduction of 58% in insulin sensitivity in a 79 patient cohort of congestive heart failure patients (Swan et al., 1997). This observation was particularly true in patients with coronary artery disease rather than dilated cardiomyopathy, with elevated plasma triglyceride levels and significantly higher insulin levels reported in the

former (Swan et al., 1997). There is also an increased incidence of new-onset diabetes reported in heart failure trials at follow-up (Vermes et al., 2003). A multicentre study demonstrated that among 663 heart failure patients, 287 (43%) exhibited blood glucose levels above normal and elevated plasma insulin though only 27% had been previously diagnosed with diabetes (Suskin et al., 2000).

It has been suggested that treatments to counteract heart failure and hypertension including beta-blockers, angiotensin converting enzyme inhibitors, and angiotensin receptor blockers may increase the risk of developing new onset diabetes (Gress et al., 2000; Kostis and Sanders, 2005). Taken together, these findings support the involvement of sympathetic nervous system (SNS) in the development of both diabetes and heart failure. Altered sympathetic nervous signaling has been suggested as a key hub in the concomitant development of left ventricular dysfunction in diabetes (Kostis and Sanders, 2005).

1.2 Diabetic Heart Disease

A number of physiological myocardial maladaptations underlie the high incidence of cardiovascular morbidity and mortality in diabetes. The mechanisms involved in ventricular dysfunction are diverse and unclear, with several pathways having been implicated including disrupted cardiac metabolism, oxidative stress and apoptosis, as well as macromolecule glycosylation and interstitial fibrosis (Fig 1.3). Left ventricular dysfunction can be characterized as either systolic or diastolic. Systolic dysfunction is defined as impaired ventricular contraction, culminating in lower ejection fraction and reduced supply of oxygenated blood to the body (Aronow, 2006). By contrast, diastolic dysfunction is defined as abnormal relaxation of the ventricle due to reduced compliance, characterized by preserved ejection fraction and altered ventricular filling pressure (Aronow, 2006; Paulus et al., 2007). Diastolic dysfunction is frequently asymptomatic, though pulse-wave Doppler

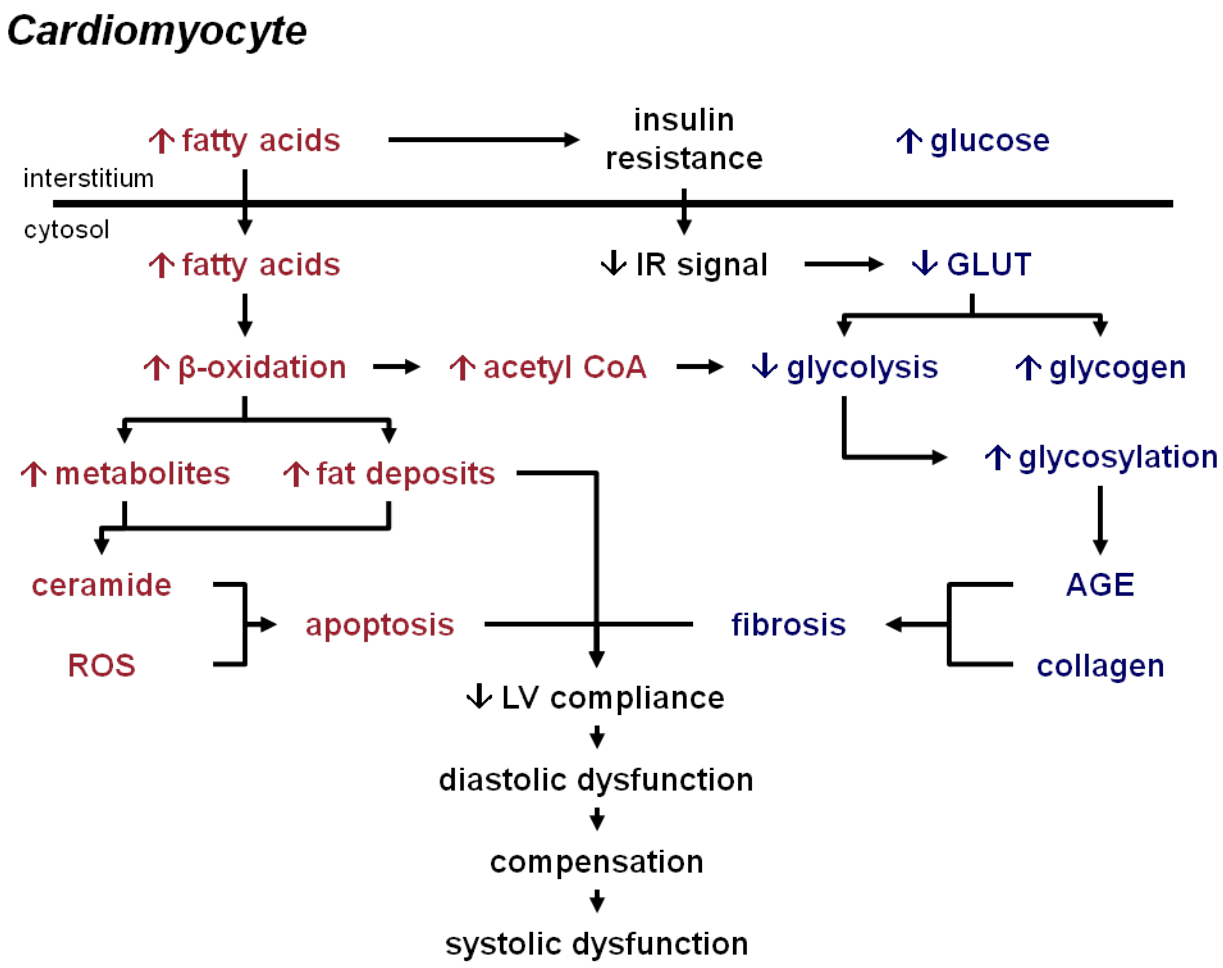

Figure 1.3 Detrimental adaptations in the diabetic heart. Increased uptake of long chain fatty acids drive elevated β-oxidation and generation of fatty acid metabolites that remain in the cytosol as fat deposits. Some metabolites can be converted to ceramides, which contribute to the generation of reactive oxygen species (ROS) and cardiomyocyte apoptosis. Rising levels of acetyl CoA inhibit pyruvate dehydrogenase to further dysregulate glucose metabolism. Rising blood and interstitial levels of nonesterified fatty acids and glucose contribute to the development of insulin resistance, which dampens the signaling of the insulin receptor (IR). This results in a decrease of glucose transporter (GLUT) translocation and reduced glucose transport contributing to rising blood glucose concentration. Decreased glucose transport reduces glycolysis and increases glycogen stores, leading to glycosylation of proteins and lipids and generating advanced glycation endproducts (AGE) that accumulate with collagen in the myocardium, contributing to interstitial fibrosis of cardiomyocytes. The combination of myocyte apoptosis with collagen and fat accumulation drive a decrease in left ventricular (LV) compliance during diastole, leading to filling abnormalities consistent with diastolic dysfunction. Adaptations to counteract this diastolic abnormality can lead to remodeling of the left ventricle and subsequent systolic dysfunction.

echocardiography has provided for non-invasive screening of patients (Galderisi, 2006; Nakao et al., 2007; Paulus et al., 2007).

1.2.1 Metabolic Abnormalities

The healthy heart relies predominantly on long chain fatty acids for ATP production (Fig 1.1). The heart relies on energetic contribution from fatty acids, glucose and lactate sources (Bertrand et al., 2008; Taegtmeyer et al., 1980). This metabolic flexibility allows adjustment to periods of high demand by enhancing glucose oxidation via AMPK- or insulin-induced GLUT4 translocation (Bertrand et al., 2008).

In the diabetic heart, incapacity to take in glucose and accumulation of non-esterified fatty acids leads to a further shift toward fatty acid metabolism (Randle et al., 1963; Young et al., 2002). This shift is perpetuated by the Randle cycle, in which high levels of myocardial fatty acid metabolites, particularly acetyl CoA, block the entry of glucose metabolites into the TCA cycle by inhibition of pyruvate dehydrogenase (Randle et al., 1963). Elevated non-esterified fatty acid levels further inhibit downstream insulin receptor signaling elements including IRS, Akt, and PKC, contributing to insulin resistance and impairing the translocation of GLUT4 to the sarcolemma (Hajduch et al., 2008).

Overexpression of the ligand-activated transcription factor peroxisome proliferator-activated receptor α (PPARα) in mice augments cardiac fatty acid metabolism in a similar manner to diabetes. PPARα transgenic mice exhibit heightened gene expression of fatty acid oxidation genes acyl CoA oxidase and CPT1, and faster fatty acid metabolic rate as measured by ^{11}C-palmitate positron emission tomography, and a reduction of glucose uptake, potentially owing to the Randle cycle (Finck et al., 2002).

Studies in isolated perfused rat hearts have shown an increase in malonyl Co-A decarboxylase (MCD), an enzyme that converts the β-oxidation product malonyl Co-A back to acetyl CoA, removing the inhibition on the rate-limiting CPT1 transport to the

mitochondria (Dyck et al., 1998; Goodwin et al., 1998; Sakamoto et al., 2000). This shift in fatty acid metabolism is similar to phenomena observed in severe ischemia. Treatment with a selective MCD inhibitor has been demonstrated to restore glucose oxidation and improve cardiac mechanical function in isolated hearts of diabetic Yorkshire pigs (Dyck et al., 2004).

1.2.2 Oxidative Stress and Apoptosis

Elevated fatty acid oxidation leads to accumulation of fatty acid metabolites including ceramide and diacylglycerol which contribute to lipotoxicity (An and Rodrigues, 2006). The formation of lipid radicals has been shown using electron paramagnetic resonance spectroscopy, and is associated with the accumulation of toxic hepatic radicals in obese diabetic rats (Kadiiska et al., 2012).

Elevated levels of oxidative stress in the heart of diabetic animal models have been described. Oxidative stress can interfere with the normal phosphorylation of Akt and other insulin signaling proteins, potentially contributing to insulin resistance (Hajduch et al., 2008; Savage et al., 2005). Administration of the anti-oxidant Q10 has been shown to reduce cardiac hypertrophy and restore Akt signaling in db/db diabetic mice (Huynh et al., 2012), supporting restoration of insulin sensitivity. Superoxide dismutase levels are depressed in diabetic rats but restored by treatment with riboflavin. This finding was associated with reduction in cholesterol levels and a favourable shift in lipoprotein LDL to HDL in treated rats (Wang et al., 2011).

It has been suggested that high rates of fatty acid oxidation at the expense of glyoclysis reduces available ATP for use by ion transporters (An and Rodrigues, 2006; Entman et al., 1977). Such an abnormality impairs Ca^{2+} homeostasis and interferes with normal excitation/contraction coupling. In 3 month old Akita type 1 diabetic mice, a threefold increase in FAT/CD36 expression, palmitate oxidation, and ceramide and diacylglycerol

accumulation in the heart was associated with impaired diastolic function measured by echocardiography and reduced expression of SERCA2A (Basu et al., 2009).

1.2.3 Collagenation and Fibrosis

Chronic hyperglycemia induces the accumulation of advanced glycation endproducts, the irreversible consequence of nonenzymatic glycosylation of proteins and lipids (Cooper, 2004; Schmidt et al., 1994). Diabetic hearts exhibit reduced compliance manifesting as a diastolic abnormality, which has been suggested to derive from collagen crosslinking of glycosylated macromolecules (Norton et al., 1996). Immunohistochemistry and PCR studies have demonstrated a marked increase in left ventricle receptor for advanced glycation endproduct accumulation in and protein expression of connective tissue growth factor in diabetic rat hearts (Candido et al., 2003). Treatment of these hearts with ALT-711, a cross-link breaker, reduced interstitial collagen type III, receptor for advanced glycation end products, and connective tissue growth factor to control levels, suggesting a critical role of glycosylation in the development of ventricular diastolic dysfunction in diabetes (Candido et al., 2003).

In mRen-2 transgenic rats overexpressing the renin gene, induction of diabetes by STZ was shown to markedly increase immunostaining for collagen type I. The fibrosis of the left ventricle was further associated with reduced expression of SERCA 2A, elevated transforming growth factor β, and a steeper slope of pressure volume loop obtained from left ventricular micromanometer catheterization studies (Connelly et al., 2009). STZ-induced diabetic transgenic mice overexpressing insulin-like growth factor 1R show a reduction in picrosirius red staining of collagen deposition in left ventricle, associated with a modest recovery of mitral valve deceleration and left ventricular filling velocities as determined by echocardiography (Huynh et al., 2010). Histological studies in STZ diabetic mice exhibit a twofold elevation in collagenation area of the left ventricle as compared to non-diabetic mice

(Li et al., 2010a; Li et al., 2011). Collagen accumulation was reduced in mice lacking the Rac1/NADPH oxidase gene, indicating a role of oxidative stress in myocardial fibrosis (Li et al., 2010a). Dysregulation of calcium regulatory proteins including SERCA2A contributes to abnormal left ventricular function and excitation/contraction uncoupling and support the interaction of diabetes with cardiac SNS signaling.

1.2.4 Functional Consequences

Growing evidence indicates that early stages of diabetic cardiomyopathy manifest as abnormalities in ventricular filling, characteristic of diastolic heart disease. The presence of heart failure with preserved ejection fraction has been frequently described in the diabetic population (Chareonthaitawee et al., 2007; Young et al., 2009), with prevalence among type 2 diabetic patients estimated to be as high as 60% (Poirier et al., 2001). From and colleagues demonstrated an independent association between the presence of diastolic dysfunction, defined as elevated E/e' ratio and increased left atrial volume, and the subsequent development of heart failure (From et al., 2010). Patients presenting with diastolic dysfunction were 20% more likely to develop heart failure during 5 year follow-up period (From et al., 2010). Abnormalities in ventricular filling have been described in type 1 and type 2 diabetic animal models. In the Type 2 diabetic Otsuka Long-Evans Tokushima Fatty rat, prolonged mitral valve deceleration time develops within days to weeks of the onset of diabetes (Mizushige et al., 2000). Echocardiography parameters have been corroborated by gold standard measurements of left ventricular pressure-volume relationships using catheter-micromanometers (Connelly et al., 2006; Radovits et al., 2009). Whereas type 1 diabetic rats tend to exhibit systolic dysfunction including decreased ejection fraction and cardiac output (Basu et al., 2009), type 2 diabetic rats tend to first exhibit diastolic dysfunction, characterized by preserved ejection fraction, increased left ventricle end diastolic pressure, and a sharper slope of the pressure-volume relationship (Radovits et al., 2009).

It has been suggested that treatment of diastolic dysfunction, particularly in early asymptomatic stages, may prevent subsequent degradation of systolic function and progression of cardiac remodeling (Aneja et al., 2008; Kim et al., 2003). It stands to reason that early indicators of cardiac dysfunction are crucial to effective treatment of diabetic heart disease.

1.3 Autonomic Nervous System

The autonomic nervous system is the primary extrinsic control of cardiac inotropy and chronotropy. At rest, the heart is predominantly under parasympathetic nervous control by the vagus nerve. However, stimulation of the SNS evokes a myriad of systemic fight or flight responses, including increased heart rate and contractility.

1.3.1 Parasympathetic Myocardial Innervation

Parasympathetic efferent neurons originate from the brain stem within nucleus ambiguous and project via the vagus cranial nerve to postganglionic fibres located within intrinsic cardiac ganglia (Ardell, 2004). Immunostaining has demonstrated right to left and base to apex gradients in both tyrosine hydroxyalse-positive sympathetic and acetylcholine-positive parasympathetic neuronal fibres (Crick et al., 1999). Acetylcholine is synthesized by choline acetyltransferase from choline and acetyl-CoA. Synthesized acetylcholine is taken into storage vesicles by the acetylcholine transporter and released into the synapse during parasympathetic neural stimulation. Acetylcholine is broken down by acetylcholinesterase in the synapse. Choline is recovered into the neuron to be reincorporated into acetylcholine. Paraympathetic signal is conducted to target tissues via nicotinic and muscarinic receptors. The heart expresses predominantly M_2 muscarinic receptors, which act to reduce heart rate by slowing neuronal depolarization and to reduce the contractile force by G_i inhibition of adenylate cyclase (Ardell, 2004). Altered muscarinic receptor expression has been identified in diabetes (Latifpour and McNeill, 1984), atrial fibrillation (Jayachandran et al., 2000), post

myocardial infarction (Mazzadi et al., 2009), idiopathic dilated cardiomyopathy (Le Guludec et al., 1997), and familial amyloid polyneuropathy (Delahaye et al., 2001; Delforge et al., 1990).

1.3.2 Sympathetic Myocardial Innervation

Sympathetic innervation consists of preganglionic and postganglionic efferent fibres. Preganglionic efferent neurons originate in the locus coeruleus of the medulla oblongata, projecting to the hypothalamus, cranial nerves, and the interomedial lateral tract of the spinal cord (Ardell, 2004). Exiting the spinal cord at T1-T5 rami, these efferent neurons synapse within the paravertebral ganglia or at the adrenal gland. Postganglionic fibres project to the heart from the stellate ganglion and other upper thoracic paravertebral ganglia (Pardini et al., 1989). These neurons coalesce with the cardiac extensions of the vagus nerve to form the cardiac neuronal plexus at the base of the heart. From this plexus, sympathetic efferents follow the coronary vasculature to innervate the myocardium, focused at the epicardium whereas parasympathetic fibres penetrate the outer layers to innervate the endocardium. Sympathetic neurons are distributed in a relatively uniform manner throughout the atria and ventricles, with focal innervation of sinoatrial and atrioventricular nodes (Wehrwein et al., 2008).

Terminal release of neurotransmitter occurs from localized swellings of the axons, termed varicosities or boutons, effectively the neuroeffector junctions of the cardiac SNS. Within the varicosity, norepinephrine (NE) is stored in neuronal vesicles and synthesized from tyrosine in a series of enzyme-catalyzed reactions: tyrosine is converted to dihydrxoyphenylalanine (DOPA) by tyrosine hydroxylase; DOPA is converted to dopamine by DOPA-decarboxylase; dopamine is converted to NE by dopamine β-hydroxylase; NE is converted to epinephrine by phenylethanolamine-*N*-methyltransferase. Following sympathetic nerve impulse, vesicles dock to the axonal membrane of the varicosity via scaffolding proteins including soluble N-

ethylmaleimide-sensitive factor attachment protein receptor (SNARE) complexes (Blanes-Mira et al., 2003; Jung et al., 2008). The contents of the vesicle are released into a synaptic cleft that is wider than in the central nervous system (Woolard et al., 2004).

Sympathetic signaling is conducted postsynaptically by neurotransmitter stimulation of G protein-coupled adrenoceptors expressed at the target tissue surface (Fig 1.4). Adrenoceptors comprise two major subtypes and multiple isoforms. Alpha-adrenoceptors exist in two isoforms: α_1-adrenoceptors which are localized mainly in the vasculature and α_2-adrenoceptors of which the α_{2A}-adrenoceptors are localized on presynaptic neurons. Beta-adrenoceptors are found in three well characterized isoforms: β_1-adrenoceptors found in highest quantity in cardiac and skeletal muscle and adipose tissue; β_2-adrenoceptors found in greatest concentration in bronchioles; and β_3-adrenoceptors predominantly expressed by adipocytes (Armour, 2004).

1.3.3 Presynaptic Function

Sympathetic signaling is terminated by: i) active recapture of neurotransmitter into the varicosity by NE reuptake transporter (NET) via the uptake-1 pathway, ii) negative feedback by stimulation of presynaptic α_{2A}-adrenoceptors to reduce subsequent NE release, and iii) catabolism of neurotransmitter by synaptic catechol-O-methyltransferase (COMT) and neuronal monoamine oxidase (MAO).

1.3.3.1 Uptake-1 Expression and Activity

As first described by Iversen, the primary termination of sympathetic signal is the active recapture of NE into the neuronal varicosity by the uptake-1 pathway via NET (Iversen et al., 1972). It has been estimated that 80-90% of the NE used by the heart is synthesized within cardiac sympathetic neurons (Eisenhofer et al., 1996; Kopin and Gordon, 1963), receiving relatively little input from circulating NE secreted by the adrenal glands. As such, the active recapture and storage of NE is essential for maintenance of cardiac sympathetic neurons.

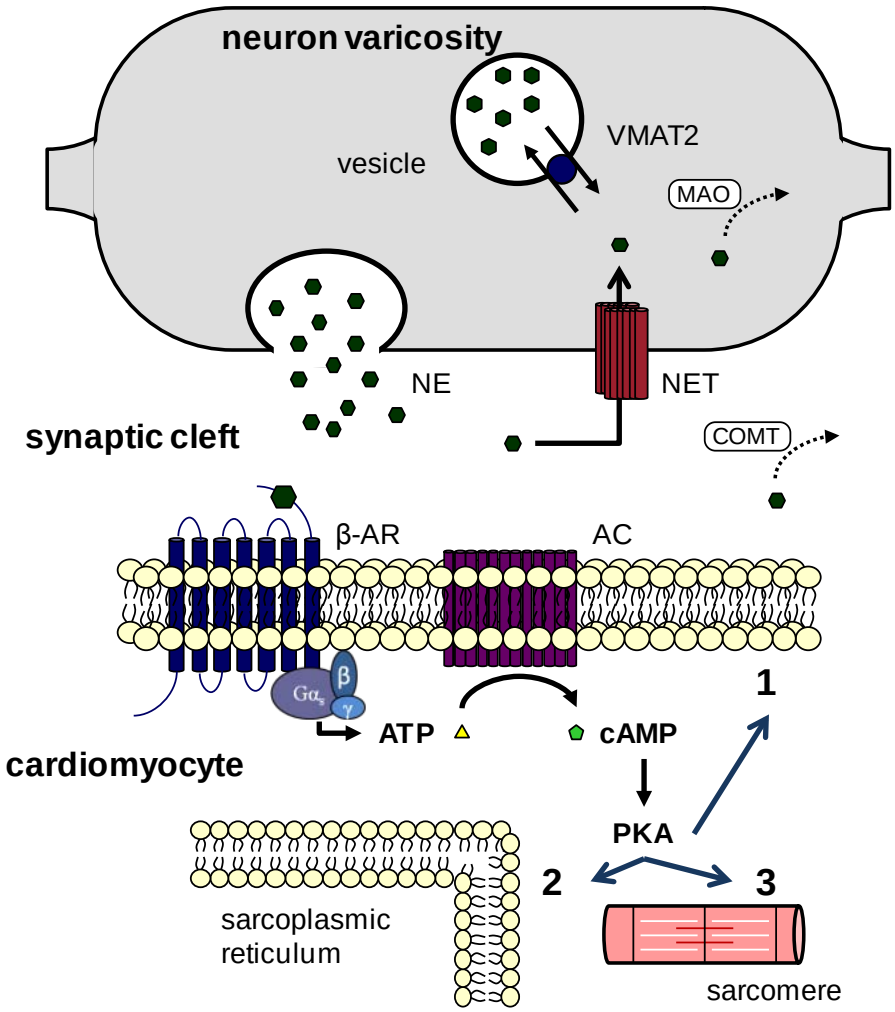

Figure 1.4 Sympathetic signal transduction and termination in the heart. Norepinephrine (NE) is released from the neuronal varicosity into the synaptic cleft. Binding of NE by β-adrenoceptors (β-AR) on the cardiomyocyte membrane causes a release of the G_s protein. $G\alpha_s$ stimulates adenylyl cyclase (AC) which converts adenosine trisphosphate (ATP) to the second messenger cyclic AMP (cAMP). cAMP activates protein kinase A, which phosphorylates calcium handling and contractile proteins at distinct sites: 1) membrane L-type calcium channels to augment Ca^{2+} influx; 2) sarcoplasmic reticulum proteins ryanadine receptor and sarcoplasmic reticulum ATPase type 2 which concentrate intracellular Ca^{2+}, and 3) sarcomere proteins myosin-binding protein-C and troponin facilitating the interaction of myosin and actin and promoting contraction. Sympathetic signal is terminated by active recapture of NE into the neuronal varicosity by the sodium-dependent NE reuptake transporter (NET), where it is subject to vesicular packaging by vesicular monoamine transporter type 2 (VMAT2) or metabolism by monoamine oxidase (MAO). The remainder of synaptic NE is metabolized by catechol-O-methyltransferase (COMT) or spills over to the circulation.

NET is a sodium-dependent 12-transmembrane domain transport protein expressed at the cell surface of neurons (Bruss et al., 1995). Transport of NE is dependent on the presence of Na+ in the tissue medium, and facilitates cotransport of neurotransmitter across the cell membrane (Sammet and Graefe, 1979). The intracellular C-terminus is necessary for targeting of the protein to axonal membrane (Burton et al., 1998). Genetic analyses have identified specific moieties of the transporter necessary for endocytic regulation of NET-1, including several sequences at the intracellular C-terminal region (Holton et al., 2005). There are five putative serine or threonine phosphorylation sites in the intracellular loops of NET (Blakely et al., 1994). Phosphorylation is followed by endocytosis of the transporter, reducing surface expression and activity of NET (Apparsundaram et al., 1998; Bonisch et al., 1998). Microscopy and immunoprecipitation studies suggest association of NET with large protein scaffolds including syntaxin 1A and t-SNARE (Beckman et al., 1998; Geerlings et al., 2000; Haase et al., 2001). Syntaxin 1A suppression with antisense oligonucleotids markedly reduced V_{max}, suggesting that these scaffolds may be important in regulating NET transport (Sung et al., 2003).

NET is expressed in adrenergic chromaffin, ganglion, and neuronal cells in the central nervous system, and mRNA is concentrated in the brainstem and locus coeruleus (Lorang et al., 1994; Sanders et al., 2005). By contrast, in the peripheral nervous system, expression of NET is predominantly limited to the catecholaminergic neurons (Phillips et al., 2001a; Schroeter et al., 2000).

In the rat heart, highest binding of NET ligands is observed in the left ventricle (~750 fmol/mg protein) with lower binding observed in right ventricle (~600 fmol/mg protein) and atrial tissue (230-300 fmol/mg protein) (Wehrwein et al., 2008). Immunoreactivity of NET is specific to sympathetic nerve fibres, as demonstrated by overlay fluorescence microscopy and colocalization with tyrosine hydroxylase antibodies (Wehrwein et al., 2008). Binding

assays with the selective inhibitor ^{3}H-mazindol have shown baseline NET expression in the rat heart of ~460 fmol/mg protein (Raffel and Chen, 2004).

Reuptake has a maximal capacity, such that excess NE will spillover from an organ (i.e. the difference between NE venous efflux and arterial influx) at a rate roughly proportional to sympathetic nerve firing (Esler et al., 1984). Spillover of NE from the heart during exercise increases by up to 1700% to resting baseline (Esler et al., 1997). Administration of the NET inhibitor desipramine (0.5 mg/kg iv, 30 min) evokes a marked increase in NE spillover to plasma from the heart but not from kidney or forearm measurements (Esler et al., 1990), reflecting the high dependence on local NE synthesis in the myocardium and tighter synaptic junction than is observed in skeletal muscle (Birkenfeld et al., 2002).

1.3.3.2 Uptake-1 Regulation

In vitro studies have identified a number of factors involved in the internalization and downregulation of surface NET for activity regulation. Electron microscopy studies demonstrated that internalized NET were localized to lipid rafts within the cytosol (Wong and Scott, 2004). Chronic KCl-depolarization in cultured superior cervical ganglia neurons evoked elevation of NET mRNA. This observation was dependent on NE production, as it was attenuated by the tyrosine hydroxylase inhibitor α-methyl-*para*-tyrosine and augmented by addition of the precursor to the tyrosine hydroxylase cofactor BH4 sepiapterin (Habecker et al., 2006). Conversely, activation of PKC by the active phorbol ester β-phorbol myristate acetate reduced NE reuptake in hNET stably transfected cells by significantly decelerating V_{max} and reduced surface NET expression (Wong and Scott, 2004). Addition of the PKC inhibitor staurosporine effectively blocked this response (Jayanthi et al., 2004). During chronic temperature stress, the proportion of NET-positive neurons was increased to 50% of axons with a parallel increase in active tyrosine hydroxylase, as demonstrated by immunocytochemistry (Miner et al., 2006). NET is also regulated by growth factors

including transforming growth factor-β and neurotrophin-3. Addition of these neurotrophins to cultured neural crest cells resulted in a significant increase in NET mRNA and activity (Ren et al., 2001). Taken together, neuronal activation stimulates translocation of NET to the cell surface to reduce synaptic overstimulation enhanced recapture of neurotranmitter. By contrast, long-term sympathetic activation and NE release may evoke an opposite result, possibly relating to catecholamine toxicity. Mao and colleagues demonstrated that exposure of PC12 cells to 100 μM NE evoked a 33% reduction in both Michaelis-Mentin V_{max} and B_{max}, concurrent with a temporal rise in indicators of oxidative stress including phoshorylated endoplasmic reticulum kinase. Expression of NET was partially restored by treatment with superoxide dismutase to attenuate oxidative stress (Mao et al., 2005). Elevation of endogenous or exogenous cAMP by forskolin or dibutyryl-cAMP administration has been shown to reduce ^{3}H-NE uptake in PC12 cells (Bryan-Lluka et al., 2001). Mardon and colleagues have shown that five day intravenous infusion of NE (0.02 μg/min) to rats evoked a twofold increase in circulating NE and a 35% decrease in myocardial uptake of ^{3}H-NE or its analogue ^{125}I-metaiodobenzylguanidine (^{125}I-MIBG). This observation was associated with a 33% reduction of NET B_{max} in rats administered NE compared to saline (Mardon et al., 2003).

Pharmacological treatments can extrinsically regulate the activity and expression of NET *in vivo*. Chronic treatment of Sprague Dawley rats with tricyclic antidepressant desipramine (10 mg/kg, 21 days) has been shown to reduce brain expression of NET in the locus coeruleus by 17% as shown by ^{3}H-nisoxetine autoradiography (Hebert et al., 2001). Reduced NET binding was also observed in the ventromedial hypothalamic nucleus by 47% following a similar treatment regimen (Benmansour et al., 2004). Zhu et al showed no change in NET immunoblot density after 3 days but ~40% reduction after 14 days of desipramine treatment (Zhu et al., 2002). Blockade of NET function with the selective inhibitor reboxetine reduced

systolic blood pressure and muscle sympathetic nerve activity in response to cold pressor testing, suggesting an impairment of autonomic reflexes (Tank et al., 2003). Similarly, in Sprague Dawley rats, chronic administration of desipramine ablated the mean arterial pressure response to treatment with the catecholamine releasing agent tyramine (Carson et al., 2002).

1.3.3.3 Uptake-1 in Disease States

Abnormalities in the regulation of NET have been suggested to play a role in cardiovascular and psychological disease. Esler and colleagues demonstrated a significantly higher degree of DNA methylation in the promoter region of the NET gene among patients with panic disorder as compared to healthy controls (Esler et al., 2006). The authors suggested that the impaired NET amplifies the effect of sympathetic signaling during panic attacks, particularly in the heart (Esler et al., 2006). Supporting this concept, systemic knockout of NET has been shown to augment plasma dopamine, epinephrine, and NE by approximately threefold, whereas cardiac levels are reduced by 25-30% (Keller et al., 2004). This disconnection reflects the local production and dependence on reuptake for maintained NE stores in the myocardium. Radiotelemetry monitoring of NET-/- mice demonstrated a larger increase in heart rate and mean arterial pressure during activity versus rest as compared to NET +/+ mice (Keller et al., 2004). NET knockout mice also show increased locomotor activity and supersensitivity to psychostimulants (Xu et al., 2000).

Similar to NET knockout, rats with biventricular hypertrophy induced by aortic banding exhibited an increase in plasma NE but reduced cardiac NE levels (Backs et al., 2001). This is concurrent with lower ^{3}H-NE uptake, a 48% decrease in ^{3}H-desipramine binding to left ventricular NET with no change in glyoxylic acid immunofluorescence of sympathetic nerve endings (Backs et al., 2001). Administration of recombinant NET to myocardium of rabbits with pacing-induced heart failure maintained ^{3}H-NE uptake kinetics, restored expression of

postsynaptic sympathetic signaling proteins, and attenuated decreases in fractional shortening and ventricular pressure (Munch et al., 2005). These experiments strongly suggest an important role for NET in the development of heart failure and regulation of NE signaling in post-infarction stages of myocardial pathogenesis.

1.3.3.4 Negative Feedback

A secondary mechanism of sympathetic signal termination is negative feedback by stimulation of presynaptic α_{2A}-adrenoceptors to reduce action potential propagation in sympathetic neurons (Freeman, 2006).

Spontaneously hypertensive rats exhibited a blunted increase in myocardial NE overflow following treatment with α_2-adrenoceptor blocker yohimbine with parallel reduction in α_2-adrenoceptor mRNA content (Zugck et al., 2003). Blockade of α_2-adrenoceptors by yohimbine in healthy dogs evokes an increase in heart rate, blood pressure and coronary flow (Heyndrickx et al., 1984). Genetic deletion of the α_{2A}- or α_{2C}-adrenoceptor in aortic banded heart failure mice is associated with elevated circulating NE, greater reduction in ejection fraction, and exacerbated hypertrophy (Brede et al., 2002). Collectively, these findings suggest that impaired negative feedback and resultant sympathetic nervous overactivity may contribute to development of cardiovascular disease.

1.3.3.5 Catecholamine Metabolism

Excess NE is degraded by enzymes localized within the neuronal cytoplasm and the postsynaptic tissue. MAO is expressed predominantly in the neuronal varicosity where it breaks NE down to dihydroxyphenylethyleneglycol (Fillenz and Stanford, 1981; Ganguly et al., 1986). COMT is mainly found within the synapse and postsynaptic tissue, where it breaks NE down to normetanephrine (Ganguly et al., 1986; Hirano et al., 2005). The final metabolic product of NE is vanillyl mandelic acid. Measurement of NE metabolites has been used as a

surrogate measurement of systemic sympathetic hyperactivity (Esler et al., 1990; Wang et al., 1999).

Inhibition of MAO in the brain by tranylcypromine evoked a dose-dependent increase in local NE content (Routledge and Marsden, 1987). NET knockout mice displayed a decrease in circulating levels of NE metabolites dihydroxyphenylglycol and 3,4-dihydroxypehnylacetic acid (Keller et al., 2004). This finding reflects the necessity of uptake-1 for the breakdown of catecholamines, particularly by MAO.

1.3.4 β-Adrenoceptors of the Heart

Both β_1 and β_2-adrenoceptors are coupled to the stimulatory G protein (G_s). Dissociation of the α-subunit of G_s activates adenylate cyclase and generates the second messenger cAMP. Subsequent activation of protein kinase A (PKA) phosphorylates a series of proteins involved in Ca^{2+} regulation including ryanadine receptor, sarcoplasmic reticulum Ca^{2+} ATPase, and L-type calcium channels . This signal culminates in an influx of Ca^{2+} which, by binding and inactivating the regulatory protein calmodulin, facilitates the interaction of actin and myosin at the sarcomere and effectively increases the force of cardiomyocyte contraction (Fig 1.4) (Brodde, 1991; Wehrens et al., 2006). β_2-Adrenoceptors are also coupled to the inhibitory G protein (G_i). The dissociated α-subunit of G_i inhibits adenylate cyclase, resulting in a reduction of cAMP production. This counters the action of the G_s stimulation and acts as a regulator of cardiac contractility. Cardiac β_3-adrenoceptors have been shown to contribute to negative inotropic effects in reducing the amplitude and accelerating the repolarization phase of the cardiac action potential in isolated ventricular myocytes (Gauthier et al., 1996). In the healthy rat heart, β-adrenergic subtype expression patterns are roughly 62% β_1, 30% β_2, and 8% β_3 adrenoceptors (Bristow et al., 1986; Dincer et al., 2001).

Continuous stimulation of β-adrenoceptors evokes uncoupling of sympathetic signaling from calcium regulation. Seven day infusion of epinephrine resulted in a decrease in β-

adrenoceptor B_{max} by dihydroalprenolol binding assay, and was associated with an earlier shift in phospholipid composition of the sarcolemma (Benediktsdottir et al., 1999). This observation supports the membrane clathrin pit internalization model of β-adrenoceptor internalization and downregulation. Using membrane preparations from failing human hearts post transplant, Bristow and colleagues demonstrated a 50-56% reduction in β-adrenoceptor density and a significant attenuation of muscle contractility (Bristow et al., 1982). Chronic treatment with β-blockers increases the expression of β-adrenoceptors. This adaptation has been shown to improve sympathetic signaling in remodeling heart to restore noradrenergic input to the cardiac muscle. Radiotelemetry studies in rats have demonstrated the effect of adrenergic blockade on heart rate, blood pressure, and heart rate variability (Bertram et al., 2000). Beckers and colleagues described a depression of low frequency heart rate variability following treatment with the β-blocker propranolol (Beckers et al., 2006).

1.4 Sympathetic Nervous System in Heart Disease

Activation of the SNS is a synergistic indicator of cardiovascular and metabolic disorders including diabetes. Heightened sympathetic drive to stimulate inotropy and chronotropy is an initial adaptive response to reduced cardiac output and efficiency. Continuous overactivity of the SNS disrupts the balance of autonomic signaling, altering the expression and sensitivity of sympathetic signaling elements, to the ultimate detriment of myocardial function.

1.4.1 Sympathetic Nervous System in Heart Failure

Heart failure is the common endpoint of primary cardiopathologies, defined as the inability of the heart to supply adequate oxygenated blood to the organs of the body. A failing heart attempts to compensate for pathophysiological deficits via several mechanisms including cardiac remodeling, altered contractility, and stimulation of the SNS.

1.4.1.1 Norepinephrine in Heart Failure

Microdialysis measurements of myocardial interstitial fluid have demonstrated an exponential increase in catecholamine release over the first 60 minutes after occlusion of the left anterior descending coronary artery in pigs (Lameris et al., 2000). In a canine model of congestive heart failure, plasma NE was elevated sixfold with a corresponding decrease in left ventricular NE as determined by glyoxylic acid staining and reduced NE uptake activity (Himura et al., 1993). Dahl salt sensitive rats with hypertension exhibited a decrease in ^{3}H-NE uptake and progressive reduction of sympathetic nerve density and left ventricular NE beginning within 7 days and sustained over 50 days of high salt feeding (Kreusser et al., 2008). Renal sympathetic nerve activity (RSNA) recordings show elevated activity in congestive heart failure rats 6 weeks after LAD ligation as compared to sham operated controls, associated with a decrease in left ventricular ejection fraction (Francis et al., 2001). In comparable studies at 4 weeks of heart failure, enhanced basal RSNA was associated with a relative decrase in low frequency pulse interval by spectral analysis of heart rate variability, suggesting a dysregulation of heart rate and pulse pressure (Tobaldini et al., 2009). Imaging studies have demonstrated that the area of sympathetic neuronal defect defined by retention of ^{123}I-MIBG tends to be larger than the ischemic region defined by myocardial perfusion single photon emission computed tomography (SPECT) imaging with ^{99m}Tc-sestamibi (Matsunari et al., 2000), which has been replicated using positron emission tomography (PET) tracers (Sasano et al., 2008).

Significant overflow of NE from the heart to the circulation is observed in patients with heart failure (Esler et al., 1990). Plasma catecholamine levels are acutely elevated in the first hours after onset of chest pain, and sustained over 48 hours (Nadeau and de Champlain, 1979). Levine and colleagues proposed that heart failure patients could be categorized based on catecholaminergic and angiotensin activity, wherein plasma NE was associated with

hemodynamic measures of left ventricular dysfunction (Levine et al., 1982). Cohn and colleagues established an inverse relationship between plasma NE concentration and survival, wherein heart failure patients with plasma NE levels exceeding 1000 pg/mL had a 50 month survival rate of less than 5% as compared to those with plasma NE levels of 200 pg/mL who had a 25-30% survival rate (Cohn et al., 1984).

1.4.1.2 Uptake-1 in Heart Failure

Regional density of NET at sympathetic nerve terminals is altered in rats following myocardial infarction. Li and colleagues demonstrated a decrease in ^{3}H-nisoxetine binding in the left ventricle but not the right ventricle or stellate ganglion in rats one week after left anterior descending coronary artery occlusion compared to sham operated rats (Li et al., 2004). While sympathetic neurons localized to the infarct region are reduced, sympathetic density has been shown to be elevated in periinfarct and remote myocardium (Cao et al., 2000). Further, whereas the left ventricle distal of the coronary artery occlusion showed significantly reduced tyrosine hydroxylase immunostaining, myocardium proximal to the occlusion showed threefold elevation of tyrosine hydroxylase with a parallel elevation in NET mRNA (Parrish et al., 2008). This heterogenetity of innervation was not seen in transgenic rats deficient of brain angiotensinogen, removing the angiotensin II augmentation of sympathetic nervous drive (Parrish et al., 2008). Barber and colleagues demonstrated the presence of denervated and non-denervated myocardium following transmural infarct in dogs (Barber et al., 1983). In dogs with right heart failure induced by right atrial balloon constriction, NE spillover was enhanced to 0.45 ng/mL compared to 0.17 ng/mL in sham operated dogs. After 5-19 weeks, NE reuptake was reduced 51% in parallel with a 57% decrease in NE reuptake inhibitor ^{3}H-mazindol binding and a 26% reduction in postsynaptic β-adrenoceptor binding by ^{3}H-dihydroalprenolol (Liang et al., 1989).

1.4.1.3 β-Adrenoceptors in Heart Failure

The density of β_1-adrenoceptors was reduced by 71% at 8 weeks after pulmonary artery occlusion and right atrial constriction in dogs. By contrast, β_2-adrenoceptor density remains relatively unchanged. This corresponded to a shift in G protein subtype expression, with a marked increase in the proportion of G_i coupled β_2-adrenoceptors to dampen the adrenergic signal (Lai et al., 1996). Comparable reductions in cAMP generation in response to isopropterenol treatment have been shown in canine right heart failure, indicating reduced sympathetic signaling capacity (Kawai et al., 2000). Taken together, these studies demonstrate sympathetic hyperactivation in failing hearts with compensatory downregulation of presynaptic NET and postsynaptic G_s-coupled β-adrenoceptors to dampen sympathetic stimulation.

Clinically, patients with sympathetic and baroreflex abnormalities as assessed by muscle sympathetic nerve recordings were shown to have a higher incidence of ventricular arrhythmia and were at greater risk of sudden cardiac death (Grassi et al., 2004). A myriad of studies have demonstrated that β-adrenoceptor density is reduced in congestive heart failure (de Jong et al., 2005; Gaemperli et al., 2010; Sethi et al., 2004). Use of β-blockers to induce upregulation of the β-adrenoceptor pool and normalize noradrenergic signaling in the failing heart remains a first-line therapy in the control of heart failure (Bristow et al., 2004).

1.4.1.4 Other Sympathetic Factors in Heart Failure

Part of the increase in sympathetic drive is believed to be mediated by higher brain regions. Intracerebroventricular administration of the cytokine synthesis inhibitor pentoxifylline reduced circulating NE in heart failure rats (Kang et al., 2008). The authors postulated that cytokine inhibition reduced the inflammatory response post infarction in rats. Administration of lidocaine to cardiac sympathetic afferent neurons reduced renal sympathetic nerve activity in a canine model of congestive heart failure (Wang and Zucker, 1996). Activation of

sympathetic neurons by capsaicin application of electrical stimulation evokes an attenuation of the baroreceptor reflex consistent with sustained elevation of basal sympathetic tone (Gao et al., 2005). This abnormal cardiac sympathetic reflex in myocardial infarction rats was improved by chronic treatment with the superoxide dismutase mimetic tempol (Shi et al., 2009). Reduced oxidative stress was associated with a reduction in renal sympathetic nerve activity following capsaicin stimulation and a reduction in plasma NE concentration. Alternatively, augmentation of endothelin by a novel endothelin converting enzyme inhibitor showed a reduction in mean arterial pressure in parallel with reduced myocardial but not adrenal gland NE secretion among heart failure rats (Rufanova et al., 2009).

1.4.2 Sympathetic Nervous System in Diabetic Heart Disease

A full review of basic and clinical evidence for cardiac sympathetic nervous dysregulation in diabetes is covered in Chapter 4. Following is a brief summary.

Overactivity of the SNS and enhanced NE levels are observed in obesity, insulin resistance, type 2 diabetes and hypertension (Anderson et al., 1991; Esler et al., 2001; Gallego et al., 2003; Grassi et al., 2005; Masuo et al., 2003). Glucose transport is regulated by insulin receptor binding and partially by NE signaling (Calera et al., 1998; Taegtmeyer et al., 2002), with translocation of GLUT4 to the sarcolemma requiring short term NE stimulation (Czech and Corvera, 1999; Morisco et al., 2005). Disruption of the cross-talk between NE and insulin signaling has been implicated as a potential causative factor in the coincidence of insulin resistance and heart failure (Esler et al., 2001; Morisco et al., 2005). Chronic blockade of β-adrenoceptors has been associated with development of new-onset diabetes among congestive heart failure patients (Swan et al., 1997). Insulin potentiates the SNS and release of NE (Anderson et al., 1991; Kern et al., 2005; Masuo et al., 2003). Acute insulin treatment decreases ^{3}H-NE uptake in PC12 cells, indicating a desensitization or downregulation of NET comparable to chronic overexposure to catecholamines (Figlewicz et

al., 1993a; Figlewicz et al., 1993b). Application of insulin evokes downregulation of β_3-adrenoceptors in cultured adipocytes (Feve et al., 1994). Treatment of monogenic obese and hyperinsulinemic mice with diazoxide, a K_{ATP} channel blocker that blocks pancreatic glucose sensing and insulin secretion, has been shown to reverse insulin and NE-induced downregulation of β-adrenoceptors (Surwit et al., 2000). Glucose is also a strong promoter of NE release, and has been associated with dysregulation of SNS signaling in obese and diabetic animals (Esler et al., 2001; Levin and Sullivan, 1989). In type 2 diabetes, insulin resistance and progressive hyperglycemia increase plasma NE which may subsequently impair β-adrenoceptor-mediated signal transduction (Esler et al., 2001; Morisco et al., 2005; Thackeray et al., 2011a). Indeed, presence of type 2 diabetes, insulin resistance and hyperglycemia has been strongly associated with elevations in cardiac NE content (Gallego et al., 2003; Ganguly et al., 1987), enhanced SNS activity (Grassi et al., 2005), altered resting heart rate (Carnethon et al., 2003b), and depressed heart rate variability (Fazan et al., 1997; Howarth et al., 2006). Elevated NE levels have been described in several animal models of diabetes (Table 1.1). Moreover, a prominent link has been established in type 1 diabetes between hyperglycemia and reduced cardiac β-adrenoceptor densities (Altan et al., 2007; Dincer et al., 2001; Sellers and Chess-Williams, 2001; Thackeray et al., 2011a), and it has been suggested that these measurements can predict cardiovascular deterioration (Flaa et al., 2008; Jyotsna et al., 2009; Rosengard-Barlund et al., 2009). In a pair of prospective clinical studies, reduced heart rate variability or enhanced NE response to a cold pressor test (i.e. impaired autonomic regulation) were predictive of subsequent insulin resistance and diabetes (Carnethon et al., 2003a; Flaa et al., 2008). Additionally, sympathetic nervous activation has Long term diabetes is associated with the loss of autonomic neurons termed diabetic autonomic neuropathy. The five year mortality rate of patients with cardiac autonomic

Table 1.1 Plasma and cardiac norepinephrine levels in diabetic animals

		Plasma NE (ng/mL)		Cardiac NE (ng/g)		
Diabetic Model	Duration	Diabetic	Control	Diabetic	Control	Ref
WK, STZ 65 mg/kg iv	2 weeks	N/D	N/D	880±51	812±68	a
	4 weeks	N/D	N/D	947±68	812±68	
	8 weeks	N/D	N/D	1015±68	744±51	
SD, STZ 55 mg/kg iv	4 weeks	N/D	N/D	8710±2970	3920±510	b
SD, STZ 65 mg/kg iv	8 weeks	3.9±0.2	1.8±0.1	510±15	217±10	c,d
SD, STZ 45 mg/kg ip	2 weeks	0.10±0.06	0.10±0.08	1052±251	771±57	e
high fat feeding	8 weeks	0.24±0.09	0.11±0.06	1120±299	935±296	
Goto Kakizaki	8 weeks	9.4±2.4	9.4±2.1	344±35	354±31	f
Zucker Diabetic Fatty	14 weeks	0.8±0.2	0.3±0.1	N/D	N/D	g

WK, Wistar Kyoto; SD, Sprague Dawley; N/D not determined

a (Akiyama et al., 1989)
b (Kiyono et al., 2001)
c (Ganguly et al., 1987; Ganguly et al., 1986)
e (Thackeray et al., 2011b)
f (Kiyono et al., 2002a)
g (Marsh et al., 2007)

neuropathy has been estimated at 16-53% (O'Brien et al., 1991). In a cohort of 73 diabetics, 40 patients (55%) had abnormal autonomic function as tested by Valsalva manouevre ratio, sustained handgrip testing, and orthostatic change in blood pressure (Ewing et al., 1980). The mortality rate of patients with abnormal tests was 44% after 2.5 years and 56% after 5 years, compared with 15% among patients with normal autonomic tests (Ewing et al., 1980). The majority of mortality was attributed to sudden cardiac death. Many imaging studies have related the decrease in radiotracer uptake to sympathetic denervation (Muhr-Becker et al., 1999; Schmid et al., 1999; Stevens et al., 1998b; Stevens et al., 1999). The presence of sympathetic dysinnervation in diabetes prior to neuronal death remains somewhat contentious. Histological examination of sympathetic ganglia revealed neuroaxonal dystrophy in STZ-induced type 1 diabetic rats but no ultrastructural neuronal damage in Zucker type 2 diabetic rats (Schmidt et al., 2003a; Schmidt et al., 2003b). Understanding the time course and process of altered sympathetic signaling would provide mechanistic insight into the role of NE in the progression of diabetic left ventricular dysfunction.

1.5 Animal Models of Diabetes

Several animal models of human diabetes have been developed for scientific research (Table 1.2). While models of insulin insufficiency can be readily generated to exhibit characteristics of type 1 diabetes, it is difficult to replicate the natural pathogenesis of the disease from inception in an animal model. Moreover, mimicry of multifaceted type 2 diabetes has proved elusive, with several candidate models in widespread use, each with similarities and differences compared to its human counterpart.

Table 1.2 Rodent models of diabetes

Model	Type	Origin	Systemic Phenotype	Cardiac Phenotype	Ref
Mice					
STZ	Type 1	beta cell toxicity	severe hyperglycemia, hypoinsulinemia, dyslipidemia	fibrosis, metabolic shift, systolic dysfunction, diastolic dysfunction	a,b
OVE26	Type 1	o/e calmodulin minigene insulin promoter, beta cell destruction	severe hyperglycemia, hypoinsulinemia, dyslipidemia	fibrosis, systolic dysfunction, diastolic dysfunction	a,c
Akita	Type 1	spontaneous mutation, insulin 2 gene, insulin deficiency	moderate hyperglycemia, hypoinsulinemia,	fibrosis, metabolic shift, systolic dysfunction, diastolic dysfunction	d
ob/ob	Type 2	leptin knockout	mild hyperglycemia, hyperinsulinemia, dyslipidemia, obesity	hypertrophy, lipotoxicity, oxidative stress, metabolic shift, systolic dysfunction, diastolic dysfunction	e
db/db	Type 2	leptin receptor knockout	mild hyperglycemia, hyperinsulinemia, hyperlipidemia, obesity	lipotoxicity, oxidative stress, metabolic shift, systolic dysfunction, diastolic dysfunction, hypertension	f,g
Rats					
STZ	Type 1	beta cell toxicity	severe hyperglycemia, hypoinsulinemia, dyslipidemia, weight loss	fibrosis, metabolic shift, systolic dysfunction, diastolic dysfunction	h
STZ Hi Fat	Type 1/2	insulin resistance, beta cell toxicity	moderate hyperglycemia, progressive hypoinsulinemia, weight stagnancy, dyslipidemia	metabolic shift, diastolic dysfunction	i,j,k
GK	Type 2	spontaneous mutation, insulin resistance	mild hyperglycemia, hyperinsulinemia, insulin resistance, non-obese	metabolic shift, systolic dysfunction, diastolic dysfunction	l
OLETF	Type 2	spontaneous mutation, insulin resistance	moderate hyperglycemia, hyperinsulinemia, hypertriglyceridemia, mild obesity	metabolic shift, diastolic dysfunction	m,n
ZDF	Type 2	leptin receptor knockout, insulin resistance	moderate hyperglycemia, hyperinsulinemia, hypertriglyceridemia, obesity	hypertrophy, lipotoxicity, oxidative stress, metabolic shift, systolic dysfunction, hypertension	o,p,q

a (Hsueh et al., 2007)
b (An and Rodrigues, 2006)
c (Li et al., 2011)
d (Basu et al., 2009)
e (Wang and Unger, 2005)
f (Goncalves et al., 2009)
g (Li et al., 2010b)
h (Sharma et al., 2008a)
i (Reed et al., 2000)
j (Marsh et al., 2009)
k (Thackeray et al., 2011b)
l (Howarth et al., 2008)
m (Bi et al., 2005)
n (Mizushige et al., 2000)
o (Marsh et al., 2007)
p (Shoghi et al., 2008)
q (Etgen and Oldham, 2000)

1.5.1 Pharmacological Models

1.5.1.1 Streptozotocin

The most common animal model of diabetes used in medical research is induced by various administration protocols of the pancreatic β-cell toxin 2-deoxy-2-(3-(methyl-3-nitrosoureido))-D-glucopyranose or STZ, a natural toxin of the bacterium *Streptomyces achromogenes* (Szkudelski, 2001). STZ is provided either as a single intravenous or intraperitoneal injection (30-70 mg/kg) to generate insulin insufficiency in adult rats or in multiple low doses in mice or neonatal rats. The toxin is taken up into pancreatic β-cells by GLUT2, as demonstrated by reduced efficacy in cells with knocked down GLUT2 expression (Schnedl et al., 1994). The mechanism of toxicity includes direct DNA alkylation (Delaney et al., 1995; Elsner et al., 2000) and donation of nitric oxide, contributing to the generation of free radicals including toxic peroxynitrite (Kroncke et al., 1995; Turk et al., 1993). Some evidence suggests that loss of β-cell mass relates to secondary immune response to the toxin (Wright and Lacy, 1988).

Intravenous injection of relatively high doses of STZ to rats generates type 1 diabetes characterized by insulin deficiency, severe hyperglycemia, weight loss, polydipsia, and polyuria (Bugger and Abel, 2009). STZ-induced type 1 diabetic rats exhibit cardiovascular abnormalities, particularly long term systolic dysfunction as measured by reduced left ventricular ejection fraction and fractional shortening in echocardiography studies (Huynh et al., 2010; Joffe et al., 1999). Studies in isolated hearts of STZ diabetic rats have contributed to the understanding of maladaptations in cardiovascular metabolism and signaling. Kinetic studies of radioligand distribution in isolated hearts of STZ-induced diabetic rats revealed reduced uptake of glucose with compensatory increase in uptake of long chain fatty acid palmitate (Sakamoto et al., 2000; Sharma et al., 2008a). This shift in cardiac metabolism has been linked to reduced cardiac output and force of contraction (Sharma et al., 2008a). In

addition, STZ type 1 diabetic rats exhibit abnormalities in autonomic function, as characterized by impaired baroreceptor reflex (Fazan et al., 1997), lower 24-hour heart rate variability (Howarth et al., 2005b), downregulation of β-adrenoceptors (Dincer et al., 2001; Sellers and Chess-Williams, 2001; Thackeray et al., 2011a), and altered NE turnover and reuptake rates (Ganguly et al., 1987; Ganguly et al., 1986; Schmid et al., 1999). Radiotelemetry studies in STZ diabetic rats described a 2-4 ms extension of the QRS interval, and a 40% suppression of 24-hour heart rate variability measured as standard deviation of the normal sinus rhythm (Howarth et al., 2005a; Howarth et al., 2005b). Microarray data illustrate the shift from glucose to fatty acid metabolism following STZ induction of diabetes. Genes involved in fatty acid metabolism are upregulated approximately twofold, whereas those involved in carbohydrate metabolism are downregulated by 3-4 fold (Malfitano et al., 2010; Song et al., 2009).

In addition, the STZ diabetic rat heart exhibits significant conduction abnormalities, most commonly manifesting as mild to severe bradycardia. Several explanations have been put forth to explain this phenomenon. Examination in cultured atrioventricular nodal myocytes revealed a delay in spontaneous action potential generation, relating to impaired Ca^{2+} hyperpolarization currents from the L-type Ca^{2+} channels (Yuill et al., 2010). Alternatively, impairment of ganglionic transmission to sympathetic efferents has been documented in cultured neurons, with a depression of fast synaptic transmission and inactivation of nicotinic acetylcholine receptors shown in STZ-induced, db/db, and ob/ob diabetic mice (Campanucci et al., 2011). The extension of the action potential manifesting as bradycardia may also derive from inhibition of outward K^+ current repolarization by NE via α-adrenoceptors (Gallego and Casis, 2001), consistent with elevated sympathetic tone observed in diabetic animal models. STZ diabetic rats exhibit a reduction in mean arterial pressure, heart rate and dP/dt refractory to treatment with insulin (Borges et al., 2006). Moreover, STZ diabetes has

been demonstrated to increase long term mortality following left anterior descending coronary artery occlusion in mice, parallel to a marked increase in left ventricular dilatation, cardiac remodeling, and elevation of proinflammatory cytokines (Shiomi et al., 2003).

1.5.1.2 High Fat Diet, Moderate Intraperitoneal Streptozotocin Rat

To better represent the physiology of type 2 diabetes, attempts have been made to modify the STZ profile to combine characteristics of the metabolic syndrome with STZ-induced hyperglycemia. High fat feeding in rodents is a common model of obesity. The polygenic-derived diet-induced obese rat was generated by selective breeding of Sprague Dawley rats in the highest 10% of weight gain when fed a high fat diet composed of condensed milk (Levin et al., 1989). Hyperinsulinemic-euglycemic clamp studies have revealed modest to severe insulin resistance in rats after consumption of high fat diet (Bruce et al., 2009).

Reed and colleagues combined high fat feeding (40% by calorie) for two weeks prior to a single intraperitoneal dose of 50 mg/kg STZ to induce a rat model with some similarities to type 2 diabetes. Comparing STZ-injected rats on high fat diet to those on normal chow, the high fat group displayed significantly higher blood glucose, plasma insulin, non-esterified fatty acid and triglyceride levels (Reed et al., 2000). Treatment with metformin or troglitazone reduced blood glucose levels but not to baseline (Reed et al., 2000). Comparable studies have established impaired glucose tolerance refractory to treatment with pioglitazone (Srinivasan et al., 2005). Administration of 15 mg/kg intravenous streptoztocin after 2 months of high fat feeding generated rats with mild hyperglycemia (23 mM), hypertrigylceridemia, and normal cholesterol (Zhang et al., 2003). The theory behind low dose of STZ is to partially impair the pancreas, leaving a portion of β-cells intact. Histological examination of the pancreas after 6 months of diabetes confirmed no disarray or atrophy of the pancreatic β-cells suggesting successful sparing of endocrine function (Zhang et al., 2003). The surviving β-cells overproduce insulin to compensate for the loss of

pancreatic mass, causing eventual cellular exhaustion, wasting, and programmed death (Reed et al., 2000). Preserved plasma insulin levels have been demonstrated after 6 months at low STZ doses (Zhang et al., 2003).

The cardiac phenotype of the high fat diet fed STZ rat is not well characterized, though similarities to other STZ models would be anticipated. In studying the effects of high fat diet (60%) and Western diet with high carbohydrate (45%) and fat (40%) content, Marsh and colleagues reported a marked and sustained increase in blood glucose levels over 12 weeks after STZ injection, though rats on Western diet tended to exhibit milder hyperglycemia (15-20 mM) (Marsh et al., 2009). Echocardiography assessment revealed reduced heart rate in all STZ-treated rats regardless of diet, no change in ejection fraction, but a reduction in fractional shortening in diabetic rats fed the Western diet (Marsh et al., 2009). These findings suggest that high fat feeding attenuates the severity of cardiovascular dysfunction in STZ rats, though available data are limited in scope.

1.5.2 Diabetic Rodents from Leptin Gene Mutations

In addition to pharmacological induction of insulin insufficiency, there are a number of spontaneous diabetic rodent strains and genetic knockout models that exhibit characteristics of type 2 diabetes. Of these, the best studied is the Zucker Diabetic Fatty rat (fa/fa), selectively bred for hyperglycemia from rats lacking the leptin receptor (Phillips et al., 1996). Leptin signaling controls suppression of appetite in the brain, whereby the mutation of the receptor generates obese rats with the predisposition for diabetes (Fredersdorf et al., 2004). ZDF rats are hyperinsulinemic and insulin resistant from 6 weeks of age, and develop progressive hyperglycemia by 10-12 weeks of age. In comparison with lean littermates, ZDF rats could be effectively clamped at euglycemia by 89% lower infusion of glucose during hyperinsulinemic euglycemic clamp studies (Leonard et al., 2005). At maturity, ZDF rats exhibit hyperinsulinemia, hyperglycemia, insulin resistance, hyperleptinemia, and elevated

plasma concentration of nonesterified fatty acids and triglyceride (Fredersdorf et al., 2004; Leonard et al., 2005; Shoghi et al., 2009). Cardiac metabolism in ZDF rats is impaired, with a marked shift to fatty acid over glucose oxidation, exemplified by a decrease in phosphorylated AMPK and Akt expression and a further decrease in glycogen synthase (Golfman et al., 2005; Lajoie et al., 2006; Shoghi et al., 2009; van den Brom et al., 2009). Small animal PET studies in ZDF rats established a reduction in myocardial uptake of the glucose analogue ^{18}F-fluoro-deoxyglucose (^{18}F-FDG), with a corresponding reduction in sarcolemma GLUT4 expression (Shoghi et al., 2008).

Over time, ZDF rats have been shown to develop both diastolic and systolic cardiac dysfunction, culminating in cardiomyocyte fibrosis, hypertrophy and steatosis (Fredersdorf et al., 2004; Marsh et al., 2007; Radovits et al., 2009; Zhou et al., 2000). Histological analysis has demonstrated increased cardiomyocyte volume by 2.5-fold at 19 weeks in ZDF rats compared to lean controls, with a parallel accumulation of perivascular fibrosis (Fredersdorf et al., 2004). Moreover, ZDF rats exhibit a reduction in fractional shortening due to systolic dilatation as determined by M-mode echocardiography (Zhou et al., 2000). This functional alteration was associated with a dramatic increase in ceramide and lipid accumulation in the heart, suggestive of lipotoxicity (Zhou et al., 2000). Similar findings have been reported in mouse models deficient in leptin (ob/ob) or leptin receptor (db/db). In db/db mice, hypertension and reduced heart rate variability were shown to develop by 12 weeks of sustained diabetes with a marked augmentation of heart rate response to the β_1-adrenoceptor inhibitor metoprolol (Goncalves et al., 2009).

1.5.3 Polygenic Spontaneous Diabetic Rodents

Other spontaneous diabetic rodent models include the non-obese Goto Kakizaki (GK) rat and the Otsuka Long-Evans Tokushima Fatty (OLETF) rat. Unlike ZDF, these animals derive diabetes from a polygenic origin, which may be more representative of the clinical

manifestation. GK rats are a Wistar substrain which exhibits mild hyperglycemia, insulin resistance, and hyperinsulinemia in the absence of obesity (Howarth et al., 2008; Kiyono et al., 2002a). Cardiac studies have demonstrated consistently lower heart rates in GK rats compared to control by ~60 bpm, with a parallel reduction in heart rate variability, sustained to 15 months of age (Howarth et al., 2008). OLETF rats exhibit mild adiposity with progressive hyperglycemia developing by 30 weeks of age (Yagi et al., 1997). Longitudinal echocardiography studies with transmitral pulse wave Doppler demonstrated a persistent prolongation of mitral valve deceleration time in OLETF rats compared to strain controls, with a concurrent reduction in peak early ventricular filling velocity. While collagen content in the left ventricle was higher at 15 weeks of diabetes, there was no sustained difference in myocardial fibrosis (Mizushige et al., 2000).

1.6 Diabetic Therapy

Treatment of diabetes is focused on normalization of blood glucose levels. In the case of type 1 diabetes, this is generally accomplished by insulin replacement therapy, injecting insulin following meals to facilitate the uptake of glucose by cells. By contrast, pharmacological treatment of type 2 diabetes is more complex, with a number of target organs and mechanisms including: i) reduced hepatic gluconeogenesis; ii) reduced adipocyte lipolysis to ameliorate circulating lipids; iii) reestablishment of balanced fat and carbohydrate metabolism by striated muscle via stimulation of AMPK; collectively contributing to iv) restoration of whole body insulin sensitivity (Fig 1.5).

1.6.1 Insulin

In the treatment of type 1 diabetes and terminal stages of type 2 diabetes, exogenous insulin provides for a restoration of insulin receptor-mediated GLUT4 translocation to skeletal and cardiac muscle membranes, normalizing the uptake of glucose and its oxidation. Effective glucose control with insulin has been shown to reduce glycosylated hemoglobin (HbA1c) to

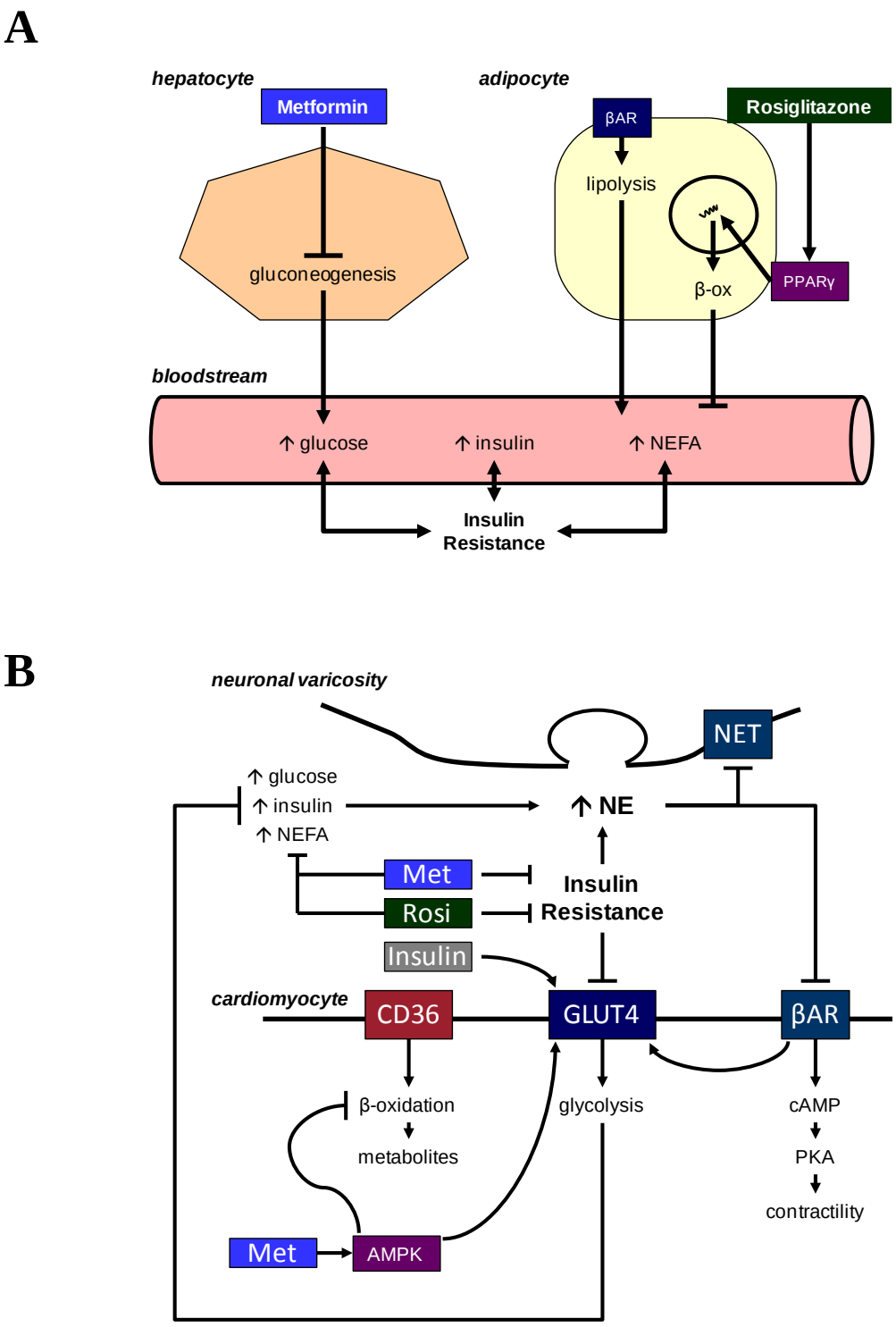

Figure 1.5 β-Adrenergic signaling in the diabetic heart and mechanisms of glycemic therapy. (**A**) Systemic effects of the insulin sensitizing agents metformin and rosiglitazone. Metformin acts on hepatocytes to decrease gluconeogenesis, counteracting the increase in blood glucose in diabetes. Rosiglitazone acts via peroxisome proliferator activated receptor-γ (PPARγ) a nuclear targeted

receptor that alters transcription in adipocytes to enhance β-oxidation and disposal of fatty acids, reducing circulating nonesterified fatty acid concentration (NEFA). Stimulation of β-adrenoceptors (βAR) drives lipolysis and an increase in NEFA in the blood stream. The coalescence of glucose, insulin, and NEFA in the blood contribute to insulin resistance. (**B**) Myocardial effects of insulin, metformin, and rosiglitazone on metabolism and β-adrenergic signaling. Insulin resistance reduces translocation of glutcose transporter (GLUT4) to the cardiomyocyte membrane, reducing glycolysis and increasing the relative rate of fatty acid uptake and β-oxidation. βAR activation contributes to normal GLUT4 translocation. Persistent elevation of glucose, insulin, and NEFA increase circulating and local norepinephrine (NE) release, evoking downregulation of βAR and presynaptic NE reuptake transporter (NET) to increase spillover of excess neurotransmitter. Insulin augments GLUT4 expression to increase glycolysis and reduce circulating blood glucose levels. Metformin counteracts insulin resistance to reduce insulin and glucose levels and stimulates AMP-activated protein kinase (AMPK) to enhance GLUT4 translocation. Rosiglitazone counteracts insulin resistance by lowering plasma NEFA levels. These actions are expected to reduce NE release and normalize sympathetic signaling protein expression.

7%, in line with the healthy population (Ziegler et al., 1998). Reduction of HbA1c by1-3% is associated with improved cardiovascular outcomes (Dluhy and McMahon, 2008). Insulin treatment has been shown to influence fatty acid oxidation as well, whereby administration to an obese male cohort led to a decrease in plasma leptin levels and a marked reduction in plasma nonesterified fatty acids (Saad et al., 1998).

Acute administration of insulin has been shown to improve glucose uptake in a dose dependent manner in cultured neonatal rat ventricular cardiomyocytes (Morisco et al., 2005). Insulin provision recovers the phosphorylation of Akt, consistent with a restoration of normal insulin receptor signaling via IRS1/2 (Morisco et al., 2005). Radioligand studies in isolated perfused hearts of insulin-treated STZ diabetic rats established enhanced glucose uptake and diminished long chain fatty acid uptake, consistent with a restoration of metabolic balance (Sharma et al., 2008a). Insulin treatment was further associated with a recovery of cardiac output (Sharma et al., 2008a).

Providing 10 days of subcutaneous injections of synthetic insulin daily to rats after 6-9 weeks of sustained STZ-induced diabetes markedly reduced circulating glucose levels and restored the force-shortening velocity ratio to non-diabetic values (Fein et al., 1981). This improvement was associated with heightened myocardial Ca^{2+} ATPase activity, recovered completely to control levels by 4 weeks of insulin therapy (Fein et al., 1981). In the Akita mouse model of type 1 diabetes, administration of insulin normalized left ventricle diastolic function with shorter mitral valve deceleration time and a relative recovery of E/A transmitral flow velocity ratio and E´ tissue Doppler measurements. Increases in SERCA2A and ameliorated diacylglycerol and ceramide content supported an improved contractile function and attenuation of lipotoxicity (Basu et al., 2009).

Radiotelemetry studies have demonstrated a normalization of dP/dt_{max} in response to β_1-adrenoceptor agonist dobutamine (Goncalves et al., 2009), consistent with a recovery of β-

adrenoceptor density and sensitivity at the sarcolemma. Insulin has been demonstrated to restore expression of β-adrenoceptors in cardiomyocytes to control levels, with subtype expression pattern of 62:30:8 β_1:β_2:β_3 in treated rats (Dincer et al., 2001). Insulin treatment in STZ-diabetic rats restored functional cardiac sympathetic reuptake as measured by retention of ^{11}C-*meta*-hydroxyephedrine (^{11}C-HED) and was associated with a reduction of the diabetes-induced elevation of cardiac nerve growth factor (Schmid et al., 1999). This result indicated that the deterioration of sympathetic neurons in type 1 diabetes was arrested and suggests a potential for reinnervation.

Additionally, insulin has been shown to regulate signaling in the central nervous system, particularly in stimulating sympathoadrenal response to hypoglycemia to augment peripheral GLUT translocation and fatty acid oxidation via NE (Fisher et al., 2005). Studies in neuron-restricted insulin receptor knockout mice revealed a blunted responsiveness of hypothalamic neurons in glucose sensing, manifesting as a reduction in GLUT3 and GLUT4 expression in knockout brains and a 40-50% reduction in catecholamine secretion in response to falling glucose levels (Diggs-Andrews et al., 2010; Fisher et al., 2005). Despite this disadvantage in hypoglycemia, the effective normalization of blood glucose by insulin treatment is valuable for recovery of metabolic flexibility and reduction of sympathetic overactivity in the heart.

1.6.2 Metformin

The biguanide metformin is classified as an insulin sensitizer due to its multiple actions in liver and skeletal muscle to counteract insulin resistance. In addition to reducing hepatic gluconeogenesis, evidence suggests that metformin works to activate AMPK, driving an increase in glucose uptake and glycolysis and a reduction of fatty acid β-oxidation, thereby lowering non-esterified fatty acid levels.

Studies in cultured cardiomyocytes demonstrated a dose-dependent increase in 2-deoxy-glucose transport when metformin was added to the culture medium (Yang and Holman,

2006). This elevation was associated with elevated AMPK activity and phosphorylation of Akt susceptible to wortmannin inhibition of upstream PI3K (Yang and Holman, 2006). The authors suggested that metformin improved glucose transport by enhanced GLUT 4 residence time at the sarcolemma, facilitated by AMPK signaling and PI3K activation. Fischer and colleagues reported an increase in glucose uptake in cultured cardiomyocytes that was modestly attenuated by addition of drugs that augment noradrenergic signal transduction including isoproterenol, cholera toxin, and dibutyryl cAMP (Fischer et al., 1995), underscoring the cross-talk between insulin and noradrenergic signals.

In ZDF rats, oral treatment with metformin reduced blood glucose levels by 44%, insulin levels by 64%, nonesterified fatty acids by 50%, and triglyceride levels by 55% (Sreenan et al., 1996). Studies in isolated pancreas of ZDF rats treated with metformin showed a recovery of insulin secretion in response to elevated levels of glucose, suggesting functional glucose tolerance (Sreenan et al., 1996). In the OLETF rat, metformin treatment was shown to improve glucose tolerance and disposal, with a 50% increase in pancreatic insulin content (Choi et al., 2007).

Chronic metformin administration to ZDF rats was shown to reduce FAT/CD36 and acyl CoA oxidase mRNA at 14 and 21 weeks compared to untreated rats, with maintained ACC1 and fatty acid synthase mRNA (Forcheron et al., 2009), potentially counteracting the accumulation of deleterious fatty acid metabolites. In a small animal PET study in ZDF rats, Shoghi and colleagues demonstrated a reduction of FAT/CD36 expression and a modest 30-40% increase in glucose uptake and utilization following six weeks of treatment with metformin (Shoghi et al., 2009). Concurrent echocardiography analysis suggested that left ventricular function was improved with metformin treatment (Shoghi et al., 2009).

Isolated perfused hearts from STZ diabetic rats exhibited extended time to half relaxation in response to filling pressure by ~85%. Eight weeks of oral metformin therapy elicited a

reduction in blood glucose levels and normalized isolated heart half time to ventricular filling at variable pressures (Verma and McNeill, 1994). Aminoguanidine, a comparable drug formulation, was shown to reduce the slope of left ventricular stress-strain relationship measured by micromanometer catheterization in STZ diabetic rats (Norton et al., 1996). Taken together, these findings suggest a reduction of myocardial stiffness and recovery of diastolic function as compared to untreated diabetic rats. Metformin treatment also affects intracellular Ca^{2+} currents. Exposure of cultured cardiomyocytes to high glucose levels disrupted contractility by inhibiting intracellular Ca^{2+}transients, but was effectively normalized by addition of metformin (Ren et al., 1999).

The effects of metformin on AMPK activity have been shown to affect myocardial performance. Gundewar and colleagues demonstrated a 14% reduction in mortality among mice treated daily with 125 µg/kg metformin following coronary artery occlusion and reperfusion (Gundewar et al., 2009). Metformin treated mice showed reduced left ventricular dilatation and hypertrophy, improved left ventricular ejection fraction by echocardiography, elevated AMPK phosphorylation, and a significant increase in respiratory exchange ratio by indirect calorimetry, suggesting a shift toward glucose oxidation (Gundewar et al., 2009). Further studies in knockout and transgenic animals suggested that part of this cardiovascular improvement was related to AMPK action on endothelial nitric oxide synthase and a reduction in myocardial free radical generation and oxidative stress (Gundewar et al., 2009).

Metformin therapy is associated with a reduction by 0.8-1.5% in HbA1c levels, weight loss, and decreased circulating triglyceride (Ajjan and Grant, 2006). In the UKPDS trial, overweight patients receiving metformin exhibited a 32% reduction in diabetes morbidity and a 36% lower relative risk of all cause mortality, a result linked both to improved lipid biomarkers and restoration of insulin signaling (Peter et al., 2008). Used as the control arm of the DREAM trial evaluating the cardiovascular effects of rosiglitazone, metformin was

confirmed to confer a reduction in cardiovascular events among treated diabetic patients (Gerstein, 2002).

1.6.3 Thiazolidinediones

Thiazolidinediones such as troglitazone, pioglitazone, and rosiglitazone target the peroxisome proliferator activated receptor-γ (PPARγ), a nuclear hormone receptor that alters the transcription of several enzymes involved in carbohydrate and lipid metabolism. Acting on adipocytes, thiazolidinediones suppress lipid metabolism thereby depleting nonesterified fatty acids by 20-40% (Fonseca et al., 2000; Phillips et al., 2001b).

Troglitazone treatment in ZDF rats reduced liver glycogen content and increased expression of IRS1, IRS2, pAkt, reflecting increased insulin sensitivity. Euglycemic clamp confirmed a 40% increase in glucose infusion rate to maintain glucose levels in opposition to continuous insulin administration (Li et al., 2005). Pioglitazone treatment in low dose STZ rats with high sucrose feeding lowered plasma nonesterified fatty acid, triglyceride, and insulin concentrations with a parallel increase in skeletal muscle GLUT4 expression and IRS1 activity (Ding et al., 2005). Six weeks of pioglitazone administration increased insulin sensitivity in diet induced obese rats as illustrated by improved glucose tolerance and increased insulin response to oral glucose load (Henriksen et al., 2009). In OLETF rats, 10 week treatment with pioglitazone reduced the area under the curve in glucose tolerance test, decreased fasting insulin, nonesterified fatty acid and triglyceride to non-diabetic levels, with a twofold increase in cardiac malonyl Co-A decarboxylase activity, consistent with enhanced glucose over fatty acid utilization (Kim et al., 2003). Seven days of treatment with rosigliazone in db/db mice reduced blood glucose by 50% compared to untreated controls, with a concurrent improvement in insulin resistance index (Chang et al., 2008). In high fat diet-fed STZ diabetic rats, administration of pioglitazone or rosiglitazone was shown to modestly reduce blood glucose levels and decrease triglyceride concentrations. Isolated

aortic rings from diabetic rats showed an increase in tension in response to angiotensin attenuated by chronic treatment with thiazolidinediones (Gaikwad et al., 2007).

Moreover, cardiovascular benefits have been described in thiazolidinedione treated rodents. Circulating levels of malondialdehyde and 3-nitrotyrosine were lower in treated compared to untreated STZ diabetic rats, suggesting a reduction in oxidative stress (Kavak et al., 2008). Histological studies have demonstrated a decrease in oil red O staining in the myocardium of ZDF rats treated with rosiglitazone, reflecting an reduction of fatty acid uptake and lower potential for lipotoxicity (Golfman et al., 2005). Measurement of gene expression confirmed a decrease in malonyl CoA decarboxylase and acyl CoA carboxylase expression, in concert with increased expression of GLUT1 and GLUT4 and pyruvate dehydrogenase kinase, reflecting an increase in glucose uptake and glycolysis (Golfman et al., 2005). These changes in myocardial metabolism contributed to normalization of cardiac power measured in isolated perfused hearts (Golfman et al., 2005). Rosiglitazone treatment in diet-induced obese rats with dietary restriction showed a greater increase in myocardial fatty acid transport gene expression than with rosiglitazone alone, suggesting an added benefit of fat redistribution (Moore et al., 2008).

In vivo PET studies in ZDF rats demonstrated that prolonged rosiglitazone treated decreased ^{11}C-palmitate uptake and oxidation threefold associated with a reduction in fatty acid transport protein (FATP) and medium-chain acyl CoA dehydrogenase (MCAD) expression (Shoghi et al., 2009). The same study reported a threefold elevation of ^{18}F-FDG uptake and glucose utilization parallel to enhanced sarcolemma GLUT4 (Shoghi et al., 2009). Sidell and colleagues reported a 34% increase in insulin-stimulated glucose uptake in isolated Zucker rat hearts, with a concurrent decrease in circulating nonesterified fatty acids (63%) and triglyceride (51%) (Sidell et al., 2002). OLETF rats treated for 4 weeks with pioglitazone exhibited an improvement in hypothermia-induced phosphorylation of Akt, reflecting the

recovery of insulin signaling and PI3K phosphorylation (Taniguchi et al., 2006). In spontaneously hypertensive rats, rosiglitazone treatment has been linked to reduced superoxide dismutase staining, corresponding to a reduction in infarct size following ischemia/reperfusion injury, and a more efficient stabilization of coronary flow (Potenza et al., 2009).

These metabolic changes have functional consequences for the myocardium. Echocardiography studies demonstrated a shift in early to atrial transmitral flow velocity and faster mitral valve deceleration as compared to untreated diabetic rats (Kim et al., 2003). Ischemia-reperfusion in STZ diabetic rats revealed a faster recovery of aortic flow and cardiac output in rats treated with 1 μmol/L rosiglitazone immediately prior to coronary occlusion. This finding was associated with an increase in GLUT4 translocation to sarcolemma and attenuation of Jun amino terminal kinase activation, consistent with a reduction in oxidative stress (Khandoudi et al., 2002). Treated ZDF rats also exhibited a faster recovery of myocardial rate pressure product during the reperfusion phase, with rates similar to Zucker lean controls (Sidell et al., 2002). Left ventricular diastolic pressure during reperfusion after ischemic injury was increased to normal levels with pioglitazone, suggesting cardioprotective effects of Akt activation (Kim et al., 2003). Rosiglitazone treatment is associated with twofold increase in Akt phosphorylation, and downstream glycogen synthase 3β and forkhead transcription factor. This upregulation is suggested to play an antiapoptotic role such that after coronary artery occlusion, rats treated with rosiglitazone showed a 46% reduction in infarct size and 58% reduction in apoptotic cardiomyocytes defined by TUNEL staining (Yue et al., 2005). Rosiglitazone also appears to have anti-inflammatory effects in ApoE knockout mice prone to atherosclerosis, where rosiglitazone administration over 13 weeks resulted in greater plaque stability than in untreated ApoE -/- mice (Zhou et al., 2008).

Treatment with thiazolidinediones has been shown to reduce HbA1c by 0.5-1.5%, owing to increased skeletal muscle insulin sensitivity due to reduced circulating fatty acids (Cefalu, 2007). Early clinical trials demonstrated effective treatment of diabetes with thiazolidinediones. The PROACTIVE trial established a modest benefit of thiazolidindione glucose control over standard therapy, but saw an increase in the occurrence of congestive heart failure (Dormandy et al., 2005). The 5200 patient DREAM trial reported improved glycemic control among rosiglitazone-treated patients, with no increase in cardiovascular death recorded (Gerstein et al., 2006). The ADOPT trial demonstrated a reduction in myocardial infarction and all cause cardiovascular mortality in the rosiglitazone arm compared to standard treatment (Kahn et al., 2011). In the ADVANCE trial, patients with intensive glucose control defined by a rapid reduction of HbA1c to 6-7% achieved by a myriad of medications showed no reduction of cardiovascular events as compared to standard control over 5 years follow-up (Patel et al., 2008). The lack of improvement in survival with intensive glycemic control has been suggested to relate to the patient population, which had a long duration and relatively high severity of diabetes (Johnson and Bowker, 2011).

1.6.3.1 Rosiglitazone and Cardiac Risk

A series of meta-analyses in the late 2000s suggested an added risk of myocardial infarction among diabetic patients treated with rosiglitazone. In a retrospective analysis of 42 clinical trials, Nissen and colleagues reported a significant hazard ratio of 1.03-1.98 of myocardial infarction and cardiovascular death among patients treated with rosiglitazone compared to the control treatment groups (Nissen and Wolski, 2007). Subsequent analyses have provided both support for and contention with this finding. Shuster and colleagues suggested that the Nissen study was flawed in using a fixed effects analysis rather than random effects meta-analysis due to the relative rarity of cardiovascular events in the pooled clinical trial cohort (Diamond et al., 2007; Shuster et al., 2007). In an analysis of Quebec patient data, risk of

hospitalization for heart failure (1.94 hazard ratio) or acute myocardial infarction (1.41 hazard ratio) was elevated among elderly patients, but cardiovascular mortality was not increased (0.88 hazard ratio) (Vanasse et al., 2009). Retrospective study of United States health records revealed an increase in cardiovascular events over 3 years of treatment with rosiglitazone as compared to metformin therapy, but improved outcomes as compared to sulfonylurea pharmacotherapy (McAfee et al., 2007). Similarly, one year of rosiglitazone administration was associated with a significant relative risk of 142 for myocardial infarction and 2.09 for congestive heart failure (Singh et al., 2007). Among older patients, the risk of hospitalization for heart failure and/or myocardial infarction was significantly increased to 1.60 and 1.40, with a parallel increase in hazard ratio for cardiovascular death 1.29 as compared to other oral glycemic therapies (Lipscombe et al., 2007). In a comparison of thiazolidinediones in 30000 patients, the risk ratio of pioglitazone was found to be lower than rosiglitazone by ~22% (Gerrits et al., 2007).

The cause of this increased risk has been suggested to relate to the thiazolidinedione effect on blood volume expansion, driving an elevation in blood pressure and the incidence of hypertrophy. Studies in diet induced obese rats support this theory, with an increase in water content over 6 weeks of therapy with pioglitazone but not the newer generation balaglitazone as determined by serial magnetic resonance studies (Henriksen et al., 2009). Prolonged exposure to increasing doses of rosiglitazone was associated with an increase in total plasma volume from 3 mL/100 g to 4 mL/100g and a corresponding increase in heart mass, over a 7 day study in Zucker obese rats (Chang et al., 2008). Blood pressure, cardiac remodeling and hypertrophy are associated with modification of SNS signaling, suggesting a potential synergistic role of noradrenergic signaling in cardiovascular risk of rosiglitazone.

1.6.4 Other Agents

There are a number of other oral glycemic agents that have been used in the treatment of type 2 diabetes. These include sulfonylureas, non-sulfonylurea secretagogues, α-glucosidase inhibitors, and glucagon-like peptide-1/ dipeptidylpeptidase IV inhibitors.

Sulfonylureas (tolbutamide, glibenclamide) act at pancreatic K_{ATP} channels to enhance insulin secretion in response to glucose sensing (Stumvoll et al., 2005). Use of sulfonylureas has been associated with reduced microvascular complications of diabetes (UKPDS, 1998). The long-acting nature of the drug has been suggested to induce antecedent hypoglycemia in some cases (Amoroso et al., 1990; Waldhausl, 1996).

Non-sulfonylurea secretagogues (repaglinide, nateglinide) operate in a similar mechanism to sulfonylureas to increase pancreatic insulin secretion (Stumvoll et al., 2005). The shorter action of these agents was proposed to reduce the risk of hypoglycemic events in treated patients.

Inhibitors of α-glucosidase (acarbose) suppress the absorption of glucose in the gastrointestinal tract while stimulating glucagon-like-peptide-1 release (Cefalu, 2007). The reduction in post-prandial blood glucose fluctuations has been linked to reduction in diabetic symptoms and cardiovascular disease (Chiasson et al., 2003).

GLP1 agonists (exendatide) and/or DPP-IV inhibitors (sitagliptin) stimulate pancreatic β-cell function and inhibit glucagon secretion. The reduction in HbA1c levels is comparable to other oral hypoglycemic agents, with an increase in weight loss also reported (Cefalu, 2007). Cardiovascular effects are not known at present.

1.6.5 Lifestyle Modification

Perhaps the most effective means of treating type 2 diabetes is modification of lifestyle, incorporating a reduction of fat and carbohydrate feeding with a modest exercise regimen to stimulate weight loss and improve blood lipid profile. Provision of individualized

consultations with dieticians and resistance training sessions in an overweight Finnish population generated a reduction of 4.5 kg in the first year as compared to 1.0 kg in the standard medical care cohort, with a significantly greater reduction of serum triglyceride, fasting glucose, and glucose clearance rate (Lindstrom et al., 2003). Similar findings were reported by the Indian Diabetes Prevention Programme, which reported a 39.3% incidence of new onset diabetes over 3 years follow-up in at risk patients receiving lifestyle modification consultation as compared to 55% of the control group (Ramachandran et al., 2006). A longer term prospective study demonstrated a 41.1-46.0% incidence of diabetes in patients that received advice and monitoring of diet, exercise or both as compared to 67.7% in the non-consulted group (Pan et al., 1997). The importance of modifying behaviours was underscored by the American Heart Association scientific statement on diet and lifestyle issued in 2006, which recommended restriction of saturated and trans fat intake and promoted whole, high fibre foods to counter the rising incidence of obesity and type 2 diabetes and improve lipid levels and cardiovascular outcomes (American Heart Association, 2007).

Basic research in diabetes has indicated a role for exercise in altering SNS activity and the expression of β-adrenoceptors. A daily regimen of running on a motorized treadmill in healthy Wistar rats reduced β_1-adrenoceptor expression in ventricles and atria as measured by immunoblotting, with a reduction in basal heart rate variability (Barbier et al., 2006). By contrast, evidence suggests that adrenoceptor expression is augmented in exercised diabetic rats. After 4 weeks duration of STZ diabetes, rats were randomized to undergo a scaled exercise program from 10 min/day at 10 m/min, 0% grade to a maximum of 60 min/day at 10 m/min, 5-10% grade, 5 days/week over 3 weeks (Bidasee et al., 2008). Exercised diabetic rats exhibited higher ejection fraction than non-exercised diabetics and enhanced responsiveness to adrenergic stimulation by isoproterenol as measured by dP/dt via catheter micromanometer. This improvement was attributed to the restoration of β-adrenoceptor

expression, whereas sedentary diabetics showed a 60% reduction in β_1-adrenoceptor and a 20% reduction in β_2-adrenoceptor expression (Bidasee et al., 2008). Treadmill training was shown to increase heart rate variability in STZ-diabetic ovarectomized Wistar rats, with improved tachycardiac and bradycardic responses (Souza et al., 2007). This was associated with a decrease in mortality rate by ~20% compared to untrained diabetic ovarectomized rats.

1.7 Cardiac Positron Emission Tomography

PET is a dynamic and noninvasive molecular imaging technology that allows dynamic visualization of the distribution of a radiolabeled biological or pharmacological ligand, substrate or analogue within the body (Fig 1.6).

1.7.1 Principles of Cardiac PET

These radiotracers are produced using a cyclotron, accelerating a positively charged hydrogen nucleus by magnetic centripetal acceleration and bombarding a target material. A nuclear chemical reaction generates an unstable radioisotope. In the case of carbon-11, nitrogen gas is bombarded with a stripped hydrogen nucleus, essentially a proton. The resulting reaction is a substitution of a proton for an alpha particle, generating carbon-11, a positron-emitting isotope (Finn and Schlyer, 2002).

After administration to the subject, the isotope undergoes β-decay, releasing a positron, a particle with the mass of an electron and a positive charge. The positron annihilates upon collision with an electron from the ionized tissue, generating two antiparallel photons of 511 keV. A PET camera comprises a ring of detectors capable of coincidence timing detection of these photons. Computerized iterative and non-iterative reconstruction algorithms generate a map of the activity distribution within the field of view over time, producing a dynamic image and time-activity curve for various regions of interest in the subject (Koeppe, 2002; Thompson, 2002).

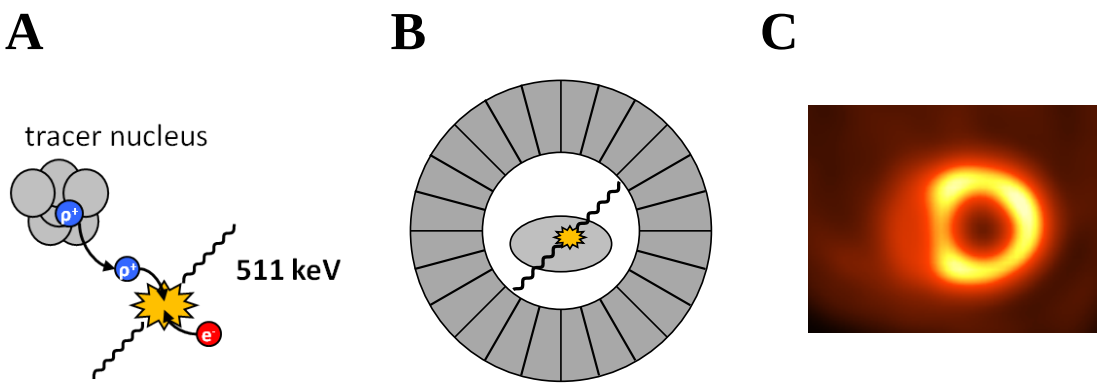

Figure 1.6 Principles of positron emission tomography (PET). (**A**) A radiolabeled substrate distributes according to its inherent pharmacokinetics and dynamics and decays by positron (ρ^+) emission. The released positron annihilates with an electron (e^-) to generate two 511 keV photons at 180^o coincidence. (**B**) In a PET camera, coincidence detection of these photons allows for the computerized calculation of the location of the annihilation event. The sum of these individual counts allows the reconstruction of a PET image. (**C**) Sample short axis myocardial PET image of ^{11}C-*meta*-hydroxyephedrine (^{11}C-HED) in a rat heart.

The development of small animal imaging technology has facilitated the application of clinical PET radiotracers for research studies in rodents. The continuing improvement in resolution and sensitivity has permitted quantification of a variety of radiotracer kinetics in basic research. This modality allows for serial noninvasive measurements to be taken in individual animals, allowing for accurate assessment of pathogenesis and pharmacological agent efficacy within subjects and between groups. Transgenic and knockout models of human disease further enhance the utility of small animal PET for the development and evaluation of novel drugs (Roselt et al., 2004). Small animal PET is a valuable tool in the investigation of diabetic cardiomyopathy.

1.7.2 Perfusion Imaging

The most common clinical screening conducted in cardiac PET centres is the evaluation of myocardial blood flow. The distribution of ^{13}N-ammonia or ^{82}Rb in the myocardium can identify regions of reduced perfusion either at rest or stress reflecting scar or ischemic tissue, respectively. Quantitative measurement of uptake rate can be used to calculate myocardial blood flow from ^{13}N-ammonia distribution in the myocardium (Klein et al., 2010b). Positron range and subsequent blurring limits the application of ^{82}Rb in small animals.

1.7.3 Metabolic Imaging

Nuclear cardiology allows for the noninvasive assessment of myocardial metabolism in heart failure, hibernating myocardium, and in diabetes. The most widely used PET tracer ^{18}F-FDG is a glucose analogue, uptake of which is proportional to expression of GLUT4 and reflects glucose uptake by cardiomyocytes (Shoghi et al., 2008). The rate of myocardial glucose uptake has been shown to be markedly reduced in diabetic animal models including STZ-induced diabetes (Menard et al., 2010) and ZDF rats (Shoghi et al., 2009).

Fatty acid metabolism can be evaluated with a number of distinct radiotracers. Uptake of ^{11}C-palmitate reflects the activity of fatty acid transport into the cardiomyocyte and can be used

to estimate β-oxidation. Long chain fatty acid transport can also be assessed by ^{18}F-fluorothiamluoro-6-thia-heptadecanoic acid (FTHA), which is trapped in the cell, providing an index of fatty acid uptake (Taylor et al., 2001). Finally, the washout of ^{11}C-acetate as ^{11}C-CO_2 provides an index of fatty acid contribution to the citric acid cycle, wherein monoexponential washout of ^{11}C-CO_2 is proportional to the breakdown of the intermediate acetate (Yoshinaga et al., 2007). In ZDF rats, ^{11}C-palmitate uptake was reduced by insulin sensitizing rosiglitazone but not metformin (Shoghi et al., 2009; van den Brom et al., 2009). Uptake of ^{18}F-FTHA was similarly reduced in STZ rats, with a concurrent reduction in terminal in vitro measurements of FAT/CD36 expression and oxidative enzyme levels (Ci et al., 2006; Menard et al., 2010).

1.7.4 Neurohormonal Imaging

Evaluation of traditional biomarkers of cardiovascular disease by molecular imaging has gained traction in recent years. The majority of radiotracers used at present target innervation at the uptake-1 site, where tracer retention reflects myocardial sympathetic nervous density, functional NET expression, and sympathetic activity by washout.

Radiolabeled receptor ligands have been developed to noninvasively assess the expression of β-adrenoceptors. Myocardial binding of ^{11}C-CGP12177 or its analogue ^{11}C-CGP12388 has been shown to be blocked by specific inhibitors of β-adrenoceptors (Delforge et al., 2002; Elsinga et al., 1998; van Waarde et al., 1995a). Subchronic treatment with isoproterenol over 14 days has been shown to decrease ^{3}H-CGP12177 binding in ex vivo biodistribution studies, suggesting sensitivity to overstimulation receptor internalization (Thackeray et al., 2011a). Clinical evaluations have demonstrated a reduction in ^{11}C-CGP12177 binding in acute myocardial infarction, congestive heart failure, and other cardiomyopathies (Caldwell et al., 2008; Link et al., 2003; Tsukamoto et al., 2007). It has been suggested that ^{11}C-CGP12177

binding may identify idiopathic cardiomyopathy patients most likely to respond to β-blocker therapy (Naya et al., 2009).

Intracellular signaling targets have also been investigated including the phosphodiesterase-4 specific inhibitor (*R*)-^{11}C-rolipram. Phosphodiesterase-4 breaks down cAMP under the regulation of PKA, providing an indirect index of cAMP activity following β-adrenoceptor activation (Kenk et al., 2007). Binding of (*R*)-^{11}C-rolipram is elevated by acute elevation of NE by desipramine, reflecting an increase in phosphodiesterase production in response to increased cAMP activity (Lourenco et al., 2006; Thomas et al., 2011). The desipramine-induced increases in (*R*)-^{11}C-rolipram binding were attenuated in disease states with elevated basal sympathetic activity including obesity (Greene et al., 2009), adriamycin-induced acute cardiotoxicity (Kenk et al., 2010), and congestive heart failure (Kenk unpublished). This loss of responsiveness reflects a downregulation of β-adrenoceptor density in conditions of high sympathetic tone.

1.8 Presynaptic Sympathetic Nerve Radiotracers

A number of compounds have been developed for molecular imaging of the intrinsic SNS. Radiotracers take advantage of similar structure to the endogenous neurotransmitters to gain transport across the neuronal membrane via NET. For single photon emission computed tomography, the archetype tracer is ^{123}I-MIBG, which has been used clinically for several years in Europe and Japan, but has only recently moved to late stage clinical trials in North America (Bengel, 2009). In PET, the predominant radiotracers are the labeled catecholamine ^{11}C-epinephrine and the false neurotransmitter ^{11}C-HED, of which the latter has enjoyed more widespread use due to ease of synthesis and analysis methods. Other candidate compounds have been developed and assessed including ^{11}C-phenylephrine (Raffel et al., 1996), ^{11}C-methylreboxetine (Ding et al., 2003), ^{11}C-nisoxetine (Haka and Kilbourn, 1989), ^{18}F-fluorometaraminol (Langer et al., 2000), and the ^{11}C-labeled phenethylguanidine series

(Raffel et al., 2005). Each of the presynaptic tracers exhibits a number of pharmacological characteristics that are both beneficial and detrimental.

1.8.1 ^{123}I-Metaiodobenzylguanidine (^{123}I-MIBG)

In SPECT, use of the NE analogue ^{123}I-MIBG has been limited to research purposes in North America due to regulatory challenges. As an analogue of NE, ^{123}I-MIBG is a substrate of the uptake 1 NET carrier, taken actively into nerve terminals where it is either packaged into vesicles by the vesicular monoamine transporter or diffuses back into the synaptic cleft. Developed for the analysis of tumours of the adrenal medulla, significant uptake was observed in the heart, prompting further exploration. A study in pheochromocytoma in which ^{131}I-MIBG was applied as a therapeutic agent, reported an inverse correlation between myocardial uptake and concentration of plasma and urinary catecholamines (Nakajo et al., 1983), suggesting an influence of sympathetic tone on tracer retention.

The expansion of small animal molecular imaging has facilitated studies of the dynamic uptake and washout of ^{123}I-MIBG in a variety of rodent models of disease. Kusmic and colleagues have demonstrated an enhanced myocardial washout in STZ diabetic mice from 30-120 min after injection of ^{123}I-MIBG, consistent with elevated sympathetic tone and reduced neuronal reuptake. Bladder accumulation of ^{123}I-MIBG was significantly higher in diabetic mice, supporting higher clearance of tracer (Kusmic et al., 2008). Elevated washout was also observed in STZ diabetic rats with or without concurrent hypertension, with an average of 15% augmentation of washout rate (Dubois et al., 1996).

The ADMIRE HF trial identified an independent prognostic value of ^{123}I-MIBG imaging in the identification of heart failure patients (NYHA Class II and III) at greatest risk of progression. Patients with late frame heart to mediastinal activity ratio measurements below the cut-off value of 1.60 exhibited a 2-year mortality rate for cardiac death of 11.2% and for all-causes of 16.1%, a marked increase from the 1.8% and 3.0% observed among patients

with normal heart to mediastinal ^{123}I-MIBG retention ratios (Jacobson et al., 2010). A substudy of ADMIRE HF identified an even greater risk among diabetic patients with low late heart to mediastinal ^{123}I-MIBG ratio, wherein diabetic heart failure patients exhibited a 34% incidence for heart failure progression compared to 11% in diabetic patients with normal ^{123}I-MIBG scans (Gerson et al., 2011). This incidence rate is markedly higher than observed in the non-diabetic heart failure population, underscoring the additive risk of comorbidity.

1.8.2 ^{11}C-*meta*-Hydroxyephedrine (^{11}C-HED)

One of the most routinely used radiotracers for imaging of the myocardial SNS is ^{11}C-HED. As an analogue of NE devoid of postsynaptic activity, ^{11}C-HED is actively taken up by NET to the presynaptic varicosity, where it is packaged to vesicles, released with neurotransmitter, or passively diffuses back to the synaptic cleft (Raffel and Wieland, 2001b). As such, retention of ^{11}C-HED reflects the complete presynaptic function of the sympathetic neuron (Fig 1.7).

1.8.2.1 Chemistry

^{11}C-HED exhibits two stereocentres, and can therefore be synthesized in two series and four stereoisomers: the erythro series (*1R,2S*) and (*1S,2R*), and the threo series (*1S,2S*) and (*1R,2R*) (Foley et al., 2002; Van Dort and Tluczek, 2000). Structure activity relationship studies identified the greatest selectivity for NET over DAT (1:10) and SERT (1:71) in the (*1R,2S*) enantiomer (Foley et al., 2002). Use of a stereospecific precursor compound, *1R,2S*-metaraminol, allows the synthesis of predominantly (*1R,2S*)-^{11}C-HED.

^{11}C-HED is synthesized by N-^{11}C--methylation of metaraminol freebase with ^{11}C-MeI as described (Rosenspire et al., 1990). ^{11}C-CO_2 is produced by cyclotron acceleration of protons at 11 MeV and the nuclear reaction $^{14}N(p,\alpha)^{11}C$ in the presence of 1% oxygen. Methyliodide

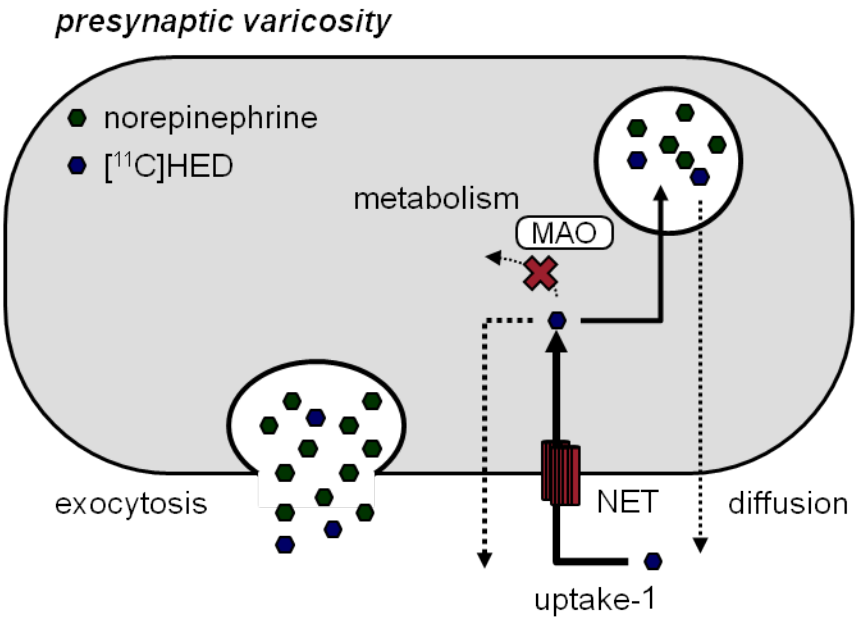

Figure 1.7 Schematic of neuronal uptake, retention and washout of ^{11}C-*meta*-hydroxyephedrine (^{11}C-HED). ^{11}C-HED is actively transported from the synapse to the presynaptic varicosity by the endogenous uptake-1 pathway via norepinephrine reuptake transporter (NET). ^{11}C-HED is resistant to breakdown by cytosolic monoamine oxidase (MAO). Once inside the varicosity, ^{11}C-HED is partially packaged into vesicles by vesicular monoamine transporter 2 and actively released with norepinephrine and other vesicular contents during sympathetic stimulation. Due to its lipophilicity, ^{11}C-HED passively diffuses across the vesicular and neuronal membranes. Measurement of ^{11}C-HED retention effectively measures the cyclic uptake and active/passive washout from the neuronal varicosity.

is produced either by wet chemistry method, the reduction of $^{11}C\text{-}CO_2$ with lithium aluminum hydride in the presence of tetrahydrofuran and hydroiodic acid, or by the recirculating gas phase MeI system, nickel catalyst conversion of $^{11}C\text{-}CO_2$ to $^{11}C\text{-}CH_4$ and reaction with iodine. The gas phase method has been demonstrated to yield significantly higher specific activity (Valdivia et al., 2011). *N*-^{11}C-Methylation of metaraminol freebase is carried out in the presence of dimethylformamide at 90^{o}C with high radiochemical yield, purified by semi-preparative HPLC using a C18 column, solvent evaporated, and reformulated in an isotonic buffer for injection. For each production run, quality control HPLC with absorbance and radiation detection is completed to verify chemical identity and specific activity.

1.8.2.2 Pharmacological Characterization

Biodistribution studies in male and female rats demonstrated high and prolonged retention (1-3% injected dose/g) of ^{11}C-HED in regions with complex adrenergic networks including heart, adrenal glands and spleen with a gradual accumulation by liver (Rosenspire et al., 1990). Uptake in left ventricle, spleen, and adrenal glands was reduced by 62-92% by pretreatment with the NET inhibitor desipramine, with an increase in hepatitc tracer accumulation (Rosenspire et al., 1990), reflecting NET specific uptake of tracer (Law et al., 1997; Rosenspire et al., 1990). In addition to specificity of retention for uptake-1, increasing doses of precursor metaraminol reduced left ventricular retention of ^{11}C-HED at 34 minutes after injection by a maximum of 90% (Law et al., 1997), suggesting a competitive uptake effect. This is a reasonable assumption as the affinity of metaraminol for NET (k_i = 21.8 nM) is similar to that of ^{11}C-HED (k_i = 20.9 nM) (Raffel and Chen, 2004). Studies in hearts denervated with increasing doses of the neurotoxin 6-hydroxydopamine revealed a direct relationship between B_{max} of NET and the retention of ^{11}C-HED by binding assay with ^{3}H-mazindol (Raffel et al., 2006).

Studies in isolated perfused rat hearts demonstrated nearly complete elimination of ^{11}C-HED uptake in the immediate presence of desipramine. Addition of desipramine to the buffer after 10 minutes accelerated the clearance rate by a factor of 20 (DeGrado et al., 1993). Addition of exogenous NE (10 nM) had a competitive effect on ^{11}C-HED kinetics, with a similar initial uptake rate but a 3-fold increase in clearance (DeGrado et al., 1993). However, NE infusion dose-dependently increased basal heart rate and cardiac output, confounding interpretation of these findings (DeGrado et al., 1993). PET studies in dogs confirmed the specificity of ^{11}C-HED uptake to nerve terminals, and was utilized to confirm that a blood-tissue exchange model could be applied to quantify retention of ^{11}C-HED (Caldwell et al., 1998).

Reversed phase HPLC metabolite analysis in guinea pigs showed accumulation of ^{11}C-labeled metabolites in the plasma and liver at 30 minutes after injection, but no presence of metabolites in myocardial tissue (Rosenspire et al., 1990). In rats, at 30 minutes after injection, 24.9% of radioactivity remaining in plasma is unchanged ^{11}C-HED whereas myocardial activity is almost entirely (99.5%) non-metabolized (Law et al., 1997). Lack of labeled metabolites in target tissue provides for simplified kinetic analysis. Metabolite analysis in human subjects has demonstrated a similar metabolite profile, with a rapid accumulation of ^{11}C-labeled metabolites in the blood over 10-20 min after injection (Link et al., 1997). Corrections for metabolite concentrations in blood are generally applied to correct the input function activity in quantifying ^{11}C-HED retention.

1.8.2.3 Preclinical Imaging with ^{11}C-HED

To date, much of the preclinical evaluation of ^{11}C-HED has been focused on tracer kinetic evaluation. Studies in large animals have identified utility for sympathetic integrity measurements in cardiac pathology. For instance, a porcine model of hibernating myocardium with high incidence of sudden cardiac death exhibited a significant defect of

^{11}C-HED retention in the region of mismatch between ^{13}N-ammonia and ^{18}F-FDG retention (Luisi et al., 2005). This deficit was not normalized by reperfusion in the pigs, suggesting an irreversible damage sustained by the neuronal network(Fallavollita et al., 2010)

The growth of small animal imaging has facilitated dynamic analysis of the uptake and retention of ^{11}C-HED in rodents. Tipre and colleagues completed a comparison of three presynaptic imaging tracers in rats: ^{11}C-HED, ^{11}C-epinephrine, and ^{11}C-phenylephrine. Rats injected with ^{11}C-HED showed clear uptake in lateral, septal, and apical wall with global retention index of 7.4%/min at 40 minutes after injection. Image contrast was excellent with slow but linear clearance from myocardium. Injection of desipramine 15 minutes after tracer resulted in accelerated washout, and pretreatment blocked myocardial ^{11}C-HED uptake with increased liver accumulation (Tipre et al., 2008). In comparison to ^{11}C-epinephrine and ^{11}C-phenylephrine, ^{11}C-HED demonstrated higher overall retention and greater response to despiramine treatment. The enhanced washout rate was attributed to heightened basal sympathetic tone in rodents (Tipre et al., 2008). Law and colleagues demonstrated myocardial uptake of ^{11}C-HED in mice susceptible to displacement by increasing doses of cold metaraminol bitartrate (Law et al., 2010). Clearance of left ventricular activity, expressed as cps/image, was accelerated in a dose-dependent manner as higher concentrations of the cold compound were administered (Law et al., 2010).

1.8.2.4 Clinical Applications of ^{11}C-HED

Since its development, ^{11}C-HED has been utilized routinely for the assessment of sympathetic nervous innervation and presynaptic function in a variety of cardiovascular disorders.

One of the first cardiac applications of ^{11}C-HED was in the evaluation of post-transplant reinnervation. Tracking of ^{11}C-HED retention in transplant patients revealed a recovery of left ventricular innervation over 2-12 years, corresponding to a recovery of tyramine-induced

NE release as measured from coronary sinus blood sampling (Munch et al., 2000; Odaka et al., 2001; Uberfuhr et al., 2000).

Administration of desipramine affects the washout rate of ^{11}C-HED in healthy volunteers, with a gradual increase in the time activity curve decay gradient with desipramine doses of 50-100 mg (Malizia et al., 2000). Following myocardial infarction, a decrease in ^{11}C-HED retention is observed in the infarcted area that extends beyond the borders of the ^{13}N-ammonia perfusion defect to affect up to a 20% greater proportion of the left ventricle (Allman et al., 1993). In NYHA class II heart failure, ^{11}C-HED defect area has been shown to encompass 80% of the left ventricle (Hartmann et al., 1999). Patients with hypertrophic cardiomyopathy exhibit a distinct 40% reduction in ^{11}C-HED volume of distribution as compared to healthy controls, proportional to estimated difference in β-adrenoceptor B_{max} in this population (Schafers et al., 1998).

In coronary artery disease patients with normal left ventricular function, abnormalities in sympathetic innervation measured by ^{11}C-HED uptake were described in 61% of patients despite normal resting perfusion (Bulow et al., 2003). Hartmann reported that ^{11}C-HED retention index was proportional to left ventricular ejection fraction and NYHA heart failure class, but not to plasma NE concentration (Hartmann et al., 1999). This observation supports an influence of sympathetic tone on ^{11}C-HED retention, even in the absence of denervation. PET studies in combination with tissue analysis in explanted hearts demonstrated a regional correlation between flow-corrected ^{11}C-HED retention and uptake-1 density determined by binding assay (Ungerer et al., 2000). ^{11}C-HED retention was further correlated β-adrenoceptor kinase-1 activity levels (Ungerer et al., 2000), reflecting regional overstimulation of β-adrenoceptors in the presence of high catecholamines. Attempts to match pre-and post-synaptic function have demonstrated regions of matched and mismatched defects in hibernating myocardium and coronary artery disease (John et al., 2007). The ratio

of presynaptic function measured with ^{11}C-HED to postsynaptic β-adrenoceptor expression measured with ^{11}C-CGP12177 showed a mismatch in congestive heart failure patients, suggesting a regional heterogeneity of innervation and receptor density (Link et al., 2003). Conversely, single-tissue compartment distribution volume of ^{11}C-HED was modestly reduced in hibernating myocardium and further reduced in infarcted myocardium as compared to healthy controls, a result that matched to β-adrenoceptor density as determined by ^{11}C-CGP12177 binding (John et al., 2007).

The utility of ^{11}C-HED as a marker of sympathetic nervous function was tested against traditional autonomic function tests including blood pressure variability and baroreceptor reflex sensitivity in congestive heart failure patients, with a positive correlation of r=0.75 found to blood pressure measurements and a r=0.43 found to baroreflex sensitivity (Vesalainen et al., 1999). As such, retention of ^{11}C-HED in patients is believed to reflect sympathetic nervous integrity, whereby reduced accumulation of tracer indicates worse prognosis.

1.8.3 Other Presynaptic Sympathetic Nerve Radiotracers

Other presynaptic neuronal tracers include ^{11}C-epinephrine and ^{11}C-phenylephrine, of which the former is more routinely used. The pharmacological characterisitics and ease of synthesis limit the use of these tracers in nuclear cardiology. ^{11}C-Epinephrine shows specificity for NET with a greater proportion of vesicular uptake by vesicular monoamine transporter, but quantification is complicated by susceptibility to monoamine oxidase and catechol-*O*-methyltransferase (Raffel and Wieland, 2001b). ^{11}C-Phenylephrine shows greater membrane permeability than either ^{11}C-HED or ^{11}C-epinephrine, and a higher conversion rate of catecholamine metabolism (Raffel et al., 1996; Tipre et al., 2008).

1.9 ^{11}C-HED Image Quantification

Quantification of ^{11}C-HED uptake is based in the extended retention of the tracer in the presynaptic varicosity. The combined effects of reuptake, vesicular packaging, passive diffusion and active exocytosis of ^{11}C-HED following injection leads to a pseudo-equilibrium in human subjects, where a plateau of the myocardial time activity curve is apparent at 5-10 minutes after injection. This behavior led to the utilization of the retention index as the primary clinical measurement of ^{11}C-HED retention. Some variability in retention index calculations between centres limits the comparability of imaging data. The lack of a steady state equilibrium in rodents with a modest washout of tracer evident in the myocardial time activity curves has also fueled the search for additional quantitative measurements of ^{11}C-HED, including standardized uptake values and indices of tracer washout.

1.9.1 Retention Index

The clinically utilized retention index is a ratio of activity in the myocardium to the blood input function. Myocardial activity is measured in a relatively late frame, generally 30-40 minutes after tracer injection, and divided by the integral of the blood activity derived from the image using the blood pool from the left ventricle cavity. Retention index (RI) is calculated as:

Equation 1 $$RI = \frac{C_m(30-40)}{\int_0^{40} C_b dt}$$

where C_m(30-40) is activity in the myocardium at 30-40 minutes and $C_b$dt is blood input function. Retention index is expressed as %/min, and has shown some reliable translation from humans to rats (Tipre et al., 2008), though the lack of equilibrium in small animals complicates the reliability of the measurement. Moreover, the blood input function as denominator requires accurate correction for ^{11}C-labeled metabolites contributing to the radioactivity signal.

1.9.2 Standardized Uptake Value

The standardized uptake value (SUV) is a quantification of activity in a single or summed frame, normalized to the injected dose and the body weight of the subject. This normalization is required in comparing subjects of different sizes with a consistent dose administered (Law, 1993). SUV is calculated as:

Equation 2 $$SUV = \frac{C_m/W_m}{ID/W_b}$$

where C_m is the activity in the myocardium in a set frame in Bq, W_m is the tissue weight in grams, ID is the injected dose in Bq, and W_b is body weight in grams. SUV is expressed as cc/g or as a unitless ratio depending on the measurement of tissue weight. The SUV is calculated in the same way as tracer retention measurements from ex vivo biodistribution gamma well counting (Kenk et al., 2010; van Waarde et al., 2004), facilitating comparison between methods.

1.9.3 Washout Rate (k_{mono})

The clearance of ^{11}C-HED from the varicosity follows a monoexponential function. Measurements of tracer washout have been successfully applied in small animals with ^{11}C-acetate (Herrero et al., 2006), ^{123}I-MIBG (Kusmic et al., 2008), and ^{11}C-HED (Law et al., 2010; Tipre et al., 2008). Washout rates are determined by fitting a monoexponential function to the myocardial time activity curve to estimate the clearance of tracer from the varicosity, which accounts for the lack of equilibrium observed in rodents. K_{mono} washout is expressed as %/min, and is calculated from the myocardial time activity curve alone, without influence of the blood input function.

1.10 Clinical Significance

The strength of small animal imaging research approaches lies in the translation from basic research to clinical practice. There are a number of aspects of this project that bear important impact for the evaluation and management of diabetic heart disease.

1.10.1 Insight on Diabetic Heart Disease Progression

The impact of glycemic control on impaired sympathetic nervous signal transduction and cardiac outcomes is poorly understood. The high incidence of comorbid heart failure and type 2 diabetes suggests there are common pathogenic processes involved. A prominent association between the two conditions is dysfunctional noradrenergic signaling, exacerbated and possibly driven by excessive glycemia. The progression of left ventricular dysfunction and sympathetic signaling abnormalities can be noninvasively and longitudinally tracked using small animal PET to provide mechanistic insight into the timeframe and relationship between these conditions. Response to glucose-lowering therapy further advances the understanding of the interaction of glycemia and sympathetic nervous signaling.

1.10.2 Risk Stratification

Molecular imaging approaches have been recently employed to identify patients at greatest risk of disease progression in heart failure (Jacobson et al., 2010) and in diabetes (Gerson et al., 2011; Young et al., 2009), even in the absence of cardiac symptoms. The high rate of silent heart disease among diabetic patients underscores the necessity of better screening approaches to identify particularly vulnerable patient populations. Early changes in autonomic function have been suggested to predict the subsequent development of diabetes (Flaa et al., 2008) and may influence the progression of heart failure among patients (Gerson et al., 2011). Delineating the temporal progression of left ventricular dysfunction and sympathetic nervous dysfunction provides insight into the prognostic value of ^{11}C-HED retention as a complement to functional echocardiography measures.

1.10.3 Monitoring of Therapy

Recent clinical studies have identified prominent effects of hypoglycemic agents on cardiac function (Nissen and Wolski, 2007). Differences in cardiac sympathetic signaling following treatment with various agents would provide insight on the mechanism of deleterious cardiac effects of one or more antidiabetic therapies. Serial PET provides the opportunity to evaluate the cardiovascular impact of glycemic control and may inform subsequent treatment with sympathetic agents to improve cardiac function during the progression of diabetes. Evidence suggests that β-blocker therapy can influence cardiac metabolism, function, and insulin resistance (Kostis and Sanders, 2005; Sharma et al., 2008a). Serial PET measurements may provide useful information on the titration of oral glycemic agents and the impact of glycemic control on cardiac function.

1.11 Hypotheses

1.11 Primary Hypothesis

The primary hypothesis of the doctoral research project is that hyperglycemia in diabetes precipitates enhanced circulating and myocardial NE leading to impairment of sympathetic neuronal reuptake in a high fat diet-fed, intraperitoneal STZ rat model of diabetes with insulin resistance. Restoration of glycemic state by insulin or insulin sensitizing therapy will reduce sympathetic overstimulation, normalize sympathetic neuronal integrity reuptake, and recover left ventricular function.

1.11.2 Secondary Hypotheses

The specific hypotheses of the doctoral research project are: i) clinically relevant measurements of [^{11}C]HED retention can be reliably and reproducibly applied in rats; ii) retention of [^{11}C]HED is directly proportional to NET availability and inversely proportional to cardiac and/or plasma NE levels; iii) the diabetic animal model will be insulin resistant with impaired glucose oxidation and reduced metabolic flexibility; iv) diabetic rats will exhibit progressive elevation in plasma and cardiac NE levels resulting in depressed heart rate variability and a reduction in [^{11}C]HED retention; v) abnormal sympathetic function will be paralleled by diastolic and/or systolic left ventricular dysfunction in the presence of sustained hyperglycemia; vi) myocardial relative expression of NET and β-adrenoceptors will be downregulated in persistent hyperglycemic rats; vii) insulin normalization of blood glucose will reduce circulating and cardiac NE levels with a recovery of heart rate variability, restoration of normal [^{11}C]HED retention and NET/β-adrenoceptor expression profiles; viii) early treatment of diabetes with insulin, metformin, or rosiglitazone will reduce circulating and cardiac blood glucose and prevent deterioration of sympathetic neuronal integrity in the myocardium with maintained [^{11}C]HED retention; ix) abnormal echocardiographic

parameters of left ventricular function will be improved by late insulin treatment and prevented by early treatments restoring insulin sensitivity.

1.12 Objectives

The objectives of the doctoral research project are: i) to calculate test-retest variability and population variability of small animal [^{11}C]HED PET quantification measurements in rats; ii) to evaluate the specific retention of [^{11}C]HED by blockade of the NET; iii) to determine the impact of elevated NE on the retention of [^{11}C]HED retention by continuous infusion of exogenous NE; iv) to serially assess [^{11}C]HED retention in full kinetic studies using small animal PET in an animal model of high fat diet fed STZ diabetes with insulin resistance and non-diabetic controls at 0, 8, and 16 weeks of diabetes with insulin or metformin treatment initiated at 9 weeks of diabetes; *or* at 0 and 8 weeks of diabetes with or without insulin, metformin or rosiglitazone treatment initiated at 1 week of diabetes; v) to longitudinally evaluate cardiac systolic and diastolic function by echocardiography; vi) to serially monitor hemodynamics and heart rate variability by implantable telemetry; vii) to determine whole body metabolic substrate utilization by indirect calorimetry; viii) to assess insulin sensitivity by hyperinsulinemic euglycemic clamp at 8 and 16 weeks of diabetes; ix) to serially measure levels of physiological markers (i.e. glucose, insulin, catecholamines, nonesterified fatty acids, triglyceride); x) to validate PET measurements using immunoblot analysis of NET and β-adrenoceptor expression; xi) to assess cardiomyocyte health by histopathology.

1.13 Introduction to Manuscripts

1.13.1 Manuscript #1

The first manuscript addresses the pharmacological retention profile of [^{11}C]HED at 30 minutes after tracer injection by ex vivo biodistribution. Drugs blocking NET reduce retention of [^{11}C]HED in heart, lung, pancreas and interscapular brown adipose tissue by 49-89%, consistent with rich noradrenergic innervation of these tissues. Elevation of

endogenous NE by inhibition of monoamine oxidase with tranylcypromine or exogenous NE by continuous subcutaneous infusion reduced retention of [^{11}C]HED in these regions in a dose dependent manner, reflecting competitive reuptake at the NET uptake-1 site. Analysis of radiolabeled metabolites described accumulation of 39% ^{11}C-labeled metabolites in plasma at 30 minutes from the total radioactivity signal, with only 5-8% metabolite in heart, pancreas, and brown adipose tissue. Low tissue concentrations of radiolabeled metabolites significantly simplify modeling of tracer kinetics. These findings support the utility of [^{11}C]HED for the determination of sympathetic nervous dysfunction including denervation and neuronal hyperactivity in brown adipose tissue in obesity and in the heart in hyperadrenergic states including heart failure, obesity, and diabetes.

1.13.2 Manuscript #2

Building on this previous work, the second manuscript examines the application of [^{11}C]HED in small animal PET imaging with the Inveon small animal PET camera. The population and retest variability of measurements of [^{11}C]HED myocardial retention including the clinically used retention index and of washout including a monoexponential fit to assess reproducibility. Pretreatment and chase treatment with the NET inhibitor desipramine was applied to determine the dynamic effect on tracer kinetics and evaluate quantification methods. Continuous acute infusion of exogenous NE dose-dependently reduced retention of [^{11}C]HED. Concurrent measurements of plasma and terminal measurements of cardiac NE were inversely proportional to [^{11}C]HED retention index and standardized uptake value and were directly proportional to [^{11}C]HED monoexponential washout. These findings support the utility of [^{11}C]HED PET for serial evaluation of tracer retention in disease models with 15% population variability and 12-20% test-retest variability. Moreover, pharmacological studies confirmed findings in manuscript #1 wherein retention of [^{11}C]HED was directly proportional to NET availability. Finally, studies with NE infusion support the use of

[^{11}C]HED to identify elevated myocardial sympathetic activity by increased competition with synaptic NE for neuronal uptake, suggesting a role in defining early cardiac disease prior to neuronal degeneration.

1.13.3 Manuscript #3

A review of the current literature supporting development of cardiac sympathetic dysregulation in diabetes, consequences for myocardial function, and opportunities for molecular imaging is presented in manuscript #3. Basic evidence for sympathetic signaling abnormalities as assessed by catcholamine turnover, radioligand adrenoceptor binding assays, and nerve activity measurements are discussed in parallel with functional evaluations of baroreceptor reflex sensitivity, hemodynamics, and downstream intracellular signaling. These findings are discussed with regard to molecular imaging approaches to longitudinally investigate the sympathetic presynaptic innervation and postsynaptic receptor expression in the progression of diabetes. Clinical and preclinical imaging studies with PET and SPECT radiotracers are addressed in the context of prospective imaging and for the evaluation of diabetic therapy. This paper explains the rationale behind the studies presented in the subsequent manuscripts.

1.13.4 Manuscript #4

The fourth manuscript evaluates the high fat diet fed STZ rat as a model of type 2 diabetes and establishes the presence of impaired sympathetic nervous function by ex vivo biodistribution. Half of STZ-treated rats exhibit insulin resistance, impaired glucose tolerance, sustained hyperglycemia and progressive insulin deficiency by 8 weeks of diabetes. Transmitral pulse wave Doppler echocardiography identified abnormal ventricular filling in streptozotcin hyperglycemic rats as defined by elevated early to atrial filling velocity and extended mitral valve deceleration time, suggesting the presence of diastolic dysfunction. Myocardial retention of [^{11}C]HED was reduced by 13-25% in hyperglycemic

STZ rats as compared to vehicle-treated controls. This was confirmed by elevated myocardial NE content and relative reduction of cardiac NET by immunoblot. Tyrosine hydroxylase immunostaining confirmed no change in sympathetic nerve density, suggesting dysregulation of sympathetic signaling rather than degeneration of sympathetic neurons. These findings describe an association between left ventricular diastolic abnormalities and elevated sympathetic nervous tone, developing over 8 weeks of hyperglycemia. Maintained sympathetic nerve density supports the potential for functional rescue of sympathetic nervous function by reduction of blood glucose and normalization of NE levels.

1.13.5 Manuscript #5

Expanding on the findings of the second and fourth manuscript, this study investigated the ability to reverse the myocardial sympathetic nervous deficit in the high fat diet STZ diabetic rat using serial small animal [^{11}C]HED imaging. After 8 weeks of diabetes, rats were stratified to receive either insulin or metformin and were treated continuously for 8 additional weeks. Small animal [^{11}C]HED imaging was conducted at prediabetic baseline, 8 week peak diabetes, and 16 weeks of diabetes with 8 weeks of therapy. Insulin reduced blood glucose levels to the non-diabetic range with a concurrent decrease in plasma NE concentration; no change in blood glucose or NE levels was observed with metformin treatment, potentially due to insulin insufficiency at 8 weeks. [^{11}C]HED standardized uptake value was reduced at 8 weeks in diabetic rats compared to non-diabetic controls and restored following insulin treatment at 16 weeks with no improvement observed with metformin treatment, supported by an acceleration of tracer washout at 8 weeks and 16 weeks with metformin. Terminal immunoblotting confirmed an increase in NET expression in insulin-treated diabetics whereas metformin-treated diabetics exhibited a 20% reduction in NET. Echocardiography measurements showed persistent diastolic dysfunction in diabetic rats at 8 and 16 weeks of treatment. Hemodynamic measurements demonstrated an unchanged modest depression of

heart rate variability in diabetic rats despite insulin provision. These findings indicate that insulin normalization of blood glucose reduces plasma NE and cardiac NE spillover with a recovery of NET expression and reuptake function. No parallel improvement is observed in cardiac function, suggesting a critical degree of left ventricular damage has not been reversed.

1.13.6 Manuscript #6

Taking into account the inefficacy of metformin and lack of cardiac functional improvement observed in the fifth manuscript, this study aimed to prevent deterioration of myocardial function and sympathetic deficit by initiating treatment early after induction of diabetes. One week after STZ treatment, diabetic rats were assigned to receive insulin, metformin, rosiglitazone or no treatment. [^{11}C]HED imaging was conducted at prediabetic baseline and at 8 weeks of treated diabetes. Insulin reduced blood glucose levels and restored glucose tolerance, metformin treatment improved glucose tolerance with no change in blood glucose levels, and rosiglitazone did not alter blood glucose levels. Echocardiography parameters demonstrated no change in diastolic function at 8 weeks of treated diabetes as compared to untreated diabetics which exhibited impaired ventricular compliance. [^{11}C]HED standardized uptake value was reduced in untreated and treated diabetic groups compared to non diabetic controls, with a corresponding elevation of plasma NE. This finding suggests that prevention of sympathetic dysinnervation in diabetes cannot be prevented with early normalization of blood glucose. This finding may reflect the interaction of insulin and β-adrenergic signaling, with the sparing of insulin in early stages of disease providing additional drive for sympathetic activation. Improved diastolic function suggests successful reduction of lipotoxic and glucotoxic effects of ventricular compliance, with a prevention of filling abnormalities. Taken together with the findings of Manuscript #5, these results support

treatment to normalize sympathetic tone in parallel with glycemic therapy to obtain normal cardiac function in diabetic rats.

Chapter 2: Manuscript #1

J Nucl Med. (2007) 48(10): 1733-40.

Presence of Specific [^{11}C]*meta*-Hydroxyephedrine Retention in Heart, Lung, Pancreas, and Brown Adipose Tissue

James Thackeray[1,2], Rob S Beanlands[1,2], and Jean N DaSilva[1,2]

[1]Cardiovascular PET Molecular Imaging Program, National Cardiac PET Centre, Division of Cardiology, University of Ottawa Heart Institute
[2]Department of Cellular & Molecular Medicine, Faculty of Medicine, University of Ottawa, Ottawa, Ontario, Canada

Key words: sympathetic nervous system, SNS function, norepinephrine transporter uptake-1, competition with norepinephrine, HPLC column-switch system

Contributions of Authors

The work described in this manuscript was initiated as part of the candidate's Masters thesis and completed during the first months of his doctoral work. The candidate was principally involved in the design and execution of all experiments, was responsible for the acquisition and analysis of data, and drafted the manuscript. Dr DaSilva (supervisor) and Dr Beanlands (co-supervisor) provided supervision and edited the manuscript.

ABSTRACT

[^{11}C]*meta*-Hydroxyephedrine (HED) is used in cardiac positron emission tomography (PET) as an index of norepinephrine (NE) reuptake transporter (NET) density and synaptic NE levels. While cardiac uptake is well documented, tracer retention in other tissues with rich noradrenergic innervation is unclear. Dysfunctional sympathetic nervous system (SNS) function in extra-cardiac metabolic storage tissues (ie adipose tissue and skeletal muscle) and endocrine organs contributes to several disorders. The aim of this study was to determine the potential of HED as an index of NE function in brown adipose tissue, lung, pancreas, skeletal muscle, and kidney by identifying NET specific retention and determining the presence of radiolabeled metabolites. **Methods:** Male Sprague-Dawley rats were administered HED and sacrificed at 30 min post-tracer injection. Tissues were rapidly excised, counted for radioactivity, and relative tracer retention was quantified. Pretreatment with NET inhibitors established specific HED accumulation. The effect of elevated NE was tested by subcutaneous mini-pump NE infusion or inhibition of monoamine oxidase. Column-switch high performance liquid chromatography (HPLC) was used to analyse the presence of radiolabeled metabolites in heart, brown adipose tissue, pancreas, and plasma. **Results:** NET specific retention was observed in heart, brown adipose tissue, lung, and pancreas, but not in liver, skeletal muscle, or kidney. A dose-dependent response of HED accumulation to treatments elevating NE levels was established in tissues exhibiting specific uptake. At 30 min following tracer administration, HPLC analysis revealed 93-95% of total radioactivity signal derived from unchanged HED in heart, pancreas, and brown adipose tissue compared to 61±8% unchanged HED in plasma. **Conclusion:** In addition to the heart, lung, pancreas, and brown adipose tissue exhibit specific and NE-responsive uptake of HED, supporting the potential for novel PET imaging studies of SNS integrity in these tissues.

INTRODUCTION

The sympathetic nervous system (SNS) is a primary extrinsic control mechanism mediating cardiac function, metabolic processes, and adaptation to stress. In normal conditions, the neurotransmitter norepinephrine (NE) is released from the presynaptic bouton into the synapse where it binds to and stimulates adrenoceptors on pre- and postsynaptic cells. Excess NE is recycled into the presynaptic neuron by active transport via the uptake-1 NE reuptake transporter (NET) (Esler et al., 1990; Raffel and Wieland, 2001b).

In myocardium, the SNS modulates heart rate, cardiac output, and stroke volume (Raffel and Wieland, 2001b). In metabolic storage tissues, SNS activation stimulates two key processes: lipolysis, the breakdown of lipids primarily in white adipocytes; and thermogenesis, the uncoupling of mitochondrial energetics promoting heat release over energy storage, primarily in brown adipocytes and skeletal muscle (Collins and Surwit, 2001). The SNS also partially controls pancreatic secretion of insulin and glucagon, hormones that regulate energy homeostasis by promoting glucose packaging and liberation, respectively (Noble and Liddle, 2005). A growing body of evidence suggests that SNS dysfunction may be concomitantly involved in several cardiac pathologies (Bulow et al., 2003; Meredith et al., 1991), obesity (Bachman et al., 2002), and diabetes mellitus (Stevens et al., 1999).

[^{11}C]*meta*-Hydroxyephedrine (HED) is routinely applied in cardiac positron emission tomography (PET) to assess sympathetic innervation (Link et al., 2003; Rosenspire et al., 1990). As an analogue of NE, the tracer is actively recaptured into the neuron via NET, providing a quantitative indication of presynaptic sympathetic nervous integrity and function (Law et al., 1997; Raffel and Wieland, 2001b; Rosenspire et al., 1990). Moreover, HED is resistant to the NE–metabolizing enzymes monoamine oxidase (MAO) and catechol-*O*-methyltransferase (Rosenspire et al., 1990). Characterization studies of HED have demonstrated dependence of retention on the functionality and availability of NET (Raffel et

al., 2006; Ungerer et al., 1998), confirming specificity in myocardium, spleen, and adrenal glands (Allman et al., 1993; Law et al., 1997; Rosenspire et al., 1990). Pharmacokinetic studies carried out in animal models and isolated organ systems (DeGrado et al., 1993; Law et al., 1997; Raffel and Wieland, 2001b; Rosenspire et al., 1990), have implied a correlation between NE concentration and clearance rate of HED (DeGrado et al., 1993; Raffel and Wieland, 2001b). Metabolite analyses in rats, guinea pigs, dogs, and humans revealed that metabolites detected in plasma and liver are not present in cardiac tissue, facilitating qualitative image analysis and clinical interpretation (Law et al., 1997; Link et al., 1997; Rosenspire et al., 1990).

While cardiac retention of HED has been well documented and applied in several cardiovascular and autonomic disorders (Allman et al., 1993; Kies et al., 2004; Link et al., 2003; Ungerer et al., 1998; Vesalainen et al., 1999), uptake in other tissues with rich noradrenergic innervation remains equivocal. In this study, we analysed the effect of treatments altering synaptic NE levels on specific retention of HED. Additionally, we examined the potential of HED to assess SNS innervation in brown adipose tissue, lung, pancreas, white adipose tissue, skeletal muscle, and kidney by identifying NET specific retention and determining the presence of radiolabeled metabolites in these tissues.

MATERIALS AND METHODS

Materials

HED was synthesized as previously described (Rosenspire et al., 1990) and purified by semi-preparative high performance liquid chromatography (HPLC) using a Luna C18 column (Phenomenex, 250x10mm, 10μm; 5/95 acetonitrile (MeCN)/0.1 M ammonium formate (v/v); 7 mL/min; retention time (Rt) 7 min). After solvent removal via rotary evaporation, HED was reconstituted in 50/44/6 0.9% saline/water/8.4% sodium bicarbonate (v/v/v) prior to

injection. High radiochemical purity (>99%) and specific activity (7.4-55.5 GBq/μmol, 400-1500 mCi/μmol) were obtained. Desipramine hydrochloride, nisoxetine hydrochloride, metaraminol bitartrate, tranylcypromine hydrochloride, and norepinephrine bitartrate were purchased from Sigma-Aldrich (Toronto, ON, Canada) and dissolved in 0.9% saline. Osmotic mini-pumps (Alzet 2001D) were obtained from Durect Corporation (Cupertino, CA, USA) and prepared for implantation in a laminar flow fume hood. Pumps were filled to maximal capacity with dissolved NE or saline. To ensure even flow at the time of the experiment, pumps were equilibrated at 37^{o}C for 3 h prior to implantation.

Animals

Animal experiments were conducted in accordance with the recommendations of the Canadian Council on Animal Care and with approval from the Animal Care Committee of the University of Ottawa. Adult male Sprague-Dawley rats (225-275 g at time of experiment) were obtained from Charles River Canada (Montreal, QC), and were housed in a temperature-controlled animal facility under a 12 h light/dark cycle with food and water ad libitum.

Osmotic mini-pumps were implanted subcutaneously under light anaesthesia (1-2% isoflurane). Briefly, a 0.5 cm oblique incision was made lateral to the midline at the lower cervical level. A subcutaneous pocket was created using surgical scissors, the pump inserted, and the incision closed using surgical clips. Animals were treated with buprenorphine (0.3 mg/kg sc) 1 h prior to experiment. Sham animals were implanted with a mini-pump containing saline using an identical surgical procedure.

Ex vivo Biodistribution

Biodistribution studies were performed in conscious animals as previously described (Lourenco et al., 2001). Briefly, 51.8-74 MBq (1.4-2.0 mCi at time of first injection) of HED was injected as a 0.1-0.3 mL bolus into the lateral tail vein of each restrained rat. Tail veins

were vasodilated using an infrared heat lamp to facilitate injection. In each individual experiment, all animals received approximately the same mass dose of HED (0.24-1.26 μg). Animals were sacrificed by decapitation at a defined time point following tracer injection (15, 30, 45, 60, and 90 min). A sample of trunk blood was collected into heparinized tubes. Heart, kidney, pancreas and samples of lung, intrascapular brown adipose tissue, abdominal white adipose tissue, and quadriceps femoris were rapidly excised, weighed, and counted (decay corrected) for radioactivity in a gamma counter along with 1% standard dilutions of HED injection volume. Tracer retention is expressed as percent of injected dose per gram of tissue (%ID/g).

Pharmacologic Studies

Drug treatments and doses were selected according to previous experiments. To evaluate NET specific retention of HED, animals were pretreated with the NET inhibitor desipramine (10 mg/kg ip 30 min prior) (Law et al., 1997; Rosenspire et al., 1990) or nisoxetine (10 mg/kg ip 30 min prior) (Wong et al., 1982). Synaptic competition for neuronal reuptake was tested by co-administration of the HED precursor and NE analogue metaraminol (1.3 mg/kg iv coinject) (Law et al., 1997). The effect of acute elevations of synaptic NE was assessed by pretreatment with the MAO inhibitor tranylcypromine (0.5-10 mg/kg ip 1 h prior) (Lourenco et al., 2006) or subcutaneous NE mini-pump infusion at 0.05, 0.15, and 0.45 mg/kg/h over 6 h post-surgery (0.3, 0.9, 2.7 mg/kg cumulative dose) (Laycock et al., 1996). Animals were sacrificed at 30 min post-tracer injection and tissues processed as described above.

HPLC Column Switch Apparatus

A combined and modified HPLC protocol incorporating the column-switch methodology developed by Hilton et al and the weak-cation exchange solid phase HED extraction reported by Link et al was applied to capture HED and similar protonated metabolites while eluting non-protonated metabolites, proteins, and other macromolecules prior to introduction onto

the analytical column (Hilton et al., 2000; Link et al., 1997). Briefly, the HPLC apparatus consisted of two pumps (Waters): one eluting solvent A 1/99 MeCN/water (v/v) at 2 mL/min across the capture cartridge (Alltech Direct-Connect refillable guard column, 2 x 20 mm) packed with 50 mg of weak cation exchange sorbent (WCX^{TM}, Waters Oasis®, Milford, MA, USA) and fitted with 2.5 μm frits (Alltech, 2 mm filter elements); and the other delivering solvent B 5/95 MeOH/aqueous 50 mM ammonium formate, 0.27 mM ethylenediaminetetraacetic acid, 0.346 mM 1-octane sulfonic acid (v/v) at 1 mL/min across the cation exchange analytical column (Phenomenex Partisil SCX^{TM}, 250 x 4.6 mm, 10 μm). Eluents of both columns were analyzed in series by UV absorbance detection at 280 nm (Waters 486) and coincidence radiation detection (Bioscan). Signals were integrated using the PeakSimple Six-Port Chromatography Data System, analysed using PeakSimple 3.29 software, and are presented as percentage of total noise- and decay-corrected radioactivity signal accounted for by ^{11}C-labeled metabolites (retained or unretained by the WCX resin) and by unmetabolized HED.

Samples (≤ 2 mL) were injected onto the capture column allowing proteins and macromolecules to elute as measured by UV detection. After 4-5 minutes column flow was then switched, delivering solvent B across the capture cartridge and eluting retained contents onto the analytical column. Under these conditions, authentic HED was retained (>99%) on the WCX sorbent (Rt: 14 min post solvent/column switch). The capture column was reactivated between runs under MeOH and water, then re-equilibrated under solvent A prior to the next injection. Standard cation exchange (MCX^{TM}, Waters Oasis®), anion exchange (MAX^{TM}, Waters Oasis®), hydrophilic lipophilic balanced (HLB^{TM}, Waters Oasis®), and activated alumina (type WA4, Sigma) sorbents were also tested for their ability to retain HED.

Plasma and Tissue Radiolabeled Metabolite Analysis

Restrained animals were injected with 370-444 MBq (10-12 mCi) of HED and sacrificed 30 min later. A high radioactive dose was used to analyse multiple tissues in a single animal, using the HPLC column-switch system described above to accommodate for radioactive decay. Heart (n=3), brown adipose tissue (n=4), and pancreas (n=3) were rapidly dissected and a plasma sample (n=6) obtained from centrifuged blood (3000 *g*, 4000 rpm, 5 min). Tissues were processed for injection on the HPLC system as described previously (Lourenco et al., 2001). Briefly, samples were homogenized in 80/20 ethanol/water (v/v) using a Polytron tissue homogenizer. Tissue homogenates were separated using an ultracentrifuge at 82000 *g* (22000 rpm) for 15 minutes. Supernatant was extracted and solvent removed by rotary evaporation. Remaining residue was reconstituted under 1/99 MeCN/water (v/v) and microfiltered at 0.22 μm (Cathivex GS) prior to injection and testing on HPLC. Standard control experiments (n=6) were assessed for each formulation using the same procedure described above, but directly adding authentic HED to tissue or plasma prior to homogenization.

Statistical Analysis

Statistical comparisons were completed using one-way analysis of variance on mean retention values applying Bonferroni post hoc tests. All statistics were performed using SPSS 14.0 software. Vehicle treated animals did not significantly deviate from untreated controls and were therefore pooled for statistical analysis. Significance was considered at $p<0.05$.

RESULTS

HED ex vivo Retention Studies

Time course evaluation revealed high uptake of HED in myocardial tissue that was maximal (1.66-2.04 %ID/g) at 30 min post-tracer injection (Fig. 2.1A). Due to the relative uniformity of myocardial tracer retention, left ventricle is considered representative of the whole heart hereafter. Moderately high HED retention was also observed in brown adipose tissue, pancreas, and lung, with comparatively lower levels in white adipose tissue, skeletal muscle, and kidney (Fig. 2.1B). Liver uptake was considerable and surpassed heart values at 45 min post injection. Pretreatment with NET inhibitors significantly reduced tracer retention in left ventricle, brown adipose tissue, lung, and pancreas to similar levels (0.20-0.29 %ID/g). Conversely, no blockade of HED distribution was discerned in liver, skeletal muscle, kidney, or blood. Reductions of tracer retention observed following co-administration of the NE analogue metaraminol followed the same tissue distribution as NET blockade (Fig. 2.2, Table 2.1). Modest reductions in tracer retention observed in white adipose tissue with these treatments were not statistically significant.

Tranylcypromine or exogenous NE infused subcutaneously dose-dependently reduced HED retention in heart, brown adipose tissue, lung, pancreas, and white adipose tissue (Fig. 2.3, Table 2.2). At the highest administered doses, significant blockade of HED uptake was comparable to NET inhibition in tissues displaying specific retention. Additionally, skeletal muscle HED accumulation was consistently and significantly reduced (9-13%) by subcutaneous infusion of NE but not by tranylcypromine treatment. No reduction in tracer retention levels following either treatment was observed in liver, kidney, or blood compared to controls (Fig. 2.3).

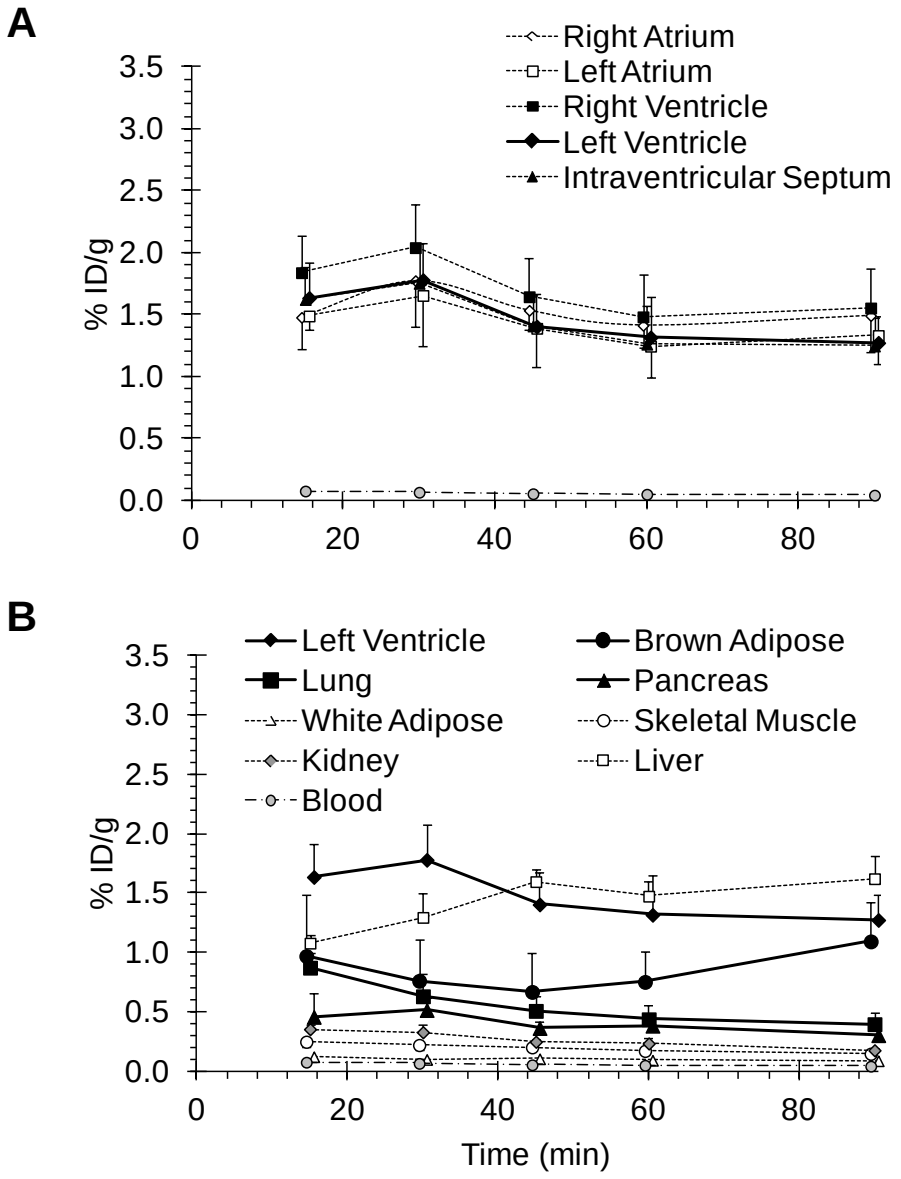

Figure 2.1 Distribution of HED in myocardium (**A**) and other peripheral tissues (**B**) at 15, 30, 45, 60, and 90 min following intravenous injection in rats. Data are shown as mean percent injected dose per gram of tissue ± standard deviation (n=26 at 30 min; n=6 at 15, 45, 60, 90 min).

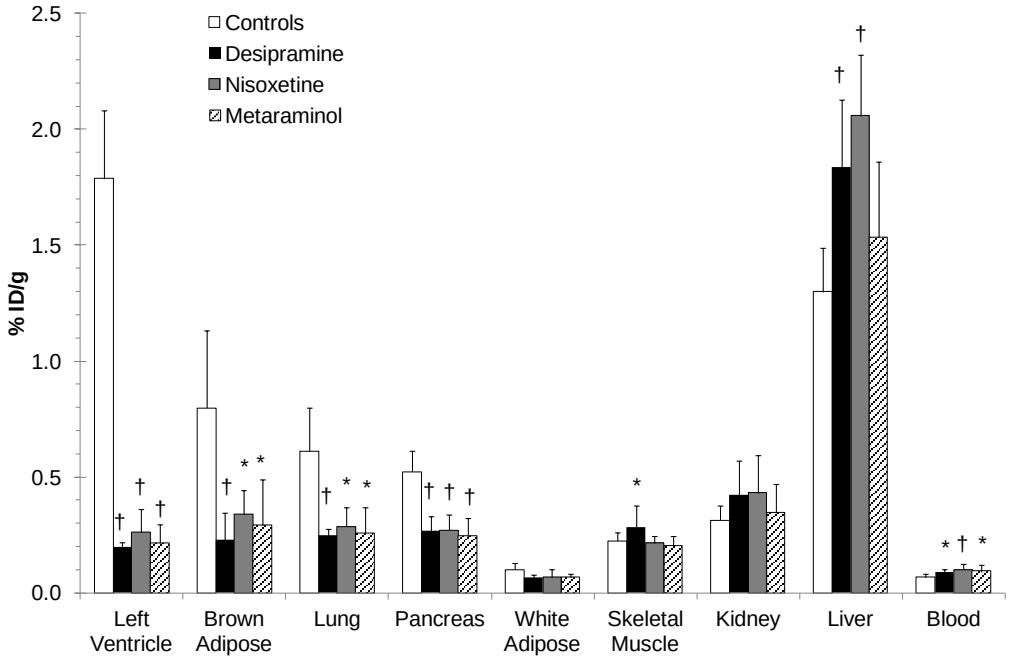

Figure 2.2 Effect of blocking norepinephrine reuptake transporter specific HED retention with NE reuptake inhibitors desipramine (10 mg/kg ip 30 min prior) or nisoxetine (10 mg/kg ip 30 min prior) or increasing competition for reuptake with norepinephrine analogue metaraminol (1.3 mg/kg iv coinjection). Animals were sacrificed at 30 minutes following HED injection. Data are shown as mean percent injected dose per gram of tissue ± standard deviation (controls n=26; desipramine n=7; nisoxetine n=6; metaraminol n=6); † $p<0.0001$; * $p<0.05$ as compared to controls using one-way analysis of variance with Bonferroni's post hoc comparisons

Table 2.1 Percent Change in HED Uptake Following Pharmacologic Treatment in Tissues Exhibiting NET-Specific Retention

Treatment and Dose	Left Ventricle	Brown Adipose	Lung	Pancreas
Desipramine (n=7) 10 mg/kg 30 min prior	-89	-71	-60	-50
Nisoxetine (n=6) 10 mg/kg 30 min prior	-85	-57	-53	-49
Metaraminol (n=6) 1.3 mg/kg iv coinject	-88	-63	-58	-54

Percent change = ((%ID/g treated) – (%ID/g control)) / (%ID/g control) x 100%
Values presented represent significant deviation ($p<0.05$) in %ID/g treated as compared to untreated controls.

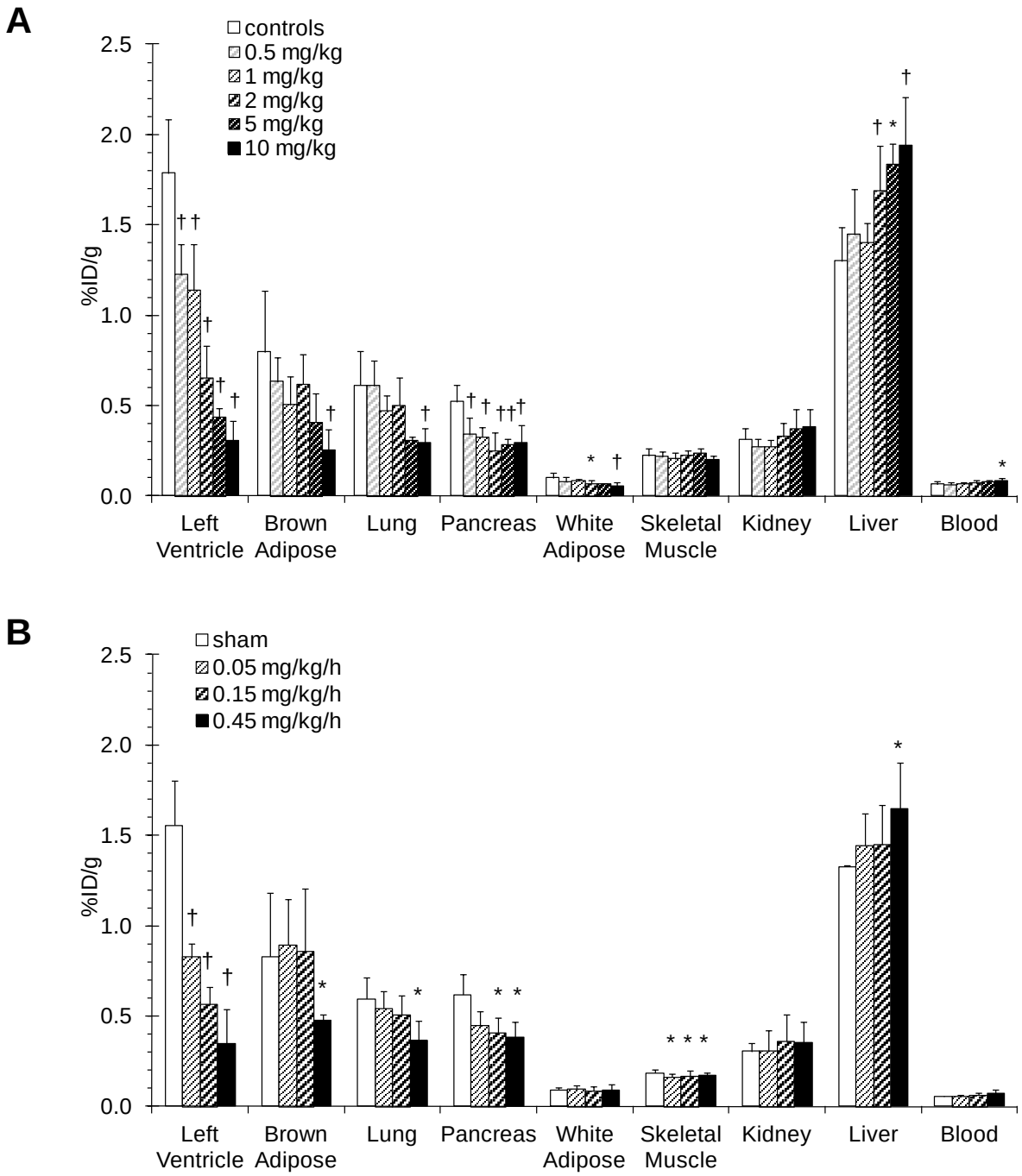

Figure 2.3 Effect of elevated norepinephrine on HED retention by pretreatment with (**A**) monoamine oxidase inhibitor tranylcypromine (0.5-10 mg/kg ip 1 h prior) or (**B**) subcutaneous infusion of norepinephrine (0.05-0.45 mg/kg/h, 6 h). Animals were sacrificed at 30 min following HED injection. Data are shown as mean percent injected dose per gram of tissue ± standard deviation (tranylcypromine: controls n=26; 0.5 mg/kg n=9; 1 mg/kg n=7; 2 mg/kg n=12; 5 mg/kg n=3; 10 mg/kg n=12; norepinephrine: sham n=8; 0.05 mg/kg/h n=6; 0.15 mg/kg/h n=10; 0.45 mg/kg/h n=9); † $p<0.0001$; * $p<0.05$ as compared to controls using one-way analysis of variance with Bonferroni's post hoc comparisons.

Table 2.2 Percent Change in HED Uptake Following Pharmacologic Treatment to Elevate Norepinephrine in Tissues Exhibiting NET-Specific Retention

Treatment and Dose	Left Ventricle	Brown Adipose	Lung	Pancreas
Tranylcypromine				
0.5 mg/kg (n=9)	-30	-20	+1	-36
1.0 mg/kg (n=7)	-35	-36	-22	-38
2.0 mg/kg (n=12)	-63	-22	-17	-53
5.0 mg/kg (n=3)	-75	-48	-49	-47
10 mg/kg (n=12)	-82	-68	-52	-44
Norepinephrine				
0.05 mg/kg/h (n=6)	-53	+13	-10	-16
0.15 mg/kg/h (n=10)	-68	+9	-17	-23
0.45 mg/kg/h (n=9)	-80	-40	-40	-29

Percent change = ((%ID/g treated) – (%ID/g control)) / (%ID/g control) x 100%
All values presented represent significant deviation ($p<0.05$) in %ID/g treated as compared to untreated controls except brown adipose tissue and lung (tranylcypromine 0.5, 1.0, 2.0, 5.0 mg/kg; norepinephrine 0.05, 0.15 mg/kg/h) and pancreas (norepinephrine 0.05 mg/kg/h).

Radiolabeled Metabolite Analysis

MCX, MAX, HLB, and alumina resins were unable to retain HED in a satisfactory manner for HPLC analysis. Contrary to the MCX sorbent, which was shown to bind too strongly to the tracer resulting in tailing of the radioactivity peak post-extraction, the WCX resin provided clear adherence and elution of authentic HED (data not shown). ^{11}C-Labeled metabolites were eluted from the WCX sorbent prior to column and solvent switching. At 30 min post-injection, 39±8% of total noise- and decay-corrected radioactivity represented metabolites in plasma, whereas 61±8% was unchanged HED (Fig. 2.4A). In contrast, predominantly unmetabolized HED was observed in heart (94±2%), brown adipose tissue (95±3%), and pancreas (92±3%) (Fig 2.4B-D). In standard control tissue samples with authentic HED, radioactivity present was solely representative of unchanged HED (data not shown).

DISCUSSION

Previous examinations of HED retention have focused primarily on myocardium. However, the SNS is ubiquitous, forming connections throughout the body to various organ systems. The data presented here indicate that HED retention is reduced by NET blockade in myocardium by more than 85%, and in brown adipose tissue, lung, and pancreas by 49-71%. These results demonstrate that HED may be aptly applied in measuring SNS innervation and function in a wider array of tissues than previously considered.

Previous examinations (Law et al., 1997; Raffel et al., 2006; Rosenspire et al., 1990) have shown higher %ID/g values in myocardium (2.7-3.2 %ID/g) than those reported here. Law et al demonstrated a slight reduction in myocardial radioactivity when HED was coinjected with 10 nmol/kg (2.2 μg/kg) unlabeled compound (Law et al., 1997). In the present study,

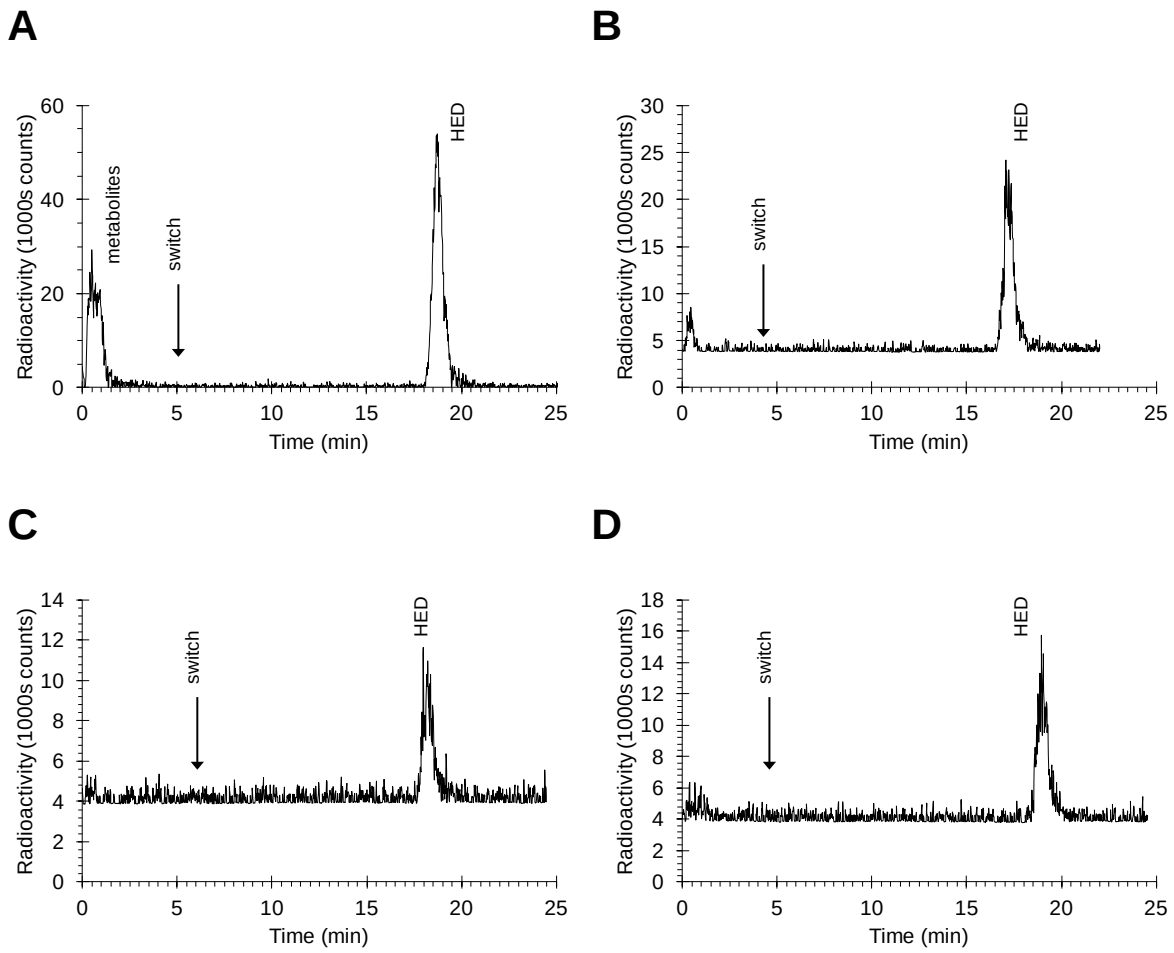

Fig. 2.4 Representative HPLC chromatograms of ^{11}C-labeled peaks at 30 min following HED injection in plasma (**A**), heart (**B**), brown adipose tissue (**C**), and pancreas (**D**). Column and solvents were switched 4-5 minutes after injection onto HPLC; unchanged HED was eluted at 14 min post-column/solvent switch. Radioactivity levels represent total counts and vary depending on time of analysis due to isotope decay.

the injected doses of HED overlap this mass dose (0.9-5.6 μg/kg) which may account for the lower uptake observed in myocardium, and reduce the apparent uptake in other tissues as well.

While a high signal is consistently detected in the heart, specific HED retention at lower levels has been previously reported in the spleen, adrenal glands, and lungs (Law et al., 1997; Rosenspire et al., 1990). Indeed, binding assays using selective NET inhibitors [^{3}H]mazindol and [^{3}H]desipramine have demonstrated NET densities as high as 250-500 fmol/mg protein in myocardium (Mardon et al., 2003; Raffel et al., 2006; Ungerer et al., 1998). As the vast majority of NE utilized by the heart is synthesized within cardiac sympathetic neurons (Kopin and Gordon, 1963), there is less dependence on circulating NE levels, and recapture of neurotransmitter is critical for normal cardiac function. The majority of research on HED has demonstrated that higher tracer uptake directly correlates to higher NET density (Liang et al., 1989; Raffel et al., 2006; Raffel and Wieland, 2001b; Ungerer et al., 1998). The observation of lower HED retention in the lungs as compared to the heart support earlier reports (Law et al., 1997; Rosenspire et al., 1990). By contrast, the selective NET inhibitor (*R*,*R*)-[^{11}C]methyl-reboxetine displayed similar binding levels for lung and heart (Ding et al., 2003). This apparently high lung uptake of (*R*,*R*)-[^{11}C]methyl-reboxetine may result from the greater lipophilicity, and hence non-specific binding. of this tracer in comparison to HED.

The presence of NET-specific HED retention in adipose tissue reflects a regulated network of NE synapses controlling lipolytic and thermogenic pathways. Unlike white adipocytes, brown adipose tissue exhibits a greater degree of sympathetic innervation as well as blood supply, owing to its dynamic involvement in both energy homeostasis and lipid clearance (Collins and Surwit, 2001; Raasmaja and York, 1988). NET densities in rat intrascapular brown adipose tissue have been estimated at 1700 fmol/mg protein, as determined with [^{3}H]nisoxetine (King et al., 1999). This higher value may derive from the lower proportion

of protein within adipocytes as compared to cardiomyocytes (Collins and Surwit, 2001). In general, previous work has reported that NET is regulated in parallel with postsynaptic β-adrenoceptors (Mardon et al., 2003). Ungerer et al demonstrated a correlation between the density of adrenoceptors and NET, as determined by the nonselective β-adrenoceptor antagonist [^{3}H]CGP12177 and [^{3}H]mazindol binding respectively, suggesting that β-adrenoceptor density may provide a useful proxy measurement of NET expression (Ungerer et al., 1998). Accordingly, brown adipose tissue β-adrenoceptor density has been shown to be two thirds of myocardial levels (Raasmaja and York, 1988), a ratio that is closely reflected by the current HED measurements at 30 min post-injection. Pancreatic ducts have been shown to contain the majority of NE in the pancreas, indicating that SNS control is not directly acting on the heavier secretory cells (Yi et al., 2004). Expression levels of NET and adrenoceptors in pancreatic ductile cells remains contentious.

Lack of specific tracer accumulation in skeletal muscle, kidney, and liver following NET blockade has been reported here and elsewhere (Law et al., 1997). A greater dispersal of NET and wider synaptic clefts in skeletal muscle may render blockade of reuptake ineffective (Esler et al., 1990). Studies with the highly selective NET inhibitor sibutramine have suggested that doses capable of elevating NE in the heart do not significantly affect NE levels or vasoconstriction in skeletal muscle (Birkenfeld et al., 2002). [^{3}H]NE uptake assays have shown lower V_{max} in kidney as compared to heart (Liang et al., 1989), which may suggest reduced or diffuse NET expression, though specific B_{max} values for kidney have not been reported to our knowledge.

Interestingly, non-specific retention of HED as determined by NET blockade is comparable among heart, brown adipose tissue, lung, and pancreas, and aligns with total retention in skeletal muscle and kidney where only non-specific retention is observed. This uniformity

indicates that tissue differences in total HED accumulation likely derive from NET-specific uptake of the tracer, reflecting differential SNS neuronal density and/or NET expression.

Elevations of endogenous NE (via tranylcypromine) or exogenous NE (subcutaneous infusion) reduced myocardial, brown adipose, lung, pancreatic, and to a lesser extent, white adipose retention of HED in a dose-dependent manner. Tranylcypromine treatment has been reported to increase tissue NE levels by 60% within 1 h of administration (Routledge and Marsden, 1987), evoke elevations of blood pressure and heart rate (Keck et al., 1991), and increase the cache of endogenous neuronal NE stores (Fillenz and Stanford, 1981). Additionally, tranylcypromine has low affinity for NET (k_i = 5 μM) (Raffel and Chen, 2004). Despite this, direct inhibition of the transporter is not anticipated at the low doses used in the present study that nevertheless evoked significant reductions of cardiac HED retention. Similar results were obtained with the NE analogue metaraminol, as reported here and elsewhere (Law et al., 1997). Studies in isolated perfused rat hearts have suggested that although initial HED uptake is unhindered, clearance is hastened in the presence of NE (DeGrado et al., 1993; Raffel and Wieland, 2001b), a result that is supported by our data. Subcutaneous infusion of NE has been shown to elevate tissue (synaptic) and plasma levels of the neurotransmitter (Mardon et al., 2003). The moderate reduction in skeletal muscle observed with NE infusion, but not with MAO inhibition, NET inhibition, or metaraminol treatment, suggests that a non-specific mechanism such as NE-induced vasoconstriction may contribute to a global reduction in tracer uptake due to reduced delivery (Pop-Busui et al., 2004). However, the decrease in skeletal muscle HED uptake (9-13%) is minor compared to the reductions obtained in tissues exhibiting specific retention, implying that perfusion may only partially explain the NE results. Taken together, the tranylcypromine, NE, and metaraminol results strongly suggest that enhanced synaptic NE significantly reduces HED

retention by competitive reuptake, decreased neuronal storage capacity, or increased vesicle release.

The capture of physiologically protonated HED and metabolites by weak cation-exchange resin in the presence of a saline gradient has been previously reported (Link et al., 1997). Here, we have demonstrated the ability to adhere protonated HED to weak cation-exchange sorbent without a saline gradient using the HPLC column-switch approach (Hilton et al., 2000). Metabolite analyses in rats, guinea pigs, dogs, and humans indicated that at 30 min post-HED administration, metabolites represent 30-50% of total radioactivity in plasma, with no labeled metabolites present in myocardium (Law et al., 1997; Link et al., 1997; Rosenspire et al., 1990). We report here that like the heart, there is an absence of ^{11}C-labeled metabolites in brown adipose tissue and pancreas. This property, in combination with the presence of NET-specific HED retention, facilitates PET image analysis and may allow the application of existing cardiac retention models to pancreas and brown adipose tissue.

Clinical applications of HED PET have included cardiovascular disorders such as acute myocardial infarction (Allman et al., 1993), congestive heart failure (Link et al., 2003; Vesalainen et al., 1999), dilated cardiomyopathies (Ungerer et al., 1998), multi-vessel coronary artery disease (Bulow et al., 2003), and Brugada syndrome ventricular fibrillation (Kies et al., 2004), as well as systemic disorders pheochromocytoma (Shulkin et al., 1992), diabetes mellitus (Stevens et al., 1999), and parkinsonian syndromes such as multi-system atrophy (Berding et al., 2003). Imaging of brown adipose tissue, lung, and pancreas present unique and formidable challenges due to problems in localization and signal identification for brown adipose tissue (Collins and Surwit, 2001), low *in vivo* tissue density hindering acquisition of high contrast images for lung (Lourenco et al., 2006), and non-pancreatic abdominal uptake causing poor signal-to-noise ratios for pancreas (Clark et al., 2004). Recent use of [^{18}F]fluorodeoxyglucose in full body scans has revealed anomalous tracer

uptake in areas of supraclavicular fat (Cohade et al., 2003), suggesting that isolation of brown adipose tissue in large mammals may be possible. While lung tissue density remains a problem for neurohormonal imaging, the advent of fused PET/CT technology may circumvent some of the other challenges to non-cardiac imaging, allowing CT delineation of brown adipose tissue or pancreas for subsequent PET evalutations.

CONCLUSION

In addition to the heart, NET specific uptake of HED without labeled metabolites is observed in lung, pancreas, and brown adipose tissue supporting the potential for novel imaging of SNS integrity in various metabolic disease states. Moreover, the present study strongly suggests an inverse correlation between tracer retention and synaptic NE dependent on the presence of NET specific retention of HED.

ACKNOWLEDGMENTS

The authors acknowledge the contributions of the University of Ottawa Heart Institute Cardiac PET Centre Radiochemistry staff (Samantha Mason, Jeffrey Collins, and Paul Coletta) for radiochemical synthesis and would like to thank Miran Kenk and Stephanie Thorn for assistance with both the manuscript and biodistribution metabolite analysis studies, also thanks to Michael Greene, Maryam Parsa-Nezhad and the Ottawa Heart Institute Animal Care and Veterinary Staff for general assistance with the experiments.

Chapter 3: Manuscript #2

Mol Imag Biol. (Submitted)

Test-Retest Repeatability of Quantitative Measurements of Cardiac ^{11}C-*meta*-Hydroxyephedrine in Rats by Small Animal Positron Emission Tomography

James Thackeray[1,2], Jennifer M Renaud[1], Myra Kordos[1], Ran Klein[1], Robert A deKemp[1], Rob S Beanlands[1,2], and Jean N DaSilva[1,2]

[1]Molecular Function & Imaging Program, Division of Cardiology, University of Ottawa Heart Institute, Ottawa, Ontario, Canada
[2]Department of Cellular & Molecular Medicine, Faculty of Medicine, University of Ottawa, Ottawa, Ontario, Canada

Key words: HED, catecholamine, test-retest repeatability, μPET, cardiovascular disease

Contributions of Authors

All experiments described in this manuscript were designed and executed by the candidate, with assistance from data analyst Jennifer Renaud (quantification measurements), animal technician Myra Kordos (image acquisition), and engineer Ran Klein (FlowQuant software). The candidate was principally conducted data analysis and drafted the manuscript. Physicist Dr Robert deKemp provided input on the experiments and contributed to editing of the final manuscript. Dr Beanlands provided a clinical perspective on the findings. Work performed was supervised by Dr DaSilva.

Abstract

Purpose: The purpose of this study was to evaluate the repeatability of quantitative cardiac measurements of the norepinephrine analogue ^{11}C-meta-hydroxyephedrine (HED) in rats and to compare the reflective measures of reuptake blockade and acute competition with norepinephrine.

Procedures: HED PET images were acquired in Sprague Dawley rats either untreated, or administered norepinephrine reuptake inhibitor desipramine or continuous infusion of exogenous NE. HED retention was quantified by retention index, standardized uptake value (SUV), monoexponential and one-compartment washout. Plasma and cardiac norepinephrine were measured by high performance liquid chromatography.

Results: Test-retest repeatability was 15-21%, with 12-22% coefficient of variability. Desipramine lowered myocardial HED retention index by 69% and SUV by 85%. Norepinephrine dose-dependently reduced HED accumulation by 27-67% and increased washout. Plasma and cardiac norepinephrine levels inversely correlated to HED retention values.

Conclusion: Measurements of HED retention exhibit high test-retest repeatability. Uptake and washout are sensitive to acute increases in norepinephrine concentration.

Introduction

Neurohormonal imaging is emerging as a unique approach in nuclear cardiology for the assessment of cardiac health (Bengel, 2009). Abnormalities in sympathetic nervous system signaling have been implicated in the progression of cardiac pathologies including myocardial infarction (Allman et al., 1993), congestive heart failure (Ungerer et al., 2000), and coronary artery disease (Bulow et al., 2003). Noninvasive cardiac positron emission tomography (PET) with norepinephrine analogues such as [^{11}C]*meta*-hydroxyephedrine (HED) or [^{11}C]epinephrine allows for evaluation of sympathetic nervous integrity in cardiac patients (Link et al., 2003; Ungerer et al., 1998), providing complementary information about myocardial health and function. The application of these tracers in longitudinal imaging studies in rats necessitates a comprehensive evaluation of image analysis reproducibility between sessions and within subjects.

Nuclear cardiology dogma dictates that HED retention is directly proportional to norepinephrine reuptake transport function and inversely related to local norepinephrine concentrations (Law et al., 1997; Raffel and Wieland, 2001a; Rosenspire et al., 1990; Thackeray et al., 2007). However, definitive evidence that elevated norepinephrine directly influences HED retention is lacking (Hartmann et al., 1999). Attempts to correlate HED absolute retention with norepinephrine have been largely unsuccessful, with no significant correlation reported to plasma concentration (Hartmann et al., 1999) and weak statistical correlation to regional cardiac levels (Ungerer et al., 1998). In rats, administration of norepinephrine was shown to reduce HED accumulation in ex vivo biodistribution (Thackeray et al., 2007) and increase tracer washout in isolated rat hearts (DeGrado et al., 1993). Small animal PET imaging facilitates accurate evaluation of tracer kinetics in response to elevated norepinephrine (Law et al., 2010; Tipre et al., 2008).

In the present study, the test-retest repeatability of HED measurements is evaluated in rats using four distinct quantitative approaches to delineate uptake, retention, and washout. The effect of reuptake blockade or norepinephrine infusion on these parameters is evaluated *in vivo*. Repeatability of quantitative HED measures is valuable for the development of serial myocardial imaging studies in animal models of disease.

Materials and Methods

Animals

Male Sprague-Dawley rats (n=22, 321±79 g at time of study) were obtained from Charles River (Montréal Canada) and were housed in pairs on a 12 h /12 h light/dark cycle with food and water *ad libitum*. All animal experiments were conducted in accordance with the recommendations of the Canadian Council on Animal Care and with the approval of the University of Ottawa Animal Care Committee.

Small Animal PET Imaging

HED was radiosynthesized by *N*-methylation of metaraminol free base as described previously in high radiochemical purity and specific activity (Rosenspire et al., 1990; Thackeray et al., 2007). Small animal imaging was conducted using the Inveon small animal PET scanner (Siemens, Knoxville TN). Anaesthetized rats (40 mL/min isoflurane) were positioned supine on the scanner bed with the heart centered in the field of view. HED (24.9±10.8 MBq, 1.1-88.1 GBq/μmol, 0.1-7.0 μg/kg cold mass) was injected in 1 mL bolus of sodium bicarbonate in saline via a 26 gauge catheter inserted into a lateral tail vein. Images were acquired over 60 minutes. Two imaging sessions were conducted with each tracer production, 60 minutes apart, accounting for the range of specific activity. Heart rate, respiration, and body temperature were continuously monitored. To determine reproducibility, animals underwent paired PET scans with 7-10 days between sessions. HED measurements were compared between imaging sessions and tested for consistency.

Image Analysis

List-mode data was acquired for 60 minutes and subsequently histogrammed into 26 frames of 12×10 s, 3×60 s, and 11×300 s. Displacement scans were histogrammed using 30 frames of 12×10 s, 3×60 s, 2×300 s, 5×60 s, 8×300 s. Dynamic data was reconstructed on a 128×128 pixel image matrix (0.345 mm pixel size) using OSEM3D/MAP (β=1.0, OSEM3D iterations=2, MAP iterations=18) with corrections for dead-time, isotope decay, detector efficiencies, and random events. Images were analysed using FlowQuant© software (Klein et al., 2010a). Time-activity curves (TAC) were generated for the blood input function and myocardial tracer accumulation. HED in the left ventricle was quantified using four methods. Cardiac HED retention index was calculated as applied clinically (Raffel and Wieland, 2001a; Tipre et al., 2008): $RI = C_m(30\text{-}40)/{}_0\int^{40} C_b(t)dt$ where $C_m(t)$ is the activity in myocardium at 30-40 min and $C_b(t)$ is the blood input function. Tracer washout was determined by automated fitting of a monoexponential function to the dynamic data for myocardium (Yoshinaga et al., 2007) or by automated fitting a one-compartment model to the first 40 minutes of dynamic data to estimate k_2. For desipramine chase studies, fits were applied starting from 15 minute scan time (frame 18) Standardized uptake value (SUV) at 30-35 minutes (frame 21) was calculated as: $(U(t))/(ID/m_{wb})$ where U(t) is the uptake in myocardium at time t in Bq/cc, ID is injected dose, and m_{wb} is mass of whole body.

Pharmacological Assessment

Desipramine hydrochloride (Sigma Aldrich, 10 mg/kg) was administered by intraperitoneal injection 30 minutes before or 15 minutes after tracer injection. Norepinephrine bitartrate (Sigma Aldrich, 0.05 or 0.15 mg/kg/h) or saline (7.6 µL/h) was infused by surgically implanted subcutaneous osmotic minipumps over a six hour period prior to tracer injection. Rats implanted with minipumps received analgesic buprenorphine (0.3 mg/kg sc) 1 h prior to

surgery. During implantation, rats were anaesthetized with isoflurane (40 mL/min) and allowed to recover until the PET scan. Blood samples were obtained from the saphenous vein at 0, 3, 6, and 7 hours for quantification of plasma norepinephrine. At the conclusion of the scan, treated rats were sacrificed by cardiac puncture exsanguination, hearts were dissected and flash frozen under liquid nitrogen for *in vitro* analysis.

In vitro Analysis

Excised hearts were weighed and homogenized under 80/20 ethanol/0.1 M formic acid using a Polytron homogenizer, and centrifuged at 82,000*g*. Supernatant was evaporated using a rotary evaporator and the residue was reconstituted under 0.1 M formic acid. Plasma and reconstituted tissue samples were analysed for catecholamine content using HPLC with electrochemical detection as described previously (Thackeray et al., 2011b). Norepinephrine reuptake transporter protein expression was determined by standard Western blotting techniques as described previously (Thackeray et al., 2011b).

Statistics

Data are presented as mean values ± standard deviations. Statistical analyses were completed using SPSS 18.0 statistical software. For test-retest scans, Bland Altman analysis was completed. Test-retest variability was calculated for each individual animal as (TRV = (|scan1 – scan2|) / (scan1 + scan2) / 2) using the retention and washout values obtained from first and second scans and averaged. Coefficient of variability was determined as the standard deviation divided by the mean of the retention or washout values (Aznavour et al., 2009). Mean HED measurements and catecholamine levels were compared by Student's t-test. Pearson product-moment correlation coefficients were calculated between each HED measurement and plasma or cardiac norepinephrine concentration, and a one-tailed test for significance was applied.

Results

Test-Retest Repeatability

High uptake of HED was observed in the myocardium compared to blood with sustained retention and mild continuous washout. Among 11 pairs of test-retest HED scans, the mean cardiac retention index was 6.4±1.7%/min, SUV was 4.0±1.0 g/cc, monoexponential washout rate was 0.80±0.30%/min, and one-compartment washout was 0.031±0.019 /min. Bland-Altman analysis revealed that differences in values from scan 1 to scan 2 tended to zero for retention index (-0.32±1.21%/min), SUV (-0.29±0.79 g/cc), monoexponential washout (0.05±0.22%/min), and one-compartment washout (0.006±0.014 /min). The least difference within subjects between scans was found for measurements of tracer accumulation retention index and SUV, with slightly higher variability in washout measurements (Table 1). The population variability was lowest for retention index, and was modestly higher for SUV and monoexponential washout measurements. One-compartment washout had 46% variability. There was no correlation between HED retention or washout measurements and the cold mass administered (r=0.25, p=NS).

Pharmacological Assessment

Pretreatment with desipramine blocked specific retention of tracer. Left ventricle images were less defined with enhanced tracer washout evident in myocardial TAC when compared to images and TACs obtained in rats without desipramine pretreatment (Figure 1A&B). Administration of despiramine at 15 min following HED evokes accelerated washout of tracer at the time of drug injection (Figure 1C). Injection of desipramine did not affect heart rate: 413±17 bpm before vs 405±21 bpm after treatment (p=NS). Desipramine pretreatment reduced retention index at 30-40 minutes by 69% and SUV by 84%, with a parallel increase of monoexponential tracer washout by 263%. Chase treatment with desipramine reduced

Table 3.1 Repeatability statistics in test-retest analysis of 11 pairs of ^{11}C-HED PET scans

Group	**RI**	**SUV**	**k_{mono}**	**k2**
Test-Retest Variability (%)	15.4±12.4	18.7±15.2	21.2±13.4	28.9±27.4
Coefficient of Variability	0.12±0.05	0.22±0.08	0.21±0.16	0.46±0.18

RI, retention index; SUV, standardized uptake value; k_{mono}, monoexponential washout; k2, one-compartment washout

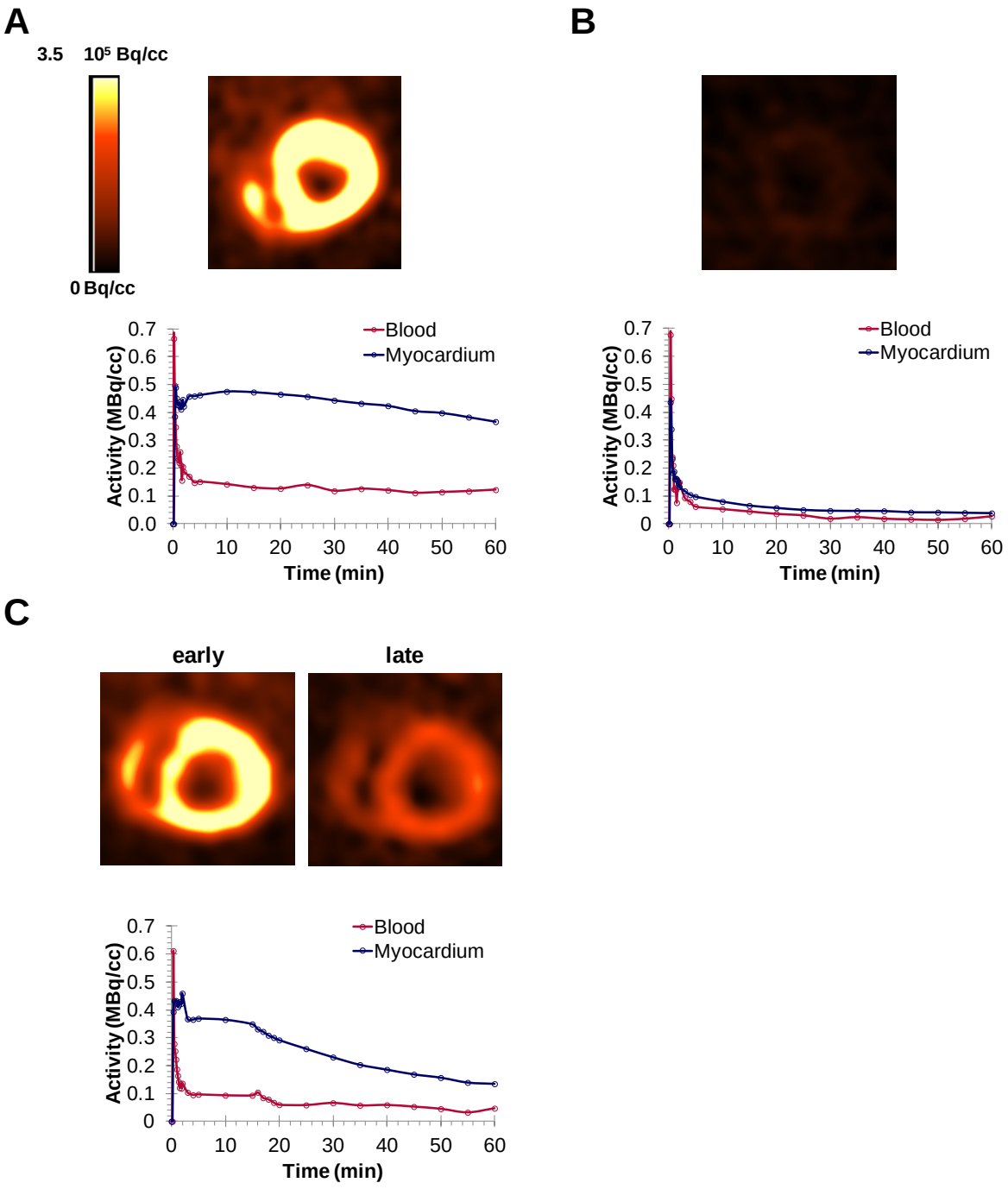

Figure 3.1 Representative transaxial images and time activity curves obtained from the same rat with (**A**) no pretreatment or (**B**) 30 min following pretreatment with NET inhibitor desipramine (10 mg/kg ip). Scans were performed one week apart. (**C**) Representative transaxial images from early (2-15 min) and late (15-40 min) frames and time activity curve HED acquisition with desipramine (10 mg/kg ip) chase injection 15 min following tracer.

30-40 minute retention index by 33% and SUV by 47%, reflecting an increase of monoexponential washout of 197% (Figure 2).

Animals administered 0.5 or 0.15 mg/kg/h norepinephrine displayed a 1.5 or 3.4-fold elevation of plasma norepinephrine concentration and were consistent at 3, 6, and 7 hours of infusion. A corresponding 1.3 or 2.5-fold elevation of norepinephrine was also observed in myocardial homogenates (Table 2). There was no difference in heart rate between groups over the duration of the PET scan. Left ventricle PET images of norepinephrine-infused rats were less defined as compared to those of saline-infused animals, with a dose-dependent increase in the declination of the myocardial time activity curve (Figure 3). Saline-infused controls showed a modest reduction in HED retention measurements and a slight increase in HED washout rates compared to the untreated control bank. Norepinephrine infusion at 0.5 or 0.15 mg/kg h reduced myocardial retention index by 26% or 67% and SUV by 36% or 68% compared to saline-infused controls (Figure 4). This reduced retention was associated with a dose-dependent acceleration in monoexponential washout by 92 or 326% and one-compartment washout by 27 or 1600% (Figure 4). Immunoblotting demonstrated no difference in relative NET expression between hearts of norepinephrine-treated and saline-treated rats.

Correlation of Retention Index to Norepinephrine

Linear regressions were plotted between HED retention measures and plasma norepinephrine concentration or cardiac norepinephrine content (Table 3). Significant inverse correlations were established between retention index or SUV and norepinephrine content. There were significant direct correlations between monoexponential and one-compartment washout and norepinephrine levels.

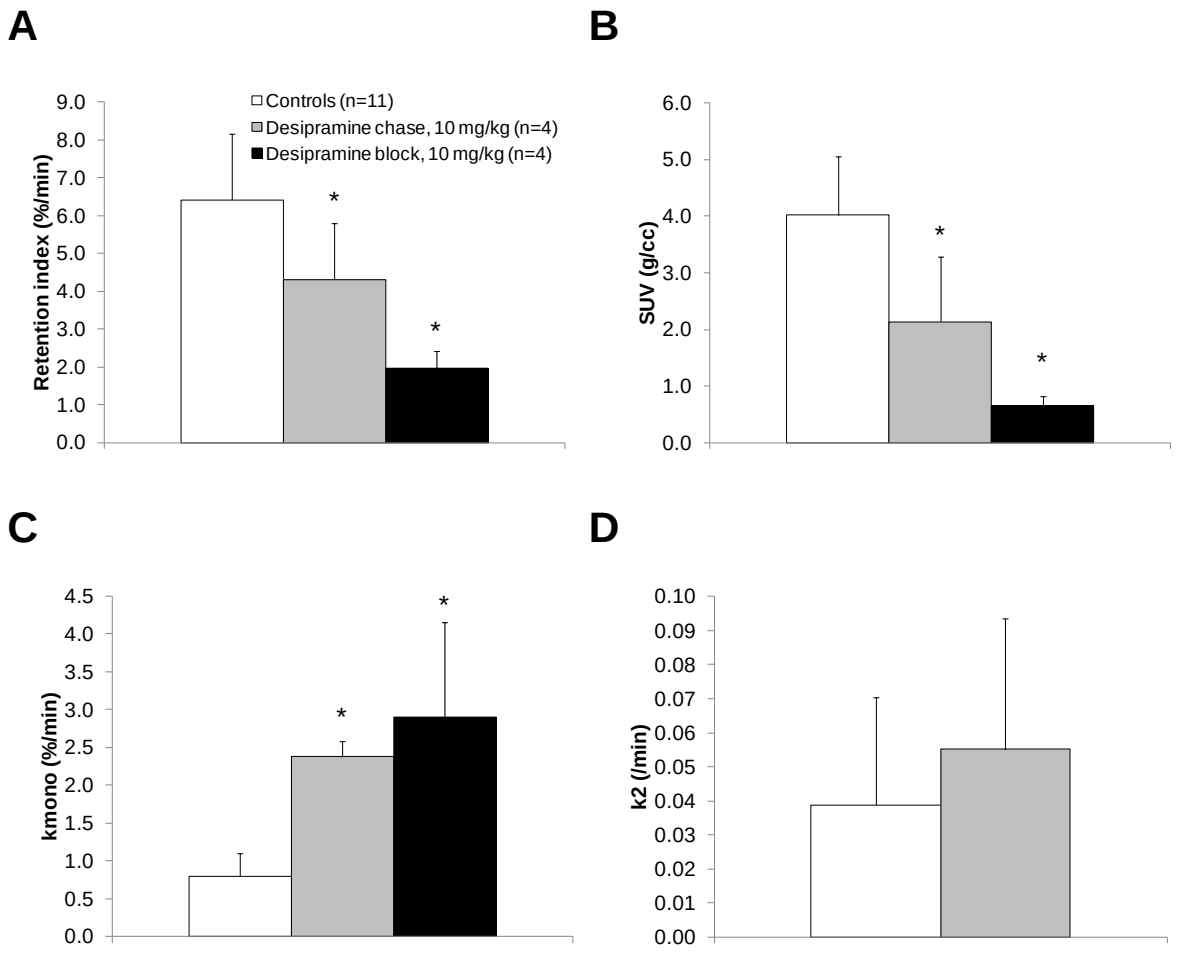

Figure 3.2 Quantitative HED analysis in untreated controls and rats administered desipramine (10 mg/kg ip) 15 minutes after or 30 minutes before tracer injection. (**A**) Retention index, (**B**) standardized uptake value monoexponential washout, (**C**) one-compartment k_2, (**D**) standardized uptake value. Because washout of tracer was complete in initial frames for desipramine pretreatment, these are not included in the analysis. Mean ± SD. * $p<0.05$ to untreated controls, one-tailed t-test.

Table 3.2 Cardiac and plasma norepinephrine level at conclusion of HED scan (7 h infusion).

Group	Plasma NE (ng/mL)	Cardiac NE (ng/mg)
Saline sc Infusion (n=4)	1.35±0.45	3.03±0.42
Norepinephrine sc Infusion		
0.05 mg/kg/h sc (n=3)	1.99±0.88	3.86±0.72*
0.15 mg/kg/h sc (n=3)	4.64±0.20*	7.70±1.56*

* $p<0.05$ to saline sc infusion, one-tailed t-test

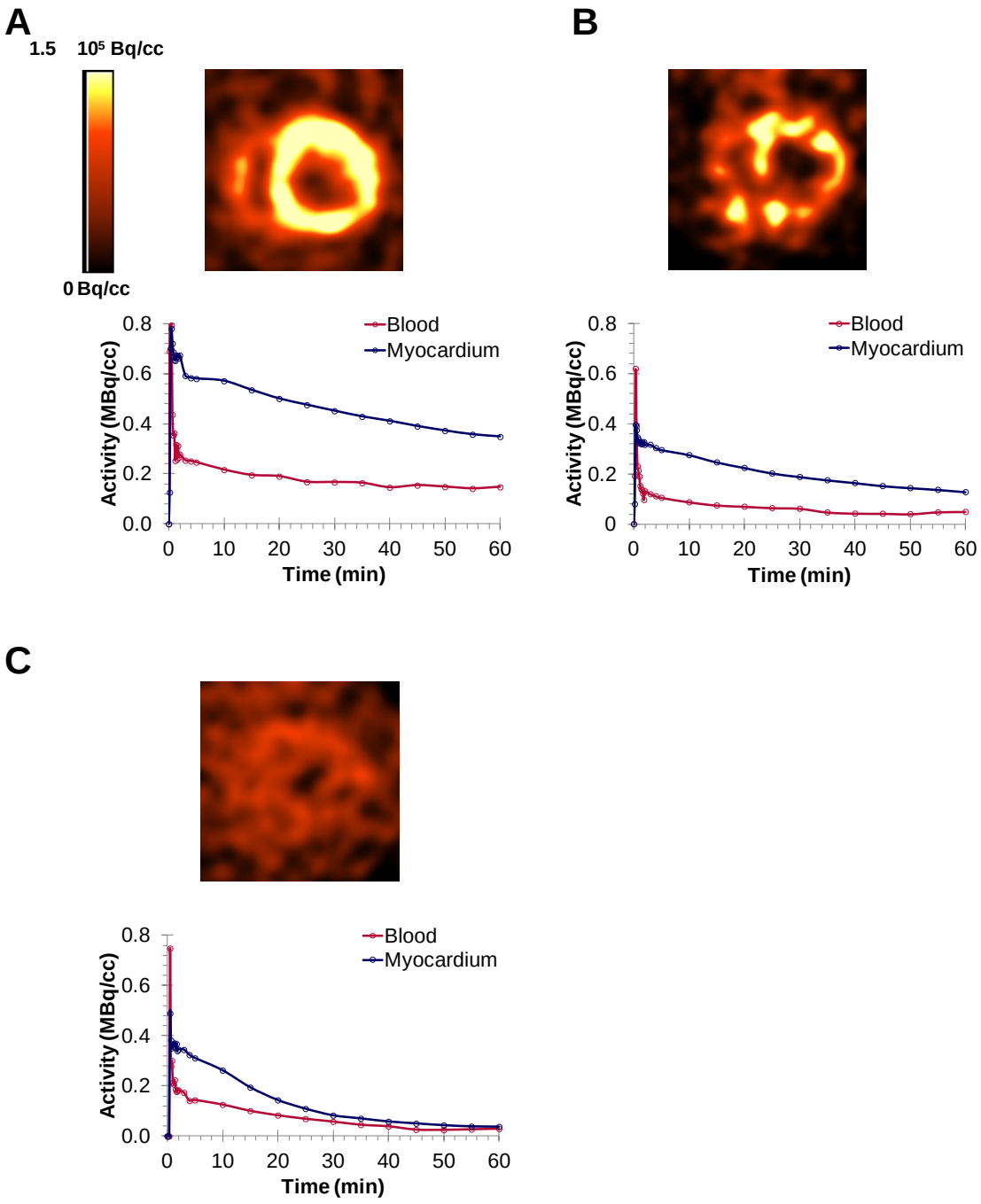

Figure 3.3 Representative transaxial images and time activity curves from animals treated with continuous infusion of (**A**) saline or norepinephrine at (**B**) 0.05 mg/kg/h and (**C**) 0.15 mg/kg/h.

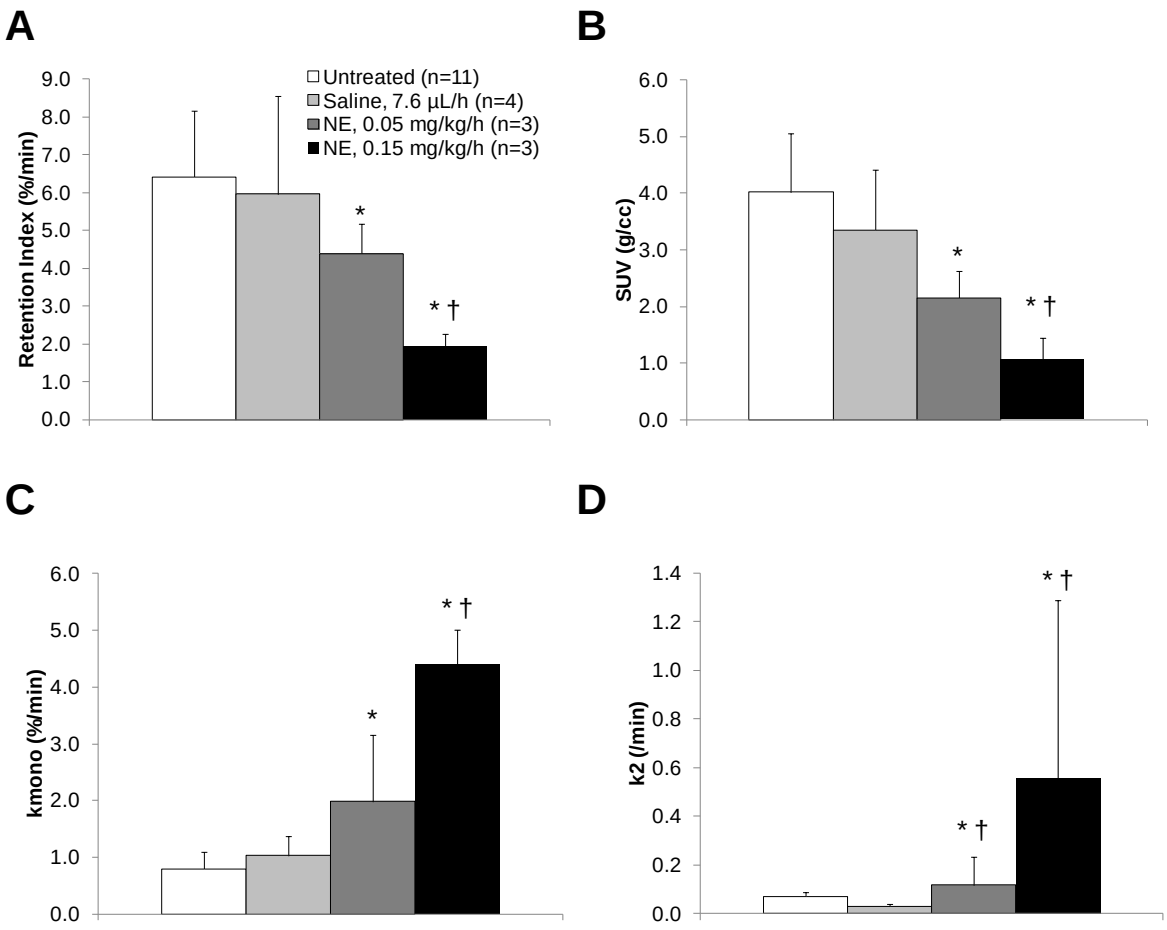

Figure 3.4 Quantitative HED analysis in untreated controls and rats treated with continuous infusion of saline or norepinephrine: (**A**) Retention index, (**B**) standardized uptake value, (**C**) monoexponential washout k_{mono}, and (**D**) one-compartment k_2. Mean ± SD. * $p<0.05$ to untreated controls, † $p<0.05$ to saline-infused rats, one-tailed t-test.

Table 3.3 Pearson correlations of plasma and cardiac norepinephrine levels to ^{11}C-HED retention.

HED Measurement	Plasma NE (r (p))	Cardiac NE (r (p))
Retention Index	-0.681(0.015)	-0.724(0.009)
Washout Rate	0.851(0.002)	0.957(0.000)
One-Compartment k2	0.788(0.003)	0.635(0.024)
Standard Uptake Value	-0.779(0.004)	-0.757(0.006)

Discussion

Repeatability of HED quantification is variable among methods. The average test-retest variability of 15±12% for retention index and 18.7±15.2% for SUV supports use of HED PET imaging for serial monitoring of the sympathetic nervous system in rodent models of cardiovascular disease. This is comparable to other receptor ligand PET tracers in small animals (Aznavour et al., 2009; Thomas et al., 2011). Of the methods tested, the clinically used retention index provided the most consistent test-retest repeatability. The present results suggest a greater sensitivity of washout measurements to norepinephrine levels. As such, monoexponential washout and one-compartment k2 measurements may be more influenced by the variability of tissue catecholamines and the increased sympathetic tone in rodents (Tipre et al., 2008).

Use of the retention index for quantification of HED kinetics assumes that steady state equilibrium is reached between tracer uptake and washout in late frames. While reasonable in human subjects (Link et al., 2003), this may not be an accurate assumption in rodents, which exhibit higher basal sympathetic tone and persistent washout following initial uptake, manifesting as a declination of the myocardial time activity curve (Law et al., 2010; Tipre et al., 2008). Moreover, retention index is affected by the blood input function, obtained from a volume of interest delineated on the left ventricle lumen, which is subject to spill-in of counts from the surrounding myocardium. The effect of myocardial spillover to the lumen is seen in relatively higher blood TAC in hearts of untreated rats compared to those treated with desipramine or norepinephrine. Spill-in to the image-derived input function results in an artificial reduction of the retention index. This phenomenon is evidenced in desipramine and norepinephrine treatment groups, wherein reduced myocardial counts contribute lower spill-in to the image-derived input function, generating lower blood TACs. Alternative measurements that are independent of the input function, such as SUV or monoexponential

washout may provide valuable quantitative data. Indeed, the relatively greater decrease in SUV (-85%) compared to retention index (-69%) following desipramine blockade reflects the contribution of the image-derived input function.

Previously, we and others have established that pretreatment with the NET inhibitor desipramine evokes up to 85% reduction in left ventricle accumulation of HED (Law et al., 1997; Rosenspire et al., 1990; Thackeray et al., 2007). Raffel et al demonstrated that increasing doses of the neurotoxin 6-hydroxydopamine resulted in reduced HED retention, proportional to the maximal binding of norepinephrine reuptake transporter assessed by [^{3}H]mazindol (Raffel et al., 2006). Administration of desipramine was shown to reduce cardiac retention of HED and [^{11}C]epinephrine in rats in vivo, predominantly due to enhanced tracer washout (Tipre et al., 2008). In the current study, the 68% reduction in cardiac retention index was directly comparable to the published reports in rats (Tipre et al., 2008). Because HED does not bind within the varicosity and exhibits limited vesicular retention (DeGrado et al., 1993), it is subject to passive diffusion across the neuronal membrane and active release with neurotransmitter. As such, measurement of HED retention reflects the cyclical reuptake and neuronal release of the tracer (DeGrado et al., 1993). The present data support this model, as myocardial time-activity curves in desipramine chase studies demonstrate enhanced tracer washout, relating to ablation of the uptake side of this equilibrium. Measurements of HED accumulation including retention index and SUV are highly sensitive to denervation and NET activity.

However, early stages of cardiac disease are not often characterized by autonomic denervation, but rather by hyperactivity of sympathetic neurons. While indirect evidence has suggested that augmented norepinephrine may reduce retention of HED (DeGrado et al., 1993), *in vivo* assessment is incomplete. Administration of the monoamine oxidase inhibitor tranylcypromine to increase endogenous monoamines, including norepinephrine, results in a

dose-dependent decrease in HED retention (Raffel and Wieland, 2001a; Thackeray et al., 2007). A similar dose-response was observed in *ex vivo* biodistribution during continuous infusion of exogenous norepinephrine (Thackeray et al., 2007). Studies in isolated perfused rat hearts have shown that addition of norepinephrine to the tissue bath enhances tracer clearance without impacting initial uptake (DeGrado et al., 1993). A previous clinical study failed to demonstrate a correlation between plasma norepinephrine levels and HED retention among patients with dilated cardiomyopathy (Hartmann et al., 1999). Recently, a significant correlation between HED washout rate (r=0.78) but not retention index (r=-0.41) and plasma norepinephrine concentration was demonstrated among 21 patients with nonischemic left ventricular dysfunction (Matsunari et al., 2010). Ungerer and colleagues established a correlation between regional HED retention and local tissue norepinephrine levels that bordered on statistical significance (Ungerer et al., 1998). The present results are consistent with increased competition for neuronal reuptake. The false neurotransmitters HED and the precursor metaraminol have similar affinity for the reuptake transporter as compared to endogenous norepinephrine (Raffel and Chen, 2004). Imaging studies in mice have shown that administration of metaraminol exceeding 9 μg/kg elicits a marked increase in HED washout and loss of specific HED retention in mice (Law et al., 2010). Importantly, HED injected dose was titrated to ensure that this threshold was not exceeded. Immunoblots of cardiac tissue confirmed that reduced HED retention in norepinephrine-treated rats was independent of altered NET protein expression. Previous evidence suggests that 3 to 5 days of elevated norepinephrine is necessary to evoke downregulation of the transporter (Mandela and Ordway, 2006).

An important consideration in interpreting the results is the physiological effect of the drugs administered. Pretreatment with desipramine administered by intraperitoneal injection did not affect heart rate. Shimizu and colleagues previously showed that treatment with

desipramine in combination with sympathetic nerve stimulation resulted in exponentially elevated dialysate norepinephrine and a marked increase in heart rate (Shimizu et al., 2009). In the present study, HPLC analysis confirmed that subcutaneous infusion of exogenous norepinephrine effectively elevated cardiac norepinephrine levels with no impact on heart rate. Additionally, the mild difference in HED measurements between untreated and saline-infused rats may reflect the influence of buprenorphine, a opioid partial agonist that results in elevated endorphins including catecholamines (Raymon and Leslie, 1994). Similarly, the impact of altered blood flow is not specifically addressed by this study. Adrenergic stimulation of coronary vessels would be expected to reduce bloodflow to the myocardium, resulting in reduced tracer delivery and uptake. The doses used in the present study are not expected to have this effect on cardiac perfusion.

The direct influence of norepinephrine on cardiac HED retention has important clinical significance. It has been stated that enhanced cardiac adrenergic activity is the first neurohormonal indication of left ventricular dysfunction (Rundqvist et al., 1997). Indeed, cardiac PET evaluation using the β-adrenoceptor antagonist [^{11}C]CGP12177 has predicted the success of beta-blocker therapy (Bristow et al., 2004). Moreover, recent studies have suggested that mismatch of perfusion and sympathetic nervous integrity, assessed by [^{11}C]epinephrine is a substrate of lethal ventricular arrhythmia in pigs (Sasano et al., 2008). This observation is supported by abnormal retention of HED in a porcine model of hibernating myocardium prone to sudden cardiac death by ventricular arrhythmia (Luisi et al., 2005). Taken with the current data, reduced tracer retention may relate to sympathetic hyperactivity, consistent with arrhythmogenic potential of heterogenous norepinephrine release at the margins of the infarct. A greater understanding of the factors influencing HED retention is beneficial to proper interpretation of clinical observations.

In conclusion, the repeatability of HED quantitative retention index, SUV, and monoexponential washout in rats between sessions and between subjects supports the suitability of small animal PET imaging for longitudinal tracking of cardiac sympathetic nervous function in health and disease states. This work underscores the complementary value of multiple quantification methods in the analysis of HED PET scans, particularly in small animals with heightened basal sympathetic tone. Moreover, each measurement reflect the physiological correlation to NET blockade and tissue and plasma norepinephrine concentration, supporting a multi-faceted approach to HED image analysis in rat models of cardiac disease.

Acknowledgments. This work is supported by grants from the Heart and Stroke Foundation of Ontario (NA6477, PRG 6242). JTT holds a Doctoral Research Award from the Heart and Stroke Foundation of Canada. RSB is a Career Investigator of the Heart and Stroke Foundation of Ontario. We thank Stephanie Thorn, Marc Lamoureux, colleagues in the Radiochemistry Laboratory and Animal Care and Veterinary Services for assistance in animal studies and with technical aspects of the manuscript.

Conflict of interest. The authors declare that they have no conflict of interest.

Chapter 4: Manuscript #3

Am J Nucl Med Mol Imaging. (In Press)

Altered sympathetic nervous system signaling in the diabetic heart: Emerging targets for molecular imaging

James Thackeray,[1,2] Rob S Beanlands,[1,2] Jean N DaSilva[1,2]

[1]Molecular Function & Imaging Program, National Cardiac PET Centre, University of Ottawa Heart Institute
[2]Department of Cellular & Molecular Medicine, Faculty of Graduate and Postdoctoral Studies, University of Ottawa

Key words: sympathetic neuronal imaging, SNS signaling, norepinephrine, β-adrenoceptor, norepinephrine reuptake transporter

Contribution of Authors

The literature review and composition of this manuscript was undertaken by the candidate, with editing assistance and corrections from Dr DaSilva. Dr Beanlands provided expertise on clinical perspective of the material.

Abstract

Diabetes is commonly associated with increased risk of cardiovascular morbidity and mortality. Perturbations in sympathetic nervous system (SNS) signaling have been linked to the progression of diabetic heart disease. Glucose, insulin, and free fatty acids contribute to elevated sympathetic nervous activity and norepinephrine release. Reduced left ventricular compliance and impaired cardiac function lead to further SNS activation. Chronic elevation of cardiac norepinephrine culminates in altered expression of pre- and post-synaptic sympathetic signaling elements, changes in calcium regulatory proteins, and abnormal contraction-excitation coupling. Clinically, these factors manifest as altered resting heart rate, depressed heart rate variability, and impaired cardiac autonomic reflex, which may contribute to elevated cardiovascular risk. Development of molecular imaging probes enable a comprehensive evaluation of cardiac SNS signaling at the neuron, postsynaptic receptor, and intracellular second messenger sites of signal transduction, providing mechanistic insights into cardiac pathology. This review will examine the evidence for abnormal SNS signaling in the diabetic heart and establish the physiological consequences of these changes, drawing from basic biological research in isolated heart and rodent models of diabetes, as well as from clinical reports. Particular attention will be paid to the use of molecular imaging approaches to non-invasively characterize and evaluate sympathetic signal transduction in diabetes, including pre-synaptic norepinephrine reuptake assessment using ^{11}C-*meta*-hydroxyephedrine (^{11}C-HED) with PET or ^{123}I-metaiodobenzylguanidine (^{123}I-MIBG) with SPECT, and post-synaptic β-adrenoceptor density measurements using CGP12177 derivatives. Finally, the review will attempt to define the future role of these non-invasive nuclear imaging techniques in diabetes research and clinical care.

Introduction

Diabetes is a prominent risk factor for the development of cardiovascular disease. Patients with diabetes carry 4 times greater risk of cardiovascular mortality, and constitute a disproportionate cohort of large scale heart failure studies. The interaction between diabetes and heart failure is diverse, with many pathways having been implicated. One factor in common between the conditions is impairment of the cardiac sympathetic nervous system (SNS), characterized initially by hyperactivity and elevated norepinephrine spillover, eventually culminating in sympathetic denervation and reduced capacity for norepinephrine release. Acute sympathetic activation evokes increased heart rate and contractility, whereas chronic activation can depress SNS sensitivity.

Continued advances in molecular imaging have led to the characterization of multiple radiotracers for the interrogation of the cardiac SNS. In a preclinical setting, longitudinal non-invasive imaging studies of sympathetic regulation during the development of diabetes and subsequent left ventricular dysfunction can provide important mechanistic insights into cardiac pathology. Long-term clinical application of imaging techniques could be used to stratify cardiovascular risk among diabetic patients.

Sympathetic Nervous System Signal Transduction

The autonomic nervous system is the primary extrinsic control of heart rate and contractility. Sympathetic projections from the central nervous system synapse at the stellate and thoracic ganglia, where postganglionic fibres project to the heart (Ardell, 2004; Crick S.J., 2000). A complex network of sympathetic neurons innervates the epicardium, with a homogeneous distribution of fibres to the entire heart. Localized varicosities (boutons) along the length of the terminal axon act as storage and release points of norepinephrine forming relatively dispersed synapses compared to central nervous system junctions (Ardell, 2004). Regional tissue concentrations of norepinephrine are considered the gold standard measurement of

cardiac sympathetic activation. The highest norepinephrine concentration is localized to the sinoatrial node, atrioventricular node, and atria as compared to the ventricles (Crick S.J., 2000). Sympathetic stimulation of the conduction system produces elevated heart rate.

Activation of sympathetic neurons evokes release of the neurotransmitter norepinephrine into the synaptic cleft where it binds to G protein-coupled adrenoceptors at the cardiomyocyte membrane (Brodde et al., 2006) (Fig 4.1). β-Adrenoceptors are positively coupled to stimulatory G protein $G\alpha_s$, which activates the cAMP/PKA signaling cascade, culminating in enhanced Ca^{2+} influx and cardiac contractility (Adams and Cuevas, 2004). The β_2- and β_3-adrenoceptor isoforms are also coupled to inhibitory G protein $G\alpha_i$, which reduces cAMP production, providing balance in noradrenergic signaling (Brodde et al., 2006).

The sympathetic signal is terminated by active recapture of the neurotransmitter into the neuronal varicosity by the sodium-dependent norepinephrine reuptake transporter (NET) via the uptake-1 pathway (Backs et al., 2001; Hoffman and Lefkowitz, 1995). Norepinephrine is further packaged into neuronal vesicles by vesicular monoamine transporter-2 (VMAT2) (DaSilva et al., 1993; Hoard et al., 2008) or metabolized by monoamineoxidase (MAO) and catechol-*O*-methyltransferase (COMT) (Raffel and Wieland, 2001a).

Diabetic Heart

Metabolic and Contractile Adaptation

The complex changes in metabolic and contractile cardiac function in the progression of diabetes have been extensively reviewed (Taegtmeyer et al., 2002; Young et al., 2002). Briefly, the diabetic heart exhibits a shift in metabolic substrate preference to almost exclusive utilization of fatty acids over glucose (Bruce et al., 2009; Kerbey et al., 1976). This shift exacerbates insulin resistance (Hajduch et al., 2008; Savage et al., 2005) and contributes to the accumulation of lipid metabolites (Huynh et al., 2012; Wang et al., 2011)

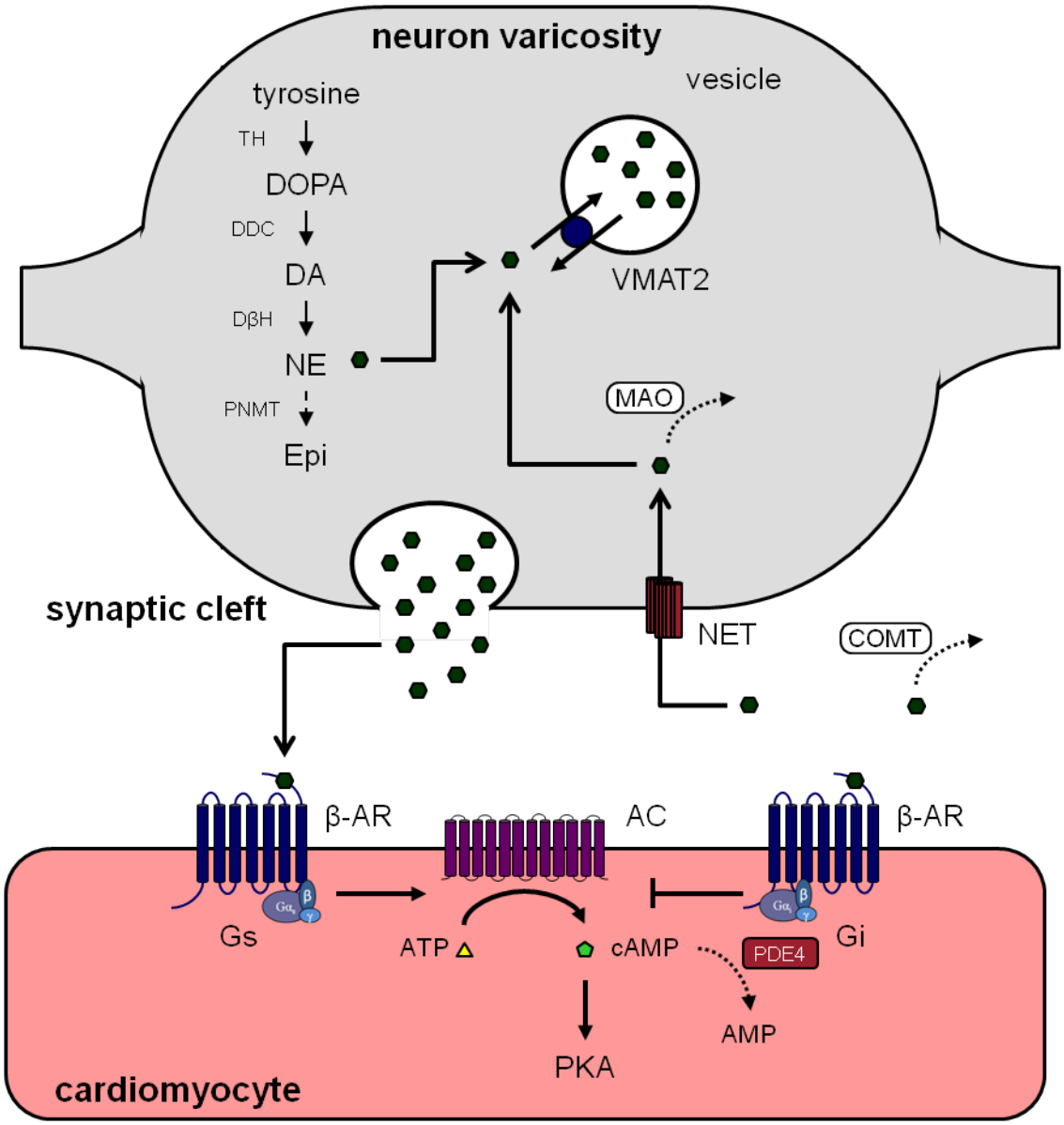

Figure 4.1 Noradrenergic neuroeffector junction. Norepinephrine (NE) is released into the synaptic cleft where it is bound by postsynaptic β-adrenoceptors (β-AR). Stimulation of G_s-coupled β-AR activate adenylate cyclase (AC) production of cAMP and downstream activation of protein kinase A (PKA). cAMP is broken down by phosphodiesterase-4 (PDE4). NE is recovered to the varicosity by NE reuptake transporter (NET). Abbreviations: TH, tyrosine hydroxylase; DOPA, dihydroxyphenylalanine; DDC, dopamine decarboxylase; DA, dopamine; DβH, dopamine β-hydroxylase; PNMT, phenetanolamine-*N*-methyltransferase; Epi, epinephrine; VMAT2, vesicular monoamine transporter-2; MAO, monoamine oxidase; COMT, catechol-O-methyltransferase.

and advanced glycation end products (Candido et al., 2003; Norton et al., 1996), leading to oxidative stress and myocardial fibrosis. These structural and metabolic changes culminate in the deterioration of contractile function, manifesting initially as reduced ventricular compliance and abnormal diastolic function, progressing to mild systolic impairment (Li et al., 2010a; Li et al., 2011). To compensate for failing systolic function, the SNS may be activated.

Circulating Factors

In addition to the compensatory activation, elevated plasma concentration of several factors have been shown to augment SNS activity. Elevated endogenous or exogenous glucose produces elevated circulating levels of norepinephrine (Ganguly et al., 1987; Levin et al., 1998; Thackeray et al., 2011b). Similarly, hyperinsulinemia has been linked to increased SNS activity (Fein et al., 1981; Kern et al., 2005). Administration of exogenous fatty acids enhances muscle sympathetic nerve activity by 45%, with resultant increases in heart rate and blood pressure (Florian and Pawelczyk).

Diabetic Cardiac Autonomic Neuropathy

Diabetic autonomic neuropathy is a late stage complication of prolonged diabetes characterized by the development of neuroaxonal dystrophy, a swelling of distal neuronal axons without relative neuron loss (Schmidt et al., 2003b). Whereas early diabetes has been associated with elevated sympathetic tone, autonomic neuropathy results in a decrease in cardiac norepinephrine content and an accumulation of neurotrophins consistent with damage sustained by sympathetic neurons (Ieda and Fukuda, 2009; Schmid et al., 1999). Accumulation of advanced glycation end products, activation of apoptotic signals, oxidative stress, and elevated basal firing rate contribute to the degeneration of sympathetic neurons (Ewing et al., 1986; Stevens et al., 1998a).

SNS in Diabetes

The presence of abnormal SNS signaling in the diabetic heart has been well established, as evidenced by direct and indirect measurements. It is unclear as to the order of sympathetic hyperactivity and development of insulin resistance, with some investigators purporting that insulin resistance is precipitated by a primary increase in sympathetic tone (Facchini et al., 1996; Landsberg et al., 1984), and others claiming independent development of insulin resistance and hyperinsulinemia promoting sympathetic drive (Jamerson et al., 1993). Because of the complex interaction of SNS activity, hyperglycemia, hyperinsulinemia, metabolism, and insulin resistance it is difficult to define the primary insult. Recent clinical evaluations have attempted to define a temporal progression from sympathoadrenal activation to insulin resistance. A recent meta-analysis has suggested that SNS dysfunction is present in 51.9% of diabetic patients, but is likely underestimated due to reliance on somewhat crude tests (Jyotsna et al., 2009).

Norepinephrine Measurements

Elevated norepinephrine turnover and accumulation of neuronal norepinephrine have been found in diabetic animal models. Ganguly and colleagues demonstrated a twofold increase in cardiac and plasma norepinephrine concentration after 8 weeks of diabetes induced by streptozotocin (STZ) in rats (Ganguly et al., 1987). Studies in isolated perfused diabetic hearts revealed enhanced catecholamine turnover, evidenced by elevated tyramine-induced norepinephrine release, increased initial rate of uptake of ^{3}H-norepinephrine, and reduced half time of ^{3}H-norepinephrine turnover. These parameters were normalized by treatment with insulin at 4 weeks after diabetes induction (Ganguly et al., 1987; Ganguly et al., 1986). Elevated norepinephrine levels have been described in a number of animal models and durations of diabetes, including STZ-induced type 1 diabetes (Akiyama et al., 1989), insulin-resistant intraperitoneal STZ-induced diabetes (Marsh et al., 2009; Thackeray et al., 2011b),

Zucker Diabetic Fatty rats (Marsh et al., 2007), and non-obese Goto-Kakizaki type 2 diabetic rats (Kiyono et al., 2002a).

These findings are supported by histofluorescence studies using glyoxylic acid, demonstrating increased fluorescent noradrenergic varicosities after 1 month of STZ-induced diabetes. In the same study, high performance liquid chromatography-quantified ventricular norepinephrine levels were elevated by 48-58% in 1 month diabetics compared to controls (Felten et al., 1982). At 4 weeks of diabetes, STZ rats show reduced dopamine content in stellate ganglia, but an increase of ventricular norepinephrine, suggesting enhanced local conversion of neurotransmitter. No change in brain or plasma norepinephrine content was observed at this time point (Gallego et al., 2003).

Sympathetic Nerve Activity

Electrode measurement of renal sympathetic nerve activity showed a reduced ability to adapt to volume expansion in STZ diabetic rats compared to controls, associated with a blunted change in heart rate following phenylephrine administration (Patel and Zhang, 1995). Splanchnic sympathetic nerve activity response to phenylephrine was dampened in obese adult Zucker rats compared to age-matched lean Zucker rats in the absence of overt diabetes (Schreihofer et al., 2007).

Baroreceptor Reflex

The baroreceptor reflex is an indirect indicator of SNS activation in the heart, reflecting responsiveness to α-adrenergic stimulation. Left aortic depressor nerve activity measurements taken in OVE26 transgenic type 1 diabetic mice demonstrated a reduction in baroreflex control of heart rate in response to phenylephrine or sodium nitroprusside (Gu et al., 2008). Pressure transducer evaluation in type 1 diabetic rats at baseline compared to non-diabetic controls describe reduced mean arterial pressure (-12%), heart rate (-13%) and lower

rates of isolvolumic pressure development and decay following phenylephrine challenge (Borges et al., 2006).

Heart Rate Variability

Advancement of implantable telemetry transducer/receiver technology has facilitated longitudinal analysis of sympathetic tone in diabetic rats. Power spectral analysis provides a surrogate measurement of baroreceptor reflex activity and the quantification of heart rate variability (Bertram et al., 2000; Kuwahara et al., 1994; Mills et al., 2000; Ramaekers et al., 2002).

Heart rate variability (standard deviation of normal heart rhythm, SDNN) has been demonstrated to be reduced by 50% (18 vs 36 bpm) within days of diabetes induction by STZ compared to non-diabetic controls (Howarth et al., 2005a; Howarth et al., 2005b). Low frequency to high frequency power ratio progressively increased over time, suggesting declination of high frequency (parasympathetic) and mid frequency (sympathetic) density (Howarth et al., 2005b). Treatment with insulin was insufficient to restore heart rate variability to control levels, though there was a a modest recovery of heart rate: 362 vs 266 vs 303 bpm in non-diabetic, diabetic, and insulin-treated diabetic rats, respectively (Howarth et al., 2006).

In Goto-Kakizaki non-obese type 2 diabetic rats a less prominent but significant reduction of heart rate variability SDNN compared to non-diabetic controls was observed at 2 months (-24%) and 7 months (-16%), but was attenuated at 15 months of age (-5%) (Howarth et al., 2008). This is consistent with reduced heart rate variability during aging (Howarth et al., 2008), with parallel changes in NET expression and reuptake function reported (Kiyono et al., 2002b). The differences in heart rhythm derive in part from extended duration of electrocardiogram QRS complex with no difference in QT interval between groups (Howarth

et al., 2008). Prolonged QRS is consistent with delayed repolarization as observed in STZ rats (Chen et al., 2009; Gallego and Casis, 2001; Hekimian et al., 1985).

Continuous telemetric monitoring in db/db type 2 diabetic mice describes a blunting of baroreflex regulation of heart rate, calculated by sequence method and cross-spectral analysis. Whereas blockade of sympathetic signaling with metoprolol decreased heart rate substantively in db/db mice, the effect was negligible in db/+ mice, consistent with constitutive activation of the cardiac SNS (Goncalves et al., 2009). Atropine blockade of parasympathetic tone was also blunted in db/db mice compared to db/+ controls (Goncalves et al., 2009). Conversely, study of non-obese diabetic mice showed the presence of sympathetic neuropathy, evidenced by elevated baroreceptor reflex activity that was not attenuated by metoprolol administration (Gross et al., 2008). Heart rate variability measurement demonstrated reduced standard deviation of R-R interval in db/db mice compared to db/+ controls (Goncalves et al., 2009).

Power spectrum density analysis of systolic arterial pressure in diabetic rats revealed a progressive reduction of intermediate frequency (0.25-0.65 Hz), the range generally corresponding to sympathetic modulation of vascular tone, remaining fairly consistent over 1 to 18 weeks after STZ induction of diabetes (Fazan et al., 1997).

These findings have been replicated in the clinical population. A study of young Norwegian males demonstrated that those in the highest quartile elevation of plasma norepinephrine during cold pressor test showed elevation of fasting plasma glucose level and homeostasis model assessment of insulin resistance at 18-years follow-up. This observation suggests that early sympathetic dysfunction may partially underlie subsequent development of insulin resistance and pre-diabetes (Flaa et al., 2008). A similar result was obtained by heart rate variability analysis over 8 year follow up in the Atherosclerosis Risk in Communities (ARIC) trial. In this case, individuals falling in the lowest quartile of heart rate variability (either

standard deviation of R-R interval or low-frequency power) were 60% more likely than the highest quartile to develop insulin resistance or diabetes (Carnethon et al., 2003a). It has been reasoned that sustained sympathetic activation may augment lipid metabolism, leading to elevated circulating fatty acids and insulin resistance (Carnethon et al., 2003a).

β-Adrenoceptor Expression

The persistent elevation of catecholamines evokes downregulation of cardiomyocyte β-adrenoceptors, and a shift in the isoform population to favour G_i-coupled β_2-adrenoceptors. This pattern is well characterized in the development of heart failure (Bristow, 1993; Dell'Italia and Ardell, 2004), and has been extensively described in diabetes as well, including rats (Dincer et al., 2001; Sellers and Chess-Williams, 2001), large animal models (Avendano et al., 1999), and the patient population (Swan et al., 1997). Reduced β-adrenoceptor expression has been consistently described in type 1 diabetic heart (Table 4.1), evidenced by significant reductions in total β-adrenoceptor binding in radioligand binding assays (Atkins et al., 1985; Beenen et al., 1997; Dincer et al., 2001; Ingebretsen et al., 1983; Kashiwagi et al., 1989; Latifpour and McNeill, 1984; Matsuda et al., 1999).

Latifpour and McNeill established time dependent changes in cardiac autonomic receptor expression patterns in type 1 diabetic STZ-treated rats (Latifpour and McNeill, 1984). At 3 months of diabetes compared to age-matched non-diabetic controls, only ^{3}H-prazosin binding to α-adrenoceptors was reduced (B_{max} 66.6 vs 78.8 fmol/mg protein), with no difference in ^{3}H-dihydroalprenolol or ^{3}H-quinuclidinyl benzilate binding to β-adrenoceptors and muscarinic cholinergic receptors, respectively. By 6 months of untreated diabetes, binding to all three receptors was reduced by 21-28% (α-adrenoceptor: 56.4 vs 72.2; β-adrenoceptor: 22.5 vs 28.6; muscarinic: 84.8 vs 117.4 fmol/mg protein) (Latifpour and McNeill, 1984).

Reduced β-adrenoceptor density in diabetes reflects a shift in relative expression of β-

Table 4.1 β-Adrenoceptor Expression in Diabetic Heart

Diabetic Model	Duration	Measurement	Isoform(s)	B_{max} *	% Diff†	Ref
SD, alloxan 35 mg/kg iv	5 days	^{3}H-DHA binding	all	47±4	-51%	a
SD, STZ 65 mg/kg ip	2 weeks	^{3}H-DHA binding	all	35±4	-6%	b
		CGP20712 block, high affinity	β_1AR	10±1	-46%	
		CGP20712 block, low affinity	β_2AR	24±1	+37%	
WK, STZ 45 mg/kg iv	4-6 weeks	^{3}H-CGP12177 binding	all	33±7	-51%	c
WK, STZ 60 mg/kg iv	6 weeks	Western immunoblotting	β_1AR		-65%	d
			β_2AR		+61%	
			β_3AR		+140%	
WK, STZ 55mg/kg iv	8 weeks	^{125}I- CYP binding	all	36±4	-31%	e
SHR, STZ 55 mg/kg iv	8 weeks	^{125}I- CYP binding	all	35±5	-34%	e
SD, STZ 45 mg/kg ip,	8 weeks	^{3}H-CGP12177 *ex vivo* biodist.	all		-40%	f
high fat feeding		Western immunoblotting	β_1AR		-15%	
			β_2AR		+12%	
SD, STZ 65 mg/kg iv	10 weeks	^{3}H-CGP12177 binding	all	92±4‡	-41%	g
WK, STZ 45 mg/kg iv	14 weeks	Western immunoblotting	β_1AR		-45%	h
			β_2AR		-17%	
			β_3AR		+200%	
SD, STZ 65 mg/kg iv	13 weeks	^{3}H-DHA binding	all	28±3	-13%	i
	26 weeks			23±2	-21%	

* fmol/mg protein; † (Diabetic – Control) / Control × 100%; ‡ fmol/10^6 cells
SD, Sprague Dawley rat; WK, Wistar Kyoto rat; SHR, Spontaneously Hypertensive Rat; DHA, dihydroalprenolol; ^{125}I-CYP, ^{125}I-cyanopindolol; biodist, biodistribution

a (Ingebretsen et al., 1983)
b (Sellers and Chess-Williams, 2001)
c (Matsuda et al., 1999)
d (Sharma et al., 2008b)
e (Beenen et al., 1997)
f (Thackeray et al., 2011a)
g (Kashiwagi et al., 1989)
h (Dincer et al., 2001)
i (Latifpour and McNeill, 1984)

adrenoceptor subtypes as determined by Western immunoblotting (Dincer et al., 2001). Quantification of Coomassie staining showed a shift in β_1:β_2:β_3 expression profile from 62:30:8 in control to 40:36:23 in diabetic rat hearts (Dincer et al., 2001). This shift is similar to that observed during sympathetic hyperactivity in the development of heart failure (Bristow, 1993). In the same study, normalization of blood glucose by daily insulin injection for only 2 weeks following 12 weeks of chronic diabetes was sufficient to revert expression patterns to normal, with a β_1:β_2:β_3 expression profile of 57:33:10 (Dincer et al., 2001). Displacement of ^{3}H-dihydroalprenolol by cold CGP20712 to distinguish high affinity β_1-adrenoceptor binding from low affinity β_2-adrenoceptor identified a shift in relative expression (β_1:β_2) from 52:48 in control to 30:70 in untreated diabetics, restored to 40:60 by insulin (Sellers and Chess-Williams, 2001). These findings establish the critical involvement of glycemia in the maintenance of β-adrenoceptor expression.

After 2.5 months of diabetes, internalization of β-adrenoceptors is evident, as determined by binding assays with the cell-surface impermeable ^{3}H-CGP12177 compared to lipophilic ^{125}I-iodocyanopindolol (Kashiwagi et al., 1989). This observation suggests an increase in the internalization of β-adrenoceptors during diabetes, prior to overt degradation, which, in the context of other dihydroalprenolol studies, is suggested to occur by 6 months of diabetes. Treatment over 48 hours with insulin partially restored membrane surface ^{3}H-CGP12177 binding sites (Kashiwagi et al., 1989). The rapid response to insulin suggests that early internalization and impairment of β-adrenoceptor signaling is readily reversible by glycemic control.

The altered expression patterns of myocardial β-adrenoceptors bear functional consequences. The reduced maximum rate of left ventricle dP/dt_{max} was associated with a reduction of isoproterenol-induced adenylate cyclase activity after 4 weeks of untreated diabetes, suggesting alteration of upstream signaling mediators (Atkins et al., 1985). Paradoxically,

pressure transducer evaluation in type 1 diabetic rats following administration of low-dose β_1-adrenoceptor agonist dobutamine (1 μg/kg) showed nearly double maximal isovolumic pressure development and decay compared to controls. Insulin treatment normalized the response in diabetic rats. This suggests an increased sensitivity to β-adrenergic stimulation, consistent with an upregulation of β_1-adrenoceptors (Borges et al., 2006). However, no attempt to quantify adrenoceptors was performed in this study.

In isolated perfused diabetic hearts (6 weeks post STZ), left ventricular developed pressure was significantly lower than controls by as much as 50% at higher left atrial filling pressure, associated with a 50% reduction in relative β_1-adrenoceptor expression (Sharma et al., 2008b). Treatment with the β_1-adrenoceptor antagonist metoprolol not only increased expression of β-adrenoceptors in diabetic hearts, but also improved mechanical performance in left ventricular pressures (Sharma et al., 2008b). Sharma and colleagues further demonstrated concomitant improvement in metabolic performance in metoprolol-treated rats, characterized by an 80% increase in glucose oxidation, 39% decrease of palmitate oxidation, driven in part by a reduction in carnitine palmitoyl transferase-1B expression and activity (Sharma et al., 2009; Sharma et al., 2008a).

Downstream Noradrenergic Signaling

In addition to changes in innervation and receptors, downstream targets of the SNS have also been studied in diabetes. As early as 8 days after diabetes induction, the response of adenylate cyclase to β-adrenergic stimulation was ablated, whereas other pathways of adenylate cyclase activation remained intact (Gotzsche, 1983). No difference in dihydroalprenolol binding was observed (Gotzsche, 1983), suggesting a functional uncoupling of adenylate cyclase from myocardial β-adrenoceptors. Additional evidence suggests that adenylate cyclase and cAMP inotropic effects are independently impaired in diabetes, with reduced contractile force observed in isolated perfused hearts following

stimulation with adenylate cyclase activator forskolin, exogenous dibutyryl cAMP, or 3-isobutyl-1-methylxanthine (IBMX) (Gando et al., 1997). Reduced expression of β-adrenoceptors in isolated perfused 4 week diabetic heart also affects calcium mobilization, wherein diabetic rats exhibit lower intracellular Ca^{2+} following stimulation with isoproterenol (op den Buijs et al., 2005). This anomaly would impair the contractile response to sympathetic stimulation and stress.

SNS Imaging Targets with PET and SPECT

Tracer-based imaging of the SNS has gained traction in recent years, progressing toward more mainstream clinical application. Targets of molecular imaging include evaluation of neuron integrity at the NET and evaluation of postsynaptic expression of β-adrenoceptors at the cardiomyocyte membrane (reviewed in (Raffel and Wieland, 2001a; Yoshinaga et al., 2005)) (Fig 4.2A). Additional autonomic targets include muscarinic receptors (Delahaye et al., 2001), angiotensin II type 1 receptors (Hadizad et al., 2009; Higuchi et al., 2010) and intracellular signaling elements phosphodiesterase-4 (DaSilva et al., 2002) and diacylglycerol (Otani et al., 2005), though the validation of these tracers is at present unclear (Kenk et al., 2011). The bulk of SNS imaging has been focused on presynaptic measurements of reuptake function and postsynaptic adrenoceptor density.

Neuronal imaging agents are generally analogues of norepinephrine (Fig 4.2B), that are taken up via the sodium-dependent NET (uptake-1) pathway. In SPECT, the prevalent tracer is radio-iodinated metaiodobenzylguanidine (^{123}I-MIBG). Availability and regulation has limited ^{123}I-MIBG use to research purposes, but recent advances have revealed an added-value of neuronal imaging using ^{123}I-MIBG among heart failure patients, which may accelerate its application as a clinical diagnostic tool (Bravo and Bengel, 2011; Jacobson et al., 2010). In PET, ^{11}C-*meta*-hydroxyephedrine (^{11}C-HED), ^{11}C-phenylephrine, and

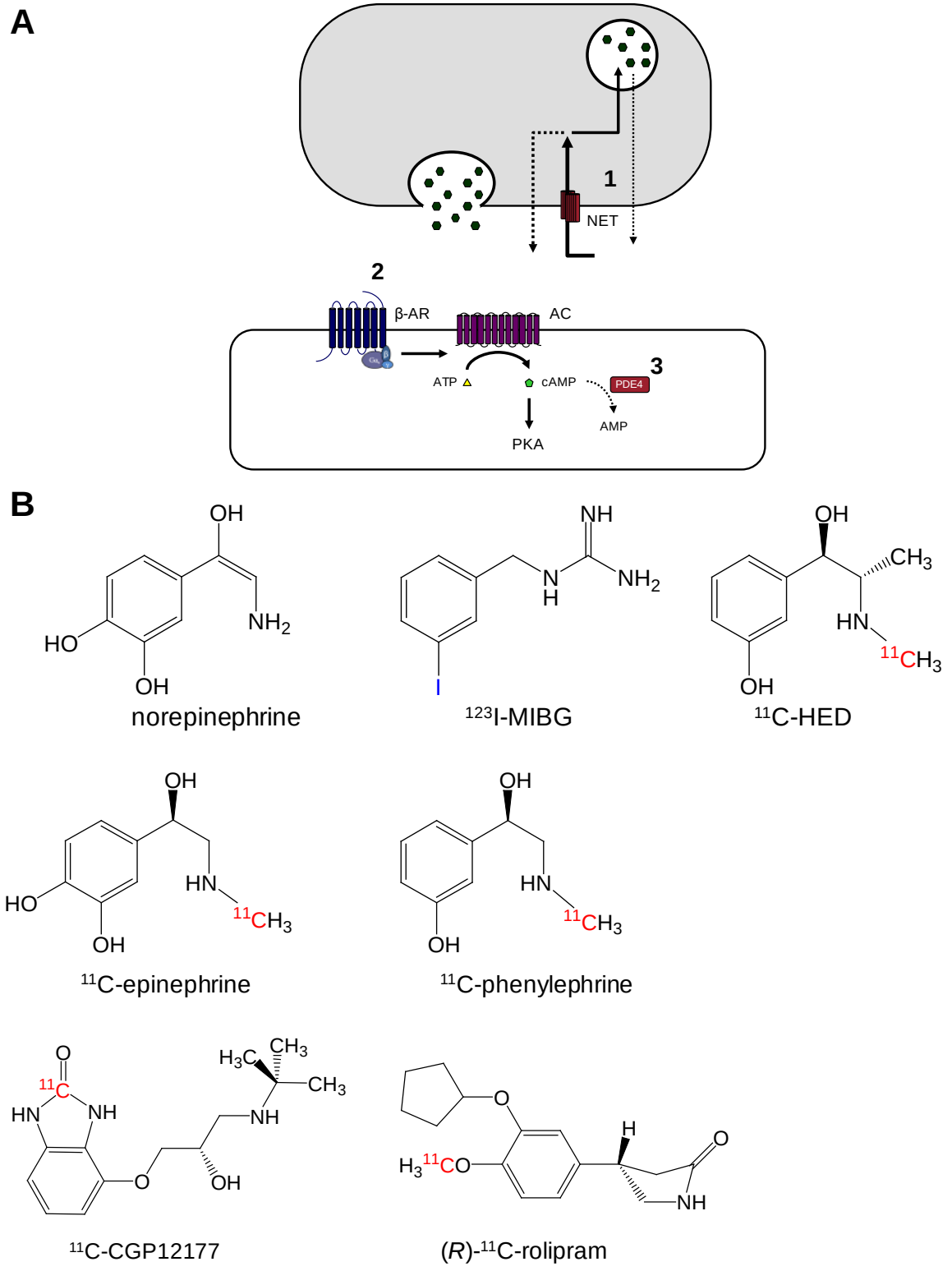

Figure 4.2 Established probes for evaluation of cardiac SNS. (**A**) Targets for molecular imaging in the sympathetic signaling include (**1**) presynaptic nervous integrity at NET; (**2**) postsynaptic β-AR density; and (**3**) indirect evaluation of cAMP levels and PKA activation at PDE4. (**B**) Chemical structures of probes for neurohormonal interrogation.

^{11}C-epinephrine have been evaluated with varying degrees of success (reviewed in (Lautamaki et al., 2007; Raffel and Wieland, 2001a)). The development, characterization, and application of these radiotracers have been extensively studied and reviewed (Lautamaki et al., 2007; Raffel and Wieland, 2001a; Tipre et al., 2008).

^{123}I-MIBG SPECT Imaging

Briefly, retention of ^{123}I-MIBG was shown to be reduced by blockade of NET (uptake-1) (DeGrado et al., 1993) and following sympathectomy by phenol application in the canine heart (Dae et al., 1992), though a high degree of extraneuronal uptake (via uptake-2) is consistently observed in many animal species. Heart transplant recipients reflect this observation, with a complete lack of early and late ^{123}I-MIBG uptake by myocardium devoid of sympathetic innervation (Raffel and Wieland, 2001a). ^{123}I-MIBG has been applied in nuclear cardiology to examine post-myocardial infarct healing (Kasama et al., 2007; Kasama et al., 2011), arrhythmia (Bax et al., 2008; Boogers et al., 2010), and progression of congestive heart failure (Currie et al., 2011). Reduced contrast between the heart and the mediastinum is characteristic of impaired neuronal function, which also manifests as enhanced late tracer washout (Boogers et al., 2010; Jacobson et al., 2010; Narula and Sarkar, 2003).

^{11}C-HED PET Imaging

Advantages of the PET tracer ^{11}C-HED include high neuronal compared to extraneuronal uptake (Raffel and Chen, 2004), long neuronal retention time due to partial packaging in vesicles (Wieland et al., 1990), and metabolic stability due to resistance to catecholamine metabolism by MAO or COMT (Fuller et al., 1981). Due to its lipophilicity, ^{11}C-HED can passively diffuse from the neuronal varicosity, and is also subject to active release during signal transduction. Kinetic studies have demonstrated the dependence of ^{11}C-HED retention on the availability of NET, established as susceptibility to blockade or displacement by the

NET inhibitor desipramine. This has been observed in isolated perfused rat heart (DeGrado et al., 1993), *ex vivo* biodistribution in rats (Law et al., 1997; Rosenspire et al., 1990; Thackeray et al., 2007) and dogs (Caldwell et al., 1998; DeGrado et al., 1993) and more recently using small animal PET in rats (Tipre et al., 2008) and mice (Law et al., 2010). Retention of ^{11}C-HED is also subject to competition for limited reuptake sites with endogenous and exogenous neurotransmitter, as demonstrated by treatments with the precursor and false neurotransmitter metaraminol (Law et al., 1997; Law et al., 2010), treatments to enhance endogenous norepinephrine such as tranylcypromine (Thackeray et al., 2007) and by infusion of exogenous norepinephrine (Thackeray et al., 2007). Clinical applications of ^{11}C-HED have included post-infarct neuronal remodeling (Allman et al., 1993), tracking of post-transplant reinnervation (Bengel et al., 2002b; Schwaiger et al., 1991), arrhythmia (Kies et al., 2004; Sasano et al., 2008), congestive heart failure (Hartmann et al., 1999; Ungerer et al., 1993; Ungerer et al., 2000), hibernating myocardium (John et al., 2007; Luisi et al., 2005), hypertrophic cardiomyopathy (Schafers et al., 1998), and coronary artery disease (Bulow et al., 2003). Evaluation of ^{11}C-HED in rats (Fig 4.3A) has demonstrated similar image quality to clinical images (Fig 4.3B), though accelerated tracer washout due to heightened basal sympathetic tone is observed in rats compared to humans (Tipre et al., 2008).

^{11}C-Phenylephrine is subject to metabolism by MAO to ^{11}C-methylamine, complicating kinetic modeling (Del Rosario et al., 1996; Tipre et al., 2008). ^{11}C-Epinephrine holds promise as a sympathetic neuronal marker with the added complication of labeled metabolites (Nguyen et al., 1997; Tipre et al., 2008). Retention properties of both of these tracers are similar to ^{11}C-HED, with advantageous and disadvantageous characteristics (reviewed in (Raffel and Wieland, 2001a)). Effectively, retention of ^{123}I-MIBG or ^{11}C-HED provides a dynamic semi-quantitative measurement of reuptake, storage, and release of norepinephrine from myocardial sympathetic neuronal varicosities.

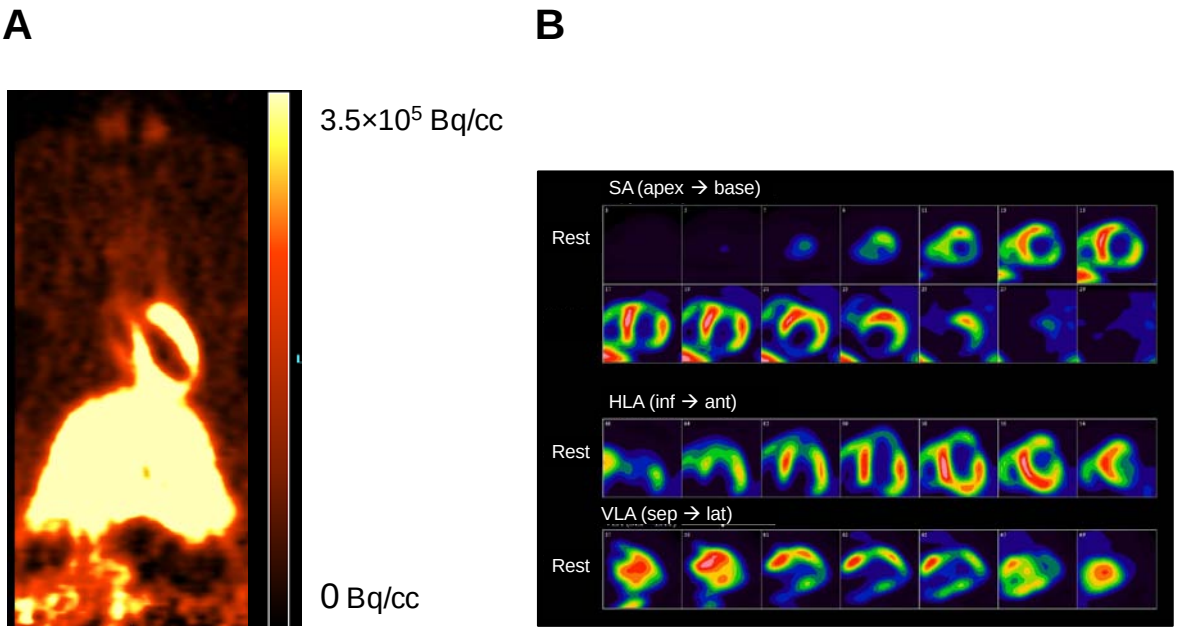

Figure 4.3 Sample ^{11}C-HED myocardial images. (**A**) Rat ^{11}C-HED coronal image obtained using Siemens Inveon DPET small animal camera showing heart and liver uptake. (**B**) Reoriented ^{11}C-HED PET cardiac image from a patient with obstructive sleep apnea obtained using GE Discovery D690 PET/VCT 64 camera.

^{11}C-CGP12177 PET Imaging

Non-invasive determination of β-adrenoceptor density is another target of interest in imaging the cardiac SNS. The bulk of research has been conducted using the non-selective ^{11}C-CGP12177 and its derivatives (Fig 4.2B). Labeled with tritium, CGP12177 has been utilized in binding assays to determine β-adrenoceptor density ex vivo (Affolter et al., 1985; Mohell and Dicker, 1989). As a radiotracer, CGP12177 shows high and sustained uptake in myocardium compared to surrounding tissues in rat hearts, and is selectively blocked up to 90% by β-blockers propranolol, atenolol and unlabeled compound (Thackeray et al., 2011a; Van Waarde et al., 1995b). Complicated synthesis has limited the use of ^{11}C-CGP12177 to some extent, though some clinical applications have emerged, including use in post-myocardial infarction (Link et al., 2003), heart failure (Caldwell et al., 2008; Ungerer et al., 2000), hibernating myocardium (John et al., 2007), and non-ischemic cardiomyopathy (Naya et al., 2009; Tsukamoto et al., 2007). A correlation has been described between pre- and post-synaptic function, as assessed with ^{11}C-HED and ^{11}C-CGP12177, respectively, with similar reduction in sympathetic neuron integrity and myocardial β-adrenoceptor density observed among subjects with congestive heart failure (Caldwell et al., 2008; Ungerer et al., 1993). A similar correlation was described to early and delayed late heart-to-mediastinal ratio of ^{123}I-MIBG (Tsukamoto et al., 2007). In a small scale trial in patients with stable chronic heart failure due to idiopathic cardiomyopathy, β-adrenoceptor density measured by ^{11}C-CGP12177 PET predicted 20 month response to carvedilol treatment, wherein the patients with the lowest CGP12177 binding showed the greatest improvement in left ventricular ejection fraction (Naya et al., 2009). Application of CGP12177 in the diabetic heart has been limited to preclinical evaluations, but ex vivo biodistribution studies suggest that CGP12177 is a suitable radiotracer for longitudinal evaluation of β-adrenoceptor density in the diabetic heart (Thackeray et al., 2011a).

(R)-^{11}C-Rolipram PET Imaging

(*R*)-^{11}C-Rolipram (Fig 4.2B) has been characterized in small animals for evaluation of phosphodiesterase-4 expression in the heart, providing an indirect index of intracellular cAMP activation. Preliminary evaluation of (*R*)-^{11}C-rolipram imaging has illustrated quality myocardium-to-blood and myocardium-to-background contrast and specific binding in rats (Fig 4.4AB) and dogs (Fig 4.4C) (Lortie et al., 2012; Thomas et al., 2011). Cardiac binding of (*R*)-^{11}C-rolipram was enhanced by treatments elevating endogenous norepinephrine and reduced when phosphodiesterase-4 is blocked (Kenk et al., 2007; Thomas et al., 2011). By contrast in animal models of chronic obesity and acute adriamycin-induced cardiotoxicity, characterized by elevated sympathetic drive and catecholamine levels, no increase in (*R*)-^{11}C-rolipram cardiac binding was observed in response to blockade of the NET by desipramine and increased synaptic norepinephrine (Greene et al., 2009; Kenk et al., 2010). This finding is consistent with downregulation of β-adrenoceptors.

Preclinical Imaging of SNS in Diabetes

The development of specific radiotracers and dedicated small animal imaging systems has facilitated the interrogation of cardiac sympathetic nervous integrity in rodent models of diabetes using SPECT and PET imaging, ex vivo biodistribution, and autoradiography techniques (Table 4.2).

^{123}I-MIBG Preclinical Imaging in Diabetes

A small number of preliminary imaging studies have been conducted using radioiodinated ^{123}I-MIBG in diabetic rodents. Small animal SPECT imaging revealed maintained uptake but enhanced myocardial washout of ^{123}I-MIBG over 30-120 min after injection among STZ diabetic C57/Bl6 mice compared to controls (41 vs 21%). Liver washout and urinary

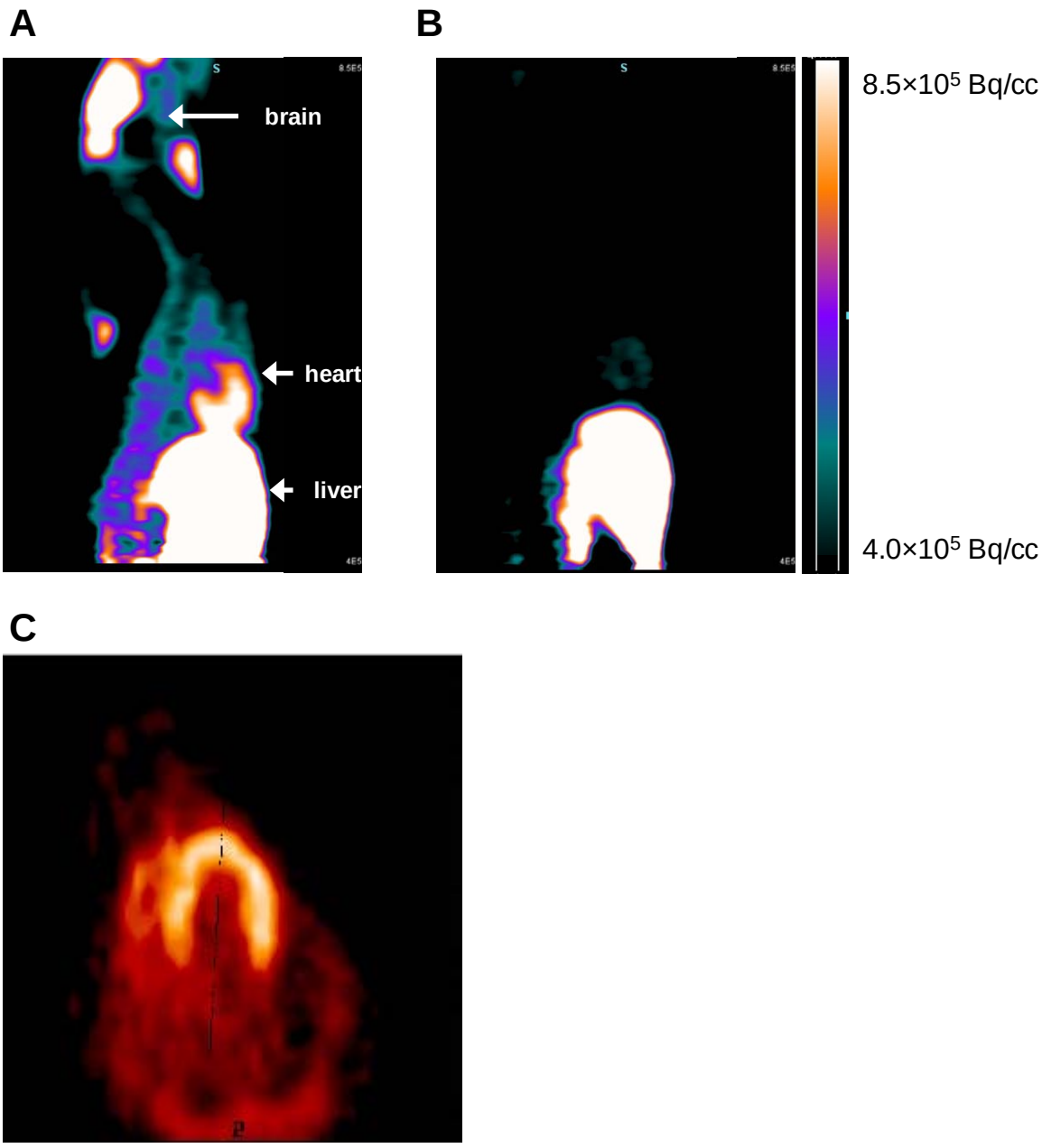

Figure 4.4 Sample (*R*)-^{11}C-rolipram images. (**A**) Rat (*R*)-^{11}C-rolipram sagittal whole body image obtained using Siemens Inveon DPET small animal camera showing heart, brain, and liver uptake. (**B**) Coinjection of cold (*R*)-rolipram blocks the specific binding of (*R*)-^{11}C-rolipram to phosphodiesterase-4 in brain and heart. (**C**) Summed canine (*R*)-^{11}C-rolipram coronal image obtained using ECAT-ART cardiac PET camera shows myocardial uptake.

Table 4.2 Summary of Preclinical Myocardial Presynaptic Imaging Studies in Diabetic Rodents

Model	Duration	Tracer	Method	Finding	Ref
SD, STZ 55 mg/kg iv	4 weeks	^{125}I-MIBG	*ex vivo* autoradiography	-13% inferior LV retention	a
SD, STZ 45 mg/kg ip, high fat feeding	8 weeks	^{11}C-HED	*ex vivo* biodistribution	-12% LV retention	b
WK, STZ 50 mg/kg ip	6 months	^{11}C-HED	*ex vivo* biodistribution	-33% distal LV retention	c
	9 months			-40% proximal LV retention -44% distal LV retention	
Goto Kakizaki	8 weeks	^{125}I-MIBG	*ex vivo* autoradiography	-23% anterior LV retention -41% inferior LV retention	d
WK, STZ 60 mg/kg iv	8 weeks	^{123}I-MIBG	pinhole SPECT	-58% counts x kg / pixel +61% washout rate	e
SHR, STZ 60 mg/kg	8 weeks	^{123}I-MIBG	pinhole SPECT	-58% counts x kg / pixel +34% washout rate	e
Zucker Obese	22 weeks	^{123}I-MIBG	pinhole SPECT	+272% counts x kg / pixel +44% washout rate	e
WK, STZ 60 mg/kg iv	8 weeks	^{123}I-MIBG	small animal SPECT	+64% washout rate	f
mice, STZ 35 mg/kg ip × 5d	7 months	^{123}I-MIBG	small animal SPECT	+95% LV washout rate +14% initial LV uptake	g

SD, Sprague Dawley; WK, Wistar Kyoto; SHR, Spotaneously Hypertensive Rat; ^{123}I-MIBG, metaiodobenzylguanidine; ^{11}C-HED, hydroxyephedrine

a (Kiyono et al., 2001)
b (Thackeray et al., 2011b)
c (Schmid et al., 1999)
d (Kiyono et al., 2002a)
e (Dubois et al., 1996)
f (Goethals et al., 2009)
g (Kusmic et al., 2008)

excretion were also accelerated. ^{3}H-Desipramine binding assay demonstrated a reduction of NET density (B_{max}) in hearts of diabetic compared to non-diabetic mice (136 vs 244 fmol/mg protein) with no change in binding affinity (k_d) (Kusmic et al., 2008). Maintained initial uptake with enhanced washout suggests the presence of functional sympathetic nerve terminals and elevated sympathetic tone, with downregulation of NET consistent with other models of diabetes (Kiyono et al., 2002a; Thackeray et al., 2011b).

Similar observations were made using pinhole SPECT in Wistar STZ rats, with washout acceleration to 21.0 as compared to 12.8 %/h in non-diabetic controls (Goethals et al., 2009). Evaluation of ^{123}I-MIBG in STZ rats at 8 weeks demonstrated reduced uptake at 60 min after injection compared to age-matched healthy controls and accelerated washout over 4 hours (36 vs 22%). The altered tracer kinetics were corroborated by an elevation of plasma norepinephrine (3.6 vs 2.4 nmol/l) and reduced β-adrenoceptor expression measured by ^{125}I-cyanopindolol binding assay (36 vs 52 fmol/mg protein) (Dubois et al., 1996). In comparing Zucker obese with lean rats at 22 weeks of age, obese animals displayed higher initial uptake of ^{123}I-MIBG (0.67 vs 0.18 counts × kg body weight / pixel × injected dose). However, the washout was significantly accelerated in obese compared to lean rats (44 vs 19%) (Dubois et al., 1996). No change in norepinephrine was observed, but β-adrenoceptor density was 15% lower in Zucker obese rats.

In ex vivo studies, regional distribution of ^{125}I-MIBG was compared with sestamibi (MIBI) using autoradiographic techniques in STZ diabetic rats to discern sympathetic neuronal density and perfusion, respectively. A decrease in inferior wall ^{125}I-MIBG distribution absorption ratio was observed in 10 week diabetic rats, with no comparable decrease observed in MIBI distribution. By contrast, no difference was reported in control rats. These observations correlated to an increase in regional norepinephrine levels in diabetic compared to non-diabetic rats (8.2 vs 4.3 μg/g anterior wall; 8.7 vs 3.9 μg/g inferior wall) and a

moderate decrease in inferior wall NET density (641 vs 809 fmol/mg protein) as measured by ^{3}H-desipramine binding assay (Kiyono et al., 2001). This suggests that while blood flow was maintained, a regional impairment of anterior sympathetic innervation was apparent. In non-obese type 2 diabetic Goto-Kakizaki rats (8 weeks old), the same investigators described maintained MIBI and a moderate decrease in ^{125}I-MIBG inferior to anterior wall distribution absorption ratio. No difference in regional cardiac norepinephrine concentration was detected between Goto-Kakizaki and non-diabetic rats, but a dramatic reduction of NET density was observed by binding assay (263 vs 364 fmol/mg protein anterior wall; 251 vs 459 fmol/mg protein inferior wall) (Kiyono et al., 2002a).

^{11}C-HED Preclinical Imaging in Diabetes

Distribution of ^{11}C-HED has been assessed in STZ-induced diabetic rats using gamma counting techniques. At 6 months of diabetes, STZ rats exhibited a significant 33% reduction of ^{11}C-HED retention restricted to the distal left ventricle compared to non-diabetic controls, with a mild but significant increase in left ventricle norepinephrine (711 vs 600 ng/g proximal; 613 vs 491 ng/g distal). By 9 months of diabetes, this defect was observed in the entire left ventricle, with reduced ^{11}C-HED accumulation by 40-44% in proximal and distal left ventricle segments. At the 9 month timepoint, significant reduction of norepinephrine (503 vs 694 ng/g proximal; 351 vs 536 ng/g distal) and nerve growth factor (4.1 vs 10.1 ng/g proximal; 2.9 vs 7.4 ng/g distal) was described. Taken together these data indicated that while autonomic neuropathy was present at 9 months, this was preceded (at 6 months) by a regional dysregulation of sympathetic neurons during which norepinephrine release was not impeded (Schmid et al., 1999).

A similar result was obtained at 2 months of diabetes in STZ diabetic rats fed high fat diet to produce insulin resistance. Retention of ^{11}C-HED in cardiac regions was globally reduced by 15-30%, with a corresponding increase in cardiac norepinephrine levels (20%) and a

decrease in NET expression (-17%) compared to age-matched, high fat diet-fed controls. Immunostaining for tyrosine hydroxylase confirmed the maintenance of intact sympathetic neurons in the left ventricle of diabetic rats (Thackeray et al., 2011b). Collectively, these studies have built a foundation for further longitudinal evaluation of sympathetic dysregulation in the diabetic rodent heart.

Postsynaptic Preclinical Imaging in Diabetes

To date, no small animal imaging has been conducted using ^{11}C-CGP12177 derivatives to visualize cardiac β-adrenoceptors. In high fat diet-fed STZ diabetic rats, 8 weeks of hyperglycemia was shown to reduce specific binding of ^{3}H-CGP12177 to cardiac β-adrenoceptors by 30-40% compared to controls (Thackeray et al., 2011a). This result was in conjunction with a significant decrease in relative myocardial β_1-adrenoceptor expression and no change in relative β_2-adrenoceptor expression compared to controls (Thackeray et al., 2011a), consistent with receptor internalization and degradation following sustained hyperglycemia. Norepinephrine levels in hyperglycemic rats were elevated 2.5 fold in plasma and 1.2 fold in myocardium (Thackeray et al., 2011b). This study supports the suitability of ^{11}C-CGP12177 for longitudinal study of membrane β-adrenoceptor expression during the development and treatment of diabetes.

The evidence of altered adenylate cyclase regulation (Gotzsche, 1983) suggests a potential role for the phosphodiesterase-4 inhibitor (*R*)-^{11}C-rolipram as a surrogate marker of cAMP activity during the development of diabetic cardiomyopathy. In conditions of sympathetic hyperactivity such as diabetes, examination of myocardial phosphodiesterase-4 expression and activity may provide insight into the development of signaling abnormalities.

Clinical Imaging of SNS in Diabetes

^{123}I-MIBG Clinical Imaging in Diabetes

SNS imaging studies in the diabetic patient population have largely been limited to investigation of presynaptic nervous integrity using ^{123}I-MIBG SPECT or ^{11}C-HED PET. Evaluation of post-synaptic β-adrenoceptors in human subjects has been limited. The trials have overwhelmingly focused on type 1 diabetes and the development of autonomic neuropathy, though some instances of early sympathetic dysregulation in diabetes have also been described (Table 4.3).

Mean late heart-to-mediastinal ratio of ^{123}I-MIBG uptake was significantly lower in diabetic subjects compared to non-diabetic subjects, regardless of heart failure progression. Among diabetic patients, lower heart-to-mediastinal ^{123}I-MIBG late uptake ratio (<1.60) was associated with three times greater rate of heart failure progression as compared to diabetic patients with a normal (>1.60) heart-to-mediastinal ^{123}I-MIBG uptake ratio (33.5 vs 11.2% event rate) (Gerson et al., 2011). There was no difference in plasma norepinephrine levels between diabetic and non-diabetic subjects, suggesting greater prognostic power from neuronal imaging.

Greater impairment in baroreflex sensitivity was found among hypertensive type 2 diabetic patients as compared to normotensive diabetics, paralleled by a modest decrease in ^{123}I-MIBG uptake (heart-to-mediastinum ratio) at early and delayed stages and an increased washout rate (Takahashi et al., 2001). No difference in high and low frequency power heart rate variability or plasma norepinephrine was found between these subgroups of diabetics (Takahashi et al., 2001).

In a study of 114 patients, autonomic function testing by heart rate variability and reflex tests identified 16 patients with cardiac autonomic neuropathy. Patients with neuropathy exhibited

Table 4.3 Summary of Clinical Myocardial Presynaptic Imaging Studies in Diabetic Patients

Tracer	N	Groups	Finding	Ref
^{11}C-HED	10	type 1 diabetic	- reduced retention index (-30%) in diabetics	a
	11	healthy controls	- increased retention index (+25%) 3 y follow-up, good control	
			- decreased retention index (-14%) 3 y follow-up, poor control	
^{11}C-HED	16	diabetic MNA	- increased area of retention defects (36% of LV) in MNA patients compared to diabetic controls (<1% of LV)	b
	12	diabetic		
	10	non-diabetic		
^{11}C-HED	23	CAD	- slightly lower retention (-2.5%, p=0.0007) at 1 y follow up in diabetic CAD patients	c
	10	type 2 diabetic		
	13	non-diabetic	- no change in non-diabetic CAD patients at 1 y	
^{123}I-MIBG	11	diabetic	- reduced 1-y follow-up uptake score in poor glucose control	d
			- no change 1 y follow-up ^{123}I-MIBG uptake in good glucose control	
^{123}I-MIBG	7	CAN	- reduced H/M ratio in CAN patients	e
	26	healthy controls	- correlation of H/M ratio to early diastolic tissue velocity	
			(r^2=0.32, p=0.01)	
^{123}I-MIBG	33	type 2 diabetic	- enhanced washout in hypertensive diabetic (+20%)	f
	15	hypertensive	- lower H/M ratio in hypertensive diabetic (-14%)	
	18	normotensive		
^{123}I-MIBG	961	NYHA II-III	- lower H/M ratio in diabetics vs non-diabetics	g
	343	diabetic	- lower H/M ratio in diabetics with heart failure progression	
	618	non-diabetic		

^{11}C-HED, hydroxyephedrine; ^{123}I-MIBG, metaiodobenzylguanidine; MNA, microangiopathy; CAD, coronary artery disease; CAN, cardiac autonomic neuropathy; NYHA II-II, New York Heart Association Class II or III heart failure; H/M, heart to mediastinum

a (Stevens et al., 1999)
b (Pop-Busui et al., 2004)
c (Fricke et al., 2008)
d (Muhr-Becker et al., 1999)
e (Sacre et al., 2010)
f (Takahashi et al., 2001)
g (Gerson et al., 2011)

modest decrease in ^{123}I-MIBG heart to mediastinal ratio compared to those without (1.6 vs 1.8) which significantly correlated with reduced resting tissue Doppler peak early diastolic velocity (4.7 vs 6.3 cm/s) (Sacre et al., 2010). Regional analysis demonstrated denervation particularly localized to the anterior and lateral walls of the ventricle (Sacre et al., 2010).

^{11}C-HED Clinical Imaging in Diabetes

Stevens and colleagues described a defect in ^{11}C-HED retention in ~7-9% of the distal left ventricle of diabetic patients, consistent with sympathetic denervation or dysinnervation (Stevens et al., 1999). At 3 years follow up, among patients who subsequently achieved good glycemic control this deficit of ^{11}C-HED retention index was reduced by 77% compared to the first scan, and average retention index score in proximal and distal segments improved by 30%. By contrast, among patients with poor glycemic control the size of the apical defect was increased by 340%, with distal segments showing a further 21% decrease in retention index (Stevens et al., 1999). Interestingly, no improvement in autonomic reflex test scores was observed among the patients with good glycemic control (Stevens et al., 1999). A similar capacity for recovery was shown in a 1 year follow-up scintigraphy study among type 1 diabetic patients, wherein patients achieving glycosylated hemoglobin <8% exhibited significant reduction of global and regional ^{123}I-MIBG uptake score (Muhr-Becker et al., 1999).

In the presence of coronary artery disease, fixed defects of ^{11}C-HED retention remain, but were not complicated by the presence of diabetes. The defect size of ^{11}C-HED did not increase in size or severity over a 1 year follow up among coronary artery disease patients during normal therapy (Fricke et al., 2008). These patients exhibited good glucose control, with HbA1c levels of 6.9±0.9%, matching the cutoff value for glycemic control previously identified (Stevens et al., 1999). However, in segments with severely reduced coronary flow

reserve, a significant reduction of ^{11}C-HED retention was observed, which was purported to reflect ischemic rather than hyperglycemic neuronal damage (Fricke et al., 2008).

Indeed, in a small cohort Pop-Busui and colleagues identified a significant difference in ^{11}C-HED retention as affected area among type 1 diabetic patients with early microangiopathy as compared to the stable patient population. Diabetic patients showed generally lower plasma norepinephrine levels at rest, an amplified response to the cold pressor test, baroceptor reflex impairment, and echocardiographic indicators of diastolic dysfunction (Pop-Busui et al., 2004). In addition, myocardial blood flow reserve was reduced in diabetics compared to healthy subjects, and reduced further in the diabetic group with early microangiopathy (Pop-Busui et al., 2004). This loss of flow reserve may derive from loss of vascular response to norepinephrine stimulation, consistent with constitutively hyperactivated sympathetic nervous drive. Together, these observations support the presence of abnormal noradrenergic signaling and presynaptic sympathetic function even in the absence of diabetic autonomic neuropathy.

Recent clinical investigations with ^{123}I-MIBG have made a strong case for the prognostic value of molecular imaging of the cardiac SNS. Heart-to-mediastinal uptake ratio of ^{123}I-MIBG (<1.60 threshold) was independently predictive of heart failure progression, arrhythmic events, cardiac death, and all-cause mortality among a heart failure patient population over a two year period (Jacobson et al., 2010). While this study did not directly evaluate the benefit of ^{123}I-MIBG imaging in these patients, it provides a solid foundation for the use of sympathetic imaging data in the stratification of patient risk to inform long term treatment options. Subjects with events had a modest elevation of plasma norepinephrine compared with event-free subjects (722 vs 642 pg/ml), but norepinephrine levels alone were not of prognostic value in the study (Jacobson et al., 2010). In previous reports, plasma

norepinephrine has been identified as an independent predictor of cardiac events in heart failure patients (Cohn et al., 1984).

Collectively, the clinical data strongly support the utility of ^{123}I-MIBG SPECT and ^{11}C-HED PET imaging in stratifying risk of cardiovascular events among diabetic patients, particularly progression to heart failure and sudden cardiac death. The regression of sympathetic defects to glycemic control underscores the relationship between hyperglycemia, norepinephrine, and cardiac noradrenergic signaling, and suggests that altered regulation of sympathetic neuronal signaling precedes overt neuropathy.

Future Perspectives

Considerable evidence from basic and clinical studies has established the presence of abnormal SNS signaling in the diabetic heart, as both a consequence and cause of systolic and diastolic dysfunction. Diabetes evokes elevated systemic and cardiac norepinephrine, leading to blunted baroreceptor adrenergic reflex, reduced heart rate variability, and downregulation of signaling elements including presynaptic NET and postsynaptic β-adrenoceptors (Fig 4.5). These abnormalities partially underlie the added risk of cardiovascular morbidity and mortality incurred by the diabetic population. As molecular imaging research in this area progresses, a number of opportunities and questions stand to be addressed.

As discussed in this review, the bulk of present studies have focused on the development of sympathetic neuronal changes in type 1 diabetes, with limited imaging and non-imaging evaluation in the type 2 diabetic population. Preclinical imaging studies in established models of type 2 diabetes may provide additional insight into the progression of autonomic neuropathy and sympathetic signaling abnormalities in the development of diabetes. Some evidence suggests that neuropathy is either delayed or absent in this population, providing the

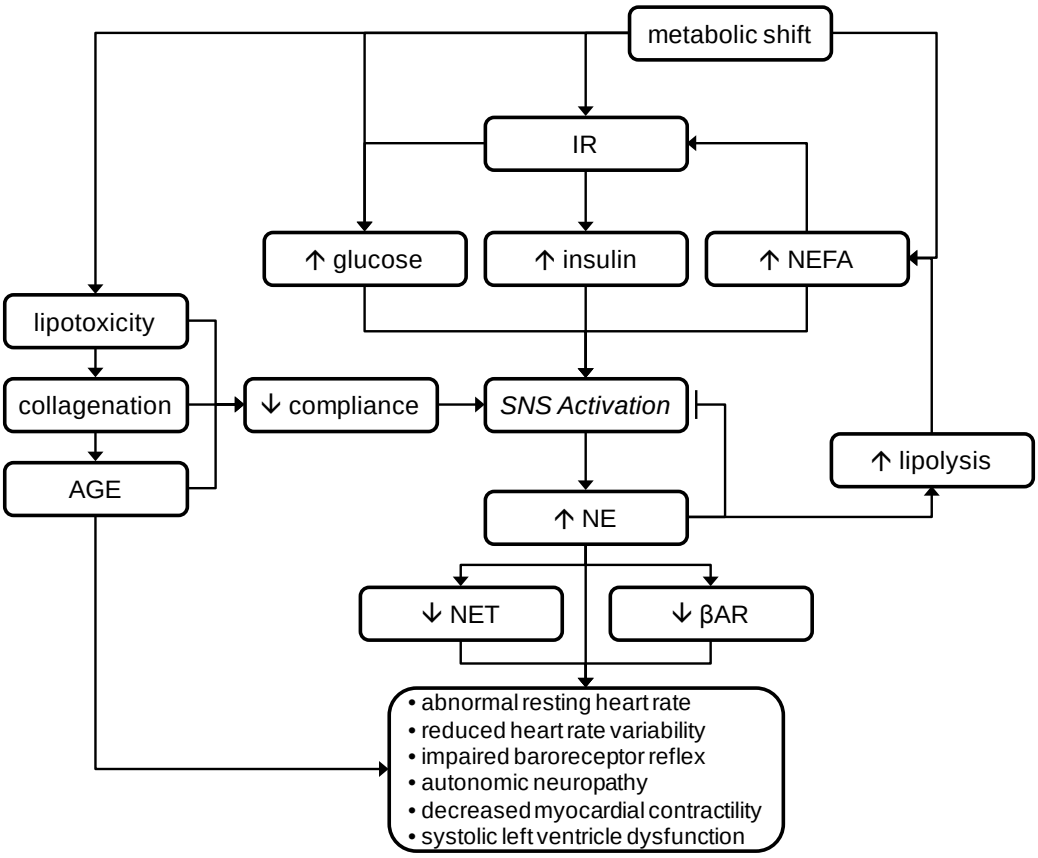

Figure 4.5 Schematic of sympathetic nervous activation in diabetes and physiological consequences. Shift in myocardial metabolism to fatty acids over glucose stimulate nonesterified fatty acid (NEFA) accumulation and insulin resistance, elevated glucose and insulin levels, and accumulation of lipid metabolites, collagen, and advanced glycation end products (AGE), leading to reduced left ventricular compliance and SNS activation. Chronic elevation of NE leads to downregualtion of NET and β-adrenoceptors with several functional consequences.

opportunity to study sympathetic hyperactivity and increased myocardial norepinephrine release and the effects of therapies to dampen this sympathetic signal.

The continued development of micro imaging techniques will permit a longitudinal assessment of diabetes progression in small animal models. Basic research suggests that denervation is preceded by a transient period of sympathetic hyperactivity, which may contribute to the deterioration of myocardial performance. Serial studies in diabetic animals would facilitate the complementary analysis of sympathetic neuronal imaging, functional measures such as echocardiography and left ventricular hemodynamics, and in vitro determination of pathological mechanisms. These studies can be further translated to clinical imaging application, wherein cardiovascular risk may be identified by PET or SPECT.

In addition to established imaging of sympathetic nevous integrity (^{11}C-HED, ^{123}I-MIBG) and β-adrenoceptor density (^{11}C-CGP12177), continuing research can explore novel neurohormonal targets in diabetes. Indirect measurements of cAMP levels by (*R*)-^{11}C-rolipram may provide a complementary measurement of sympathetic tone in diabetes. While the majority of research to date has focused on the sympathetic signaling axis, changes in parasympathetic neuronal signaling may also play a role in diabetic cardiac risk. Evaluation of myocardial muscarinic receptors using ^{11}C-methylquinuclidinyl benzilate (^{11}C-MQNB) may provide additional information on cardiac function in diabetes. The development of ^{11}C-labeled angiotensin II type 1 receptor antagonists provide the opportunity for dynamic evaluation of altered angiotensin II signaling, which partially regulates sympathetic tone. Moreover, diabetic patients treated with angiotensin II type 1 receptor blockers have been shown to exhibit improved cardiovascular outcomes.

In the long term, the literature demonstrates that abnormalities in SNS signaling identified using PET and SPECT imaging may be of value in the identification of diabetic patients at greatest risk of cardiac disease, even prior to the development of autonomic neuropathy.

Given the link between hyperglycemia and elevated norepinephrine, sympathetic neuronal imaging may be further applied to evaluate myocardial effects of, and thereby guide, anti-diabetic therapy.

Acknowledgement

JTT held a Doctoral Research Award from the Heart and Stroke Foundation of Canada. RSB is a Heart and Stroke Foundation of Canada Career Investigator, Tier 1 University of Ottawa Chair in Cardiovascular Disease Research, and the Goldfarb Chair in Cardiac Imaging Research.

Chapter 5: Manuscript #4

Cardiovasc Diabetol. (2011) 10: 75.

Sympathetic nervous dysregulation in the absence of systolic left ventricular dysfunction in a rat model of insulin resistance with hyperglycemia

James Thackeray,[1,4] Jerry Radziuk,[2] Mary-Ellen Harper,[1,5] Erik J Suuronen,[1,4] Kathryn J Ascah,[2] Rob S Beanlands,[1,2,4] Jean N DaSilva[1,2,4]

[1]Molecular Function & Imaging Program, National Cardiac PET Centre, University of Ottawa Heart Institute
[2]Division of Cardiology, University of Ottawa Heart Institute
[3]Ottawa Hospital Research Institute
[4]Department of Cellular & Molecular Medicine, Faculty of Graduate and Postdoctoral Studies, University of Ottawa
[5]Department of Biochemistry, Microbiology, and Immunology, Faculty of Graduate and Postdoctoral Studies, University of Ottawa

Key words: norepinephrine; [^{11}C]meta-hydroxyephedrine (HED); small animal echocardiography; positron emission tomography; diabetes mellitus; cardiovascular disease

Contributions of Authors

The experiments described in this manuscript were designed and executed by the candidate with the consultative assistance of the co-authors (all senior). Data were analysed and interpreted by the candidate under the supervision of Drs Beanlands and DaSilva. The manuscript was drafted and revised by the candidate. Dr Radziuk provided insight on euglycemic clamp procedures and the animal model. Dr Harper contributed to the acquisition and interpretation of indirect calorimeter data. Dr Suuronen provided assistance in immunohistochemistry. Dr Ascah provided a clinical interpretation of echocardiography results. Dr Beanlands and Dr DaSilva provided supervision on the project and edited the final manuscript.

Abstract

Background: Diabetes mellitus is strongly associated with cardiovascular dysfunction, derived in part from impairment of sympathetic nervous system signaling. Glucose, insulin, and non-esterified fatty acids are potent stimulants of sympathetic activity and norepinephrine (NE) release. We hypothesized that sustained hyperglycemia in the high fat diet-fed streptozotocin (STZ) rat model of sustained hyperglycemia with insulin resistance would exhibit progressive sympathetic nervous dysfunction in parallel with deteriorating myocardial systolic and/or diastolic function.

Methods: Cardiac sympathetic nervous integrity was investigated *in vivo* via biodistribution of the positron emission tomography radiotracer and NE analogue [^{11}C]*meta*-hydroxyephedrine ([^{11}C]HED). Cardiac systolic and diastolic function was evaluated by echocardiography. Plasma and cardiac NE levels and NE reuptake transporter (NET) expression were evaluated as correlative measurements.

Results: The animal model displays insulin resistance, sustained hyperglycemia, and progressive hypoinsulinemia. After 8 weeks of persistent hyperglycemia, there was a significant 13-25% reduction in [^{11}C]HED retention in myocardium of STZ-treated hyperglycemic but not euglycemic rats as compared to controls. There was a parallel 17% reduction in immunoblot density for NE reuptake transporter, a 1.2 fold and 2.5 fold elevation of cardiac and plasma NE respectively, and no change in sympathetic nerve density. No change in ejection fraction or fractional area change was detected by echocardiography. Reduced heart rate, prolonged mitral valve deceleration time, and elevated transmitral early to atrial flow velocity ratio measured by pulse-wave Doppler in hyperglycemic rats suggest diastolic impairment of the left ventricle.

Conclusions: Taken together, these data suggest that sustained hyperglycemia is associated with elevated myocardial NE content and dysregulation of sympathetic nervous system signaling in the absence of systolic impairment.

Background

Diabetes mellitus, hyperglycemia, and insulin resistance confer a significantly greater risk of developing cardiovascular disease and heart failure (Kostis and Sanders, 2005). The mechanisms involved in the progression of ventricular dysfunction in diabetes are diverse and unclear, with several pathways having been implicated including disrupted metabolic processes (Sharma et al., 2008a; van den Brom et al., 2009), glycation and interstitial fibrosis of myocardium (Connelly et al., 2007), oxidative stress and apoptosis (Taegtmeyer et al., 2002), and impairment of autonomic, particularly sympathetic, signal transduction (Dincer et al., 2001; Kusmic et al., 2008; Stevens et al., 1999; Taegtmeyer et al., 2002).

The sympathetic nervous system is the primary extrinsic control of heart rate and contractility. Under stress, release of the neurotransmitter norepinephrine (NE) from sympathetic nerves enhances cardiac output (Lameris et al., 2000). Signaling is terminated by recovery of NE from the synaptic cleft back into the neuron varicosity via the NE reuptake transporter (NET) (Raffel and Wieland, 2001b). Dysregulation of sympathetic innervation has been documented in congestive heart failure (Ungerer et al., 1998), acute myocardial infarction (Li et al., 2004), and diabetes (Schmid et al., 1999). Enhanced sympathetic signaling partially compensates for deteriorating myocardial function (Lameris et al., 2000).

Glucose, insulin, and non-esterified fatty acids (NEFA) are potent stimulants of NE and epinephrine release (Anderson et al., 1991; Levin and Sullivan, 1987). Diabetic animals display reduced heart rate variability, hypertension, and elevated plasma and tissue levels of NE (Dias et al., 2011; Ganguly et al., 1987; Howarth et al., 2005b; Marsh et al., 2009; Marsh et al., 2007). These animals develop systolic and diastolic cardiac dysfunction over time (Connelly et al., 2007; Marsh et al., 2009; Marsh et al., 2007; Rodrigues et al., 2011). The frequent concurrence of diabetes with cardiac disease, with each increasing the risk of

developing the other, implies a common pathogenesis (Kostis and Sanders, 2005). It has been suggested that sympathetic dysregulation may be involved in such a process (Kostis and Sanders, 2005; Stevens et al., 1999).

[^{11}C]*meta*-Hydroxyephedrine ([^{11}C]HED) has been routinely applied in cardiac positron emission tomography (PET) to interrogate sympathetic nervous integrity in a myriad of clinical conditions including acute myocardial infarction, cardiomyopathies, coronary artery disease, and heart failure (Raffel and Wieland, 2001b; Ungerer et al., 1998). Retention of [^{11}C]HED is blocked by NET inhibitors and reduced by treatments elevating synaptic NE (Raffel et al., 2006; Thackeray et al., 2007). Altered uptake of [^{11}C]HED and other presynaptic tracers has been described extensively in diabetic rats and mice (Kusmic et al., 2008; Schmid et al., 1999), as well as clinically (Stevens et al., 1999). The temporal progression of cardiac sympathetic dysregulation and its relation to left ventricular dysfunction remains unclear.

We hypothesized that sustained hyperglycemia would contribute to cardiac sympathetic nervous dysfunction which would manifest in parallel with deteriorating cardiac systolic and diastolic function. The high fat diet-fed, moderate dose streptozotocin (STZ) rat model of sustained hyperglycemia with insulin resistance was serially characterized for metabolic and cardiac function, and sympathetic nervous integrity was tested at 2 and 8 weeks of unregulated hyperglycemia using *ex vivo* biodistribution of [^{11}C]HED with NET expression and NE levels measured concurrently. This combined approach establishes an association between altered sympathetic nervous signaling and functional abnormalities during the progression of diabetes.

Methods

Drugs, chemicals, and radiochemistry

Desipramine hydrochloride, NE bitartrate, and STZ were obtained from Sigma-Aldrich (Toronto, ON, Canada). Drugs were dissolved in saline except STZ, which was in tribasic citrate. Antibodies against rat NET (AB5066P), tyrosine hydroxylase (AB1542) and GAPDH (sc32233) were obtained from Chemicon/Millipore (Billerca, MA, USA) and Santa Cruz Biotechnology (Santa Cruz, CA, USA), respectively. Secondary horseradish peroxidase conjugated IgG antibodies to mouse, rabbit and sheep were from Santa Cruz (sc2314, sc32004) or Abcam (ab6747, Cambridge, MA, USA). Histological stains were from Richard Allan Scientific (Kalamazoo, MI, USA). [^{11}C]HED was synthesized as previously described and dissolved in 50:44:6 0.9% saline/water/8.4% sodium bicarbonate (v/v/v) for injection (Thackeray et al., 2007). High radiochemical purity (>99%) and specific activity (7.3-55.5 GBq/μmol) were obtained.

Animal model

Animal experiments were conducted in accordance with the Canadian Council on Animal Care, with approval of the Animal Care Committee of the University of Ottawa. Adult male Sprague-Dawley rats (200-250 g) were obtained from Charles River Canada (Montreal, QC, Canada) and housed in a temperature-controlled animal facility under a 12 hour light/dark cycle with food and water *ad libitum*. Rats were maintained on high fat diet (Research Diets D12266B, New Brunswick, NJ, USA) composed of (by kJ) 32% fat, 51% carbohydrate, and 17% protein. After two weeks of initial feeding, a single intraperitoneal injection of moderate dose STZ (45 mg/kg, n=99) or vehicle (n=44) was administered (Marsh et al., 2009; Reed et al., 2000; Srinivasan et al., 2005; Zhang et al., 2003). Fed state blood glucose levels 2 weeks post-STZ were used to stratify treated rats by glycemic state, with blood glucose levels exceeding 11 mM considered to be hyperglycemic and the remainder

considered as a STZ-treated euglycemic control group (Marsh et al., 2009; Zhang et al., 2003). Body weights, diet consumption, and blood markers were assessed in all animals. Whole heart weights were determined at the conclusion of experiments and expressed as a ratio to body weight. STZ- and vehicle-treated rats were divided among several experimental protocols (Table 5.1). An additional group (n=5) were fed standard rodent chow (Teklad 2019, Harlan Teklad, Madison, WI, USA) for euglycemic clamp experiments.

Blood markers

Fed state blood glucose was tested weekly from the saphenous vein using a glucose meter (AccuChek, Roche Diagnostics, Laval, QC, Canada). Fasted (overnight 8-12 h) plasma insulin, NEFA and triglyceride were measured from trunk blood collected at 2 and 8 weeks post-STZ following decapitation by radioimmune assay (Linco/Millipore, Billerca, MA, USA) or microplate colorimetric assays (Biovision, Mountain View, CA, USA), respectively.

Plasma and cardiac norepinephrine

Plasma and reconstituted heart samples were analyzed for NE content using a modified inline capture, column-switching high performance liquid chromatography procedure with electrochemical detection (Thackeray et al., 2007; Wang et al., 1999). Briefly, venous blood samples were centrifuged at 3000 × *g* to separate plasma and filtered (0.2 µm) for injection. Excised hearts were homogenized under 80/20 ethanol/0.1 M formic acid, centrifuged at 82000 × *g*, and supernatant evaporated in a rotary evaporator. The residue containing NE was reconstituted under 0.1 M formic acid and filtered. Samples were injected and NE adsorbed onto a capture column (Direct Connect refillable guard column, 2 × 20 mm, Alltech, Deerfield, IL, USA) containing activated aluminum oxide (Type WA4, Sigma)

Table 5.1 Sample sizes of rat groups for individual experiments.

		Streptozotocin	
	Controls	Euglycemic	Hyperglycemic
2 Weeks			
HED[*]	6	4	4
HED + Desipramine[*]	4	3	4
Western Blot[*†]	3	3	3
None[*†]	3	5	6
2 Weeks Total	16	15	17
8 Weeks			
HED[*]	8	9	14
HED + Desipramine[*]	6	6	5
OGTT + Western Blot[*†]	3	3	3
Echocardiography[*†]	5	7	8
Clamp + Histology[*]	3	5	4
Indirect Calorimetry[*]	3	0	3
8 Weeks Total	28	30	37

[*]Blood samples taken for measurement of biochemistry markers.
[†]Heart samples used for measurement of tissue norepinephrine.

under 1.5 M Tris, 0.05 M EDTA (2 mL), rinsed with 10 mL of deionized water (1 mL/min), then eluted by 5/95 methanol / 50 mM ammonium formate, 0.27 mM EDTA, 0.346 mM octanesulfonic acid (pH 2.85, 1 mL/min) onto a cation exchange analytical column (Partisil SCX, 250 × 4.6 mm, 10 μm, Phenomenex, Torrance, CA, USA) for separation (NE retention time = 6.8 min), and quantified by flow-through coulometric electrochemical detection (Coulochem III, ESA/Dionex, Chelmsford, MA, USA) with an applied voltage of 400 mV. Amperage signals were integrated using the PeakSimple Six Port Chromatography Data System and analysed where area under the curve is representative of mass NE. This procedure was validated using NE bitartrate standards, demonstrating 95% recovery and linear reproducibility in a physiological range (0.001-20 ng).

Oral glucose tolerance

Serial oral glucose tolerance tests were performed as described elsewhere (Reed et al., 2000), at three intervals: prior to high fat feeding, 2 weeks after STZ or vehicle injection, and 8 weeks after STZ or vehicle injection.

Euglycemic clamp

The hyperinsulinemic euglycemic clamp was performed as described elsewhere (van den Brom et al., 2009). Continuous iv infusion of biosynthetic insulin (Novolin, 30 mU kg^{-1} min^{-1}) was counteracted by variable iv infusion of 20% glucose to maintain glycemia at 5 mM. Rats were considered clamped with three consecutive stable readings of blood glucose levels and glucose infusion rate, within 120 min.

Indirect calorimetry

Calorimetric measures were obtained at 2 and 8 weeks of diabetes using the 4-chamber Oxymax system (Columbus Instruments, Columbus, OH, USA) as previously described (Greene et al., 2009). Rats were sequestered in individual 11.7 L calorimetry chambers with food and water *ad libitum* for 24 h. Oxygen consumption, carbon dioxide production and

respiratory exchange ratio (RER) were measured five times per hour. RER provides an index of carbohydrate versus fatty acid substrate utilization (Greene et al., 2009).

Echocardiography

Serial echocardiography was carried out biweekly under light anesthesia (1-2% isoflurane) using the Vevo 770 system (VisualSonics, Toronto, ON, Canada) and a 23.5 MHz probe (van den Brom et al., 2009). All echocardiography studies were performed and analyzed by a single operator. Parasternal long and short axis views were recorded as sequential ECG-gated M-mode sweeps (EKV-mode) to generate two-dimensional cines of the left ventricle. Endocardial and epicardial areas were traced on the two-dimensional parasternal long axis cine and used to calculate left ventricular volumes at end systole and end diastole. Calculations for stroke volume, percent ejection fraction (%EF), cardiac output, and percent fractional area change (%FAC) were completed using VisualSonics software. Diastolic function was assessed using pulse-wave Doppler across the mitral valve from the apical four chamber view (van den Brom et al., 2009). Early (E) and late (A) flow velocity as well as mitral valve deceleration time provide an indication of diastolic function.

[^{11}C]HED ex vivo biodistribution

Biodistribution studies were performed at 2 and 8 weeks following STZ or vehicle injection in conscious animals, as described previously (Greene et al., 2009; Thackeray et al., 2007). Briefly, 50-75 MBq (0.2–1.3 μg cold mass) of [^{11}C]HED was injected as a 0.1-0.3 mL bolus into a lateral tail vein of restrained rats. Animals were killed by decapitation 30 min after tracer injection. A sample of trunk blood was collected. Hearts were rapidly excised and dissected to right and left atria, right and left ventricle free walls, and intraventricular septum, and a portion of skeletal muscle (quadriceps femoris) was taken as a reference tissue devoid of specific retention (Thackeray et al., 2007). Samples were counted for radioactivity (decay corrected) in a gamma-counter along with 1% standard dilutions of each [^{11}C]HED

formulation. Total tracer retention is expressed as percentage of injected dose per gram of tissue, normalized to body weight (% ID/g × BW). To delineate non-specific retention, a subset of animals at 2 and 8 week post-STZ or vehicle was injected with the NET inhibitor desipramine (10 mg/kg, ip) 30 min prior to tracer administration. This value was subtracted from the total [^{11}C]HED retention to determine specific retention.

Western immunoblotting

Hearts were removed and flash frozen in liquid nitrogen following decapitation. Hearts were hand powdered under liquid nitrogen and stored at -80^{o}C until use. Total cell lysate was prepared (Dincer et al., 2001; Wehrwein et al., 2008) and protein content was determined by BCA assay. SDS-PAGE was carried out using 8% polyacrylamide gels with 40 μg of protein loaded for each sample. Protein was transferred to polyvinylidine difluoride membranes. Blocked membranes were incubated in anti-NET (1:750) and anti-GAPDH (1:2000) followed by secondary antibody incubation. Protein was visualized by chemiluminescence Western lighting kit (Perkin Elmer, Waltham, MA, USA) and the Fluorchem HD Imaging System. Analysis was completed with AlphaEase FC software normalizing NET immunoblot densities to GAPDH and expressed as a percentage of controls.

Tyrosine Hydroxylase Immunostaining

To determine the relative sympathetic nerve density in the myocardium, immunostaining for tyrosine hydroxylase was carried out in paraffin-embedded short axis heart sections as described elsewhere (Cao et al., 2000; Enomoto et al., 2001; Ieda et al., 2006). Briefly, after antigen retrieval by citrate, slides were blocked in normal horse serum and incubated for 96 hours at 4^{o}C with 1:100 anti-tyrosine hydroxylase. Slides were then incubated with 1:100 anti-sheep HRP-conjugated secondary antibody and visualized using diaminobenzidine reagent (Vector Labs). Six images from each section were analysed using ImageJ software to determine the area of positive staining as a percentage of the total field of view.

Histopathology

Cardiomyocyte health was assessed by histopathology in a subset of rats. Tissues were processed for histological analysis as described elsewhere (Connelly et al., 2007; Marsh et al., 2009). Hematoxylin and eosin staining assessed cardiomyocyte morphology and fibre size. Masson Trichrome staining was used to determine collagen deposition.

Statistics

All data are presented as mean ± standard deviation. Differences between STZ-treated hyperglycemic, STZ-treated euglycemic, and vehicle-treated control groups were tested for significance by one-way analysis of variance with Bonferroni's post hoc test using SPSS 17.0 software. Indirect calorimetry data were tested with repeated measures general linear model using SAS 9.0 software. Significance was considered at $p<0.05$.

Results

Diabetic animal model

Injection of STZ was successful in inducing overt hyperglycemia in 53.5% of treated rats (n=53/99), whereas 46 animals maintained normal glucose levels (Fig 5.1A). After STZ injection, the average fed state blood glucose concentration over 8 weeks in STZ-treated hyperglycemic, STZ-treated euglycemic, and control rats was 20.7±8.7, 7.3±2.7, and 6.5±1.0 mM, respectively. Body weights of all groups were similar until the induction of diabetes, at which point STZ-treated animals displayed stunted weight gain. As diabetes progressed in hyperglycemic rats, further depletion of weight gain was apparent (Fig 5.1B). One week following treatment and for the remainder of the experiment, STZ-treated hyperglycemic rats tended to consume greater amounts of diet compared to STZ-treated euglycemic and vehicle-treated controls with an average per diem consumption of 568±92, 518±94, and 497±83 kJ, respectively. Heart weight was lower in STZ-treated hyperglycemic rats as compared to

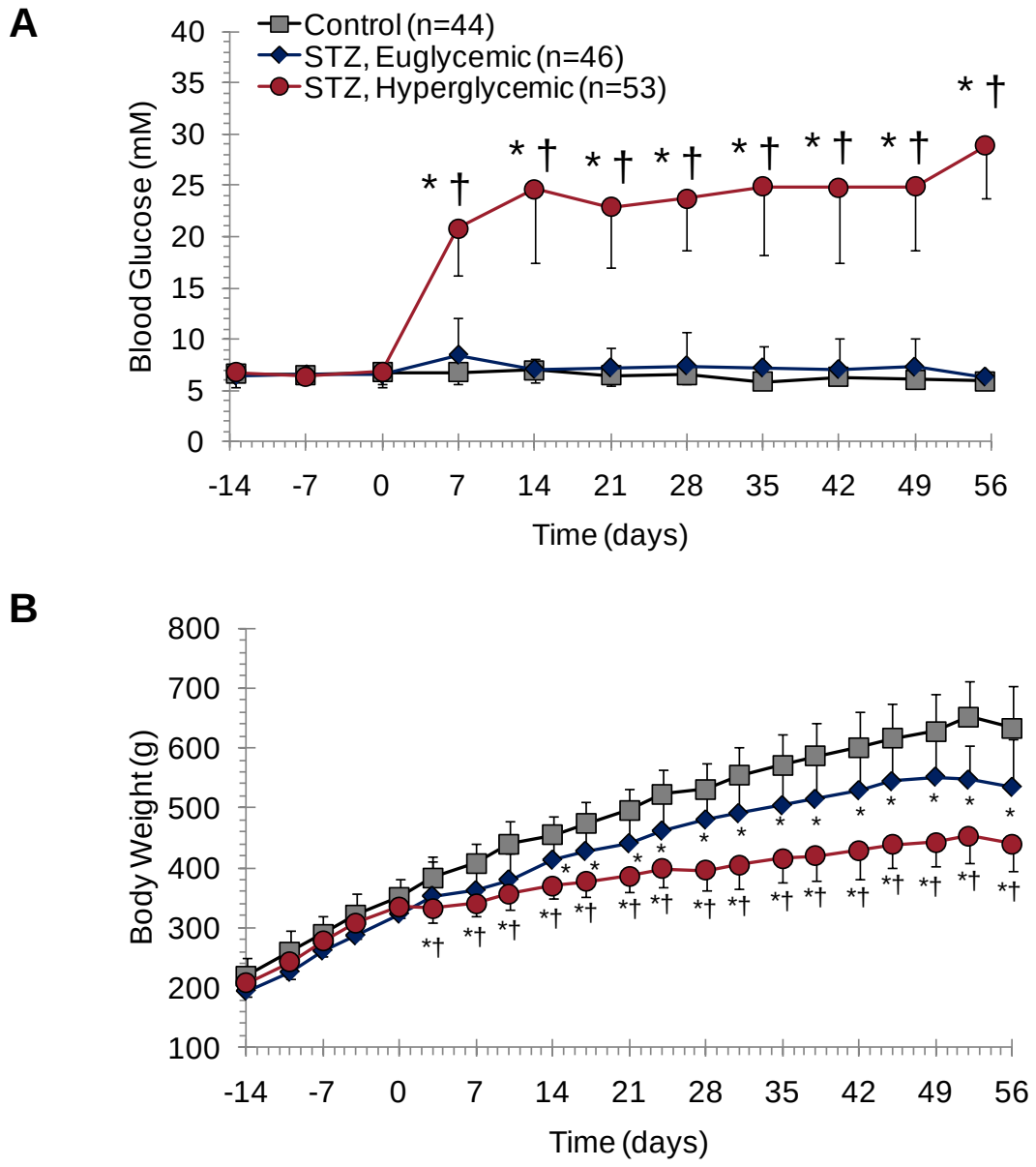

Figure 5.1 Blood glucose (**A**) and body weight (**B**) data from high fat diet fed, moderate dose STZ-induced diabetic rats over 8 weeks after STZ or vehicle administration. Mean ± SD. * $p<0.05$ to controls, † $p<0.05$ to STZ euglycemic rats, one-way ANOVA, Bonferroni post hoc.

controls. A higher heart to body weight ratio was apparent in STZ-treated hyperglycemic rats as compared to both STZ-treated euglycemic and vehicle-treated controls (Table 5.2).

Blood markers

Hyperglycemic rats displayed progressive hypoinsulinemia, with depletion of insulin levels at 8 weeks but not at 2 weeks post-STZ. Fasted NEFA and triglyceride levels were also significantly lower in STZ-treated hyperglycemic rats as compared to both vehicle-treated and STZ-treated euglycemic controls (Table 5.3).

Plasma and cardiac norepinephrine

Plasma NE concentrations were comparable between the three groups of animals at baseline, but were 2.5 fold higher in STZ-treated hyperglycemic rats at 8 weeks (Table 5.3). HPLC analysis of cardiac samples revealed a significant 1.4 fold elevation of NE in STZ-treated hyperglycemic rats compared to vehicle-treated controls at 2 weeks post-STZ, and a 1.2 fold elevation at 8 weeks post-STZ. NE levels in STZ-treated euglycemic rats were unchanged compared to vehicle-treated controls at both time points (Fig 5.2).

Oral glucose tolerance

Prior to induction of diabetes by STZ, there was no difference in clearance of oral glucose load between groups (Fig 5.3A). However, at 2 and 8 weeks following STZ injection, animals with overt hyperglycemia displayed impaired fasting glucose levels, higher peak glucose after gavage, and a longer time to return to baseline (Fig 5.3B-C). STZ-treated euglycemic rats showed similar glucose tolerance to vehicle-treated controls. The response of insulin secretion to oral glucose load was ablated in STZ-treated hyperglycemic rats and diminished in STZ-treated euglycemic rats as compared to controls with peak plasma insulin concentrations of 0.4±0.1, 1.4±1.0, and 3.8±1.4 ng/mL at 8 weeks, respectively.

Table 5.2 Terminal heart and body weights in STZ-treated hyperglycemic, STZ-treated euglycemic, and vehicle-treated control rats.

	Control		STZ, Euglycemic		STZ, Hyperglycemic	
	2 Weeks	8 Weeks	2 Weeks	8 Weeks	2 Weeks	8 Weeks
BW (g)	302.4±26.5	584.7±62.2	358.9±22.7*	535.8±43.9*	331.6±30.1	424.6±48.1*†
HW (g)	0.89±0.05	1.46±0.17	1.13±0.14*	1.38±0.11	1.02±0.06*	1.31±0.12*
HW/BW ($\times 10^{-3}$)	3.0±0.2	2.5±0.2	3.1±0.3	2.6±0.2	3.1±0.2	3.1±0.3*†

Mean ± SD.

* $p<0.05$ to age-matched control, † $p<0.05$ to age-matched STZ, euglycemic, one-way ANOVA, Bonferroni post hoc

Table 5.3 Fasted levels of metabolic blood markers in STZ-treated hyperglycemic, STZ-treated euglycemic, and vehicle-treated control rats.

	Control		STZ, Euglycemic		STZ, Hyperglycemic	
Factor	2 Weeks	8 Weeks	2 Weeks	8 Weeks	2 Weeks	8 Weeks
Glucose (mM)	7.0±1.2	6.3±0.4	7.0±1.1	5.9±0.6	24.6±7.2*†	28.8±5.1*†
Insulin (ng/mL)	0.65±0.41	1.36±0.69	0.67±0.66	0.79±0.57	0.78±0.46	0.33±0.33*†
NEFA (nM)	0.20±0.10	0.40±0.13	0.31±0.05	0.20±0.12*	0.30±0.22	0.24±0.14*
Triglyceride (nM)	0.79±0.05	0.81±0.35	0.67±0.17	0.66±0.14	0.80±0.45	0.55±0.29*
NE (ng/mL)	0.10±0.05	0.11±0.06	0.10±0.14	0.10±0.03	0.10±0.06	0.24±0.09*†

Mean ± SD.

* $p<0.05$ to age-matched control, † $p<0.05$ to age-matched STZ, euglycemic, one-way ANOVA, Bonferroni post hoc

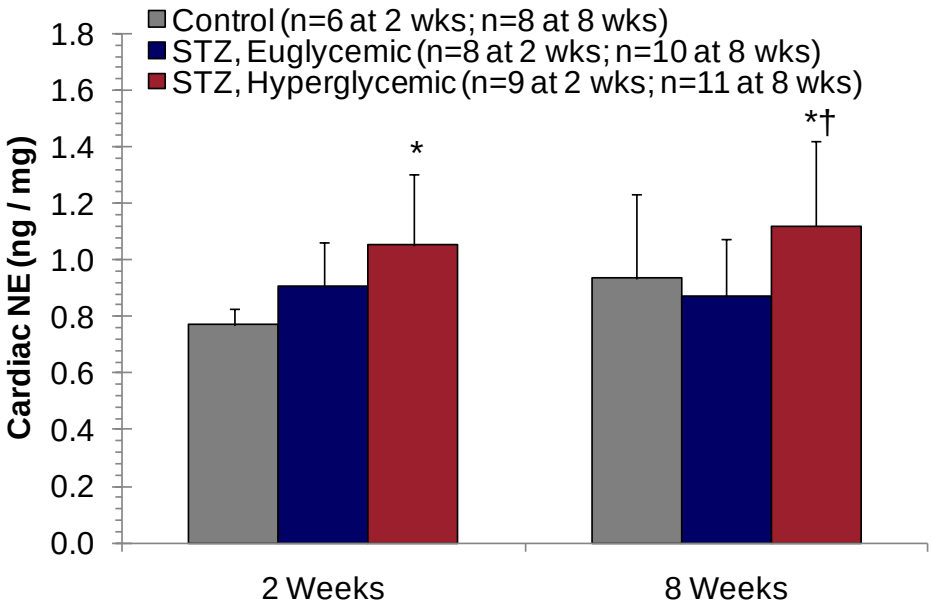

Figure 5.2 Cardiac NE content at 2 and 8 weeks after STZ or vehicle administration. Mean ± SD. * $p<0.05$ to controls, † $p<0.05$ to euglycemic, one-way ANOVA, Bonferroni post hoc.

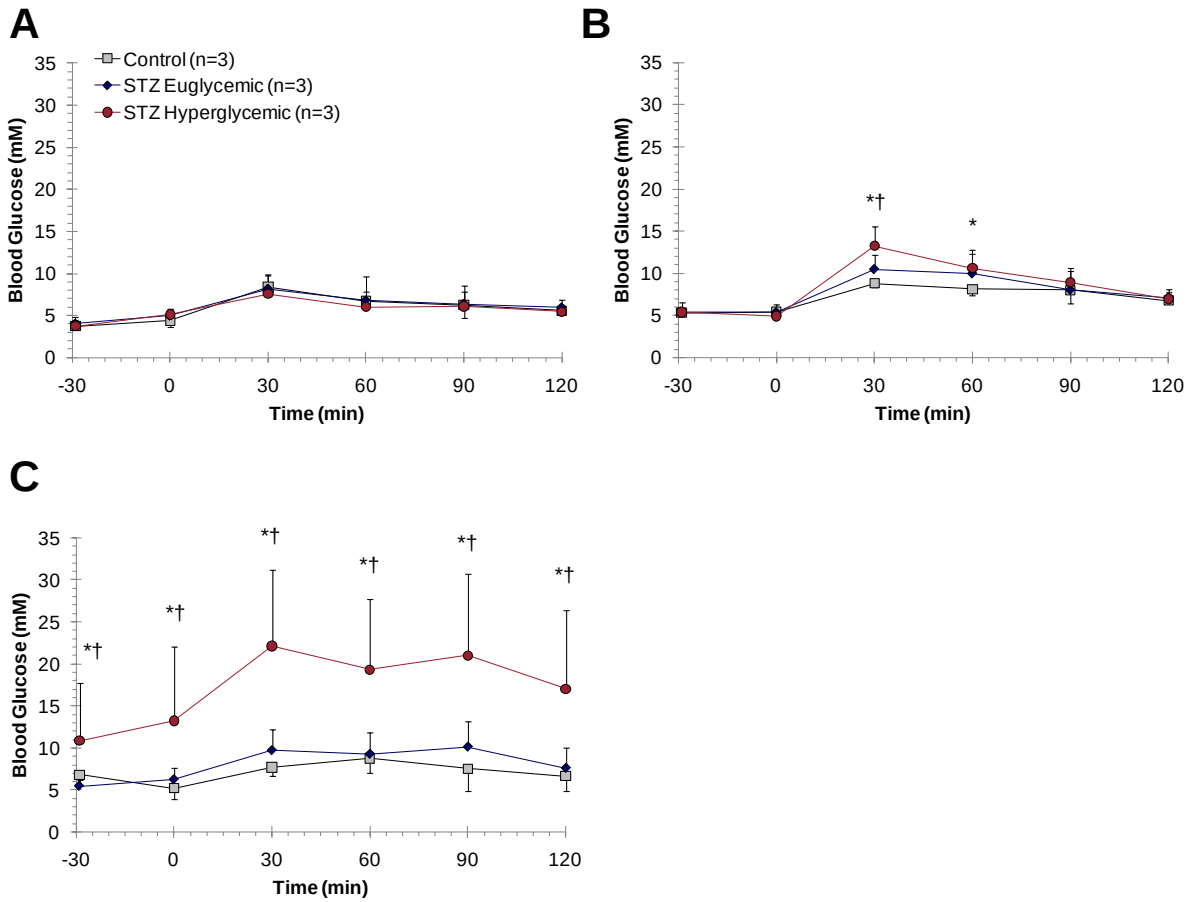

Figure 5.3 Oral glucose tolerance testing at baseline (**A**) and at 2 (**B**) and 8 weeks after STZ or vehicle administration (**C**). Mean ± SD. * $p<0.05$ to controls, † $p<0.05$ to STZ euglycemic rats, one-way ANOVA, Bonferroni post hoc.

Euglycemic clamp

Rats at 8 weeks post-STZ were successfully clamped at 5 mM blood glucose during hyperinsulinemic euglycemic clamp under anaesthesia. The glucose infusion rate required to achieve steady state fasted blood glucose concentration was 4.0±2.0, 2.9±1.8, 3.2±0.4 mg kg^{-1} min^{-1} in STZ-treated hyperglycemic, STZ-treated euglycemic, and vehicle treated control rats, respectively. The infusion rates for all high fat-fed animals were significantly lower than for chow-fed controls, which had a glucose infusion rate of 25.0±4.2 mg kg^{-1} min^{-1}.

Indirect calorimetry

STZ-treated hyperglycemic rats oxidized a lower proportion of carbohydrates as compared to vehicle-treated controls after 8 weeks but not 2 weeks of hyperglycemia (Fig 5.4A). There was a trend toward lower oxygen consumption in STZ-treated hyperglycemic rats as compared to controls (Fig 5.4B).

Echocardiography

Measures of systolic and diastolic cardiac function are summarized in Table 5.4. STZ-treated hyperglycemic rats exhibited significantly lower heart rates than euglycemic and control counterparts (Fig 5.5A). There was no difference in percent LV ejection fraction or fractional area change between groups (Fig 5.5B-C). However, STZ-treated hyperglycemic rats demonstrated elevated mean mitral valve deceleration time (Fig 5.5D) and E/A wave ratio as compared to other groups (Table 5.4).

[^{11}C]HED ex vivo biodistribution

Retention of [^{11}C]HED was uniform in myocardium and effectively blocked (81-86%) by pretreatment with desipramine in all groups of animals. At 2 weeks post-STZ, no difference in total or specific myocardial [^{11}C]HED accumulation was observed between the groups (Fig 5.6A). Conversely, 8 weeks following induction of diabetes, hyperglycemic rats

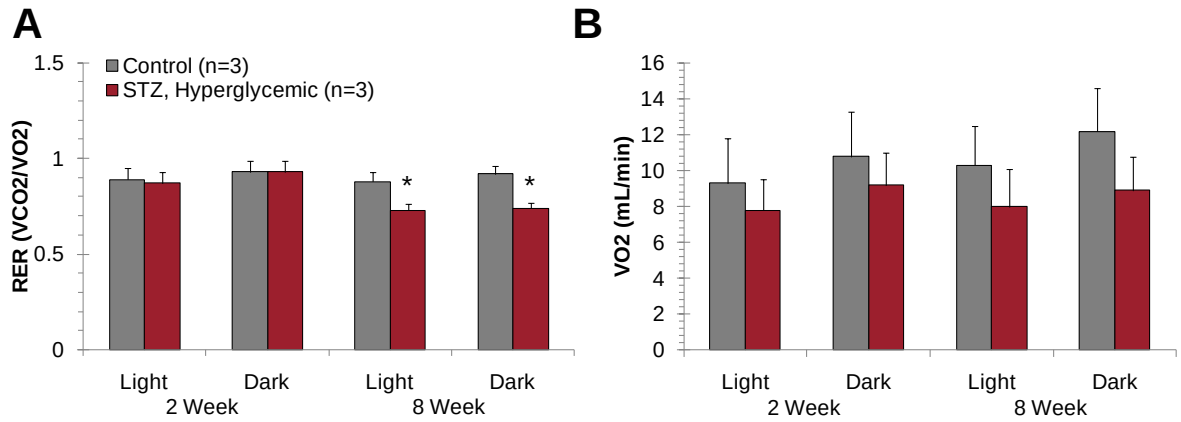

Figure 5.4 Indirect calorimetry assessment of oxygen consumption (**A**) and respiratory exchange ratio (**B**) at 2 and 8 weeks after STZ or vehicle administration. Mean ± SD. * $p<0.05$ to controls, repeated measures, general linear model.

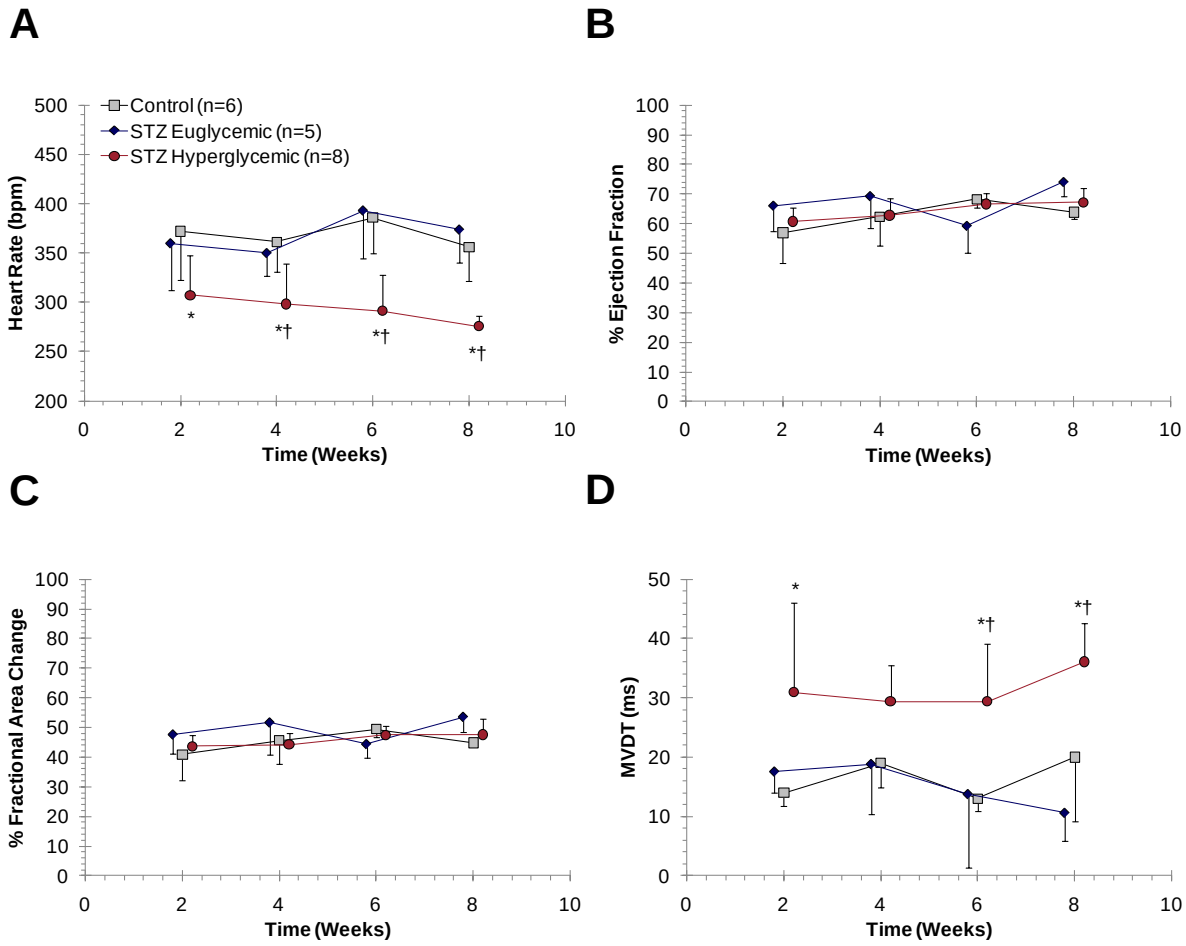

Figure 5.5 Serial echocardiographic assessment of heart rate (**A**), left ventricle ejection fraction (**B**), fractional area change (**C**), and mitral valve deceleration time (**D**) at 2, 4, 6, and 8 weeks after STZ or vehicle administration. Mean ± SD. * $p<0.05$ to controls, † $p<0.05$ to euglycemic, one-way ANOVA, Bonferroni post hoc.

Table 5.4 Echocardiography parameters in STZ-treated hyperglycemic, STZ-treated euglycemic, and vehicle treated control rats at 2, 4, 6, and 8 weeks after STZ.

	Control				STZ, Euglycemic				STZ, Hyperglycemic			
	2 Weeks	4 Weeks	6 Weeks	8 Weeks	2 Weeks	4 Weeks	6 Weeks	8 Weeks	2 Weeks	4 Weeks	6 Weeks	8 Weeks
EV (d) (µL)	477±135	477±65	431±90	353±43	570±47	457±100	400±67	363±35	435±103	497±117	483±80	369±111
EV (s) (µL)	199±49	184±72	137±35	128±19	192±33	134±39	160±9	95±23	189±57	182±42	162±36	119±37
SV (µL)	278±122	293±30	293±58	225±27	379±81	323±118	240±76	268±21	262±57	314±86	321±52	250±79
CO (mL/min)	105±52	106±15	112±16	81±11	138±47	113±37	93±18	100±13	82±23	91±18	94±19	69±22
IVCT (ms)	62±5	79±13	70±6	64±9	84±5	74±7	65±7	73±6	83±14	81±14	83±15	78±6
IVRT (ms)	22±4	33±5	25±8	32±7	23±0	30±5	31±2	24±6	27±6	25±4	34±15	33±5
A (cm/s)	62±22	77±13	85±33	77±25	59±6	83±22	65±17	97±23	50±13	65±21*†	58±39	69±19*†
E (cm/s)	98±5	118±23	92±26	98±19	105±5	119±22	92±8	125±42	92±18	104±24	98±28	99±21
E/A Ratio	1.7±0.5	1.6±0.3	1.2±0.4	1.3±0.3	1.8±0.1	1.5±0.2	1.4±0.3	1.3±0.2	1.9±0.6	1.7±0.3	2.0±1.0	1.5±0.3

* $p<0.05$ to controls, † $p\leq0.05$ to euglycemic, one-way ANOVA, Bonferroni post hoc
(EV = endocardial volume at diastole (d) or systole (s); SV = stroke volume; CO = cardiac output; IVCT = intraventricular contraction time; IVRT = isovolumic relaxation time; A = transmitral atrial (late) filling velocity; E = transmitral early filling velocity)

Calculations:

EV (d) = $(4\pi/3) \times (\text{Endo Major (d)} / 2) \times ((\text{Endo Area (d)}) / \pi (\text{Endo Major (d)}/2))^2$

EV (s) = $(4\pi/3) \times (\text{Endo Major (s)} / 2) \times ((\text{Endo Area (s)}) / \pi (\text{Endo Major (s)}/2))^2$

SV = EV(d) – EV (s)

EF = SV / EV (d) × 100%

FAC = (Endo Area (d) – Endo Area (s)) / Endo Area (d) × 100%

CO = SV × Heart Rate

exhibited a significant decrease in [^{11}C]HED retention as compared to STZ-treated euglycemic and controls (Fig 5.6B). There was no change in non-specific retention as defined by pretreatment with desipramine. Percent change in total and specific cardiac tracer retention were similar at 13-26% and 12-26%, respectively (Table 5.5).

Western immunoblotting

Immunoblots for NET resulted in consistent protein bands at 76 and 78 kDa, as per the manufacturer's documentation (Fig 5.7A). Relative NET expression normalized to GAPDH was significantly reduced in cardiac lysate of STZ-treated hyperglycemic rats by 17% compared to controls and by 15% to STZ-treated euglycemic rats (Fig 5.7B).

Tyrosine Hydroxylase Immunostaining

Tyrosine-hydroxylase-positive nerve endings were identified within the left ventricle in each group (Fig 5.8A). Quantitative analysis revealed no difference in staining between STZ-treated hyperglycemic, STZ-treated euglycemic, and vehicle-treated controls, suggesting maintained sympathetic innervation (Fig 5.8B).

Histopathology

There were no differences in cardiomyocyte morphology between STZ-treated hyperglycemic, STZ-treated euglycemic, and control rats (Fig 5.9). Masson Trichrome staining revealed no change in collagen content between groups (Fig 5.9).

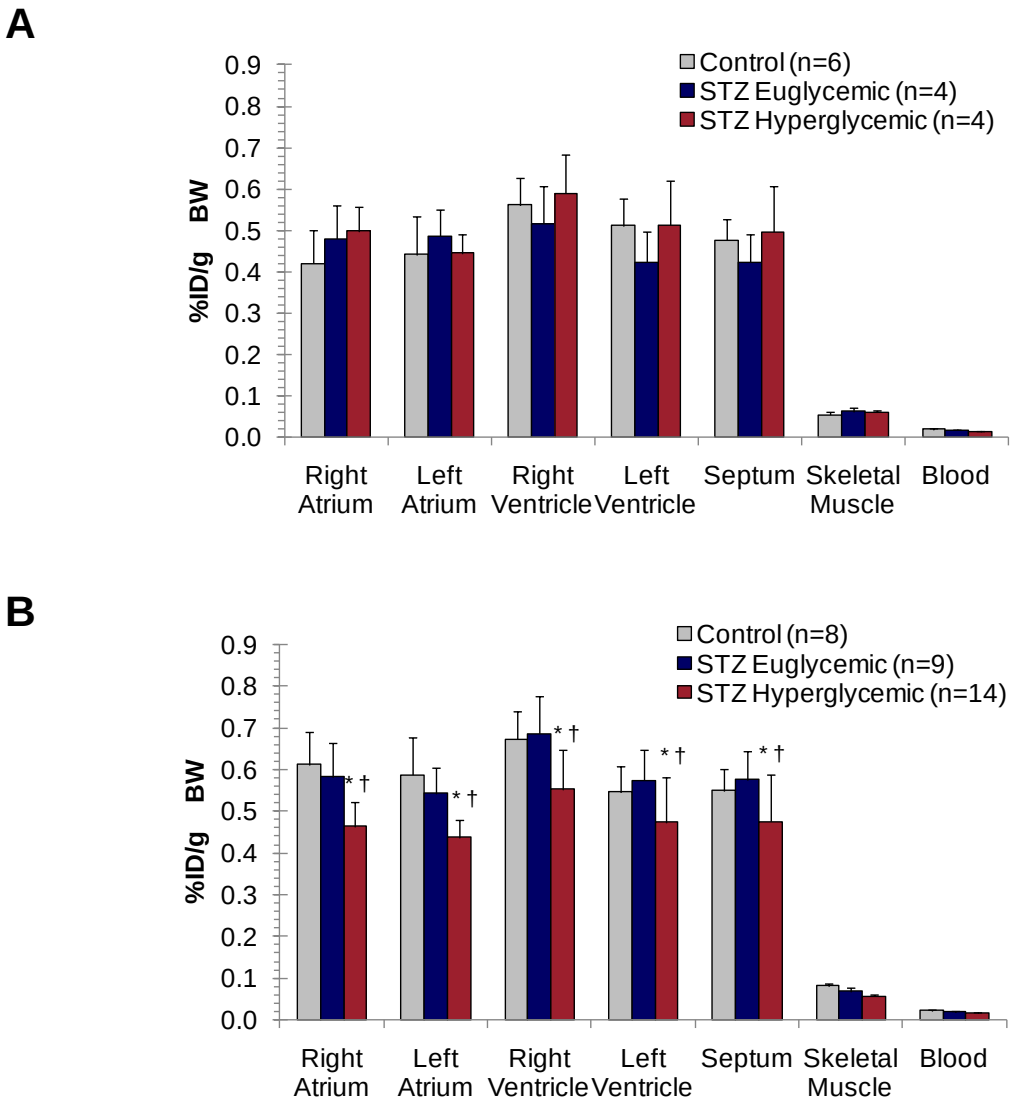

Figure 5.6 *Ex vivo* biodistribution of [^{11}C]HED 30 min post-tracer injection in cardiac regions, skeletal muscle and blood at 2 (**A**) and 8 weeks (**B**) after STZ or vehicle administration. Mean ± SD. * $p<0.05$ to controls, † $p<0.05$ to euglycemic, one-way ANOVA, Bonferroni post hoc.

Table 5.5 Percent change in total and specific cardiac HED retention compared to vehicle treated controls.

Group	Right Atrium	Left Atrium	Right Ventricle	Left Ventricle	Septum
Total Retention					
STZ, Euglycemic	-5±1	-8±1	+2±0	+5±1	+5±1
STZ, Hyperglycemic	-24±4	-26±4	-18±3	-13±3	-13±3
Specific Retention*					
STZ, Euglycemic	-6±1	-12±1	+1±0	+5±1	+5±1
STZ, Hyperglycemic	-24±4	-26±4	-19±3	-12±3	-13±3

Mean ± SD.

*Specific Retention (SR) = Total Retention (TR) – Non-Specific Retention (NSR) [desipramine]

% Change = $TR_{STZ} - TR_{control} / TR_{control}$

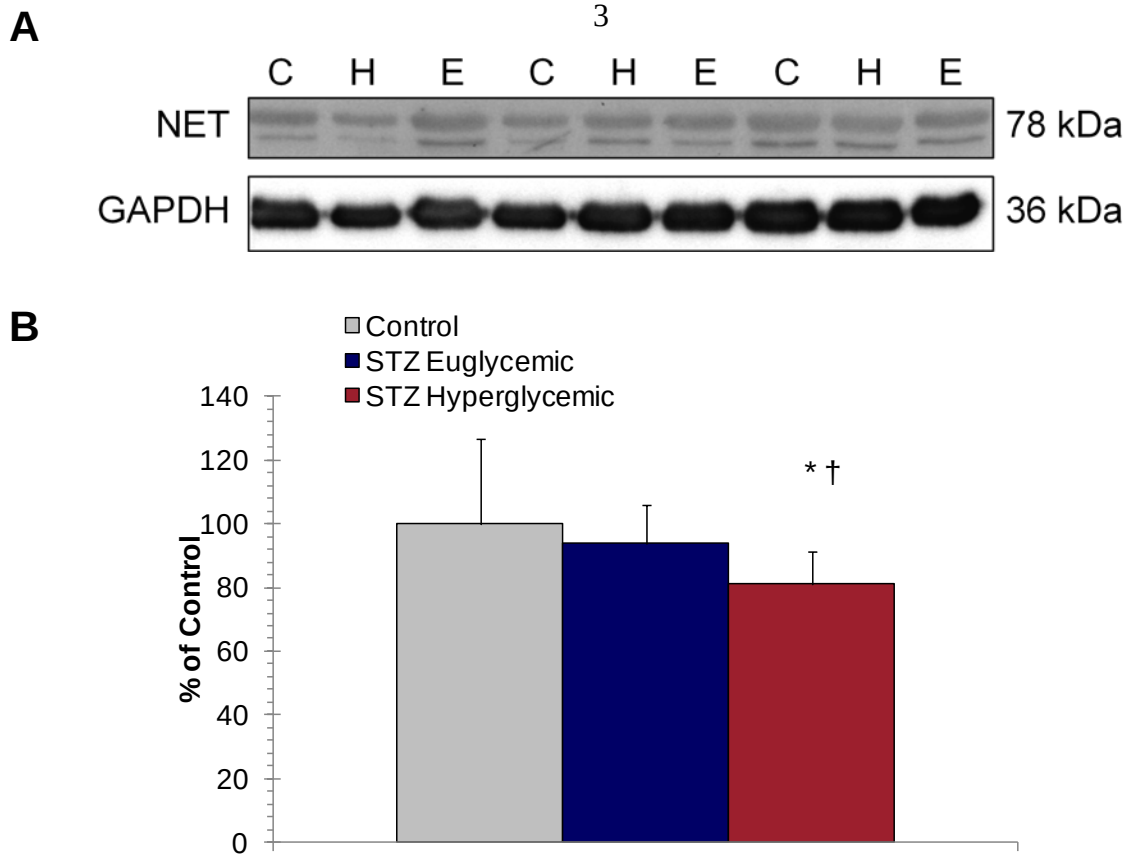

Figure 5.7 **(A)** Representative immunoblots for NET and GAPDH. (**B**) Relative quantification of immunoblot density between groups 8 weeks after STZ or vehicle administration. Mean ± SD. * $p<0.05$ to controls, † $p<0.05$ to euglycemic, two-tailed t-test. C, control; H, STZ hyperglycemic; E, STZ euglycemic.

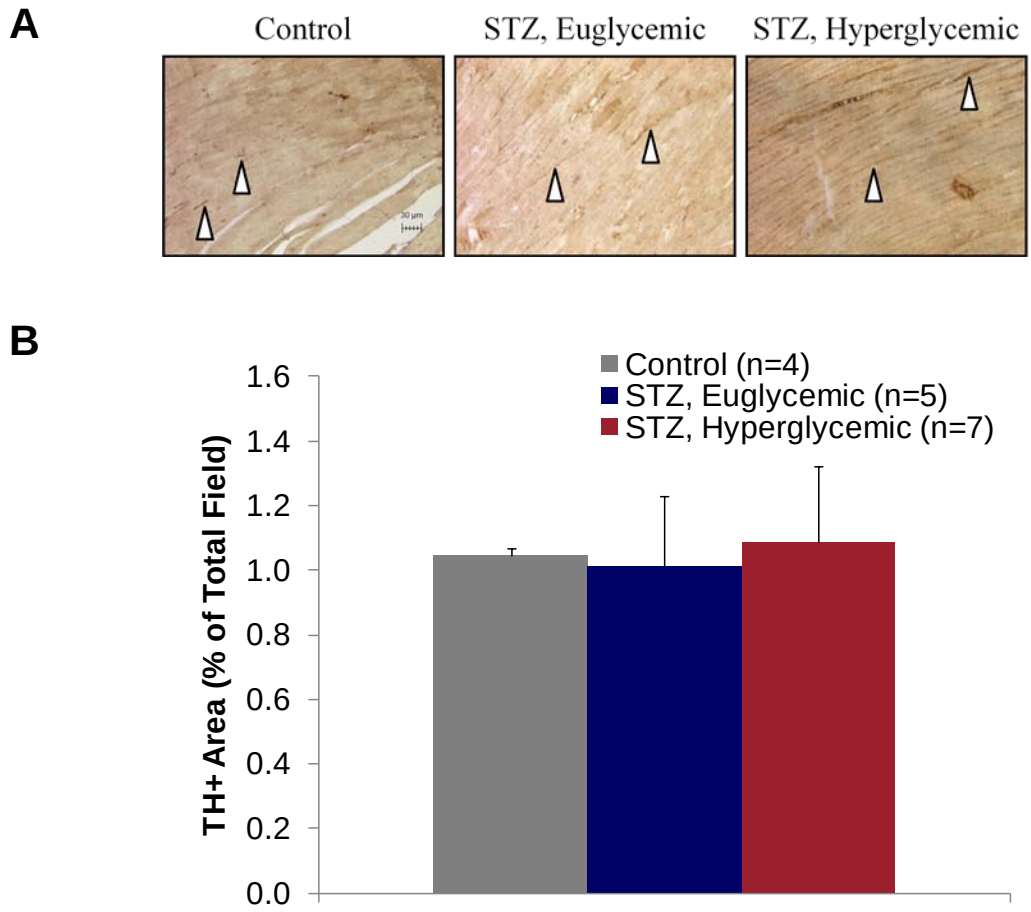

Figure 5.8 (**A**) Sympathetic nerve density assessment by tyrosine hydroxylase immunostaining of left ventricle sections at 8 weeks after STZ or vehicle administration. Representative slides from vehicle-treated control, STZ-treated euglycemic, and STZ-treated hyperglycemic. 200× magnification; white arrowheads indicate tyrosine-hydroxylase positive nerve terminals. (**B**) Relative sympathetic nerve density as percentage tyrosine-hydroxylase-positive area per field of view.

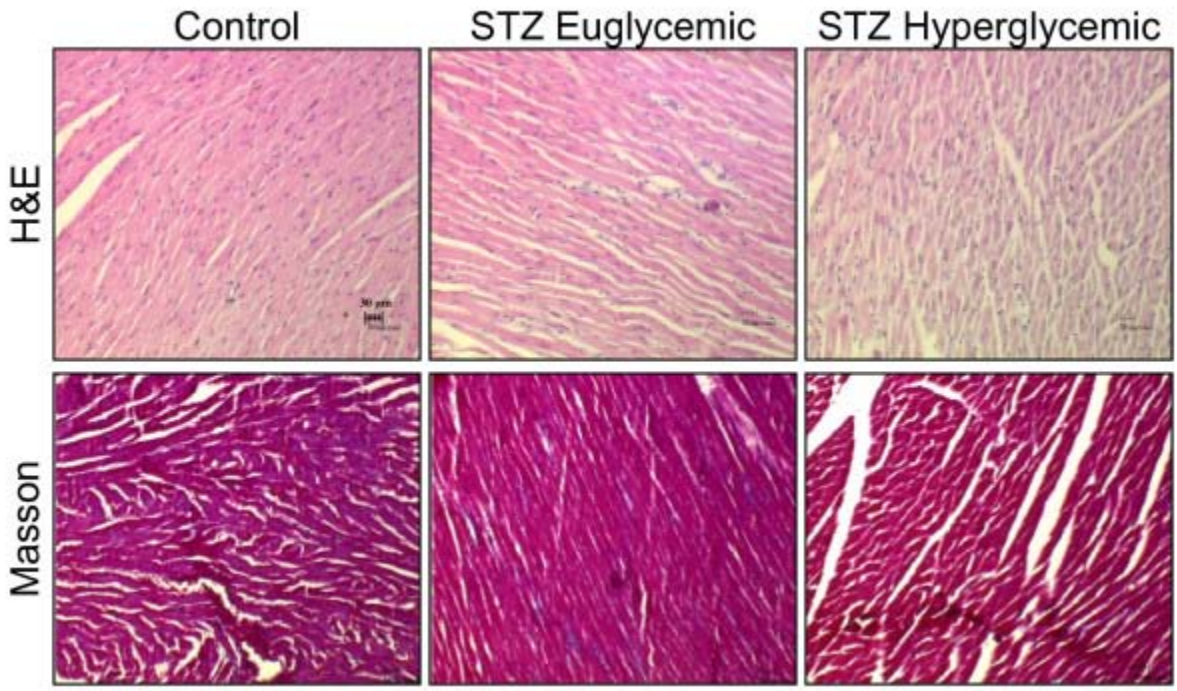

Figure 5.9 Histopathology of left ventricle at 8 weeks after STZ or vehicle administration. Hematoxylin and eosin (H&E) and Masson Trichrome staining in control, STZ euglycemic, and STZ hyperglycemic rats. 200× magnification.

Discussion

In the present article, we describe a progressive deterioration of cardiac sympathetic nervous integrity in the presence of diastolic left ventricular abnormalities in a rat model of insulin resistance with uncontrolled hyperglycemia. A reduction of 12-26% in myocardial [^{11}C]HED retention is paralleled by a modest decrease in relative cardiac NET expression and an increase in plasma and cardiac NE content at 8 weeks of diabetes with no change in sympathetic nerve density. While diastolic function appears to be abnormal, left ventricular ejection fraction is maintained, and histology is unchanged, indicating preserved systolic function.

Diabetic Animal Model

The animal model used in these experiments mimics certain aspects of clinical type 2 diabetes, exhibiting insulin resistance, sustained hyperglycemia, and progressive hypoinsulinemia (Reed et al., 2000; Srinivasan et al., 2005; Zhang et al., 2003). The STZ-treated hyperglycemic rats show reduced insulin, NEFA and triglyceride levels as compared to both sets of controls at 8 weeks, inconsistent with some previous reports describing elevated lipid levels (Reed et al., 2000). This may reflect the longer duration of insulin resistance and diabetes examined in the present study, 2 to 8 weeks post-STZ as compared to 3-7 days. Glucose tolerance deteriorates over time following STZ injection, as evidenced by greater impairment of fasting glucose and higher peak glucose levels attained in hyperglycemic rats following oral glucose loading. Zhang and colleagues demonstrated a similar result with intravenous glucose tolerance testing in this animal model (Zhang et al., 2003). High fat feeding has been shown to induce insulin resistance in rodents, a result that is reflected by the current data. Insulin resistance and glucose intolerance is further supported by the indirect calorimetry data, which demonstrate fatty acid as the preferred energy substrate in STZ-treated hyperglycemic rats, as in other diabetic animal models and in

patients (Houwing et al., 1995; Meex et al.). These diabetic rats lack the obesity and prolonged hyperinsulinemia commonly associated with type 2 diabetes, but permit the evaluation of elevated blood glucose in the presence of high fat diet-induced insulin resistance. Moreover, the inclusion of STZ-treated euglycemic rats, which show a modest development of insulin insufficiency at 8 weeks, suggests that hyperglycemia is the predominant influencing factor in sympathetic dysregulation for this model.

Cardiac Dysfunction in Diabetic Rats

Development of cardiac dysfunction has been documented in several animal models of type 1 and type 2 diabetes, with decline in systolic and diastolic function, as well as in cardiac output (Kim et al., 2003; Marsh et al., 2007; Rodrigues et al., 2011; Sharma et al., 2008a; van den Brom et al., 2009). In the present experiments, hyperglycemic rats exhibit some indicators of impaired diastolic function, as measured by consistently higher E/A ratio and prolonged mitral valve deceleration time. Diastolic dysfunction is a common early manifestation of heart disease in diabetic animal models (Kim et al., 2003) and patients (From et al., 2010). This is comparable to previous reports in the present animal model and in the Zucker Diabetic Fatty rat model of type 2 diabetes, which exhibit reduced heart rate, prolonged isovolumic relaxation time and increased chamber stiffness (From et al., 2010; Marsh et al., 2009; Marsh et al., 2007; van den Brom et al., 2009). Because diastolic parameters are influenced by the time spent in diastole, the reduction of heart rate observed in STZ-treated hyperglycemic rats poses a complication in interpreting these results. A recent study of STZ-induced diabetes in Wistar rats established that autonomic impairment, as measured by reduced baroreflex sensitivity to phenylephrine, was associated with diastolic dysfunction, characterized both by echocardiographic and left ventricular hemodynamics(Rodrigues et al., 2011). Still, further investigation of diastolic function in the present case is warranted.

Sympathetic Nervous Integrity

In the current study, there is a conclusive reduction in presynaptic sympathetic nervous integrity, consistent with previous reports in animal models of diabetes. Reduced tracer accumulation is present despite an increase in heart to body weight ratio compared to STZ-treated euglycemic and vehicle-treated controls, which in the absence of a physiological alteration to sympathetic nervous integrity would be instead expected to increase. This result suggests that reduced [^{11}C]HED retention reflects abnormal sympathetic innervation rather than an artifact of tissue weight. Schmid and colleagues have shown a progressive regional reduction of [^{11}C]HED retention in distal left ventricle in intravenous high dose STZ-induced type 1 diabetic rats as compared to non-diabetic controls, associated with elevated NE at 6 months of diabetes and depletion of nerve growth factor (NGF) at 9 months (Schmid et al., 1999). These data suggest that diabetic autonomic neuropathy associated with reduced cardiac NE content is not present at 8 weeks of diabetes, rather displaying dysregulated sympathetic signaling characterized by elevated NE release. Recently, small animal single photon emission computed tomography (SPECT) imaging using the [^{11}C]HED analogue [^{123}I]*meta*-iodobenzylguanidine (MIBG) in db/db type 2 diabetic mice demonstrated maintained tracer uptake with enhanced washout rate (Kusmic et al., 2008). These findings are consistent with elevated sympathetic activity without a pronounced decrease in NET density; that is, enhanced local release of catecholamines and vesicle-packaged MIBG. Furthermore, Kiyono and colleagues have suggested that differential factors influence MIBG retention in rat models of type 1 and type 2 diabetes (Kiyono et al., 2002a; Kiyono et al., 2001). Specifically, in intravenous STZ-induced type 1 diabetic rats, MIBG retention was moderately reduced compared to controls, paralleled by a twofold increase in cardiac NE concentration and no change in NET (Kiyono et al., 2001). By contrast, in Goto Kakizaki non-obese type 2 diabetic rats, the global and regional decrease in MIBG uptake was

correlated to no change in cardiac or plasma NE but a 30-45% reduction in NET B_{max} as assessed by [^{3}H]desipramine binding assay (Kiyono et al., 2002a). In the present study, after 8 weeks of uncontrolled hyperglycemia, a modest decrease in apparent NET expression is paralleled by a significant 20% elevation of cardiac NE, 250% elevation of plasma NE, and a significant 12-25% reduction in [^{11}C]HED retention. Importantly, the consistent tyrosine hydroxylase immunostaining between groups indicates that sympathetic denervation is not responsible for reduced [^{11}C]HED retention. Persistently elevated catecholamines evoke downregulation of cardiomyocyte β-adrenoceptor expression in parallel with NET (Mardon et al., 2003). We and others have demonstrated that adrenoceptors in diabetic myocardium are reduced by 30-40% (Thackeray et al., 2011a) and can be restored by insulin treatment (Dincer et al., 2001). This has important functional consequences, manifesting as impaired calcium transport by sarcoplasmic/endoplasmic reticulum calcium ATPase (SERCA) and loss of excitation-contraction coupling (Raimondi et al., 2004; Rodrigues et al., 2011).

Sympathetic Nervous System and Heart Disease

Cardiac deterioration is a common endpoint for most diabetic animal models and the most common cause of death in diabetic patients (Kostis and Sanders, 2005). Studies in isolated perfused hearts of STZ-induced diabetic rats have shown reduced cardiac output, depressed cardiac β-adrenoceptor expression, and partial restoration by treatment with the β-blocker metoprolol (Sharma et al., 2008a). Indeed, Mongillo and colleagues propose that presynaptic sympathetic integrity is proportional to glucose uptake in heart failure (Mongillo et al., 2007), suggesting a complementary value in [^{11}C]HED retention to myocardial viability. Considered with the present experiments, these data imply a role for sympathetic dysregulation in the progression of cardiac disease in diabetic rats. Continuous β-adrenergic stimulation by infusion of isoproterenol generates cardiac hypertrophy, bradycardia, and slowed end-diastolic relaxation rates (Nakajima-Takenaka et al., 2009). NET knockout mice

display elevated cardiac NE, hypertension and tachycardia (Keller et al., 2004). Conversely, overexpression of NET has been shown to ameliorate downregulation of β-adrenoceptors and SERCA, and restore ventricle diameters and systolic function in experimental heart failure (Munch et al., 2005). Catecholamines have been implicated in the development of cardiovascular dysfunction, acting to dysregulate calcium transport, alter angiotensin II signaling (Connelly et al., 2007; Henriksen, 2007), increase reactive oxygen species (Maiese et al., 2007), and exert direct toxicity by conversion to quinones (Rupp et al., 1994). Recent work has suggested that abnormal heart rate and heart rate variability in diabetic rats can be normalized by renal denervation using phenol, though conclusions are preliminary (Dias et al., 2011). Cardiac autonomic neuropathy is a common complication of diabetes, associated with depletion of cardiac NE stores and reduced neurotrophin expression. It is conceivable that a period of sympathetic hyperactivity precedes denervation and may provide opportunity for neuronal rescue by NGF therapy, as suggested elsewhere (Ieda et al., 2006).

Potential of PET in Diabetic Heart Disease

The current experiments suggest that non-invasive PET measures of cardiac sympathetic nervous integrity may have important prognostic value for cardiac events in diabetes. In the ADMIRE HF trial, Jacobson and colleagues demonstrated that patients with the lowest heart to mediastinal ratio in MIBG scintigraphy had ten times higher cardiac mortality than those with preserved neuronal uptake (Jacobson et al., 2010). Similarly, the Detection of Ischemia in Asymptomatic Diabetics (DIAD) trial attempted to identify patients at risk of developing cardiac dysfunction by analyzing myocardial perfusion in diabetic patients with preserved ejection fraction (Young et al., 2009). Patients who showed impaired perfusion were more likely to incur a cardiac event. The present results suggest that analysis of sympathetic nervous integrity may provide a more sensitive marker of early cardiac dysfunction in diabetes. A 3 year follow-up [^{11}C]HED imaging study in type 1 diabetic patients

demonstrated recovery of [^{11}C]HED retention in patients with good glycemic control, and greater defect size with reduced tracer uptake in patients with poor glycemic control (Stevens et al., 1999). These studies indicate the potential for molecular imaging to stratify diabetic patients for cardiac risk.

Limitations

A limitation in the use of [^{11}C]HED biodistribution to define sympathetic nervous system defects is the inability to delineate the mechanistic cause of the abnormality. Sympathetic nervous dysfunction can manifest both at the nerve terminals, which can be assessed by [^{11}C]HED PET, or in the central nervous system with efferent nerve traffic, which cannot. Previous work has demonstrated attenuation of sympathoadrenal responses, originating from higher brain centers (Diggs-Andrews et al., 2010). Moreover, direct measurement of neurotrophins was not undertaken in this study, though maintained sympathetic nerve density and elevated cardiac and plasma NE suggest functional sympathetic neurons. While the present work confirms abnormal cardiac sympathetic nervous signaling in sustained hyperglycemia, further research is warranted to more closely define the mechanism of this defect and its relation to diastolic dysfunction.

Conclusions

Sustained hyperglycemia with insulin resistance in the high fat fed moderate dose STZ rat is associated with cardiac sympathetic dysregulation manifested by elevated plasma and cardiac NE, reduced NET expression, and depleted [^{11}C]HED retention with maintained sympathetic nerve density. These findings were observed in conjunction with echocardiographic indicators of diastolic dysfunction and in the absence of systolic dysfunction of the diabetic myocardium. Taken together, these results suggest that non-invasive [^{11}C]HED PET may be a useful tool to monitor cardiac sympathetic nervous dysfunction and guide glycemic therapy in diabetic patients.

Competing Interests

The authors declare that they have no competing interests.

Author Contributions

JTT performed experiments, contributed to discussion, and drafted the manuscript. JR, MEH, EJS and KJA contributed to discussion and reviewed/edited the manuscript. RSB and JND supervised research, contributed to discussion and writing, and reviewed/edited the manuscript. All authors have read and approved the final manuscript.

Acknowledgements

This work was funded by the Heart and Stroke Foundation of Canada #NA6477 and PRG6242, a Doctoral Research Award to JTT and a Career Investigator Award to RSB. The authors thank Stephanie Thorn, Miran Kenk, and Maria Kolajova of the PET Biotesting Laboratory; Lisa Bevilacqua of the Mitochondrial Bioenergetics Laboratory; and Samantha Mason, Jeffrey Collins, and Paul Coletta of the Radiochemistry Laboratory for technical assistance in these studies.

Chapter 6: Manuscript #5

Cardiovascular Research (2012, Submitted)

Insulin restores myocardial presynaptic sympathetic neuronal integrity in insulin resistant diabetic rats

James Thackeray,[1,2] Robert A deKemp,[1] Rob S Beanlands,[1,2] Jean N DaSilva[1,2]

[1]Molecular Function & Imaging Program, National Cardiac PET Centre, University of Ottawa Heart Institute
[2]Department of Cellular & Molecular Medicine, Faculty of Graduate and Postdoctoral Studies, University of Ottawa

Key words: Diastolic dysfunction, Glycemic therapy, meta-Hydroxyephedrine (HED), Noradrenaline,

Contributions of Authors

The experiments described in this manuscript were designed and executed by the candidate with the supervisory assistance of Dr Beanlands and Dr DaSilva. The candidate analysed and interpreted all data and drafted the manuscript. Physicist Dr deKemp contributed to the interpretation of quantitive imaging results. Dr Beanlands provided a clinical perspective on the data. Dr DaSilva supervised the project and participated in editing and revising the manuscript.

ABSTRACT

Aims – Diabetes is associated with increased sympathetic nerve activity, elevated circulating noradrenaline, impaired heart rate variability, and added risk of cardiovascular mortality. This study aims to evaluate the temporal development of altered sympathetic neuronal integrity in diabetic rats and determine the effect of glycemic therapy on these abnormalities.

Methods and Results – Using the noradrenaline analogue [^{11}C]*meta*-hydroxyephedrine (HED) and positron emission tomography, we serially investigated myocardial sympathetic neuronal integrity in Sprague Dawley rats rendered diabetic by streptozotocin and insulin resistant by high fat feeding. Images were obtained at pre-diabetic baseline, at 8 weeks of diabetes, and after a subsequent 8 weeks of treatment. Rats were treated with either insulin (4 U/d) or metformin (650 mg/kg/d) to restore insulin sensitivity. Implantable telemetry and echocardiography measurements provided indication of cardiac function. Retention of HED was reduced in diabetic rats compared to age-matched non diabetics at 8 weeks by 52-57% ($p=0.01$). Treatment with insulin but not metformin restored HED retention to a level comparable to non-diabetics. Reduced tracer retention was confirmed by elevated plasma and myocardial noradrenaline and reduced relative expression of noradrenaline reuptake transporter and β-adrenoceptors in metformin-treated diabetic rats which was attenuated by insulin treatment. Diabetic rats exhibited persistently reduced heart-rate variability and impaired diastolic function. Insulin treatment was ineffective in restoring these parameters.

Conclusion – The results suggest that reduced sympathetic neuronal integrity observed in imaging studies may reflect elevated sympathetic activity rather than neuropathy. Effective glycemic control can recover sympathetic function in diabetic rats. Neurohormonal imaging may be useful in stratifying cardiovascular risk among diabetic patients.

Introduction

Sustained hyperglycemia in diabetes leads to higher rates of cardiovascular morbidity and mortality. Heightened systemic and cardiac sympathetic nervous system signaling is believed to play a role in the progression of left ventricular dysfunction in diabetes. Central and systemic release of noradrenaline levels is augmented by glucose (Levin and Sullivan, 1987), insulin (Rizk and Dunbar, 2004), and non-esterifed fatty acids (Florian and Pawelczyk). Persistent elevation of glucose and noradrenaline evokes downregulation of noradrenergic signaling components including β-adrenoceptors (Dincer et al., 2001; Thackeray et al., 2011a), neuronal noradrenaline reuptake transporter (NAT) (Thackeray et al., 2011b), and tyrosine hydroxylase (Li et al., 2004). Diabetic animals exhibit reduced heart rate variability due to imbalance of sympathetic and parasympathetic stimulation of the heart (Howarth et al., 2005b). Sympathetic nervous dysfunction in diabetes is often associated with cardiac autonomic neuropathy. The five-year mortality rate of diabetic patients with autonomic neuropathy has been reported to be as high as 50% (O'Brien et al., 1991). We have recently demonstrated the presence of cardiac sympathetic dysfunction in a rat model of insulin resistance with hyperglycemia (Thackeray et al., 2011b). These animals exhibit elevated plasma and cardiac noradrenaline, reduced NAT expression, but maintained sympathetic nerve density in the presence of diastolic dysfunction. This observation suggests that a period of aberrant noradrenergic signaling may precede the death of sympathetic neurons.

The advancement of dedicated small animal imaging has facilitated longitudinal evaluation of disease progression and regression to treatment. Positron emission tomography using the noradrenaline analogue [^{11}C]*meta*-hydroxyephedrine (HED) provides a measurement of presynaptic sympathetic function selective to NAT (Tipre et al., 2008). Retention of HED is directly proportional to NAT function and inversely proportional to synaptic and systemic noradrenaline levels (Law et al., 2010; Thackeray et al., 2012 (Submitted)-b).

Changes in presynaptic sympathetic function in the diabetic heart have been established by *ex vivo* autoradiography and biodistribution studies in streptozotocin-induced type 1 diabetic (Kiyono et al., 2001; Schmid et al., 1999), high fat diet-fed streptozotocin insulin resistant (Thackeray et al., 2011b), and Goto Kakizaki non-obese type 2 diabetic rats (Kiyono et al., 2002a). These studies have been extended to small animal imaging with SPECT in which the HED analogue ^{123}I-metaiodobenzylguanidine (MIBG) washout was accelerated by 40-90% and left ventricular tracer accumulation reduced by 30-60% in rats (Dubois et al., 1997) and mice (Kusmic et al., 2008). Similar observations have been reported clinically. Follow-up studies established that effective glucose control among diabetic patients translated to smaller defects and improved tracer retention whereas poor glucose control led to larger and more severe innervation defects (Muhr-Becker et al., 1999; Stevens et al., 1998b). By contrast, patients without diabetes exhibited no change in HED retention at 1 year of follow up with neurostimulation (Fricke et al., 2008). Comorbidities such as heart failure (Gerson et al., 2011), hypertension (Takahashi et al., 2001), and microvascular disease (Pop-Busui et al., 2004) are associated with larger defect area, accelerated tracer washout, and higher incidence of cardiac events.

We hypothesized that administration of insulin to reduce blood glucose or metformin to restore insulin sensitivity would normalize cardiac sympathetic signaling and left ventricular function in diabetic rats. In a rat model of hyperglycemia with insulin resistance, we conducted longitudinal HED PET imaging in parallel with implantable radiotelemetry assessment of autonomic drive and echocardiography measures of left ventricular function. Imaging data were validated by *in vitro* measurements of noradrenaline, NAT, β_1- and β_2-adrenoceptors.

Methods

Animals

All animal experiments were conducted in accordance with the recommendations of the Canadian Council on Animal Care and with the approval of the University of Ottawa Animal Care Committee. Male Sprague Dawley rats (Charles River, Montreal, Canada) were maintained on high fat diet matched to condensed milk diet (32% kcal, Research Diets D12266B, New Brunswick, NJ) for 19 weeks. After two weeks of feeding, diabetes was induced by intraperitoneal injection of streptozotocin (45 mg/kg, T0, Sigma, Toronto, Canada). Blood glucose levels were measured weekly using a glucose meter. Rats that did not reach blood glucose > 12 mM were excluded from the study. Rats were killed at the conclusion of 17 weeks (T17) (Fig 6.1).

Treatment

After 8 weeks of sustained diabetes (T8), rats were randomized to receive either insulin or metformin. Insulin was provided as a continuous administration by subcutaneous pellet at 4 U/day (LinShin, Toronto, Canada) (Arikawa et al., 2007). Metformin (TRC, Toronto, Canada) was provided orally in 5 mL sugar-free gelatin at a titrated dose, beginning from 350 mg/kg/d × 4 d, then 500 mg/kg/d × 6 d, to a final dose of 650 mg/kg/d beginning on the eleventh day of treatment (Verma and McNeill, 1994). Non-diabetic rats received no treatment.

Echocardiography

To evaluate left ventricular function, serial echocardiography measurements were taken at -2, 0, 4, 8, 12, and 16 weeks of diabetes using the Vevo 770 (VisualSonics, Toronto, Canada). Systolic function was evaluated by analysis of electrocardiogram-gated cines of the parasternal long axis. Diastolic function was estimated by transmitral pulse wave Doppler measurement of early and atrial velocities.

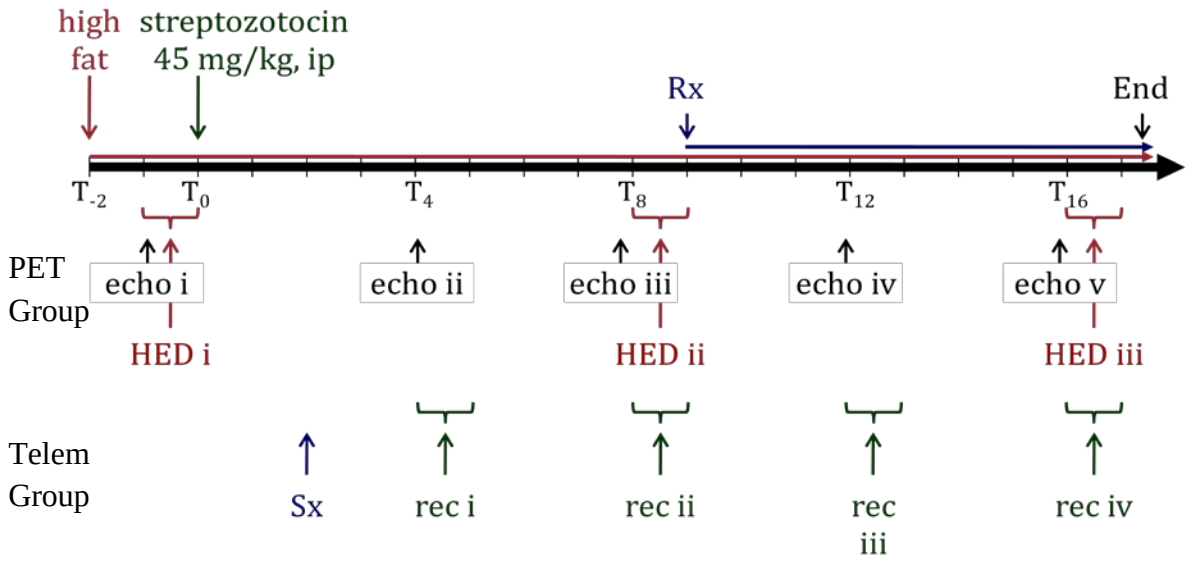

Figure 6.1 **Timeline of experiments.** Rats are fed high fat diet for two weeks prior to the administration of streptpzotocin to induce diabetes at week 0 (T0). After 8 weeks of sustained diabetes, treatment with insulin or metformin is initiated at 9 weeks (T9) and continued until the end of the experiments at 17 weeks (T17). Sympathetic neuronal integrity is assessed by ^{11}C-HED PET scans at baseline (T0), after 8 weeks of diabetes (T8), and after 8 subsequent weeks of treatment (T16). Cardiac systolic and diastolic function is measured by echocardiography at T-1, T4, T8, and T16. In a parallel group of animals, radiotelemetry monitoring was completed with surgical implantation at T2 and recording at T4, T8, T12, and T16. At the end of the protocol, rats were sacrificed and tissues were flash frozen for immunoblot analysis of catecholamine quantification by high performance liquid chromatography.

Small Animal HED PET

HED was synthesized as previously described (Thackeray et al., 2007). To evaluate myocardial sympathetic neuronal integrity, rats underwent longitudinal imaging studies using the noradrenaline analogue HED with the Inveon DPET small animal camera (Siemens, Knoxville, TN). PET scans were carried out at baseline (T0), diabetic (T8), and after treatment (T16) (Thackeray et al., 2012 (Submitted)-b). Briefly, under light anaesthesia, rats were positioned supine on small animal PET scanner bed and injected with 18.5 MBq of HED via a 26 Ga catheter inserted into a lateral tail vein. Images were acquired over 60 min. A ^{57}Co transmission scan was carried out to allow for attenuation correction. Images were reconstructed as previously described using an OSEM3D/MAP algorithm (Thackeray et al., 2012 (Submitted)-b). Left ventricle was defined using FlowQuant© software and used to generate time-activity curves for the left ventricle myocardium and blood pool input function. Following initial clearance of the blood pool activity, dynamic myocardial data were fitted to a monoexponential (k_{mono}) washout function. Standardized uptake value (SUV) was calculated at 30-35 min as Uptake(30)/(Dose/BW) where Uptake is Bq/cc from the myocardial time activity curve, Dose is the injected activity in Bq, and BW is the subject body weight in g.

Implantable Telemetry

To evaluate the physiological effect of sympathetic nervous dysregulation in diabetic rats, radiotelemetry probes were implanted for serial measurement of arterial pressure and heart rate (DSI, St Paul, MN) (Howarth et al., 2005b). Two weeks following induction of diabetes, rats (n=8 diabetic, n=4 non-diabetic) were selected for telemetry implantation. Rats received analgesic buprenorphine (0.04 mg/kg, sc) prior to and for two days following surgery. Under isoflurane anaesthesia, an incision was made in the abdomen, intestines retracted, and the descending aorta was isolated. The pressure transducer was inserted into the artery between

the iliac bifurcation and renal artery branches. The insertion point was sealed using tissue adhesive (VetBond, 3M, St Paul, MN). Electrocardiogram leads were externalized superior to the incision, tunneled subcutaneously, and secured by suture at the right pectoral (positive) and to the left of the xyphoid process (negative). Rats were allowed to recover over 2 weeks prior to initial telemetry sampling. Physiological data was recorded in hourly 20 s segments over 7 days at 4, 8, 12, and 16 weeks of diabetes. Insulin therapy was initiated in diabetic telemetry rats at 9 weeks and maintained to the conclusion of the study. Heart rate variability was calculated as the standard deviation of the average hourly rate over a twenty-four hour period (Howarth et al., 2005b).

Euglycemic Clamp

To determine the efficacy of metformin therapy for insulin sensitization in diabetic rats, a subgroup of animals underwent hyperinsulinemic euglycemic clamp (Thackeray et al., 2011b). Under light anaesthesia, insulin was continuously infused via venous catheter at 30 mU/kg/h and counteracted by variable infusion of 20% glucose to maintain fasted euglycemia (5 mM). Blood glucose concentration was monitored by sampling of the carotid artery.

Blood Markers

Blood samples were taken at the time of the PET scan and used to determine plasma concentration of noradrenaline. Concentration of catecholamines was determined in myocardial tissue and plasma as described previously using HPLC with electrochemical detection (ESA, Montreal, Canada) (Thackeray et al., 2011b). Plasma insulin levels were measured from venous blood samples obtained at the conclusion (T17) of the study by commercial ELISA (Alpco, Salem, NH). Plasma fatty acid and triglyceride levels were determined by commercial enzyme colorimetric assay kit (BioVision, Toronto, Canada).

Immunoblots

To validate small animal PET results, myocardial tissue was processed for western immunoblotting. Antibodies used were: rabbit polyclonal anti NAT (Chemicon/Millipore, Billerica, MA), rabbit polyclonal anti β_1AR (Abcam, Cambridge, MA), rabbit polyclonal anti-β_2AR (Santa Cruz, Santa Cruz, CA), rabbit anti-GLUT4 (Abcam), rabbit anti phospho-Acetyl CoA Carboxylase (Abcam). Immunoblots were analysed by chemiluminescence and integrated density values normalized toglyceraldehyde 3-phosphate dehydrogenase (GAPDH) were compared between groups.

Statistics

Data are presented as mean ± standard deviation. Imaging data were compared between groups using one-way analysis of variance with Bonferroni's post hoc test. Longitudinal data were compared using general linear model for repeated measures. Radiotelemetry measures, blood factors and immunoblots were compared to non-diabetic controls using two-tailed t-test.

Results

High fat feeding and streptozotocin induces sustained hyperglycemia and progressive hypoinsulinemia with a shift in myocardial substrate metabolism

Following induction of diabetes, rats exhibit sustained elevation of blood glucose to an average of 26.6±1.9 mM. Continuous treatment with insulin normalized circulating fed-state plasma insulin and lowered blood glucose to non-diabetic levels (Fig 6.2A). Metformin therapy had no effect on plasma insulin or blood glucose, but insulin sensitivity was enhanced despite continued high fat feeding (Fig 6.2B). Diabetic rats showed elevated levels of non-esterified fatty acids and triglycerides which were reduced by insulin but not metformin treatment (Table 6.1). To evaluate the shift in metabolic substrate utilization,

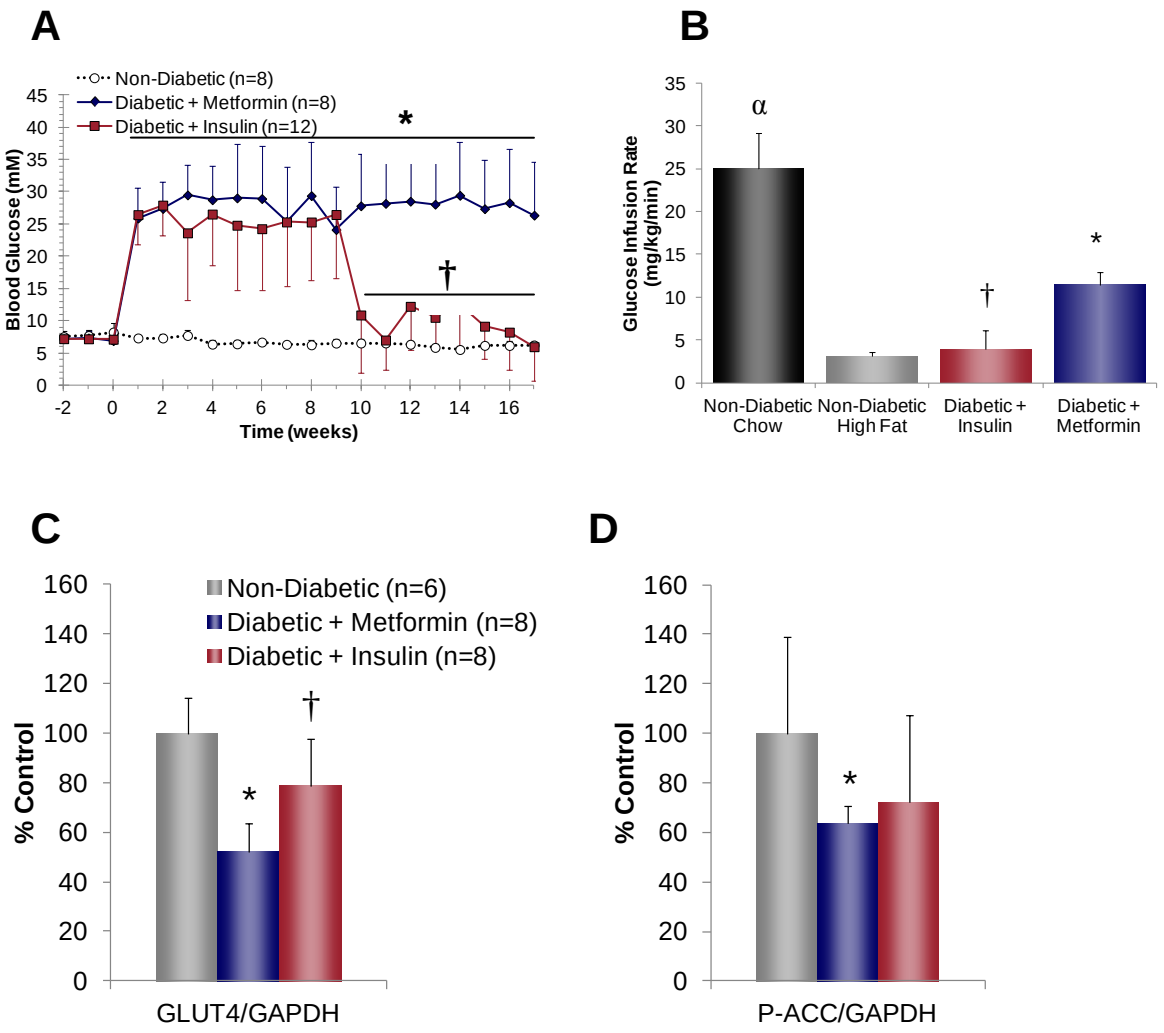

Figure 6.2 Characteristics of diabetic rats and response to insulin and metformin therapy. (**A**) Blood glucose levels taken weekly from saphenous bleed of diabetic and non-diabetic rats. (**B**) Glucose infusion rate to maintain fasted blood glucose level counteracting continuous infusion of 30 mU/kg/h insulin in hyperglycemic-euglycemic clamp. (**C**) Expression of GLUT4 in myocardial tissue normalized to GAPDH expressed as a percent of non-diabetic. (**D**) Expression of phosphorylated acetyl CoA carboxylase in myocardial tissue normalized to GAPDH expressed as a percent of non-diabetic. * $p<0.05$ to non-diabetic control; † $p<0.05$ to diabetic + metformin; α $p<0.05$ to non-diabetic high fat, diabetic, and diabetic + metformin, two-tailed t-test.

Table 6.1 Body weight, terminal insulin and lipid levels in non-diabetic and treated diabetic rats.

	Non-Diabetic (n=8)	Diabetic + Insulin (n=12)	Diabetic + Metformin (n=8)
Weight T0 (g)	229±9	220±8	229±8
Weight T8 (g)	731±63	422±44*	426±40*
Weight T16 (g)	839±82	601±47*†	471±51*
Insulin (ng/mL)	3.3±0.7	3.1±0.3†	0.6±0.1*
NEFA (ng/µL)	0.25±0.12	0.18±0.19†	0.67±0.33*
Triglyceride (ng/µL)	0.90±0.51	0.79±0.38	0.80±0.35

* $p<0.05$ to age-matched non-diabetic

† $p<0.05$ to age-matched diabetic + metformin

relative expression of proteins involved in glucose and fatty acid oxidation were evaluated by immunoblotting in cardiac muscle. Whereas metformin-treated diabetic rats showed a marked decrease in cardiac GLUT4 expression, insulin-treated diabetic rats showed increased expression compared to non-diabetics (Fig 6.2C). Cardiac expression of phosphorylated acetyl CoA carboxylase was reduced in metformin-treated and insulin-treated diabetic rats suggesting abnormalities in β-oxidation (Fig 6.2D).

Diabetic rats exhibit abnormal left ventricular filling and echocardiography markers of diastolic dysfunction

Ventricular dimensions and systolic function were unchanged in diabetic and non-diabetic rats over the 19 weeks of the study. Left ventricular ejection fraction was unchanged over the course of the study in all groups (Fig 6.3A). Ventricular dimensions did not significantly differ between groups over the course of the study (Fig 6.3B). Stroke volume and cardiac output were increased over time but did not vary between groups. However, by 4 weeks after STZ, diabetic rats began to exhibit abnormal diastolic ventricular function. Mitral valve deceleration time was extended by 201% (Fig 6.3C) and early-to-atrial transmitral filling velocity ratio was elevated by 41% in diabetic rats at 8 weeks compared to age-matched non-diabetic rats (Fig 6.3D), driven predominantly by a reduction in late transmitral velocity (Fig 6.3E). There was no improvement in diastolic echocardiographic measurements following treatment with insulin or metformin.

Presence of diabetes reduces retention and accelerates washout of HED in left ventricle which is restored by insulin treatment

A complete set of 3 longitudinal PET scans were obtained for 7, 6, and 6 rats in the insulin-treated, metformin-treated, and non-diabetic groups. Representative repeated time activity curves for each group show reduced initial uptake and accelerated washout in diabetic rats

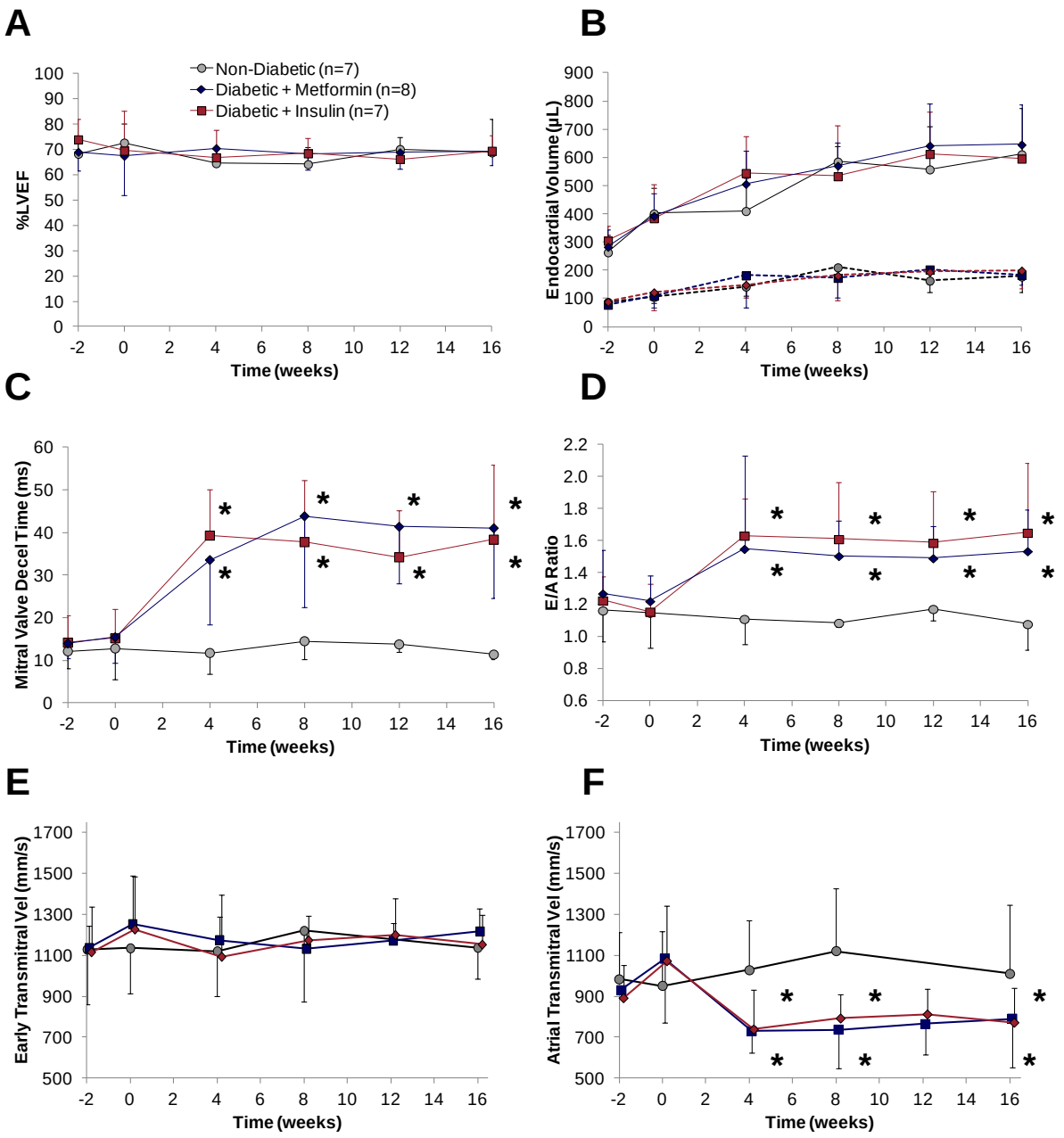

Figure 6.3 Serial echocardiography parameters of diabetic rats and response to insulin and metformin therapy. (**A**) Percent left ventricular ejection fraction (%LVEF) and (**B**) left ventricle endocardial volume at end diastole (solid lines) and end systole (dashed lines) indicate no difference in systolic function. (**C**) Mitral valve deceleration time is prolonged and (**D**) early to atrial transmitral velocity ratio is shifted with (**E**) maintained early and (**F**) lower atrial filling velocities indicating diastolic dysfunction in diabetic rats that does not respond to either therapy. * $p<0.05$ to non-diabetic, two-tailed t-test.

treated with metformin (Fig 6.4A). HED left ventricular SUV was increased over time in non-diabetic rats by 57% at 8 weeks and 52% and 16 weeks compared to baseline (T0) (Fig 6.4B). By comparison, SUV in diabetic rats was unchanged at 8 weeks, and was 42-48% lower compared to age-matched non-diabetic controls. Treatment with insulin resulted in a recovery of HED left ventricular SUV to 89% of age-matched non-diabetic controls (Fig 6.4B). There was no recovery of SUV among diabetic rats treated with metformin, which also failed to restore euglycemia remaining at 47% of controls. Monoexponential washout of HED was accelerated in diabetic rats treated with metformin at 16 weeks compared to non-diabetic controls and insulin-treated diabetics. In contrast, insulin treatment stabilized tracer washout rates compared to non-diabetic controls at 16 weeks (Fig 6.4C).

Radiotelemetry measures of arterial pressure and heart rate variability are nonresponsive to insulin treatment

To determine the functional consequences of this myocardial sympathetic defect, rats were implanted with radiotelemetry transponders to monitor arterial pressure and electrocardiogram. Diabetic rats exhibited comparable mean arterial pressure as compared to non-diabetic controls in early stages with a trend towards hypertension by the end of the study (Fig 6.5A). Heart rates were consistently lower in diabetic rats by an average of 37 bpm as compared to non-diabetic controls (Fig 6.5B). Neither therapy with insulin nor metformin restored blood pressure or heart rate toward normal. Intrabeat interval was longer in diabetics than non-diabetics (Fig 6.5C). Heart rate variability assessed as standard deviation of the 24 h heart rate was lower among diabetic rats as compared to controls at 4 and 8 weeks (Fig 6.5D). No recovery of heart rate variability was evident following treatment with insulin.

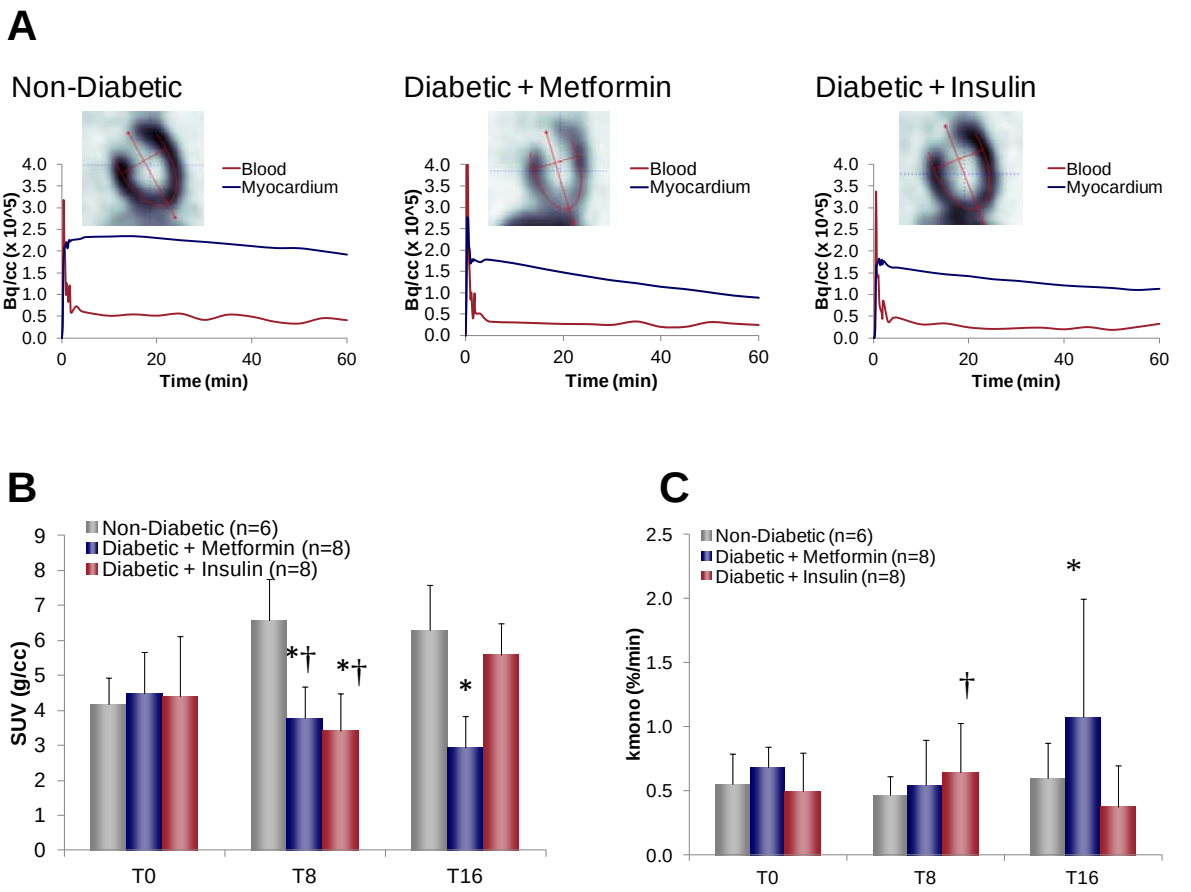

Figure 6.4 Longitudinal HED PET quantification in non-diabetic and diabetic rats before and after treatment. (**A**) Representative vertical long axis left ventricle HED images and time-activity curves for blood and myocardium in non-diabetic, diabetic + insulin, and diabetic + metformin rats at 16 weeks of diabetes and 8 weeks of treatment. Serial evaluation of (**B**) HED standardized uptake value (SUV) and (**C**) monoexponential washout rate (kmono) at baseline (T0), diabetic pre-treatment (T8), and post-treatment (T16) timepoints. * $p<0.05$ to age-matched non-diabetic controls, one-way ANOVA Bonferroni post hoc; † $p<0.05$ to T0, § $p<0.05$ to T8, repeated measure.

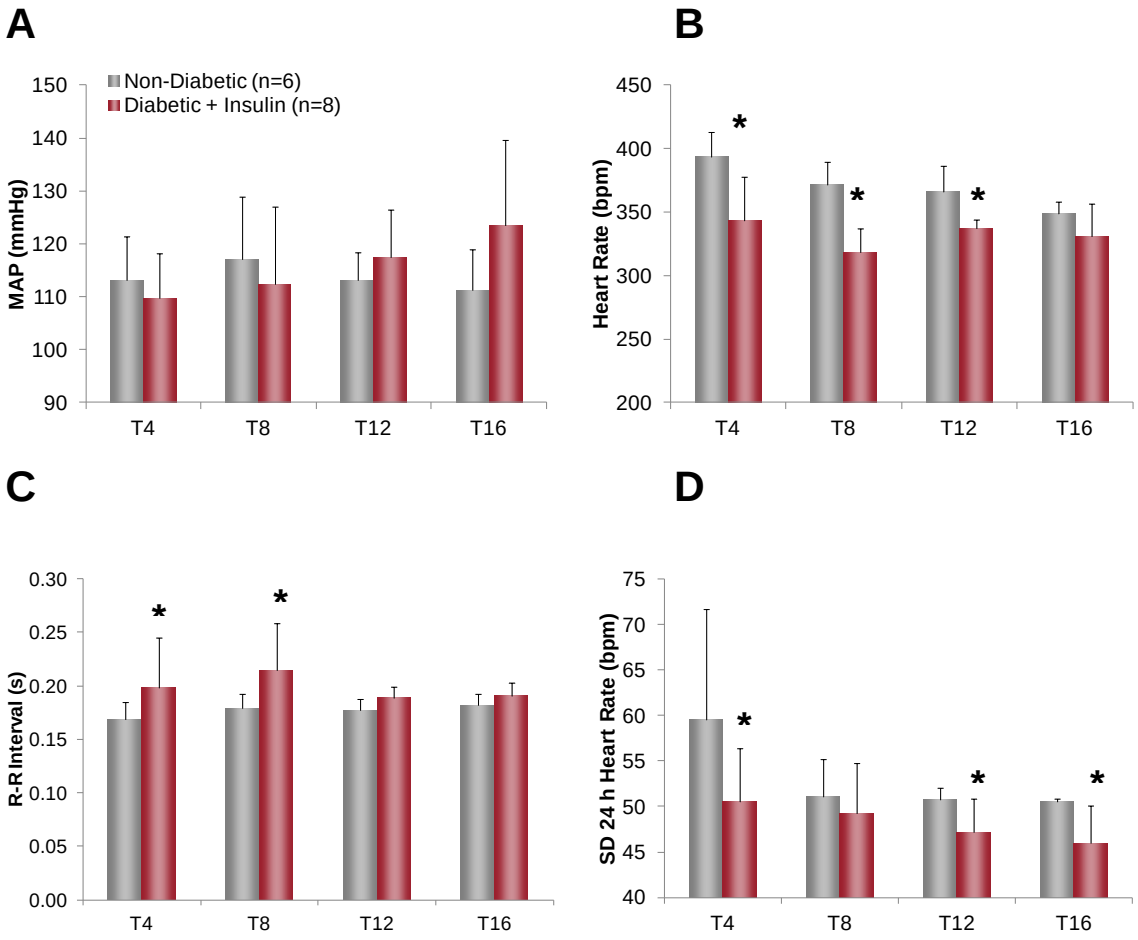

Figure 6.5 Serial radiotelemetry measurements of hemodynamics and heart rate variability in non-diabetic and diabetic rats before and after insulin treatment. (**A**) Mean arterial pressure is moderately increased at 16 weeks (T16). (**B**) Heart rate is persistently lower in diabetic rats as compared to non-diabetic controls with (**C**) elevated intrabeat R-R interval. (**D**) Standard deviation of heart rate over 24 hour period shows a trend for reduced heart rate variability in diabetic rats. * $p<0.05$ to non-diabetic control.

Plasma and cardiac noradrenaline is normalized by glycemic control with insulin

Small animal PET measurements with HED were validated by serial measurements of plasma and terminal measurements of cardiac noradrenaline levels. After 8 weeks of sustained diabetes, plasma noradrenaline concentrations were elevated by 2-3-fold compared to non-diabetic controls (Fig 6.6A). Subsequent treatment with insulin reduced circulating levels of noradrenaline by 50%. Metformin treatment did not reduce plasma noradrenaline. To determine local noradrenaline turnover, myocardial tissue was collected at the termination of the experiment. Cardiac noradrenaline was elevated in metformin-treated and insulin-treated groups compared to non-diabetic controls (Fig 6.6B).

Insulin treatment restores normal expression patterns of noradrenergic signaling components in diabetic rats

To further confirm small animal PET measurements with HED and investigate the noradrenergic signaling abnormality, relative myocardial levels of proteins involved in sympathetic signal transduction were investigated by immunoblotting at the terminal endpoint of the study (T17) (Fig 6.7A). Relative NAT expression was reduced in hearts of diabetic rats treated with metformin compared to non-diabetic controls by 28% (Fig 6.7B). After insulin treatment this reduction was attenuated to 13% of non-diabetic controls. Similarly, in sustained hyperglycemic rats treated with metformin, relative expression of postsynaptic β_1- and β_2-adrenoceptors was reduced by 45% and 27%, respectively, whereas insulin treatment partially restored expression to 77% and 90% of non-diabetics (Fig 6.7B).

Discussion

The diabetic heart exhibits a deficit in sympathetic neuronal integrity evidenced by HED in small animal PET imaging. Myocardial retention of HED was reduced and washout was accelerated in diabetic rats at 8 weeks of diabetes compared to non-diabetic controls in

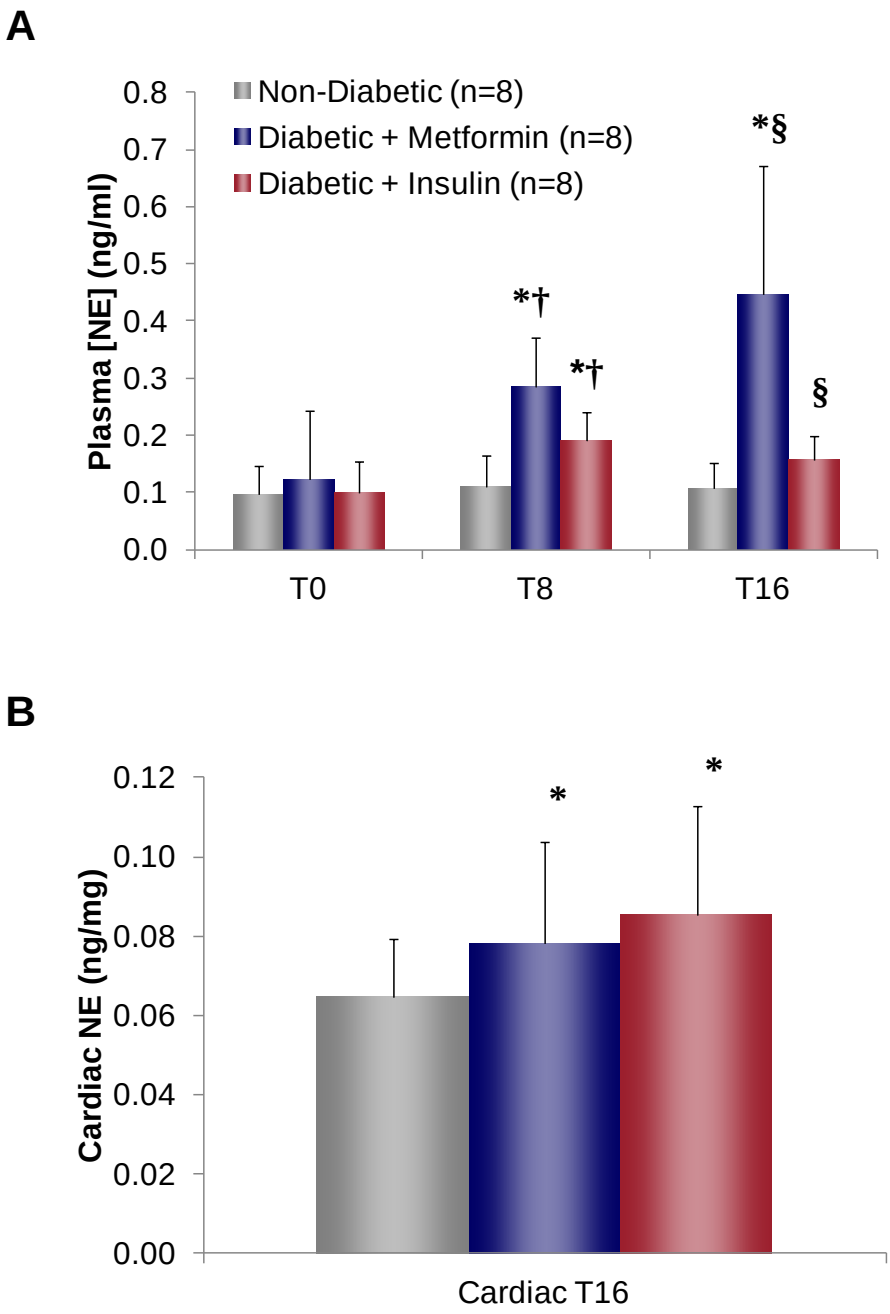

Figure 6.6 Serial plasma and terminal cardiac noradrenaline in non-diabetic and diabetic rats before and after treatment. (**A**) Plasma noradrenaline levels from tail vein samples obtained a time of PET scans at baseline (T0), diabetic pre-treatment (T8), and post-treatment (T16) timepoints. (**B**) Cardiac noradrenaline levels in whole heart samples obtained at the conclusion of the study (T16). * $p<0.05$ to age-matched non-diabetic, two-tailed t-test; † $p<0.05$ to baseline and § $p<0.05$ to T8 samples, repeated measure.

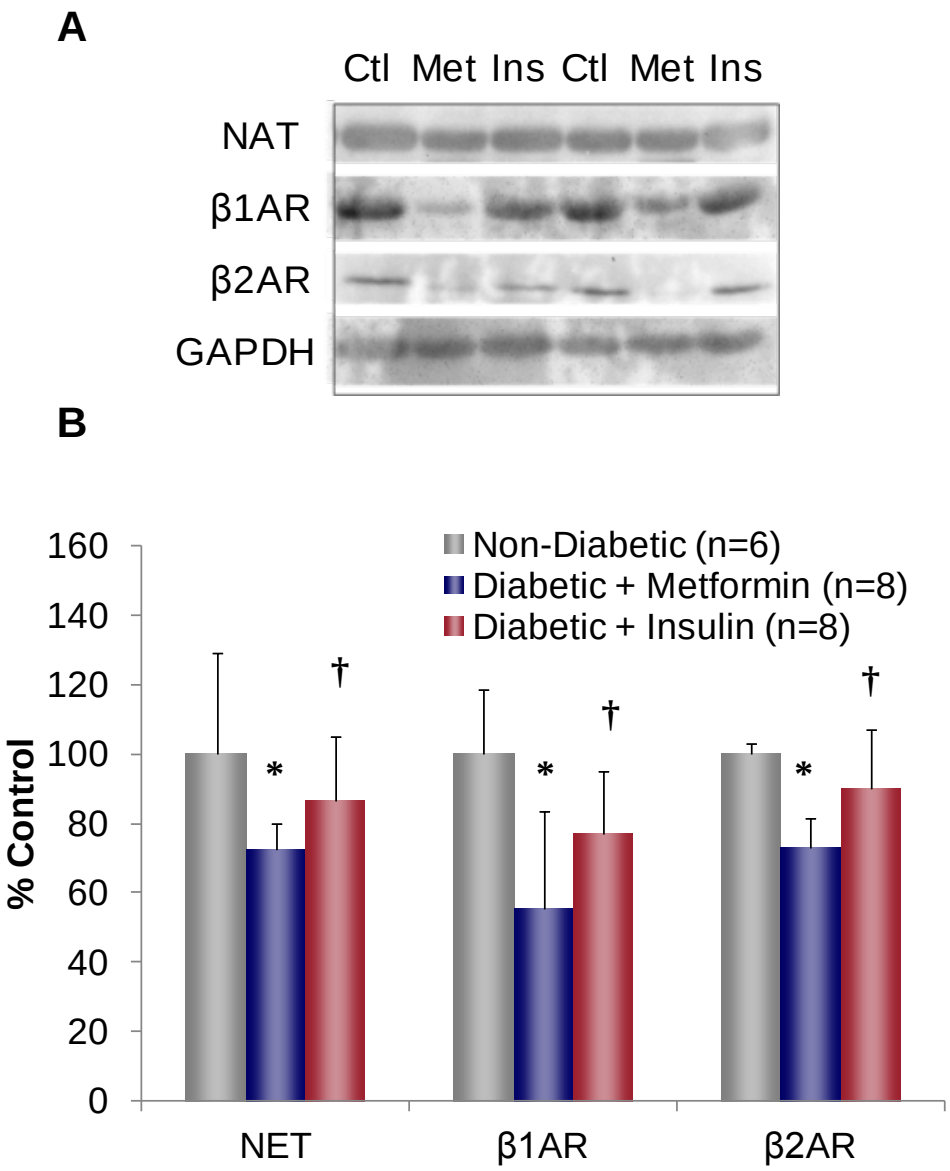

Figure 6.7 Immunoblotting of noradrenergic signaling components in myocardium of non-diabetic and diabetic rats treated with insulin or metformin. (**A**) Sample immunoblots in non-diabetic control (Ctl), metformin-treated diabetic (Met), and insulin-treated diabetic (Ins) at 16 weeks of diabetes and 8 weeks of treatment for noradrenaline reuptake transporter (NAT), β_1-adrenoceptors (β1AR), β_2-adrenoceptors (β2AR) and GAPDH loading control. (**B**) Relative expression of NAT, β1AR and β2AR normalized to GAPDH and expressed as a percent of non-diabetic. * $p<0.05$ to non-diabetic; † $p<0.05$ to diabetic + metformin, two-tailed t-test.

parallel with elevated noradrenaline, reduced expression of NAT, β_1- and β_2-adrenoceptors, lower heart rate and heart rate variability, and abnormal ventricular filling. Treatment with insulin from 8 weeks of diabetes normalized blood glucose, noradrenaline, noradrenergic signaling components, and myocardial HED retention, but did not affect heart rate variability or echocardiography measures of diastolic function. By contrast, treatment with metformin had no effect on blood glucose, noradrenaline, or left ventricular sympathetic signaling or diastolic function.

The inability of metformin to reduce blood glucose may relate to the timing of administration and the animal model used in these studies. The model exhibits a progressive insulin deficiency, which we have shown to take effect by 8 weeks after STZ administration (Thackeray et al., 2011b). In the initial report of this model, metformin therapy was shown to effectively lower blood glucose (Reed et al., 2000). In Zucker diabetic fatty (ZDF) rats, metformin has been shown to effectively reduce blood glucose to normal levels, though ZDF blood glucose is substantially lower than observed in the STZ high fat diet model (12-14 vs 20-25 mM) (Sreenan et al., 1996). However, metformin therapy was initiated immediately after diabetes induction. Lack of glucose reduction has also been observed in metformin-treated ZDF rats at a similar duration of diabetes, though glyocsylated hemoglobin was reduced to normal levels (Shoghi et al., 2009). Interestingly, heart rate variability analysis in obese type 2 diabetic patients treated with metformin demonstrated reduced low frequency (sympathetic) and elevated high frequency (parasympathetic) power, reflecting an increase in the sympathovagal balance index which corresponded to reduced plasma fatty acid concentrations and improved insulin sensitivity (Manzella and Paolisso, 2005).

A previous study has described a reduction in distal left ventricle accumulation of HED that was prevented by insulin treatment. This result was attributed in part to the sparing of autonomic neuropathy in the long-term diabetic model as reflected by nerve growth factor

expression (Schmid et al., 1999). Using the HED SPECT analogue MIBG, Kusmic and colleagues demonstrated accelerated myocardial washout in diabetic mice (Kusmic et al., 2008). We found no evidence of regional differences in myocardial HED, which may suggest that the reduction in tracer accumulation may relate to elevated sympathetic tone and compensatory NAT downregulation rather than distal neuronal cell death. Retention of HED inversely correlates with plasma and cardiac noradrenaline levels (Thackeray et al., 2007; Thackeray et al., 2012 (Submitted)-b). Balanced neuronal degeneration may also explain this finding.

The imaging findings are corroborated by *in vitro* correlative measurements. The degree of elevation in plasma and cardiac noradrenaline observed in this study compares well with reports in streptozotocin diabetic rats (Ganguly et al., 1987; Marsh et al., 2009; Thackeray et al., 2011b), Zucker diabetic rats (Marsh et al., 2007), and Goto Kakizaki rats (Kiyono et al., 2002a). Persistently high noradrenaline levels have been shown to downregulate presynaptic NAT and postsynaptic adrenoceptors over 3-5 days (Dincer et al., 2001; Thackeray et al., 2011a). The imaging and correlative data indicate that not only are the cardiac sympathetic neurons intact and functional after 8 weeks of sustained diabetes, but also that normalization of glucose and subsequent reduction of circulating noradrenaline can restore normal sympathetic nerve signaling. Recovery of β-adrenoceptor density has been shown in as little as 2 weeks of glucose stabilization (Dincer et al., 2001).

The functional consequences of sympathetic dysregulation were expected to be observed in blood pressure and heart rate variability measurements. Despite lower heart rates, diabetic rats exhibit blood pressures comparable with non-diabetic controls, which may reflect higher vasoconstriction due to elevated circulating noradrenaline. The reduction of heart rate in diabetic rats has been attributed to interference with the atrioventricular node (Yuill et al., 2010), sympathetic activity (Gallego and Casis, 2001), or nicotinic acetylcholine receptors

(Campanucci et al.). Spectral analysis of heart rate data in diabetic rats has shown a reduction in middle frequency variability, consistent with impaired sympathetic modulation (Fazan et al., 1999). Heart rate variability over 24 hours has been reported to be reduced by 25% in Goto Kakizaki rats (Howarth et al., 2005b) and by 46% in STZ diabetic rats (Howarth et al., 2006) compared to controls. In the present study, heart rate variability is slightly reduced in diabetic rats from 8 weeks of diabetes, but does not appear to improve following insulin treatment. In db/db mice heart rate and blood pressure response to β_1-adrenoceptor blocker metoprolol was substantially greater than response to the muscarinic receptor blocker atropine, reflecting enhanced basal sympathetic activity (Goncalves et al., 2009). Pharmacological challenge may provide further insight into the heart rate variability of the animals in the current study.

The persistence of diastolic dysfunction following insulin treatment may relate to advanced glycation endproduct or collagen accumulation in the ventricle that is not effectively removed. While echocardiography estimates of diastolic function are impacted by heart rate, left ventricular catheterization and pressure-volume loop assessment have revealed the presence of elevated slope of end-diastolic pressure volume relationships in diabetic animals, particularly in the presence of elevated sympathetic activity as in the mRen2 renin overexpression rat (Connelly et al., 2007). This abnormality was attributed in part to extensive fibrosis of the myocardium. Litwin and colleagues demonstrated an increase in operating chamber stiffness and abnormal pressure-volume relationship at 7 days after streptozotocin administration in rats (65 mg/kg iv), which was restored to normal by 26 days. However, at 26 days, end diastolic volume was increased and left ventricular relaxation time constant extended. Subsequent treatment with insulin normalized pressure-volume relationship, end diastolic volume, and relaxation time constant (Litwin et al., 1990). The diastolic abnormalities observed in the present study suggest a reduction of ventricular

compliance. It is conceivable that continued treatment with insulin may improve the left ventricular compliance and diastolic function.

The recovery of HED retention without recovery of echocardiography Doppler measurements suggests a role for sympathetic neuronal imaging in the assessment of cardiac risk among diabetic patients. Clinical studies have suggested that a considerable proportion of diabetic patients exhibit some degree of asymptomatic coronary disease (Chareonthaitawee et al., 2007). Progressive sympathetic neuronal defects may provide valuable insight to identify patients at greatest risk for cardiovascular complications. A long-term follow-up study demonstrated the prognostic value of sympathetic nervous measurements, wherein patients in the highest quartile of noradrenaline levels following cold-pressor test were most likely to develop subsequent insulin resistance and diabetes (Flaa et al., 2008). Previous imaging studies have suggested that effective glucose control can arrest or even reverse defects in sympathetic innervation among diabetic patients (Fricke et al., 2008; Stevens et al., 1999). In the ADMIRE HF trial, Gerson and colleagues demonstrated that diabetic heart failure patients with lowest heart-to-mediastinal MIBG late uptake ratio were three times as likely to experience a cardiac event of heart failure progression (Gerson et al., 2011). Taken together, there appears to be a point at which glycemic control can effectively counteract the deterioration of sympathetic signaling in the heart. Neurohormonal imaging of cardiac sympathetic neurons may be used to stratify diabetic patients by cardiovascular risk and to identify the efficacy of diabetic therapy on the heart.

In conclusion, the impairment of sympathetic nervous integrity observed at 8 weeks of hyperglycemia in the high fat diet fed streptozotocin diabetic model with insulin resistance is reversible by subsequent treatment with insulin but not metformin. Longitudinal imaging with HED can effectively track the progression of sympathetic neuronal dysregulation and its

regression to therapy. This sympathetic abnormality appears is associated with persistent reduction of heart rate, heart rate variability, and diastolic dysfunction which does not improve after 8 weeks of blood glucose normalization by insulin. Further study to determine the impact of noradrenergic signaling changes on ventricular filling is warranted.

Limitations

The severe deterioration of general health of diabetic animals compelled the exclusion of an untreated diabetic group carried to the full 16 week time point of the study. While longitudinal measurements (HED PET, echocardiography, telemetry, plasma noradrenaline) using repeated measures statistics, allowed each animal to be compared at multiple time points as its own control, this was not possible for terminal measurements (tissue noradrenaline, immunoblots). However, the severity of diabetes after 16 untreated weeks would also be expected to impact the comparison. The approach used in the study was designed to maintain clinical relevance.

Funding

This work was supported by the Heart and Stroke Foundation of Canada (NA7213, Doctoral Research Award to J.T., Career Investigator Award to R.B.); and the Heart and Stroke Foundation of Ontario (PRG6242).

Acknowledgements

The authors would like to thank the PET BioTesting, Imaging Physics, and Radiochemistry laboratories for their excellent technical expertise and assistance with these studies.

Conflict of Interest: none declared

Chapter 7: Manuscript #6

Am J Physiol: Heart and Circ Physiol. (Submitted)

Early restoration of insulin sensitivity delays diastolic dysfunction but not sympathetic dysinnervation in the diabetic rat heart

James Thackeray,[1,2] Robert A deKemp,[1] Rob S Beanlands,[1,2] Jean N DaSilva[1,2]

[1]Molecular Function & Imaging Program, National Cardiac PET Centre, University of Ottawa Heart Institute
[2]Department of Cellular & Molecular Medicine, Faculty of Graduate and Postdoctoral Studies, University of Ottawa

Key words: metformin; rosiglitazone; small animal positron emission tomography, norepinephrine; norepinephrine reuptake transporter; small animal echocardiography; [^{11}C]hydroxyephedrine

Contributions of Authors

The experiments described in this manuscript were designed and executed by the candidate with the supervisory assistance of Dr Beanlands and Dr DaSilva. The candidate analysed and interpreted all data and drafted the manuscript. Physicist Dr deKemp contributed to the interpretation of quantitive imaging results. Dr Beanlands provided a clinical perspective on the data. Dr DaSilva supervised the project and participated in editing and revising the manuscript. The requisite experiments will be completed following thesis submission and the paper submitted in the summer to the *American Journal of Physiology: Heart and Circulatory Physiology*.

ABSTRACT

Molecular imaging studies in diabetic subjects have demonstrated a link between abnormal cardiac sympathetic nervous system signaling and left ventricular dysfunction. Serial positron emission tomography studies in high fat diet-fed streptozotocin insulin resistant diabetic rats have shown sympathetic nervous integrity recovery following insulin treatment after 8 weeks of diabetes. Insulin sensitizing agents administered early after diabetes induction are expected to prevent deterioration of sympathetic neuronal and diastolic function. Diabetic rats were randomized to receive insulin, metformin, or rosiglitazone therapy one week after diabetes induction by streptozotocin. Small animal PET imaging using the norepinephrine analogue [^{11}C]meta-hydroxyephedrine ([^{11}C]HED) was conducted at baseline and at 8 weeks of diabetes (7 weeks of therapy) to determine sympathetic neuronal integrity. Echocardiography assessment of cardiac function was carried out concurrently. Serial measurements of plasma catecholamines and terminal immunoblotting of noradrenergic signaling proteins were performed. Insulin restored normal blood glucose and lipid levels within 3 weeks. Despite reduced circulating fatty acids, neither metformin nor rosiglitazone reduced blood glucose levels. At 8 weeks, untreated and treated diabetics displayed a 39-42% reduction in [^{11}C]HED standardized uptake values, elevated plasma norepinephrine and reduced norepinephrine reuptake transporter expression compared to non-diabetic controls. Echocardiography measures of diastolic function showed a delay in the development of prolonged mitral valve deceleration, and elevated early-to-atrial filling velocity ratio in treatment groups compared to non-diabetics. Early glycemic treatment of insulin resistant diabetic rats did not prevent deterioration of sympathetic neuronal integrity but delayed the progression of diastolic filling abnormalities.

INTRODUCTION

Diabetes is associated with progressive decline of cardiac autonomic function, manifesting as altered resting heart rate, blunted baroreceptor reflex, and reduced heart rate variability. These abnormalities partially underlie the substantive cardiovascular risk among diabetic patients. Aberrant sympathetic nervous system activity is predictive of insulin resistance, diabetes, and cardiovascular events (Carnethon et al., 2003a; Flaa et al., 2008; Rosengard-Barlund et al., 2009). Clinical and animal studies have suggested that diastolic left ventricular dysfunction and filling abnormalities may precede progression to systolic dysfunction. Sympathetic nervous system irregularities appear at a similar timeframe to diastolic dysfunction (Sacre et al., 2010; Thackeray et al., 2011b).

The positron emission tomography radiotracer and false neurotransmitter [^{11}C]*meta*-hydroxyephedrine provides an index of sympathetic neuronal uptake and release of norepinephrine (Law et al., 2010; Thackeray et al., 2007). Washout of [^{11}C]HED is accelerated by enhanced sympathetic activity and elevated synaptic norepinephrine concentration (Thackeray et al., 2012 (Submitted)-b; Tipre et al., 2008).

Longitudinal imaging studies have demonstrated the progression of sympathetic dysinnervation in the diabetic heart. We and others have reported reduced presynaptic norepinephrine reuptake and hyperactivation of the sympathetic nervous system in diabetes, developing over 4-16 weeks of disease (Schmid et al., 1999; Thackeray et al., 2012 (Submitted)-a; Thackeray et al., 2011b). Two to fourfold elevations of cardiac and plasma norepinephrine levels have been established in multiple rodent models of diabetes (Kiyono et al., 2002a; Kiyono et al., 2001; Marsh et al., 2007; Thackeray et al., 2011b). This increase in synaptic neurotransmitter evokes downregulation of postsynaptic effector β-adrenoceptors and downstream excitation/contraction uncoupling (Connelly et al., 2007; Thackeray et al., 2011a).

Restoration of euglycemia by exogenous insulin administration facilitates recovery of sympathetic nervous function in diabetic rats, including restoration of prediabetic norepinephrine levels, norepinephrine reuptake transporter expression (Schmid et al., 1999; Thackeray et al., 2011b), and β-adrenoceptor expression patterns (Dincer et al., 2001). However, abnormal diastolic left ventricular function characterized by extended mitral valve deceleration and elevated early-to-atrial transmitral flow velocity were not improved by insulin treatment after 8 weeks of sustained diabetes (Thackeray et al., 2012 (Submitted)-a). Whether this dysfunction can be prevented by early pharmacological intervention is unclear.

Metformin acts to inhibit gluconeogenesis in the liver and improves glucose metabolism and uptake in skeletal muscle via activation of AMP-activated kinase (AMPK) (Gundewar et al., 2009; Verma and McNeill, 1994). Thiazolidinedione drugs such as rosiglitazone act via perioxisome proliferator-activated receptor-γ (PPARγ) to upregulate fatty acid metabolic proteins, decrease circulating fatty acids and triglycerides, and counteract insulin resistance (Choi et al., 2007). Administration of metformin or rosiglitazone to ZDF rats evoked a shift in cardiac metabolism from fatty acid oxidation to glucose utilization, as demonstrated in isolated working heart models (Golfman et al., 2005), and *in vivo* by small animal PET with FDG and palmitate (Shoghi et al., 2009). Glycosylated hemoglobin levels were normalized, indicating prolonged restoration of circulating glucose and insulin sensitivity (Shoghi et al., 2009). While PPARγ agonists have been reported to provide cardioprotection in rodents in ischemia reperfusion and myocardial infarction injury (Sidell et al., 2002; Yue et al., 2005), clinical meta-analyses have suggested an additive risk of rosiglitazone treatment for myocardial infarction and cardiac death (Nissen and Wolski, 2007). The effect of these medications on the cardiac sympathetic nervous system integrity is not well established.

By counteracting insulin resistance with metformin or rosiglitazone therapy early in the progression of diabetes, it is hypothesized that cardiac sympathetic nervous integrity and left

ventricular diastolic function would be preserved in high fat diet-fed streptozotocin-induced insulin resistant diabetic rats as evaluated with serial *in vivo* [^{11}C]HED PET and *ex vivo* validation methods.

METHODS

Animals. Animal experiments adhered to the Canadian Council on Animal Care recommendations and were approved by the University of Ottawa Animal Care Committee. Male Sprague Dawley rats (Charles River Canada) were individually housed on a 12/12 light/dark cycle in a temperature controlled facility. For the duration of the studies, rats were provided with 32% high fat diet matched to condensed milk (Research Diets). After two weeks, rats were randomized to receive either streptozotocin (45 mg/kg ip) or tribasic sodium citrate (1 mL/kg ip) (Fig 7.1). Rats with blood glucose levels exceeding 12 mM at 1 week following streptozotocin injection were included in the study.

Treatment. Diabetic rats were randomized to receive either i) metformin at a titrated dose beginning from 350 mg/kg/d to a final dose of 650 mg/kg /d on day 11 of treatment (Shoghi et al., 2009; Verma and McNeill, 1994); ii) rosiglitazone at 4 mg/kg/d (Choi et al., 2007; Shoghi et al., 2009); iii) insulin at 4 U/d as a subcutaneous pellet (Arikawa et al., 2007; Thackeray et al., 2012 (Submitted)-a), or iv) no treatment. Metformin was dissolved in 5 mL of sugar-free gelatin and provided daily (Shoghi et al., 2009; Verma and McNeill, 1994). Rosiglitazone was dissolved in pH buffered saline and added to sugar-free gelatin for oral administration (Shoghi et al., 2009). Treatment was initiated at 1 week after diabetes induction and maintained until the end of the study. Non-diabetic rats received no pharmacological treatment.

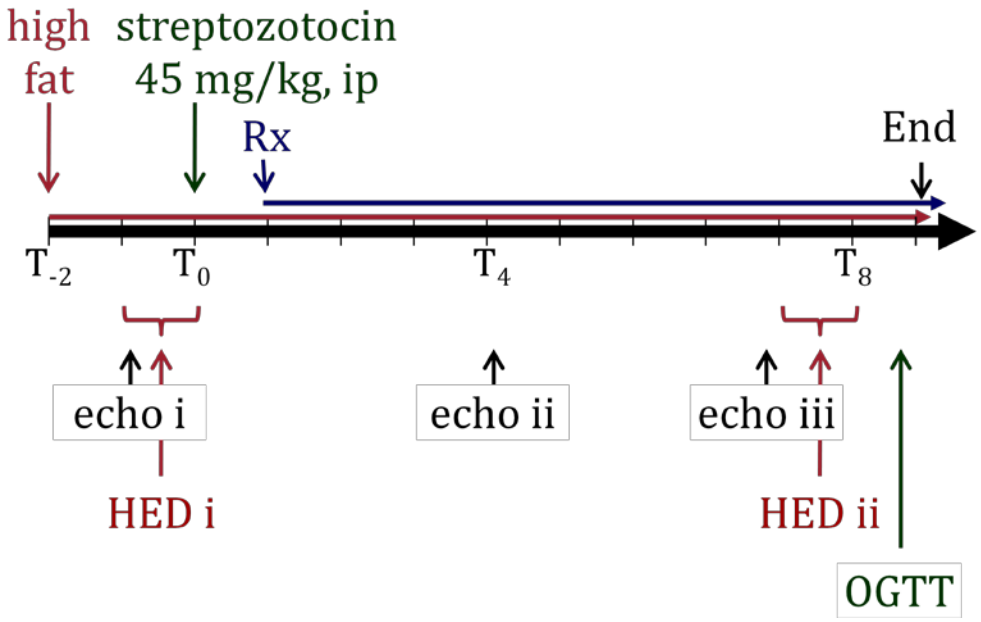

Figure 7.1 Experimental timeline. Rats are fed high fat diet for two weeks prior to the administration of streptpzotocin to induce diabetes at week 0 (T0). After 1 week. treatment with insulin, metformin or rosiglitazone is initiated at T1 and continued until the end of the experiments at 9 weeks (T9). Sympathetic neuronal integrity is assessed by [^{11}C]HED PET scans at baseline (T0) and after 8 weeks of diabetes with or without treatment (T8). Cardiac systolic and diastolic function is measured by echocardiography at T-1, T4, and T8. At 9 weeks after streptozotocin administration, rats underwent an oral glucose tolerance test (OGTT). At the conclusion of the experiments, rats were sacrificed and tissues flash frozen for immunoblot, bioassay, and catecholamine analysis.

Oral Glucose Tolerance. Two to five days after final PET scan, rats underwent an oral glucose tolerance test. Following overnight fast, rats were given an oral glucose load (2 g/kg), blood glucose levels were measured, and samples were taken for insulin measurements at 30 minute intervals over 2 hours.

Echocardiography. Cardiac function was tested by serial echocardiography at 2 and 0 weeks prior to and at 4, and 8 weeks after induction of diabetes. Left ventricular dimensions and ejection fraction were measured from parasternal long axis electrocardiogram-linked cine sweeps. Early and late ventricular filling velocity were measured by pulse-wave Doppler across the mitral valve (Thackeray et al., 2011b).

[^{11}C]HED PET. [^{11}C]HED was produced by N-methylation of metaraminol freebase by ^{11}C-methyliodide in high radiochemical purity and specific activity (Rosenspire et al., 1990; Thackeray et al., 2007). PET imaging was completed using the Inveon (Siemens, Knoxville, TN) dedicated small animal PET camera at prediabetic baseline and at 8 weeks after diabetes induction. Imaging protocol was as previously described (Thackeray et al., 2012 (Submitted)-b). Briefly, following a ^{57}Co attenuation transmission scan, anaesthetized rats were injected with 21.2±3.5 MBq of [^{11}C]HED via a lateral tail vein catheter and images were acquired over 60 minutes with the heart in the centre of the field of view. Dynamic images were reconstructed in 26 frames using OSEM3D-MAP with 2-18 iterations and β=1. FlowQuant (Ottawa Heart Institute, ON, Canada) software was used to reorient the cardiac images and generate time activity curves for left ventricle, and arterial blood derived from the left ventricle cavity (Klein et al., 2010a). Washout of [^{11}C]HED was calculated by fitting a mono-exponential curve to the data from 5-40 minutes. Standardized uptake value normalized to body weight was calculated as Uptake /(Dose/BW) where uptake is the voxel intensity in Bq/cc at 30-35 min, dose is the injected activity in Bq, and BW is the mass of the animal in grams (Thackeray et al., 2012 (Submitted)-a; Thackeray et al., 2012 (Submitted)-

b). Measurements were confirmed by analysis using the Inveon Research Workplace (Siemens, Knoxville, TN) to define regions of interest on left ventricle and blood pool images in the left ventricle cavity, left atrium, or inferior vena cava.

Catecholamines. Plasma samples collected from the tail vein at the time of each PET scan were analysed for catecholamine concentration by column-switch HPLC with electrochemical detection (Thackeray et al., 2011b). After sacrifice, samples of myocardial tissue were also processed and tested for norepinephrine.

***In Vitro* Validation.** Two to four days after the glucose tolerance test, rats were sacrificed by decapitation and trunk blood samples were collected. Plasma was analysed for insulin by ELISA (Alpco), free fatty acid and triglyceride by colorimetric enzyme assay (BioVision). Hearts and skeletal muscle were rapidly dissected, snap frozen, and hand-powdered under liquid nitrogen. Tissue samples were lysed, protein concentration determined by BCA, and analysed by Western blot for the expression of norepinephrine reuptake transporter, β_1-and β_2-adrenoceptor, tyrosine hydroxylase, glucose transporter-4 (GLUT4), phosphorylated acetyl CoA carboxylase (PACC), fatty acid transporter (FAT), and carnitine palmitoyl transferase-1 (CPT1). Relative immunoblot integrated densitometry was normalized to GAPDH as a loading control and compared to non-diabetic and untreated diabetic samples Free fatty acid levels in myocardial tissue was assessed by colorimetric enzyme assay (BioVision).

Statistics. All data are presented as mean ± standard deviation excepting oral glucose tolerance results which are mean ± standard error. Small animal PET and echocardiography results were compared to non-diabetic and untreated diabetic groups by one-way analysis of variance with Bonferroni post hoc tests. Blood biochemistry and immunoblots of treatment groups were compared separately to non-diabetic and untreated diabetics using one-tailed t-tests.

RESULTS

Efficacy of Gylcemic Therapy. Rats exhibited an immediate and sustained elevation of blood glucose from 6.8±0.8 mM at baseline to 24.6±7.1 mM at 1 week after streptozotocin injection. Treatment with insulin from 1 week of diabetes reduced blood glucose levels to non-diabetic controls over 3 weeks, with blood glucose of 7.1-8.4 mM from 4-8 weeks of treated diabetes. By contrast, neither metformin nor rosiglitazone effectively improved hyperglycemia, and remained comparable to untreated diabetic rats at doses and administration protocols well established in the literature (Fig 7.2A). Plasma insulin levels were severely depleted in untreated diabetic rats compared to non-diabetic controls. Insulin treatment restored plasma insulin levels to above non-diabetic concentrations, metformin treatment showed a modest elevation of insulin, and rosiglitazone showed insulin depletion comparable to untreated diabetic rats (Fig 7.2B). Plasma free fatty acid concentration was elevated in diabetes and normalized by insulin, metformin, or rosiglitazone treatment (Fig 7.2C). No significant changes in circulating triglyceride levels were detected between groups. Body weights were lower in diabetic rats compared to non-diabetics, with recovery of body weight in the insulin and metformin treatment groups compared to rosiglitazone treatment (Table 7.11).

Glucose Tolerance. Diabetic rats exhibit glucose intolerance with impaired fasting glucose, higher peak, and longer time to return to pre-glucose load baseline (Fig 7.3A). Treatment with insulin restored normal glucose response with continuously high insulin levels (Fig 7.3B). Metformin treatment reduced fasting blood glucose levels but the area under the curve corrected for fasting blood glucose level remained comparable to untreated diabetics and insulin levels remained depleted. Rosiglitazone treatment did not alter glucose tolerance as compared to untreated diabetics.

Table 7.1 Body weights in non-diabetic and diabetic rats before and following treatment.

	Body Weight (g)				
Group	-2 Weeks$^{\alpha}$	0 Weeks	1 Week	4 Weeks	8 Weeks
Non-Diabetic (n=6)	226±12	378±30	432±42	552±27	700±60
Diabetic (n=15)	226±7	380±15	369±17*	430±28*	460±34*
Insulin (n=6)	224±12	365±22	360±26*	520±23*†	658±69*†
Metformin (n=6)	224±6	346±25	353±21*	439±29*	501±40*†
Rosiglitazone (n=5)	215±9	335±19	337±28*†	427±28*	473±54*

α time (in weeks) relative to streptozotocin injection

* $p<0.05$ to age-matched non-diabetic control

† $p<0.05$ to age-matched untreated diabetic

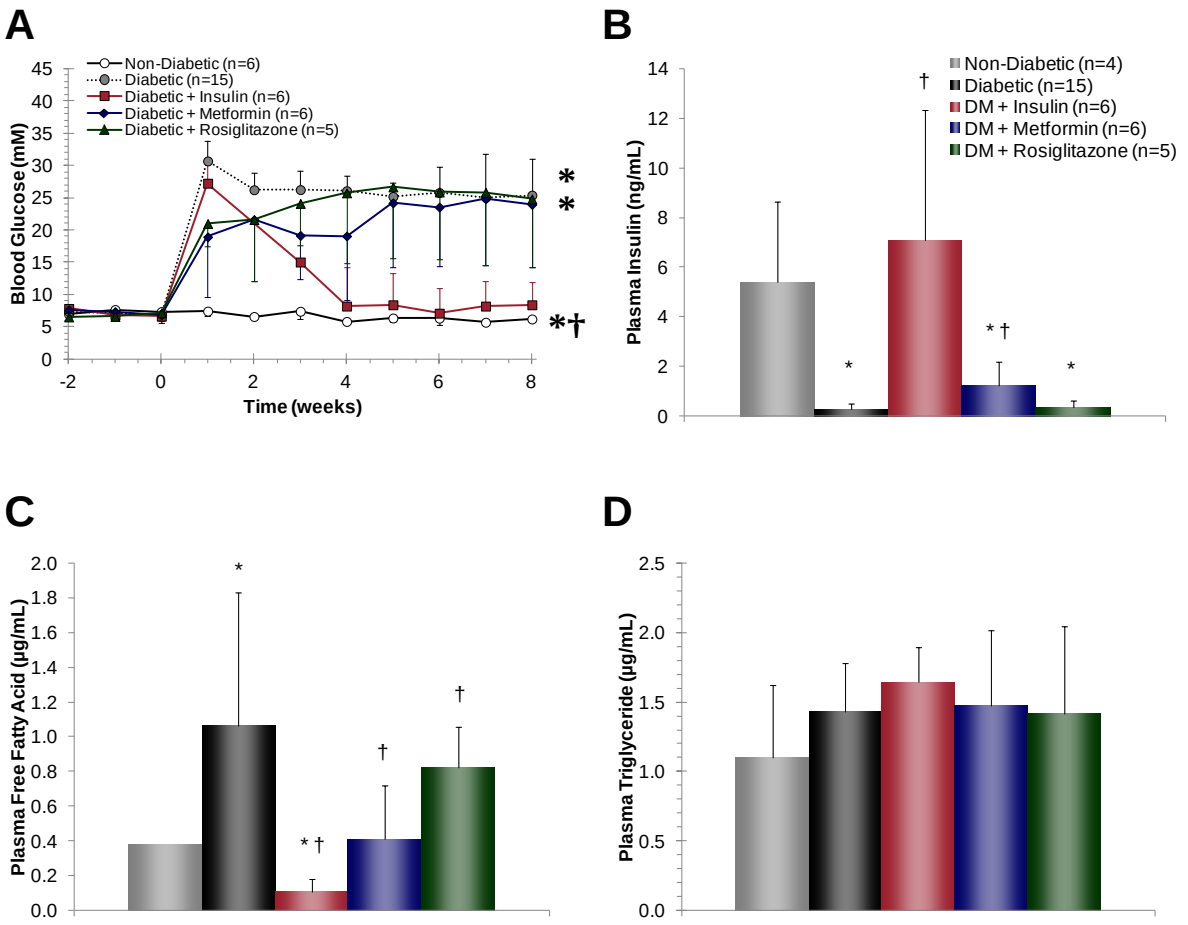

Figure 7.2 Blood biochemistry in non-diabetic and diabetic rats treated with insulin, metformin, or rosiglitazone. (**A**) Weekly measures of morning blood glucose; (**B**) terminal plasma insulin levels; (**C**) terminal plasma free fatty acid levels; (**D**) terminal triglyceride levels. * $p<0.05$ to non-diabetic control; † $p<0.05$ to untreated diabetic; one-way ANOVA, Bonferroni post hoc.

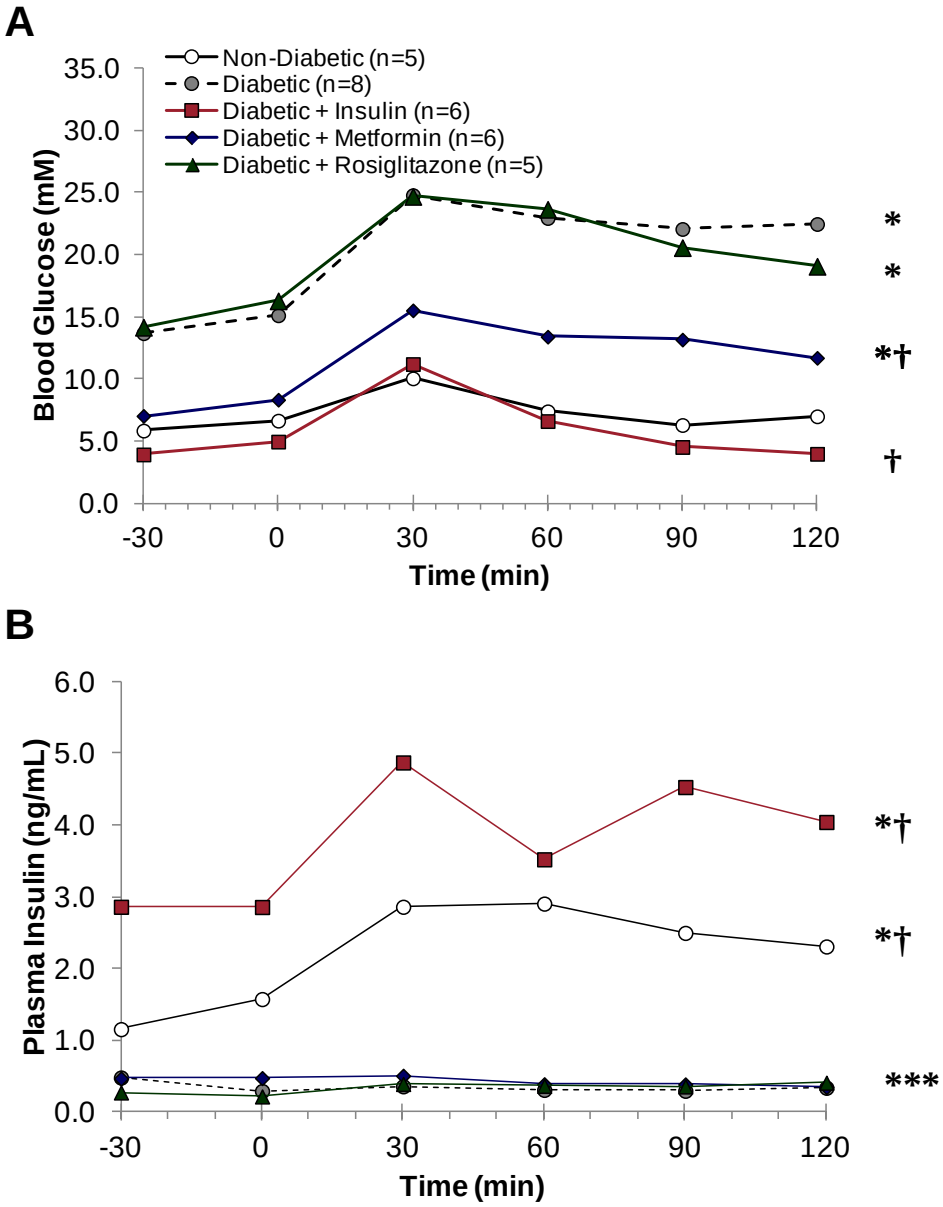

Figure 7.3 Oral glucose tolerance test in non-diabetic and diabetic rats treated with insulin, metformin or rosiglitazone. (**A**) Blood glucose and (**B**) plasma insulin levels following 2 g/kg oral glucose load over 120 minutes. * $p<0.05$ to non-diabetic control; †$p<0.05$ to untreated diabetic; one-way ANOVA, Bonferroni post hoc.

Metabolic Protein Expression. Myocardial expression of GLUT4 was markedly reduced in untreated diabetic rats. While insulin treatment attenuated this reduction of relative GLUT4 expression, neither metformin nor rosiglitazone treatment restored GLUT4 expression (Fig 7.4A). There was no difference in GLUT1 expression in any of the groups. Untreated diabetic rats exhibited a 76% increase in cardiac CD36 expression, which was significantly attenuated by insulin treatment. Phosphorylated ACC was lower in untreated and insulin-treated diabetic rats, with an increase of 36% and 108% in metformin- and rosiglitazone-treated diabetic rats, respectively (Figure 7.4B). There was no difference in myocardial non-esterified fatty acid levels between diabetic and non-diabetic rats, nor in any of the treatment groups (Fig 7.4C).

[^{11}C]HED PET. Representative vertical long axis, horizontal long axis, and short axis left ventricle images and time activity curves at 8 weeks of diabetes with or without treatment are shown in Fig 7.5. There was no evidence of regional [^{11}C]HED uptake defects in any diabetic group with or without treatment. An elevation of tracer washout is apparent from qualitative analysis of time activity curves among diabetic groups compared to non-diabetic rats. Treatment with insulin attenuates the accelerated tracer washout. Quantitative analysis demonstrated reduced [^{11}C]HED SUV in diabetic rats by 43% as compared to non-diabetics at T8 (Fig 7.6A). Insulin, metformin, and rosiglitazone treatment groups exhibited similar reductions in [^{11}C]HED left ventricle SUV at 42%, 40%, and 39% of non-diabetics, respectively (Fig 7.6A). General linear model repeated measures of tracer washout show higher mono-exponential washout rate at 8 weeks compared to baseline in diabetic untreated and treatment groups (Fig 7.6B). By contrast, non-diabetic controls exhibit a modest decline of [^{11}C]HED tracer washout.

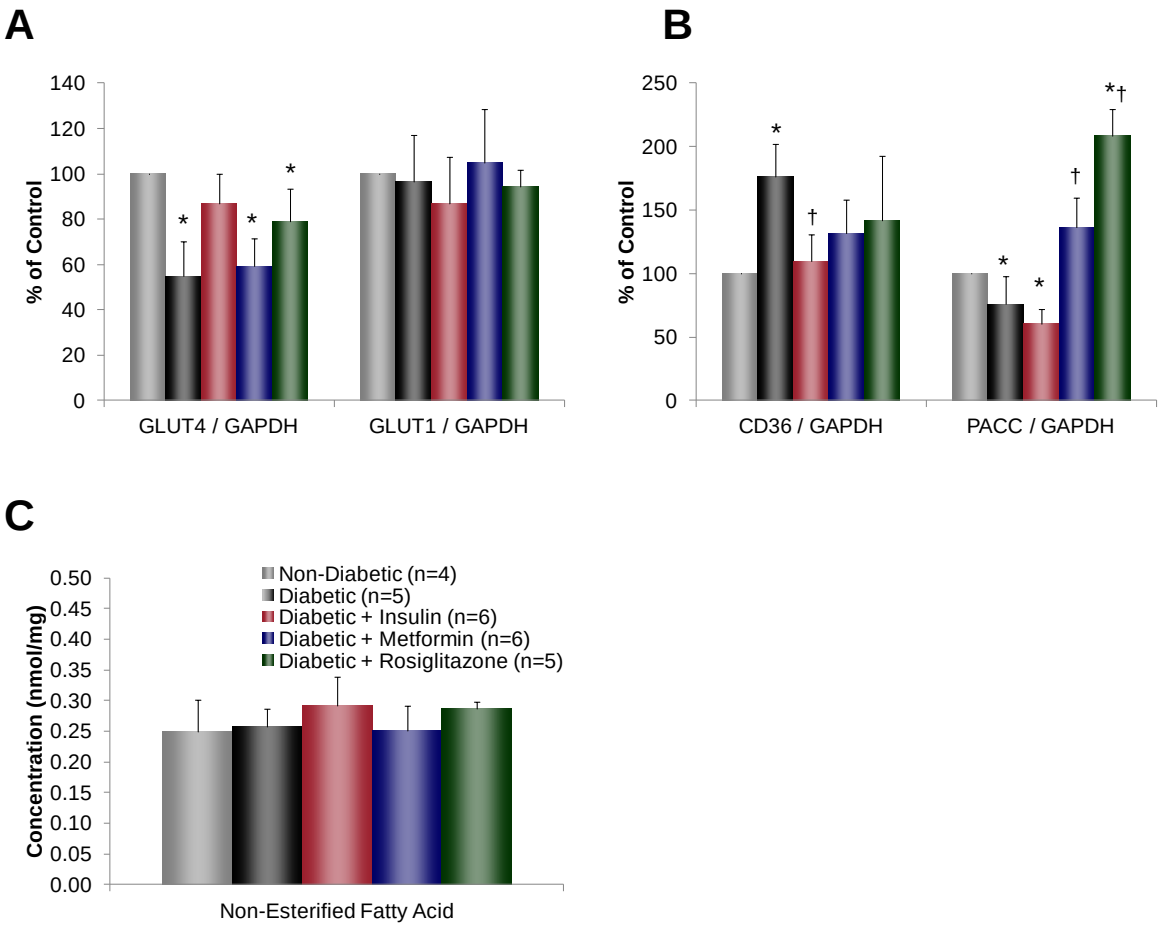

Figure 7.4 Relative expression of proteins involved in glucose and fatty acid metabolism in non-diabetic and diabetic rats treated with insulin, metformin, or rosiglitazone. (**A**) GLUT4 expression in cardiac muscle; (**B**) expression of CD36/FAT and P-ACC, in cardiac muscle; (**C**) free fatty acid levels in myocardial tissue. * $p<0.05$ to non-diabetic control; † $p<0.05$ to untreated diabetic; one-way ANOVA, Bonferroni post hoc.

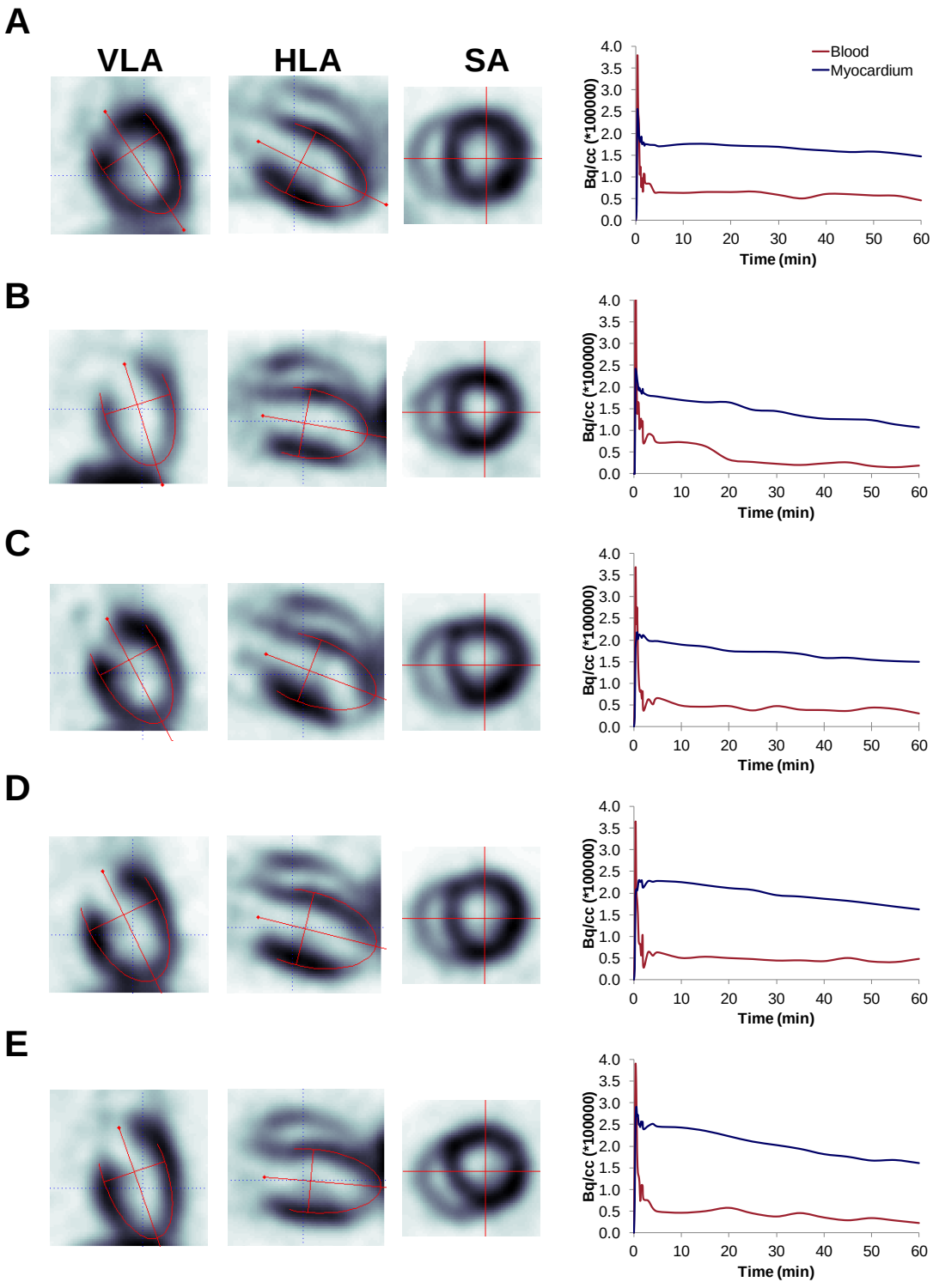

Figure 7.5 Representative [^{11}C]HED reoriented vertical long axis (VLA), horizontal long axis (HLA) and short axis (SA) myocardial PET images and time activity curves at 8 weeks after streptozotocin and 7 weeks of treatment. (**A**) Non-diabetic control; (**B**) untreated diabetic; (**C**) insulin-treated diabetic; (**D**) metformin-treated diabetic; (**E**) rosiglitazone-treated diabetic.

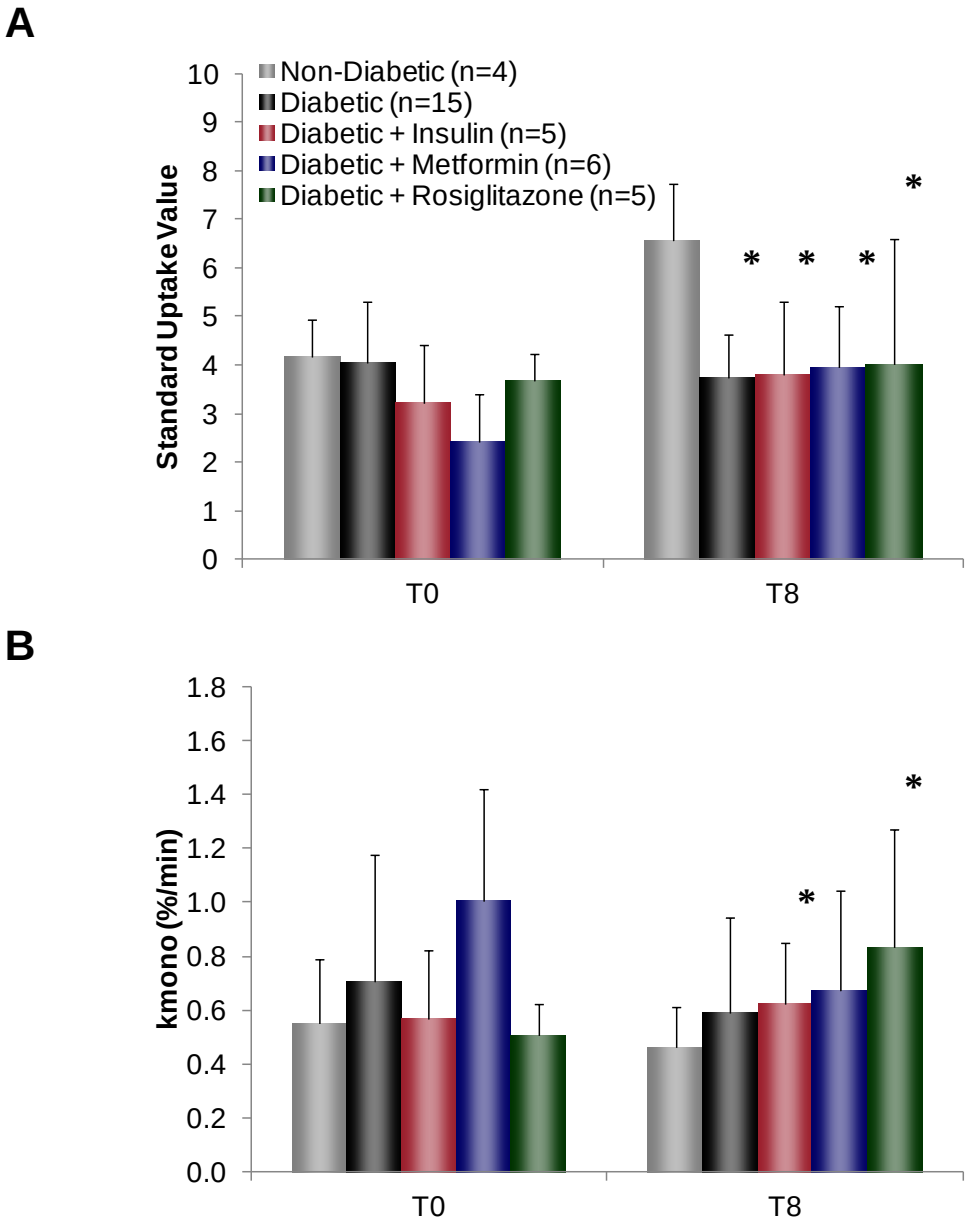

Figure 7.6 Serial quantification of [^{11}C]HED retention in non-diabetic and diabetic rats treated with insulin, metformin or rosiglitazone at pre-diabetic (T0) and after 8 weeks of diabetes (T8). (**A**) Standardized uptake value (SUV) measurement of uptake and retention; (**B**) mono-exponential tracer washout rate (kmono). * $p<0.05$ to age-matched non-diabetic control; † $p<0.05$ to age-matched untreated diabetic; one-way ANOVA, Bonferroni post hoc.

In Vitro Correlation. At baseline (T0), plasma norepinephrine levels were comparable between non-diabetic, untreated diabetic and all treatment groups. By contrast, after 8 weeks, plasma norepinephrine concentration was 138%, 24%, 105%, and 214% in untreated diabetic, insulin, metformin and rosiglitazone treatment groups as compared to their baseline values (Fig 7.7A). Myocardial norepinephrine was elevated in diabetic rats by 22%. Insulin, metformin, and rosigltiazone treatments attenuated increases in myocardial norepinephrine (Fig 7.7B). Expression of NET was lower in untreated, insulin, and metformin treated diabetics by 28, 35, and 30%, respectively. NET expression was normalized by rosiglitazone treatment (Fig 7.7C). Expression of β_1- and β_2-adrenoceptors was significantly lower in all diabetic rats, regardless of treatment (Fig 7.7C).

Cardiac Function. Echocardiography measurements demonstrated no difference in systolic function with similar end diastole and end systole dimensions between groups (Fig 7.8A, Table 7.2). Heart rates were slower in diabetic rats by 64-104 bpm. Insulin treatment prevented bradycardia. Metformin delayed the development of lower heart rate with normal cardiac rhythm observed at 4 weeks and bradycardia at 8 weeks of diabetes (Fig 7.8B). Mitral valve deceleration time was extended in diabetic rats to 16-32 ms at 8 weeks. This was attenuated to 9-15 ms in insulin-treated rats but was similar to the untreated diabetics in metformin and rosiglitazone groups (Fig 7.8C). Early-to-late left ventricle filling velocity ratio was elevated at 4 and 8 weeks of diabetes compared to non-diabetic controls with a relatively lower contribution of atrial kick to ventricular filling (Fig 7.8D). Insulin prevented the shift in E/A ratio at 4 and 8 weeks. Metformin and rosiglitazone slowed the progression of this filling abnormality, though elevated E/A ratio was evident at 8 weeks.

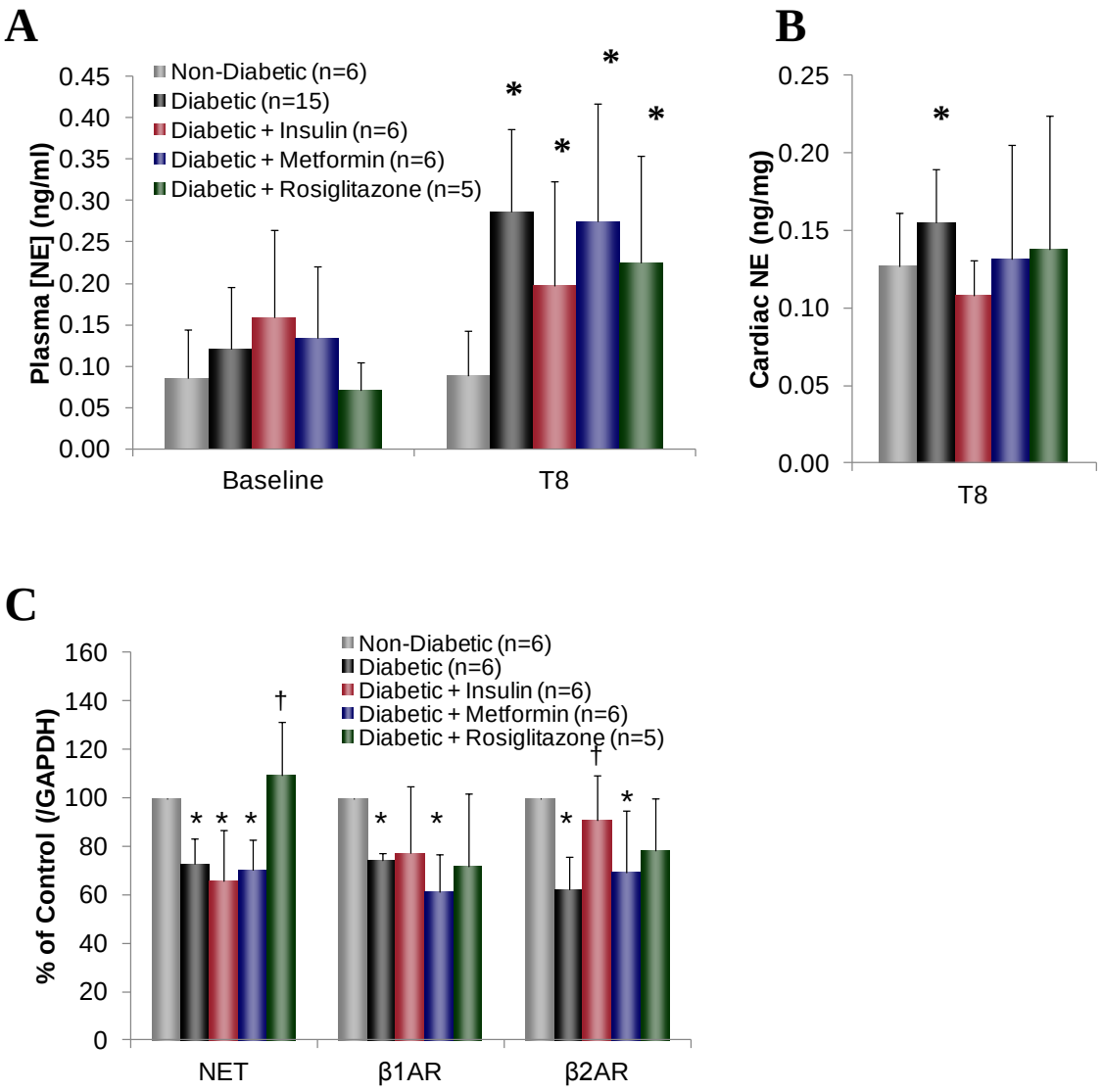

Figure 7.7 In vitro correlative measurements of sympathetic nervous function in non-diabetic and diabetic rats treated with insulin, metformin, or rosiglitazone. (**A**) Serial plasma norepinephrine levels at baseline and 8 weeks of diabetes with and without treatment; (**B**) terminal myocardial norepinephrine concentration; (**C**) relative expression of uptake-1 norepinephrine reuptake transporter (NET), postsynaptic β_1- and β_2-adrenoceptors (βAR), and tyrosine hydroxylase (TH). * $p<0.05$ to non-diabetic control; † $p<0.05$ to untreated diabetic; one-tailed t-test.

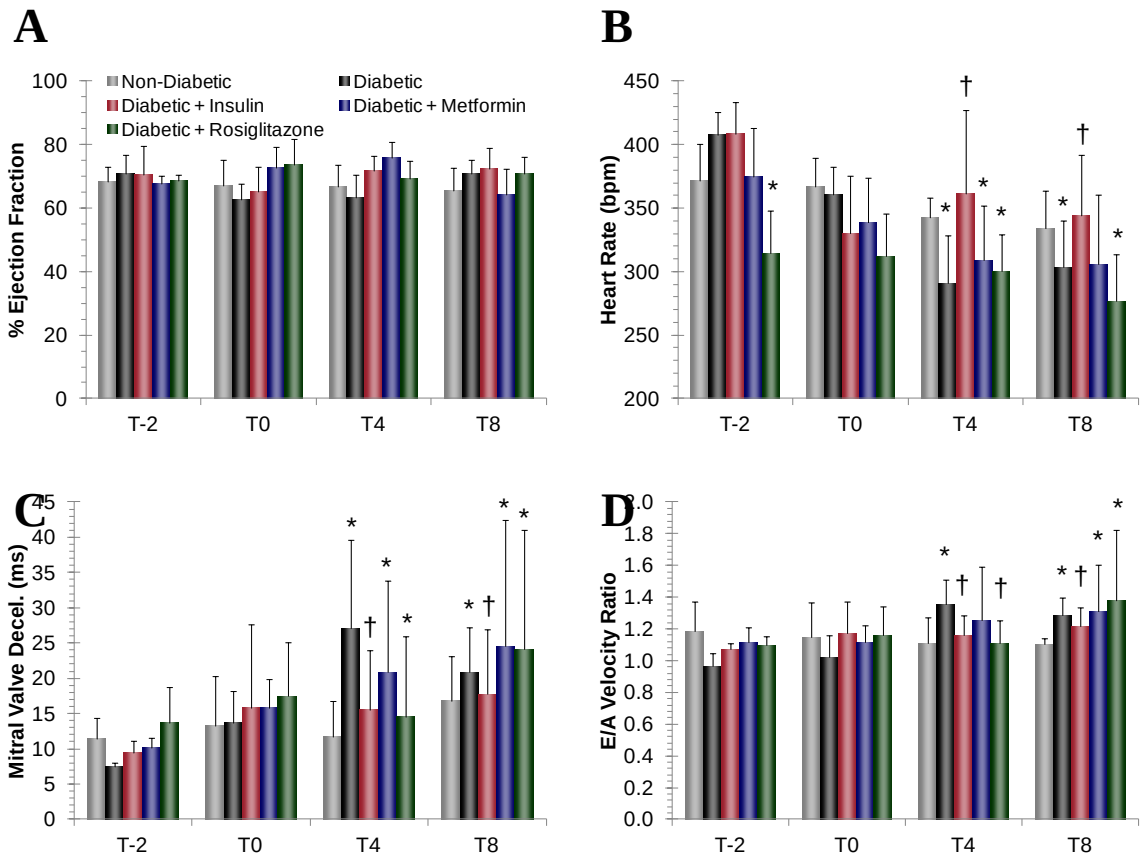

Figure 7.8 Serial echocardiography measurements of systolic and diastolic left ventricular function in non-diabetic and diabetic rats treated with insulin, metformin, or rosiglitazone. (**A**) Left ventricular ejection fraction; (**B**) M-mode derived heart rate; (**C**) mitral valve deceleration time from transmitral pulse-wave Doppler; (**D**) early to atrial transmitral filling velocity ratio. * $p<0.05$ to age-matched non-diabetic control; † $p<0.05$ to age-matched untreated diabetic; one-way ANOVA, Bonferroni post hoc.

Table 7.2 Serial echocardiography in non-diabetic and diabetic rats with and without treatment.

Parameter	Group	-2 Weeks	0 Weeks	4 Weeks	8 Weeks
FAC (%)	ND	50±4	51±13	48±7	47±6
	D	53±6	46±4	45±5	52±5
	D+I	54±7	49±7	53±5	54±6
	D+M	51±2	53±6	56±5	46±8
	D+R	49±2	54±8	51±3	51±6
EDV,d (µL)	ND	269±59	373±79	422±97	597±53
	D	273±30	370±74	485±84	615±44
	D+I	288±71	402±94	508±106	564±38
	D+M	323±32*†	423±53*	591±29*†	527±90
	D+R	297±34	418±61	496±79	560±173
EDV,s (µL)	ND	85±22	120±33	137±30	205±47
	D	80±21	126±37	176±35*	180±35
	D+I	80±17	133±33	141±30	156±35
	D+M	104±11*†	113±15	143±35	190±54
	D+R	93±11	106±21	151±25	161±45
SV (µL)	ND	184±44	253±76	285±80	392±54
	D	193±19	245±73	309±71	435±23
	D+I	207±73	252±54	366±90	408±49
	D+M	219±25	310±65	447±23	337±68
	D+R	204±26	311±75	345±75	399±140
CO (mL/min)	ND	69±15	94±29	98±24	134±27
	D	80±6	97±28	92±30	133±15
	D+I	86±32	88±23	138±45	141±18
	D+M	82±10	105±19	138±25	103±19
	D+R	66±9	98±25	104±15	111±22

E (cm/s)	ND	118±24	117±25	123±22	124±31
	D	120±13	117±12	123±15	124±17
	D+I	148±9	114±15	152±23*†	101±33
	D+M	128±17	119±19	118±24	119±25
	D+R	116±20	125±18	119±17	113±11
A (cm/s)	ND	101±21	93±26	103±25	112±28
	D	125±5	115±8	92±18*	96±18*
	D+I	138±6	101±28	133±28*†	85±32*
	D+M	114±9	107±12	97±22	92±17*
	D+R	106±18	109±19	110±25	88±23*

ND, non-diabetic; D, diabetic; D+I, insulin; D+M, metformin; D+R, rosiglitazone; FAC, fractional area change; EDV,d, endocardial volume at end diastole; EDV,s, endocardial volume at end systole; SV, stroke volume; CO, cardiac output; E, early transmitral velocity; A, late atrial transmitral velocity

* $p<0.05$ to age-matched non-diabetic

† $p<0.05$ to age-matched untreated diabetic

DISCUSSION

The high-fat diet fed streptozotocin rat model exhibits insulin resistance and persistent hyperglycemia with progressive insulin insufficiency. Treatment initiated on the same day as streptozotocin injection with metformin or the thiazolidinedione pioglitzone has been shown to counteract progression of hyperglycemia and hypoinsulinemia (Ding et al., 2005; Reed et al., 2000). In the present study, with treatment initiated one week after streptozotocin-injection, blood glucose levels were not normalized by metformin or rosiglitazone. This suggests that after one week, beta cell wasting in the pancreas is sufficient to generate a diabetic model with insulin deficiency. Glucose tolerance tests confirm a lack of insulin response to glucose in metformin and rosiglitazone treatment. Metformin reduced fasting glucose levels to normal likely by inhibiting liver gluconeogenesis, thereby lowering fasting glucose concentration. The shape of the glucose clearance curve remains consistent with impaired glucose tolerance, with a larger area under the curve normalized to fasting glucose level (Zhang et al., 2003).

Whereas both metformin and insulin treatment reduced circulating fatty acids in diabetic rats, rosiglitazone did not. This suggests that glucose oxidation was promoted by GLUT4 translocation in skeletal muscle in insulin-treated group and by AMPK stimulation in the metformin treated group (Golfman et al., 2005). The predominant site of action of rosiglitazone is adipose tissue, in which PPARγ stimulation alters fatty acid metabolism and distribution of visceral fat (Choi et al., 2007). The diabetic model used in the present exhibits low body weight and lack of appreciable fat mass. This lack of adiposity may therefore contribute to the lack of efficacy of rosiglitazone in reducing circulating lipids and consequent insulin resistance during high fat feeding. By contrast, in Zucker Diabetic fatty rats, which exhibit obesity and increased adipose tissue, plasma fatty acids are reduced,

insulin sensitivity restored, and blood glucose normalized by an identical treatment regimen of rosiglitazone (Shoghi et al., 2009).

The persistence of sympathetic neuronal dysfunction characterized by elevated plasma and norepinephrine and reduced retention of [^{11}C]HED reflect the continued high glucose levels in the diabetic rats treated with metformin or rosiglitazone. The shape of time activity curves suggests that the reduced [^{11}C]HED uptake derives in part from accelerated washout of tracer. This is consistent with elevated sympathetic activity (Tipre et al., 2008), increased synaptic norepinephrine concentration (Thackeray et al., 2012 (Submitted)-b), and impaired sympathetic neuronal function at uptake-1 NET (Raffel et al., 2006). Using small animal SPECT, diabetic mice exhibit a modest increase in initial myocardial uptake of the [^{11}C]HED analogue [^{123}I]MIBG, but an enhanced washout rate suggesting increased sympathetic activity (Kusmic et al., 2008).

Alternatively, reduced tracer uptake may reflect a change in myocardial blood flow. Reduced perfusion and myocardial flow reserve in diabetes has been well described in patients, and has been suggested to have significant impact on sympathetic nervous system imaging in these patients (Di Carli et al., 1997; Young et al., 2009). In rodents, one study has demonstrated normal [^{99m}Tc]MIBI distribution in diabetic rat hearts (Kiyono et al., 2001), though this study was conducted by *ex vivo* autoradiography. In the present case, tracer uptake was measured at the relatively late frame of 30-35 minutes which may limit the impact of perfusion abnormalities. The *in vitro* correlative findings of elevated plasma and tissue norepinephrine and reduced expression of NET, β-adrenoceptors and tyrosine hydroxylase in diabetic rats supports a neuron-specific contribution to the reduced [^{11}C]HED SUV.

The inability of insulin to prevent deterioration of [^{11}C]HED uptake, after treating from 1 week of diabetes is confounding. We have previously shown a recovery of [^{11}C]HED SUV

and kmono in insulin-resistant diabetic rats when starting insulin treatment from 8 weeks of sustained diabetes (Thackeray et al., 2012 (Submitted)-a). Insulin therapy has been shown to restore presynaptic NET function (Schmid et al., 1999) and β-adrenoceptor density (Dincer et al., 2001) in as little as one week of administration. The two week lag in glucose lowering observed in the insulin treatment group was not seen with treatment after 8 weeks of hyperglycemia. This may relate to excessive hyperinsulinemia with the early treatment, prior to depletion of insulin production. Maintained or elevated insulin levels in the high-fat diet fed streptozotocin animal model have been reported up to 2 weeks after diabetes induction (Reed et al., 2000; Thackeray et al., 2011b; Zhang et al., 2003). Because insulin is sympatho-excitatory (Rizk and Dunbar, 2004) the combination of endogenous and exogenous insulin may elevate the contribution of insulin-stimulated norepinephrine release in this case. Previous clinical imaging studies have also reported recovery of [^{11}C]HED uptake in diabetic patients with effective glucose control (Fricke et al., 2008; Stevens et al., 1999), though these studies were conducted with 1-3 years between PET scans.

Interestingly, the deterioration of diastolic function was either delayed (metformin, rosiglitazone) or prevented (insulin) in comparison to untreated diabetic rats. Reduction of blood glucose has been previously established to restore left ventricular dysfunction and normalize ventricular filling (Basu et al., 2009). Attenuation of neurohormonal signaling via anigotensin II blockade has also been shown to improve cardiac function in diabetic rats (Raimondi et al., 2004). We have previously shown that normalization of blood glucose after 8 weeks of diabetes does not ameliorate diastolic dysfunction (Thackeray et al., 2012 (Submitted)-a). The mechanism by which these treatments attenuate diastolic dysfunction is unclear. The reduction of circulating and myocardial fatty acid metabolites may improve ventricular compliance. Additionally, the promotion of myocardial glucose uptake and utilization either directly by insulin or via AMPK by metformin may reduce the

accumulation of advanced glycation endproducts in the left ventricle, thereby maintaining the equilibrium of early and atrial filling (Basu et al., 2009; Li et al., 2010b). The trend to eventual deterioration of diastolic function in metformin and rosiglitazone treatment may reflect a temporal tipping-point whereby the benefit of modestly improved glucose utilization is lost.

Taken together, the data indicate that identification of sympathetic neuronal dysinnervation may provide a useful biomarker of evolving diastolic disease in diabetes. Healthy young males in the highest quartile of norepinephrine response to cold-pressor test were more likely to develop subsequent impaired fasting glucose and insulin resistance at 18 years' follow-up (Flaa et al., 2008). Another study demonstrated an independent association of abnormal autonomic reflex tests with the presence of subclinical diastolic dysfunction in diabetic patients (Sacre et al., 2010). These observations suggest an added value to sympathetic neuronal imaging in the identification of cardiac risk in diabetic patients that cannot be detected by echocardiography alone. In a substudy of the ADMIRE HF trial, Gerson and colleagues demonstrated that diabetic patients with MIBG heart-to-mediastinal ratio in the normal range were comparable to non-diabetics. However, diabetic patients with H:M ratio <1.60 had the highest rate and earliest progression of heart failure among enlisted patients (Gerson et al., 2011).

In conclusion, the high-fat diet streptozotocin rat model of insulin resistance with diabetes cannot be effectively treated with insulin sensitizing drugs to prevent sympathetic neuronal dysregulation in the heart. Treatment with insulin prevented, and with metformin or rosiglitazone delayed the progression of echocardiographic measures of diastolic dysfunction, suggesting a role for persistent sympathetic signaling abnormalities in the development of ventricular filling abnormalities.

ACKNOWLEDGMENTS

The authors extend gratitude to the PET BioTesting, Radiochemistry, and Imaging Physics Laboratories for their technical assistance in these experiments. JTT was supported by a Heart and Stroke Foundation of Canada Doctoral Research Award. RSB is a Career Investigator of the Heart and Stroke Foundation of Canada, a Tier 1 University of Ottawa Chair in Cardiovascular Disease Research, and the Goldfarb Chair in Cardiac Imaging Research. Experiments were funded by the Heart and Stroke Foundation of Ontario (NA7213, PRG6242).

Chapter 8: Common Discussion

8.0 COMMON DISCUSSION

The increased cardiovascular risk among diabetic patients has been attributed in part to heightened sympathetic nervous activity and dysregulation of myocardial noradrenergic signaling. These abnormalities manifest as altered resting heart rate, impaired autonomic reflexes, reduced heart rate variability, and increased myocardial NE spillover, which may contribute to deterioration of left ventricular function. In diabetes, sympathetic activity is elevated by persistently high circulating glucose and fatty acids, which augment NE release and sympathetic signaling. Moreover, declining left ventricular diastolic function due to metabolic aberrations and chamber stiffness further precipitates compensatory sympathetic activation. Longitudinal assessment of myocardial sympathetic neuronal integrity may provide invaluable information in identifying risk and directing therapeutic approaches in diabetes.

In the first part of this thesis, the potential of [^{11}C]HED retention to identify altered myocardial sympathetic nervous function is established. Test-retest repeatability studies support [^{11}C]HED measurements of retention and washout as a biomarker of sympathetic function in rats. The pharmacological properties of [^{11}C]HED are investigated by *ex vivo* biodistribution and *in vivo* small animal PET imaging, establishing a direct correlation to NET availability and an inverse correlation to NE concentrations.

In the second part of the thesis, the myocardial sympathetic nervous function in diabetic rats is interrogated using [^{11}C]HED retention in parallel with evaluation of left ventricular systolic and diastolic function. Sympathetic dysinnervation and diastolic dysfunction is described in diabetic rats, characterized by increased NE spillover to plasma, reduced NET expression, and maintained sympathetic neuronal density, suggesting a capacity for recovery of normal sympathetic function. Glucose normalization by insulin treatment after prolonged diabetes restores the sympathetic signaling axis without a parallel improvement in diastolic

function. These findings support a role for the SNS in the progression of cardiac disease in diabetes that can be arrested by restoration of normal glycemia.

8.1 Quantification of [^{11}C]HED Retention in Small Animals

In line with previous examinations, our results in normal animals indicate that the clinically used retention index (C_m / $_0\int^{40}C_b dt$) evaluated at 30-40 minutes following tracer injection provides a reproducible and translatable model of [^{11}C]HED distribution in rats, with a left ventricular average of 6.5%/min as compared to 7.4%/min reported elsewhere (Tipre et al., 2008). In healthy humans, the average [^{11}C]HED retention index is 8-10%/min (Calkins et al., 1993; Stevens et al., 1998a). Use of the retention index for quantification of [^{11}C]HED kinetics assumes that steady state equilibrium is reached between tracer uptake and washout in late frames (i.e. 30-40 minutes after injection). While reasonable in human subjects (Link et al., 2003), this may not be an accurate assumption in rodents, which exhibit higher basal sympathetic tone (Law et al., 2010; Tipre et al., 2008). In current studies, persistent washout following initial tracer uptake is observed as a declination of the myocardial time activity curve, in line with previous reports in small animal imaging with [^{11}C]HED and [^{123}I]MIBG (Kusmic et al., 2008; Tipre et al., 2008) and confirmed in radioisotope studies in isolated perfused hearts (DeGrado et al., 1993). Bland-Altman analysis and test-retest variability statistics demonstrate that in late frames (i.e. 30-40 min following [^{11}C]HED injection) the average tracer retention is reliably quantifiable. Retention measurements were not affected by injected dose, specific activity, or coinjected cold mass. Beyond myocardial activity (C_m), the retention index ratio is affected by the blood input function (i.e. $_0\int^{40}C_b dt$), obtained from a volume of interest delineated on the dynamic blood pool image of left ventricle lumen. Minute differences in the input function activity can drastically affect the calculated retention index. For example, removal of metabolite correction from the FlowQuant© software automated input function calculation changes the retention index by up to 50% (unpublished

results). This effect reflects the over-estimation of unchanged [^{11}C]HED (i.e. 100% of activity) in the blood over the timecourse accounting for a falsely high activity integral.

The SUV ((C_m / W_m) / (ID / W_b)) eliminates the input function component in favour of normalization to body weight and injected dose. With consistent injected dose between subjects, this measurement is particularly susceptible to bias from the body weight as the predominant normalization factor. Body surface area is used in clinical image analysis as a more representative normalization factor, but the estimation of surface area in rodents is complex and frequently inaccurate (Farriol et al., 1997). In normal rats with comparable body weights, SUV was proportional to retention index, suggesting a congruence of measurement. However, in our experiments with diabetic animals, analysis of SUVs and retention indices yielded markedly different trends. That is, SUVs were reduced in diabetics compared to non diabetics but retention indices remained similar between groups, suggesting a falsely elevated retention index. The SUV calculation from small animal PET studies was supported by *ex vivo* biodistribution data and *in vitro* measurements of sympathetic activation including NE levels and NET expression, supporting the legitimacy of the [^{11}C]HED SUV over retention index.

This lack of agreement between retention index and SUV observed in diabetic rats may be explained by a number of factors affecting the image-derived input function. High retention index reflects reduced integral value of the input function. This could derive from left ventricular dilatation resulting in less myocardial spill-in to the blood pool of the left ventricle lumen, reducing the activity throughout the scan time. However, no difference in ventricular diameter or wall thickness between diabetic and non-diabetic animals was found with echocardiography. Alternatively, diabetic rats exhibit pronounced bradycardia and extended ventricular filling time (Basu et al., 2009; Huynh et al., 2012; Marsh et al., 2009), which would manifest as a greater duration of the cardiac cycle spent in diastole and a

relative reduction in left ventricular motion. This would also result in reduced spill-in to the blood pool, lowering the input function and raising the retention index, an explanation that seems reasonable. Secondly, the input function is corrected for metabolites using the ratio of unchanged tracer to ^{11}C-labeled metabolites obtained from the observations in healthy animals. While this is a generally accepted practice, no studies have as yet ascertained whether [^{11}C]HED metabolism is altered in the diabetic state. An increase in [^{11}C]HED metabolite production or clearance of [^{11}C]HED in diabetic rats with a metabolite correction derived from healthy control animals would reduce the input function and thus amplify the retention index.

Measurements independent of the input function that take into account only the shape of the myocardial curve such as the monoexponential washout rate may provide valuable complementary data. The results presented here and elsewhere support the correlation of washout with retention measures (Law et al., 2010; Tipre et al., 2008), and are supported in diabetic data by *in vitro* measurements of NE levels. Washout rate is a standard measurement of [^{123}I]MIBG in conjunction with very late ratios of heart to reference region (mediastinum) tracer accumulation (Jacobson et al., 2010; Kasama et al., 2011; Kusmic et al., 2008). There is evidence to suggest that washout kinetics may be more sensitive and more reflective of the presynaptic function encompassing reuptake and active release of neurotransmitter than the limited frame analysis of retention (Matsunari et al., 2010).

In clinical practice, the poor comparability of retention indices between centres (Lautamaki et al., 2007), especially in cases of diffuse or subtle disease (Schafers et al., 1998) support the exploration of alternative quantification of [^{11}C]HED. The standard measurement for receptor ligands is the Logan distribution volume (DV), a linear graphical estimation of reversible binding kinetics (Logan et al., 2005; Logan et al., 1987). Logan distribution volume is calculated as:

Equation 3 $$DV = \frac{K_1}{k_2} \times \left(1 + \frac{k_3}{k_4}\right) = \frac{K_1}{k_2} \times \left(1 + \frac{B_{max}}{K_d}\right)$$

DVs for [^{11}C]HED have been reliably reported in healthy subjects and cardiomyopathy patients, with regional decreases in DV evident in diseased myocardium (John et al., 2007; Kies et al., 2004). To accurately calculate the DV, plasma metabolite calculations should be run concurrent with each scan (Harms et al., 2011). The application of DV to small animal models may overcome the complication of high sympathetic tone and active vesicular release, but the spill-in and metabolites would continue to complicate the calculation.

This problem could be rectified by arterial blood sampling from the animals to determine a direct input function (Sharp et al., 2005) or by the use of an alternative blood pool image that is not corrupted by left ventricular motion or spill-in. Blood sampling, while providing the most accurate assessment of blood activity, is invasive and subject to volume limitations, particularly in mice. By contrast, the definition of a region of interest in the inferior vena cava or the thinner-walled left atrium may provide a superior blood pool image with reduced motion and spill-in effects, but [^{11}C]HED uptake in liver and lung tissue (Thackeray et al., 2007) can also compromise the image in later frames. Quantitative analysis of [^{11}C]HED retention in rodents may best be accomplished by a combination of measurements, taking into account both the corrected late frame myocardial activity, reflecting uptake (K_1) and retention, and the declination slope of the myocardial time activity curve, reflecting tracer clearance (k_2).

8.2 Sympathetic Dysfunction in Diabetic Rats

Defects of sympathetic innervation in hearts of diabetic subjects have been well documented. Generally, reduced cardiac uptake of sympathetic neuronal imaging agents, such as [^{11}C]HED and [^{123}I]MIBG, has been attributed to regional sympathetic denervation consistent with diabetic autonomic neuropathy (Scholte et al., 2010; Stevens et al., 1999).

Dysinneration of the apical left ventricle in conjunction with elevated nerve growth factor expression in this region supports the notion of nerve death and axonal regeneration (Schmid et al., 1999), wherein axonal neurotrophins are upregulated in response to neuronal apoptosis (Perez-Polo et al., 1990). Expression of nerve growth factor has been demonstrated to be proportional to NE levels (Cao et al., 2000; Ieda et al., 2004; Ieda et al., 2006), and may reflect the compensatory processes aimed at preserving the noradrenergic neurons in the hyperadrenergic environment.

The present studies demonstrate reduced retention of [^{11}C]HED with associated decrease in NET expression but no change in nerve density, as determined by PET imaging, Western blots and tyrosine hydroxylase immunostaining, respectively. In a normal heart, NE binds to β-adrenoceptors to initiate cAMP signal cascade to enhance contractility, with signal terminated by active recapture of NE to the presynaptic varicosity with limited overflow (Fig 8.1A). In diabetes, sympathetic tone is heightened, driving an acute increase in NE leading to hyperstimulation of β-adrenoceptors and increased spillover from the synapse (Fig 8.1B). To counter chronically heightened sympathetic tone, the myocardium and sympathetic neurons undergo compensatory adaptations to maintain normal noradrenergic signaling (Fig 8.1C). The postsynaptic internalization and downregulation of β-adrenoceptors serves to dampen the sympathetic stimulation of cardiomyocytes, and may contribute to reduced heart rate. To further reduce sympathetic signaling, cycling of active NET from the neuronal surface to intracellular vesicles is enhanced to reduce recovery of NE and augment spillover to the general circulation. The temporal increase in plasma NE concentration observed in diabetes provides evidence of heightened sympathetic tone and reduced active recapture of NE from the myocardium. The maintained nerve density suggests a dysregulation of functional innervation without overt denervation, which would allow for functional rescue of

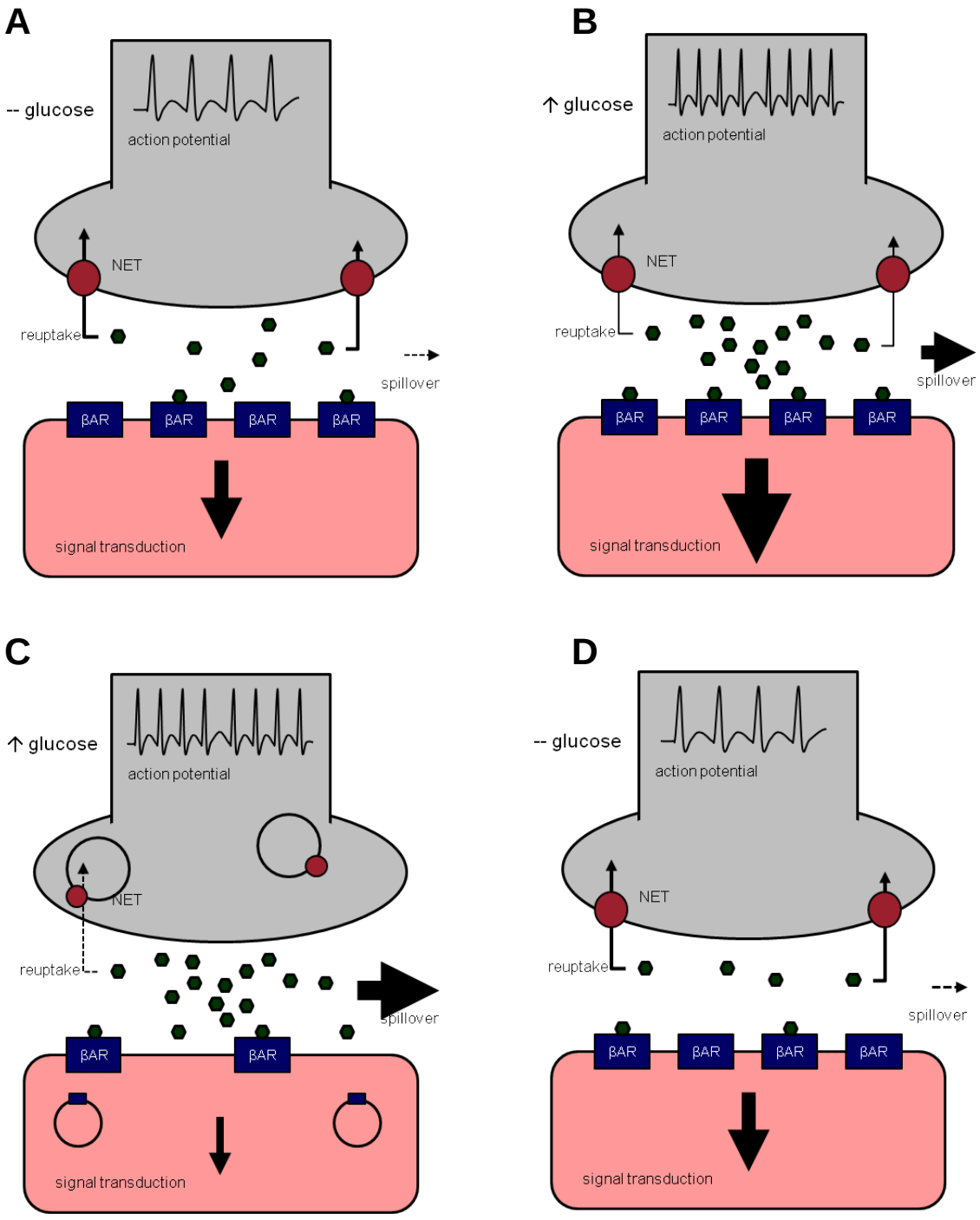

Figure 8.1 Schematic of sympathetic activation in diabetes and response to therapy to reduce sympathetic overstimulation. (**A**) Neuronal impulse action potentials stimulate norepinephrine (NE, green hexagons) release from the neuronal varicosity into the synapse where it is bound by β-adrenoceptors (βAR) on the cardiomyocyte surface and stimulates downstream signaling events via adenylate cyclase, cAMP, and protein kinase A. Synaptic NE is recovered by NE reuptake transporter (NET) via uptake-1 pathway or spills over to the circulation. (**B**) In

acute diabetes, elevated glucose augments the neuronal impulse and enhances synaptic NE, leading to heightened postsynaptic activity and increased spillover to circulation. (**C**) In chronic diabetes, persistently high NE evokes βAR and NET downregulation, dampening the sympathetic signal and further increasing NE spillover. (**D**) Treatments to reduce circulating glucose or modulate sympathetic tone attenuate the neuronal impulse and restore the expression of βAR and NET, normalizing the downstream cardiomyocyte signal, uptake-1, and spillover.

sympathetic neurons by restoration of normal adrenergic tone. PET imaging studies with infusion of exogenous NE demonstrated sensitivity of [^{11}C]HED retention to increased tissue NE, suggesting that transient increases in sympathetic tone in the global myocardium may be partially responsible for the reduced uptake of [^{11}C]HED in diabetic rats. While the SUV measurement of [^{11}C]HED retention is influenced heavily by body weight, the complementary in vitro measures of NET and NE confirm dysregulation of the SNS, particularly the compensatory dampening of the sympathetic signal. Lowering of blood glucose levels reduces sympathetic drive, resulting in reduced spillover of NE and restored NET and β-adrenoceptor expression (Fig 8.1D). The reduction of [^{11}C]HED SUV and acceleration of washout is therefore thought to reflect not only a decrease in reuptake, but also an increase in active NE release from presynaptic varicosity and spillover from the synapse to the general circulation.

The timeframe of the development of sympathetic dysfunction is comparable to previous reports, with reduced tracer accumulation detected using both ex vivo and in vivo approaches at 8 weeks of sustained hyperglycemia (Dincer et al., 2001; Kusmic et al., 2008; Muhr-Becker et al., 1999; Schmid et al., 1999; Thackeray et al., 2011a). It is conceivable that in cases of more severe or longer term diabetes, the sympathetic abnormalities may worsen and their reversibility may be impaired by permanent sympathetic denervation (Ganguly et al., 1986; Schmid et al., 1999). Indeed, in the diabetic rats treated with metformin from 8 weeks of diabetes, sympathetic markers appeared to degenerate further, though there were no indications of greater decline in left ventricular function. The metformin-treated group did exhibit a modest increase in 16-week mortality (2/8) as compared to insulin-treated (1/14) and non-diabetic controls (0/8), though sample sizes are limited.

The lack of change in both NE and [^{11}C]HED uptake observed in STZ-treated animals that remained euglycemic demonstrates a clear association between elevated blood glucose and

augmented SNS activation. Elevated glucose levels by sucrose feeding and in central administration have been demonstrated to directly increase sympathetic tone (Dutta et al., 2001; Levin and Sullivan, 1989). Moreover, the functional changes in the diabetic heart imparted by hyperglycemia culminating in fibrosis and lipotoxicity may evoke sympathetic activation to overcome reduced compliance and deteriorating systolic function (Boudina and Abel, 2007). In the present experiments, systolic function was maintained, but this may derive in part from continued adaptive sympathetic stimulation.

The functional consequences of sympathetic anomalies were expected to manifest as a pronounced decrease in heart rate variability. Acute treatment of healthy rats with β-adrenoceptor antagonist propranolol reduces heart rate and heart rate variability as determined by telemetric monitoring over 5 hours (Fig 8.2), reflecting a loss of sympathetic regulation. Alternatively, acute administration of NET inhibitor desipramine reduced the short term variability of heart rate (Fig 8.2), consistent with amplification of sympathetic tone and depressed influence of parasympathetic control. Chronic sympathetic stimulation would be expected to decrease the contribution of sympathetic afferent control of heart rate (Tobaldini et al., 2009), manifesting as smaller standard deviation of 24-hour average heart rates. While a modest depression of heart rate variability is observed in the current studies, the change is less dramatic than previously reported (Howarth et al., 2005b). The duration and severity of diabetes may impact the measurement of heart rate variability. Alternatively, the reduced sinus rhythm observed in the diabetics in previous studies may inherently depress the standard deviation, which is generally used to measure heart rate variability (Howarth et al., 2005b). Assessment of sympathetic function by pharmacological challenge with desipramine or exogenous β-agonists may provide further insight into the abnormal sympathetic signaling in these diabetic rats (Goncalves et al., 2009). Moreover, the age of

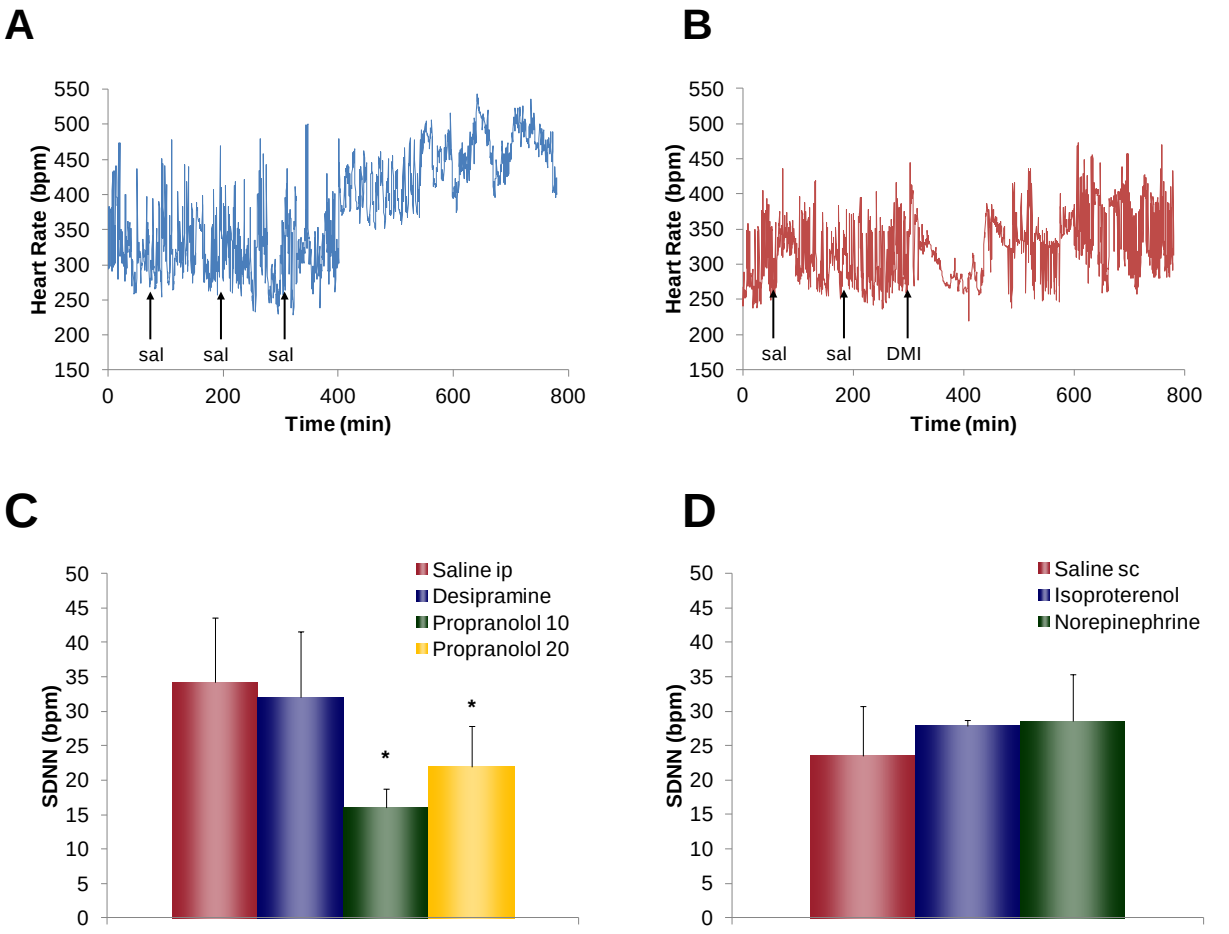

Figure 8.2 Acute effect of desipramine (DMI) administration on heart rate in healthy rat monitored by implantable radiotelemetry. (**A**) Three sequential intraperitoneal injections of saline (sal) to a healthy rat do not change the variability of heart rate. (**B**) Administration of norepinephrine reuptake inhibitor desipramine on the third injection (10 mg/kg ip) evokes reduced heart rate variability due to augmentation of sympathetic over parasympathetic regulation of heart rate. Variability is recovered at 4-6 hours after desipramine injection. Six-hour heart rate variability assessed by implantable radiotelemetry over 6 hours expressed as standard deviation of 24 h normal heart rate (SDNN) following treatment with (**C**) desipramine (10 mg/kg, ip) and β-adrenoceptor blocker propranolol (10 or 20 mg/kg, ip) or (**D**) acute subcutaneous injection of β-adrenoceptor agonist isoproterenol or norepinephrine. * $p<0.01$ to saline ip, one-way ANOVA.

rats affects the heart rate variability regardless of health status, with a progressive reduction in the differences between diabetic and non-diabetic animals apparent by 4-6 months of age (Howarth et al., 2008), which overlaps the timeframe of the present study (2-4 months of age). Alterations in heart rate variability are present after 4 weeks of diabetes, preceding the onset of measurable alterations in [^{11}C]HED retention, suggesting a progressive dysregulation of the sympathetic signal.

Depression of heart rate variability likely results from sympathetic hyperactivity and the consequent changes in presynaptic reuptake and postsynaptic signaling. While insulin treatment did not restore heart rate variability to non-diabetic levels, this may also reflect changes in parasympathetic signaling, potential upregulation of muscarinic acetylcholine receptors, or functional changes at the sinoatrial node. Recovery of sympathetic/parasympathetic balance may require longer term normalization of both glucose levels and NE.

8.3 Diastolic Dysfunction

Longitudinal echocardiography assessment suggests that diastolic dysfunction develops prior to altered [^{11}C]HED retention, with E/A shift and prolonged mitral valve deceleration present at 4 weeks of diabetes and [^{11}C]HED abnormalities appearing at 8 weeks of diabetes. This finding suggests that diastolic abnormalities precede, and may contribute to the activation of the SNS by creating a circulatory physiological requisite for compensatory augmentation of sympathetic tone. Clinical studies have demonstrated an association between impaired diastolic function and dampened autonomic reflexes (Mustonen et al., 1992; Sacre et al., 2010).

The driving factor of reduced ventricular compliance is likely a combination of the accumulation of glycation endproducts and lipid deposition (An and Rodrigues, 2006; Basu et al., 2009; Candido et al., 2003). Interstitial collagen has been described in the left ventricle

of animal models of type 1 and type 2 diabetes, often concurrent with cardiomyocyte hypertrophy. In the present study, Masson's Trichrome staining did not reveal any significant interstitial collagen deposition, though intracellular lipid accumulation and glycation both increase chamber stiffness in a similar manner. Disruption of sympathetic innervation may impact ventricular relaxation at the level of intrinsic pacemaker nodes, as both the sinoatrial and atrioventricular nodes are highly innervated by sympathetic efferents (Wehrwein et al., 2008). Dampening of the sympathetic signal contributes to the slowing of heart rate, which manifests in part as prolonged ventricular filling. However, the contribution of elevated blood glucose and the shift of cardiac metabolism towards accumulation of lipid metabolites are supported by the delay of diastolic left ventricular changes by early treatment with insulin and to a lesser extent by insulin sensitizers metformin and rosiglitazone. Normalized glycemia is expected to reduce the glycation of lipid and protein in the heart, counteracting the accumulation of advanced glycation end products and the disruption of the extracellular matrix (Basu et al., 2009; Kennedy and Baynes, 1984). Moreover, increased fatty acid metabolism in adipocytes by rosiglitazone and in cardiomyocytes via AMPK stimulation by metformin may reduce cytosolic lipid metabolites, resulting in attenuation of transmitral flow resistance. Reduced circulating levels of nonesterified fatty acids and glucose may decrease sympathetic drive in the central nervous system as well (Florian and Pawelczyk, 2010; Marsh et al., 2009). By contrast, treatment after sustained diabetes with either insulin or metformin does not improve diastolic function because ventricular compliance has already been compromised, whereby a critical degree of damage requires a longer timeframe to reverse the adaptive alteration in diastolic function in the heart. Cardiomyocyte apoptosis induced by lipotoxic ceramide or diacylglycerol would not be expected to be improved by insulin treatment alone (Hajduch et al., 2008), or may require longer treatment to reverse the incurred cardiovascular damage. Treatments to reduce reactive oxygen species (Huynh et al.,

2012), glycation (Candido et al., 2003), or fibrosis (Forcheron et al., 2009) have been demonstrated to improve cardiac diastolic function in diabetic animals.

Diastolic dysfunction measurements using echocardiography can be difficult to interpret and define, particularly with reduced heart rate observed in diabetic rats and the time dependency of variables used. Reduced heart rate extends passive filling time, prolonging the deceleration time of the mitral valve and accentuating the magnitude of the early filling velocity in relation to the atrial kick. Differences in heart rate between experimental groups can be partially accounted for by normalizing calculations to the square root of the R-R interval (Rodrigues et al., 2011). In the present studies, normalized mitral valve deceleration time was still elevated among diabetic compared to non-diabetic rats. Abnormal filling velocities have been described in diabetic mice, with additional evidence of diastolic dysfunction provided by increased mitral valve strain as determined by tissue Doppler (Basu et al., 2009; Mizushige et al., 2000). The shift may also result from differences in response to anaesthetic (Rottman et al., 2007), wherein the slower heart rates in diabetic rats are depressed more readily by prolonged exposure to isoflurane as compared to higher heart rates at baseline and in non-diabetic controls. Time under anaesthetic was kept constant between groups to minimize the influence of this potential confounding factor. Left atrial size may provide additional information on diastolic dysfunction, where reduced ventricular filling leads to increased left atrial size due to resistance. Measurements of left atrial size have correlated well with Doppler measurements of diastolic dysfunction (Blana et al., 2010). The gold standard measurement of diastolic function is left ventricle hemodynamics and pressure-volume relationship obtained using a Millar catheter micromanometer. Direct comparison of Doppler estimates and Millar catheter measurements have shown good correlation (Connelly et al., 2006), though pressure quantification is less susceptible to heart rate variables. Studies

in diabetic rats have demonstrated reduced slope of the pressure-volume loop, indicating a decrease in dP/dt consistent with impaired ventricular relaxation (Connelly et al., 2007).

Taken together, the present results suggest that left ventricular diastolic dysfunction and sympathetic dysinnervation are regulated by connected but parallel pathways (Fig 8.3). While diastolic dysfunction is intimately related to metabolic abnormalities, lipotoxicity, glucotoxicity and oxidative stress, sympathetic dysfunction is more strongly related to the central nervous system regulation of cardiac inotropy and chronotropy (Bengel et al., 2002a). To compensate for slowing heart rate and reduced compliance, the SNS would be expected to be activated in diabetic rats. The high concentration of NET in atrial tissue reflects the importance of sympathetic signaling in the regulation of atrial contraction (Wehrwein et al., 2008). In such a way, the progressive SNS alterations may play a role in the transition of diabetic heart disease from diastolic to systolic dysfunction. Reduced left ventricular ejection fraction is frequently reported in animal models and in diabetic patients (Boudina and Abel, 2007), often after significant duration of diabetes. The identification of sympathetic signaling changes early in the development of diastolic dysfunction may have prognostic value for subsequent ventricular remodeling and systolic dysfunction. Systemic activation of the SNS contributes to perturbed myocardial metabolism, as downregulation of β-adrenoceptors in the heart reduces sympathetic facilitation of GLUT4 translocation following insulin receptor signaling (Morisco et al., 2005) and in adipose tissue reduces lipolysis leading to fat accumulation and increased nonesterified fatty acid and long chain fatty acids in the circulation (Suskin et al., 2000), culminating in augmented lipid metabolism in cardiac muscle and further deregulation of glucose transport and glycolysis.

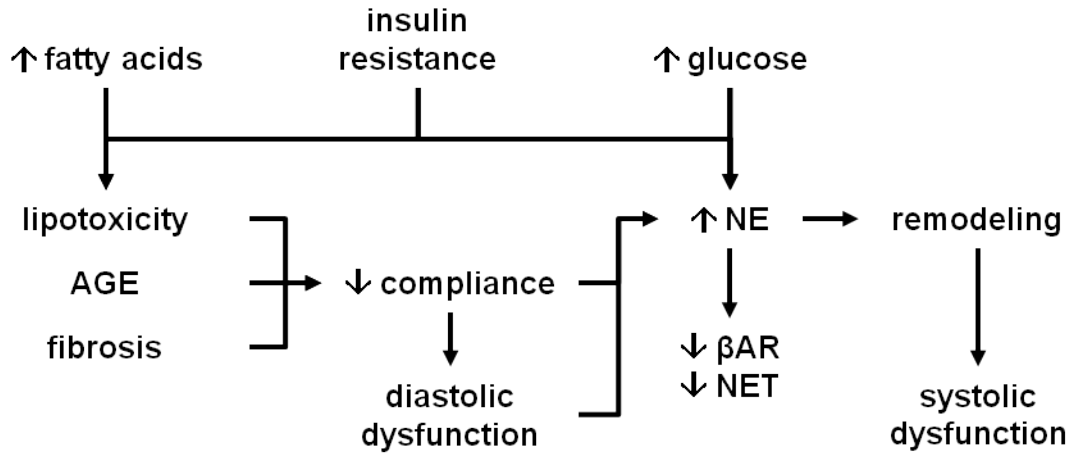

Figure 8.3 Parallel influences of ventricle stiffness and sympathetic activation to the development of left ventricular systolic dysfunction in diabetes. Elevated levels of glucose and nonesterified fatty acids in conjunction with insulin resistance contribute to the accumulation of lipid metabolites, crosslinking of advanced glycation endproducts (AGE), and collagen fibrosis in cardiomyocytes, leading to chamber stiffness, reduced compliance, and diastolic dysfunction. Left ventricular compensation for reduced compliance augments the elevation of norepinephrine release in response to hyperglycemia and hyperlipidemia, culminating in remodeling, hypertrophy, and systolic dysfunction.

8.4 Efficacy of Glycemic Therapy

The high fat diet fed STZ rat has been reported as representative of type 2 diabetes, with limited evidence suggesting responsiveness to insulin sensitizing by metformin or thiazolidinedione therapy (Reed et al., 2000). In the current studies, while diabetic rats exhibit clear insulin resistance (as demonstrated by euglycemic clamp experiments at 8 and 16 weeks after STZ), the progressive depletion of native insulin production and secretion implies the model is more accurately designated as type 1 diabetes complicated by insulin resistance. As such, while metformin treatment from 1 week after STZ was shown to improve glucose tolerance at 8 weeks, the peripheral effect of insulin sensitizing via AMPK was not observed in rats treated from 8 weeks after STZ, potentially due to the impairment of insulin production at this time point. The mechanism of AMPK stimulation by metformin in striated muscle has been questioned in recent literature (Brenman and Temple, 2007; Zhou et al., 2001). The lack of glucose reduction in the fed state observed in the present study is in line with comparable studies in ZDF rats, in which metformin treatment at a similar dose increased glucose uptake in myocardium with no change in circulating glucose levels. In the current studies, improved insulin sensitivity was established by euglycemic clamp in metformin diabetic rats, but without native insulin production, the insulin-sensitizing effect of metformin is not likely to impart any physiological effect.

By contrast, insulin replacement was effective in reducing blood glucose when provided at 8 weeks of diabetes, reflecting a functional insulin signaling apparatus limited by decreased pancreatic β-cell mass (Elsner et al., 2000). The reduction of blood glucose was associated with a parallel decrease in circulating NE levels, suggesting a dampening of glucose-induced sympathetic stimulation in the central nervous system. There was a direct relationship between plasma glycemic level and [^{11}C]HED SUV and washout rate, which, when coupled with NE measurements and immunoblots of pre- and postsynaptic signaling proteins,

supports the link between glycemia and sympathetic overstimulation. Normalization of NE levels was associated with restoration of NET, β_1- and β_2-adrenoceptors, and tyrosine hydroxylase, strongly suggesting healthy β-adrenergic signaling in insulin-treated diabetic rats, consistent with previous reports (Burgdorf et al., 2006; Dincer et al., 2001; Thackeray et al., 2011a). Additional studies have associated antecedent hypoglycemia with sympathetic activation, relating to increased muscle work and metabolic demand (Fisher et al., 2005). In the current study, delivery of insulin is continuous, with no fluctuation and the animals are allowed to regulate blood glucose by ad libitum feeding, which is expected to reduce glucose variability. Insulin levels were in line with previous reports of high fat fed rodents (Levin et al., 2005; Park et al., 2005; Reed et al., 2000).

Treatment from 1 week of diabetes established the capacity of glucose normalization and improved cardiac metabolism to delay the deterioration of diastolic function, presumably by reducing the accumulation of lipid metabolites and glycosylated intermediates. There was a 2-3 week delay in the decline of blood glucose to non-diabetic levels in insulin-treated rats, suggesting that the convergence of insulin resistance, balanced by native and exogenous insulin, may have necessitated a longer normalization period to restore glucose uptake. By contrast, rats treated at 8 weeks of diabetes are hypoinsulinemic, whereby exogenous insulin administration does not excessively raise plasma insulin or NE levels. Metformin reduced fasting glucose levels but fed state glucose remained elevated, similar to the rosiglitazone treatment, potentially owing to greater variability in glucose measurements. Similar doses have been shown to reduce HbA1c (reflecting long-term glycemic state) without a shift in fed state glucose levels (Shoghi et al., 2009). Despite this, altered cardiac fatty acid metabolism was evident from immunoblot studies, and have been reported elsewhere following acute (Verma and McNeill, 1994) and chronic treatment (Shoghi et al., 2009), as measured in isolated perfused hearts. Both treatments showed a reduction of circulating lipids, consistent

with previous studies (Reed et al., 2000; Shoghi et al., 2009). However, NE levels were elevated and [^{11}C]HED retention reduced in all treatment groups. These findings support a prominent role of hyperglycemia in the activation of the SNS and heightened NE spillover with a lesser contribution of compensatory signaling to counteract abnormal ventricular filling.

Among treatment regimens, the highest washout rate of [^{11}C]HED was found in rosiglitazone-treated diabetic rats, which may suggest an additional sympathetic activation in this treatment. The added cardiovascular risk reported with rosiglitazone has been suggested to relate to expansion of blood volume and elevated blood pressure (Chang et al., 2008; Henriksen et al., 2009). Sustained hypertension would correlate to further dysregulation of the myocardial sympathetic nervous signal, particularly to reduce heart rate and vasoconstriction in response to expanded volume. This may be an additional explanation of the persistent and progressive sympathetic dysregulation in rosiglitazone-treated diabetics.

It is conceivable that in an animal model with more characteristics of type 2 diabetes, metformin or rosiglitazone treatment would more efficiently reduce glucose levels due to milder hyperglycemia and continued native insulin production in these models. Restoration of euglycemia or reduction of glycosylated hemoglobin has been reported with metformin or thiazolidinedione therapy in GK, OLETF (Choi et al., 2007), and ZDF (Shoghi et al., 2009) rats. Considering the parallel decrease in blood glucose and NE in diabetic rats at 8 weeks post-STZ, these treatments may reduce sympathetic overactivity in type 2 diabetes, which would be expected to result in weight loss, recovered heart rate variability, and normal retention of [^{11}C]HED.

Taken as whole, the results of these studies suggest that while control of blood glucose levels may effectively and significantly delay the deterioration of diastolic function, abnormal cardiac sympathetic signaling and heightened NE levels may progress in spite of this

treatment. The consequences of this sympathetic abnormality are not entirely clear, though evidence points to added cardiovascular risk (Gerson et al., 2011). As such, long term modification of cardiac sympathetic signaling using pharmacological agents may be of value in prevention of diabetic cardiac complications.

8.5 Sympathetic Modulation in Diabetes

Continuous noradrenergic stimulation by elevated sympathetic drive evokes downregulation of presynaptic NET and postsynaptic β-adrenoceptors (Lefkowitz and Caron, 1985; Rockman et al., 2002). In heart failure, chronic β-blocker therapy has been demonstrated to upregulate the expression of β-adrenoceptors at the cardiomyocyte membrane, restoring sympathetic efferent signal to the myocardium (Bristow et al., 1992). Because of systemic effects on adipocytes and vasculature, β-blockade has been associated with increased incidence of new onset diabetes in heart failure patients, relating to the inhibition of lipolysis and resulting in increased visceral adiposity in treated subjects (Kostis and Sanders, 2005). The crosstalk of β-adrenergic and insulin receptor signaling in the translocation of GLUT4 (Morisco et al., 2005) suggest that recovery of sympathetic signaling may contribute to increased glucose uptake in striated muscle. Moreover, preventative modulation of the sympathetic signal may aid in the prevention of systolic dysfunction in diabetic heart, counteracting the adverse compensatory remodeling in response to reactive oxygen species, interstitial collagen and lipid deposition. In a series of experiments in isolated perfused hearts, five week chronic treatment with metoprolol, a selective β_1-adrenoceptor antagonist, increased cardiac output and hydraulic power with reduced palmitate oxidation and a compensatory increase in glucose uptake. Modified fatty acid metabolism was mediated in part by a reduction in carnitine palmitoyl transferase-1 activity by a PGC1α/PPARα-mediated mechanism. Chronic metoprolol increased myocardial expression of β_1-, β_2- and β_3-adrenoceptors, with an increased association of β_2-adrenoceptors with G_s over G_i, consistent with a restoration of

noradrenergic sensitivity (Sharma et al., 2009; Sharma et al., 2008a; Sharma et al., 2008b). Continuous modulation of the sympathetic signal by metoprolol reduces overstimulation of cAMP and PKA, which may counter the development of left ventricular dysfunction.

Persistent NE elevation is also associated with upregulation of G protein-coupled receptor kinases, involved in the desensitization and internalization of adrenoceptors. A recent study demonstrated that upregulation of GRK2, both naturally in ischemia and artificially in transgenic mice, impaired the uptake of [^{18}F]FDG and dampened the phosphorylation of Akt in response to insulin, consistent with insulin resistance (Ciccarelli et al., 2011). Control of sympathetic efferents in diabetes could provide protection from metabolic abnormalities exacerbated by excessive NE signaling. Indeed, ongoing heart failure trials with the third generation β-blocker carvedilol, which exhibits partial α-agonist activity have been reported to reduce the incidence of new-onset diabetes (Jacob et al., 1998).

β-Blockade has been shown to increase the expression of presynaptic NET (Mardon et al., 2003), which allows more efficient acute clearance of neurotransmitter from the synapse. Cardiac overexpression of NET has been shown to ameliorate some of the deleterious remodeling in failing hearts, owing to a dampening of the persistent sympathetic signal (Backs et al., 2001). Consequently, downstream elements involved in cardiomyocyte Ca^{2+} regulation are maintained, preserving functional contractile behavior. In heart failure, β-adrenoceptor polymorphisms have been identified as additive risk factors in the progression of the pathology (Bengtsson et al., 2001). The same may be true in diabetic patients (Masuo et al., 2005), which may facilitate identification of risk populations in a shift toward personalized medicine.

The mechanistic contribution of β-adrenergic signaling in diabetic heart disease may partially explain the efficacy of angiotensin targeted drugs in the reduction of cardiac morbidity and mortality among diabetic patients. Overexpression of renin, the starting material in the

production of angiotensin, exacerbates the cardiac phenotype in STZ-induced diabetes, with greater degree of interstitial collagen deposition and diastolic dysfunction progressing to impaired ejection fraction (Connelly et al., 2007; DeMarco et al., 2011). Elevated plasma angiotensin is associated with increased plasma catecholamines and hypertension (Xiao et al., 2011; Yu et al., 2012). Angiotensin receptor blockers and angiotensin converting enzyme inhibitor suppress sympathetic tone (Scheen, 2004), an action which, in conjunction with antioxidant and antiapoptotic properties, may contribute to improved cardiac health in treated diabetic patients.

Therefore, while glycemic control can effectively normalize the cardiac sympathetic nervous signal, additional therapeutic approaches to reduce the elevation of cardiac NE release and adrenergic signaling may have beneficial outcomes both in signaling and metabolism of the diabetic heart. The combination of removing glucose-stimulated noradrenergic stimulation in the central nervous system with targeted modulation of signaling elements at the myocardium may counteract left ventricular dysfunction.

8.6 Prognostic Imaging

One of the potential applications for molecular imaging of the cardiac SNS is in the identification of patients at greatest risk of progressive heart disease. This information is valuable in informing treatment decisions for the patient and may provide a crucial quantifiable biomarker that can be used in assessing the efficacy of therapies. This is particularly important in the context of the present findings, in which the sympathetic defects observed in diabetic rats appear to result from sympathetic overactivity rather than denervation, and may provide a window of opportunity for the normalization of sympathetic activity and left ventricular function.

The DIAD trial compared diabetic patients screened with myocardial perfusion imaging for the presence of silent ischemia with those that did not undergo screening. While the presence

of a large myocardial perfusion defect was modestly predictive of subsequent cardiac events (Young et al., 2009), there was no difference in event rate between screened and non-screened patients at 5 year follow up (Bansal et al., 2010). The reported event rate was quite low compared with previous studies (Bansal et al., 2010). By contrast, categorization of high risk was demonstrated in a comparable study among diabetic patients without known coronary artery disease with significant separation between Kaplan-Meyer curves evident by 10 years of follow up (Miller et al., 2004; Rajagopalan et al., 2005). Taken together, these findings reflect the potential benefit of glycemic control for cardiac function, acting in part through normalization of sympathetic innervation which would not require dedicated myocardial therapy. It also suggests that alternative targets including the neurohormonal signaling axis may provide complementary information in the identification of patient risk (Sasso et al., 2010).

In the ADMIRE HF trial SPECT scans with [^{123}I]MIBG conducted 3 weeks after ST-segment elevation myocardial infarction revealed an association between increased tracer washout rate and subsequent major adverse cardiovascular events over 3-5 years (Kasama et al., 2011). The degree and homogeneity of myocardial sympathetic innervation has been suggested to provide the substrate of lethal ventricular arrhythmias (Bax et al., 2008; Sasso et al., 2010). Imaging studies with [^{123}I]MIBG identified large late frame defect as a predictive measure of inducible ventricular fibrillation, information that directed the appropriate implantation of cardioverter defibrillator devices (Boogers et al., 2010). These findings underscore the added value of molecular imaging information in the treatment of cardiac patients.

The link between sympathetic dysregulation and diabetic cardiomyopathy has been well established using both indirect and direct noninvasive evaluation of sympathetic innervation and activity. The predictive value of NE levels and heart rate changes following cold pressor

testing has established the prognostic potential of SNS biomarkers in the tracking of diabetes progression (Carnethon et al., 2003a; Flaa et al., 2008). Similar to the larger ADMIRE cohort, diabetic heart failure patients with lowest retention of [^{123}I]MIBG were significantly more likely to experience a major adverse cardiovascular event (Gerson et al., 2011). Imaging studies have identified sympathetic neuronal deficits in diabetic hearts, progression of which can be arrested or reversed by normalization of glucose levels (Fricke et al., 2008; Stevens et al., 1998b), illustrating the potential of neurohormonal PET to monitor response to therapy.

The decrease and insulin-induced normalization of [^{11}C]HED SUV identified in diabetic rats suggest a value in [^{11}C]HED imaging to identify therapeutic efficacy and recovery of sympathetic signaling which occurs prior to detectable echocardiography systolic abnormalities. In combination with a PET measurement of cardiac metabolism, neurohormonal imaging could provide crucial insight to possibly identify patients who would benefit from preventative therapy with β-blockers or angiotensin blockers to potentially prevent the progression to systolic dysfunction. Reduced [^{11}C]HED retention is observed prior to detectable reduction in ejection fraction or fractional shortening, suggesting that alterations in the sympathetic drive may contribute to eventual cardiac remodeling, and normalization of this signaling may impart protection against further deterioration of left ventricular function.

8.7 Conclusions

Clinically utilized retention index, SUV, and monoexponential washout provide sound, reproducible measures of [^{11}C]HED kinetics in healthy rats. The retention and clearance of [^{11}C]HED is directly proportional to NET availability and inversely proportional to myocardial and plasma NE concentration. As such, [^{11}C]HED imaging may be useful for the detection of sympathetic hyperactivity and elevated tissue NE in early stages of myocardial

disease. Calculation of SUV with complementary evaluation of washout rates may provide the most meaningful data for this project, as these measurements corroborate the reduction in myocardial [^{11}C]HED accumulation established by *ex vivo* biodistribution and reflect the physiological increase in plasma and cardiac NE levels and reduced NET expression observed in diabetic rats.

Rats fed high fat diet and treated with STZ (45 mg/kg, ip) exhibit insulin resistance with sustained hyperglycemia, modest hyperlipidemia, and progressive insulin deficiency. Prolonged hyperglycemia in these rats alters sympathetic tone with increased tissue and plasma NE, reduced neuronal reuptake, and lower global [^{11}C]HED accumulation, but no change in sympathetic nerve density. Transmitral pulse wave Doppler measurements indicate left ventricular filling abnormalities consistent with diastolic dysfunction. Normalization of blood glucose levels by insulin replacement after 8 weeks of sustained diabetes reduces circulating NE, upregulates expression of NET, β-adrenoceptors and GLUT4, and normalizes myocardial [^{11}C]HED SUV and washout, with no corresponding recovery of diastolic function. Treatments early in diabetes progression with insulin, metformin, or rosiglitazone slow the progression of left ventricular diastolic abnormalities, but do not prevent rising NE, reduced NET, and global deficit of [^{11}C]HED retention, potentially due to latent reduction of blood glucose levels. Sympathetic neuronal regulation is secondary to the development of diastolic dysfunction, but appears to exacerbate its progression. Treatments targeted to normalize sympathetic signaling (β-blockers, angiotensin blockers) concurrent with glycemic therapy may drastically improve cardiac outcomes in diabetes.

8.8 Future Directions

Definition of an appropriate kinetic model for the accurate quantification of [^{11}C]HED in disease state is a critical step for the progression of studies. This would require the development of an appropriate metabolite correction with dynamic measurements of plasma

metabolites in both healthy and diseased rats to calculate a reliable distribution volume. The ability to obtain an accurate input function from the image is additionally important. Future studies should assess the impact of heart rate on retention indices, evaluating blood time activity curves in individual rats with or without treatments to reduce heart rate for comparison to the diabetic population. Further, perfusion PET studies ([^{13}N]ammonia) should be completed in diabetic rats to determine if the [^{11}C]HED measurements are susceptible to changes in myocardial blood flow.

Additionally, the effect of treatments modulating sympathetic drive on noradrenergic signaling and left ventricular function is of great interest. Studies with a similar design could follow treatment arms with 3 generations of β-blockers (propranolol, metoprolol, and carvedilol) and blockers of the renin angiotensin system (enalapril, losartan) in the presence and absence of normalized blood glucose levels. Such studies would identify the relative impact of glycemic therapy, mainly insulin, on the sympathetic drive and additive effect of direct normalization of the myocardial sympathetic nervous signal on the release of NE, reuptake kinetics, and the retention of [^{11}C]HED. Coupled with interrogation of metabolic parameters using small animal PET measurements of glucose uptake ([^{18}F]FDG) and fatty acid uptake ([^{18}F]FTHA) or oxidation ([^{11}C]palmitate), insight into the glucose-NE signaling axis would be gained from these experiments. To this end, genetic manipulation of diabetic rats to modify sympathetic signaling could also be investigated, overexpressing or knocking out NET to define the specific role of NE reuptake in the preservation of left ventricular function in the presence of diabetes.

Thirdly, expansion of the current findings into alternative animal models of type 2 diabetes is an attractive opportunity. Insulin sensitizing therapies would be expected to have a greater effect in obese and/or hyperinsulinemic rats. The progression of sympathetic abnormalities in ZDF or GK rats or in db/db mice is less clearly characterized than in STZ diabetes. Studies

using metformin or rosiglitazone may provide insight into the progression of volume-expansion hypertrophy and cardiac risk in rosiglitazone-treated animals.

Lastly, the findings can be translated to the clinical arena. Evaluation of sympathetic neuronal integrity using [^{11}C]HED among diabetic patients can establish a database of normal and abnormal tracer uptake and retention, which can be subsequently correlated with the risk of cardiovascular events. Assessment of treatment parameters and glycemic control among these screened patients can provide support for the application of [^{11}C]HED PET imaging to identify sympathetic neuronal dysfunction in the early stages of diabetic cardiomyopathy. This approach may further define prevention strategies for diabetic patients with pharmacotherapy targeting glucose control, cardiac metabolic balance, and/or sympathetic modulation.

Chapter 9: References

REFERENCES

Adams DJ, Cuevas J. 2004. Electrophysiological Properties of Intrinsic Cardiac Neurons. In: Armour JA, Ardell JL, editors. Basic and Clinical Neurocardiology. New York: Oxford University Press. p 1-60.

Affolter H, Hertel C, Jaeggi K, Portenier M, Staehelin M. 1985. (-)-S-[3H]CGP-12177 and its use to determine the rate constants of unlabeled beta-adrenergic antagonists. Proc Natl Acad Sci U S A 82(3):925-929.

Ajjan RA, Grant PJ. 2006. Cardiovascular disease prevention in patients with type 2 diabetes: The role of oral anti-diabetic agents. Diab Vasc Dis Res 3(3):147-158.

Akiyama N, Okumura K, Watanabe Y, Hashimoto H, Ito T, Ogawa K, Satake T. 1989. Altered acetylcholine and norepinephrine concentrations in diabetic rat hearts. Role of parasympathetic nervous system in diabetic cardiomyopathy. Diabetes 38(2):231-236.

Allman KC, Wieland DM, Muzik O, Degrado TR, Wolfe ER, Jr., Schwaiger M. 1993. Carbon-11 hydroxyephedrine with positron emission tomography for serial assessment of cardiac adrenergic neuronal function after acute myocardial infarction in humans. J Am Coll Cardiol 22(2):368-375.

Altan VM, Arioglu E, Guner S, Ozcelikay AT. 2007. The influence of diabetes on cardiac beta-adrenoceptor subtypes. Heart Fail Rev 12(1):58-65.

American Diabetes Association. 2006. Diagnosis and classification of diabetes mellitus. Diabetes Care 29 Suppl 1:S43-48.

American Heart Association Consensus Statement. 2007. Standards of medical care in diabetes--2007. Diabetes Care 30 Suppl 1:S4-S41.

Amoroso S, Schmid-Antomarchi H, Fosset M, Lazdunski M. 1990. Glucose, sulfonylureas, and neurotransmitter release: role of ATP-sensitive K+ channels. Science 247(4944):852-854.

An D, Rodrigues B. 2006. Role of changes in cardiac metabolism in development of diabetic cardiomyopathy. Am J Physiol Heart Circ Physiol 291(4):H1489-1506.

Anderson EA, Hoffman RP, Balon TW, Sinkey CA, Mark AL. 1991. Hyperinsulinemia produces both sympathetic neural activation and vasodilation in normal humans. J Clin Invest 87(6):2246-2252.

Aneja A, Tang WH, Bansilal S, Garcia MJ, Farkouh ME. 2008. Diabetic cardiomyopathy: insights into pathogenesis, diagnostic challenges, and therapeutic options. Am J Med 121(9):748-757.

Apparsundaram S, Galli A, DeFelice LJ, Hartzell HC, Blakely RD. 1998. Acute regulation of norepinephrine transport: I. protein kinase C-linked muscarinic receptors influence transport capacity and transporter density in SK-N-SH cells. J Pharmacol Exp Ther 287(2):733-743.

Ardell JL. 2004. Intrathoracic Neuronal Regulation of Cardiac Function. In: Armour JA, Ardell JL, editors. Basic and Clinical Neurocardiology. New York: Oxford University Press. p 118-152.

Arikawa E, Ma RC, Isshiki K, Luptak I, He Z, Yasuda Y, Maeno Y, Patti ME, Weir GC, Harris RA, Zammit VA, Tian R, King GL. 2007. Effects of insulin replacements, inhibitors of angiotensin, and PKCbeta's actions to normalize cardiac gene expression and fuel metabolism in diabetic rats. Diabetes 56(5):1410-1420.

Armour JA. 2004. Cardiac neuronal hierarchy in health and disease. Am J Physiol Regul Integr Comp Physiol 287(2):R262-271.

Aronow WS. 2006. Epidemiology, pathophysiology, prognosis, and treatment of systolic and diastolic heart failure. Cardiol Rev 14(3):108-124.

Atkins FL, Dowell RT, Love S. 1985. beta-Adrenergic receptors, adenylate cyclase activity, and cardiac dysfunction in the diabetic rat. J Cardiovasc Pharmacol 7(1):66-70.

Avendano GF, Agarwal RK, Bashey RI, Lyons MM, Soni BJ, Jyothirmayi GN, Regan TJ. 1999. Effects of glucose intolerance on myocardial function and collagen-linked glycation. Diabetes 48(7):1443-1447.

Aznavour N, Benkelfat C, Gravel P, Aliaga A, Rosa-Neto P, Bedell B, Zimmer L, Descarries L. 2009. MicroPET imaging of 5-HT 1A receptors in rat brain: a test-retest [18F]MPPF study. Eur J Nucl Med Mol Imaging 36(1):53-62.

Bachman ES, Dhillon H, Zhang CY, Cinti S, Bianco AC, Kobilka BK, Lowell BB. 2002. betaAR signaling required for diet-induced thermogenesis and obesity resistance. Science 297(5582):843-845.

Backs J, Haunstetter A, Gerber SH, Metz J, Borst MM, Strasser RH, Kubler W, Haass M. 2001. The neuronal norepinephrine transporter in experimental heart failure: evidence for a posttranscriptional downregulation. J Mol Cell Cardiol 33(3):461-472.

Bandyopadhyay G, Standaert ML, Galloway L, Moscat J, Farese RV. 1997. Evidence for involvement of protein kinase C (PKC)-zeta and noninvolvement of diacylglycerol-sensitive PKCs in insulin-stimulated glucose transport in L6 myotubes. Endocrinology 138(11):4721-4731.

Bansal S, Wackers FJ, Inzucchi SE, Chyun DA, Davey JA, Staib LH, Young LH. 2010. Five-year outcomes in high-risk participants in the Detection of Ischemia in Asymptomatic Diabetics (DIAD) study: a post hoc analysis. Diabetes Care 34(1):204-209.

Barber MJ, Mueller TM, Henry DP, Felten SY, Zipes DP. 1983. Transmural myocardial infarction in the dog produces sympathectomy in noninfarcted myocardium. Circulation 67(4):787-796.

Barbier J, Reland S, Ville N, Rannou-Bekono F, Wong S, Carre F. 2006. The effects of exercise training on myocardial adrenergic and muscarinic receptors. Clin Auton Res 16(1):61-65.

Basu R, Oudit GY, Wang X, Zhang L, Ussher JR, Lopaschuk GD, Kassiri Z. 2009. Type 1 diabetic cardiomyopathy in the Akita (Ins2WT/C96Y) mouse model is characterized by lipotoxicity and diastolic dysfunction with preserved systolic function. Am J Physiol Heart Circ Physiol 297(6):H2096-2108.

Bax JJ, Kraft O, Buxton AE, Fjeld JG, Parizek P, Agostini D, Knuuti J, Flotats A, Arrighi J, Muxi A, Alibelli MJ, Banerjee G, Jacobson AF. 2008. 123 I-mIBG scintigraphy to predict inducibility of ventricular arrhythmias on cardiac electrophysiology testing: a prospective multicenter pilot study. Circ Cardiovasc Imaging 1(2):131-140.

Beckers F, Verheyden B, Ramaekers D, Swynghedauw B, Aubert AE. 2006. Effects of autonomic blockade on non-linear cardiovascular variability indices in rats. Clin Exp Pharmacol Physiol 33(5-6):431-439.

Beckman ML, Bernstein EM, Quick MW. 1998. Protein kinase C regulates the interaction between a GABA transporter and syntaxin 1A. J Neurosci 18(16):6103-6112.

Beenen OH, Batink HD, Pfaffendorf M, van Zwieten PA. 1997. Beta-andrenoceptors in the hearts of diabetic-hypertensive rats: radioligand binding and functional experiments. Blood Press 6(1):44-51.

Belke DD, Betuing S, Tuttle MJ, Graveleau C, Young ME, Pham M, Zhang D, Cooksey RC, McClain DA, Litwin SE, Taegtmeyer H, Severson D, Kahn CR, Abel ED. 2002. Insulin signaling coordinately regulates cardiac size, metabolism, and contractile protein isoform expression. J Clin Invest 109(5):629-639.

Benediktsdottir VE, Curvers J, Gudbjarnason S. 1999. Time course of alterations in phospholipid fatty acids and number of beta-adrenoceptors in the rat heart during adrenergic stimulation in vivo. J Mol Cell Cardiol 31(5):1105-1115.

Bengel FM. 2009. Clinical cardiovascular molecular imaging. J Nucl Med 50(6):837-840.

Bengel FM, Permanetter B, Ungerer M, Nekolla SG, Schwaiger M. 2002a. Alterations of the sympathetic nervous system and metabolic performance of the cardiomyopathic heart. Eur J Nucl Med Mol Imaging 29(2):198-202.

Bengel FM, Ueberfuhr P, Hesse T, Schiepel N, Ziegler SI, Scholz S, Nekolla SG, Reichart B, Schwaiger M. 2002b. Clinical determinants of ventricular sympathetic reinnervation after orthotopic heart transplantation. Circulation 106(7):831-835.

Bengtsson K, Orho-Melander M, Melander O, Lindblad U, Ranstam J, Rastam L, Groop L. 2001. Beta(2)-adrenergic receptor gene variation and hypertension in subjects with type 2 diabetes. Hypertension 37(5):1303-1308.

Benmansour S, Altamirano AV, Jones DJ, Sanchez TA, Gould GG, Pardon MC, Morilak DA, Frazer A. 2004. Regulation of the norepinephrine transporter by chronic administration of antidepressants. Biol Psychiatry 55(3):313-316.

Berding G, Schrader CH, Peschel T, van den Hoff J, Kolbe H, Meyer GJ, Dengler R, Knapp WH. 2003. [N-methyl 11C]meta-Hydroxyephedrine positron emission tomography in Parkinson's disease and multiple system atrophy. Eur J Nucl Med Mol Imaging 30(1):127-131.

Bertram D, Barres C, Cheng Y, Julien C. 2000. Norepinephrine reuptake, baroreflex dynamics, and arterial pressure variability in rats. Am J Physiol Regul Integr Comp Physiol 279(4):R1257-1267.

Bertrand L, Ginion A, Beauloye C, Hebert AD, Guigas B, Hue L, Vanoverschelde JL. 2006. AMPK activation restores the stimulation of glucose uptake in an in vitro model of insulin-resistant cardiomyocytes via the activation of protein kinase B. Am J Physiol Heart Circ Physiol 291(1):H239-250.

Bertrand L, Horman S, Beauloye C, Vanoverschelde JL. 2008. Insulin signalling in the heart. Cardiovasc Res 79(2):238-248.

Bi S, Scott KA, Hyun J, Ladenheim EE, Moran TH. 2005. Running wheel activity prevents hyperphagia and obesity in Otsuka long-evans Tokushima Fatty rats: role of hypothalamic signaling. Endocrinology 146(4):1676-1685.

Bidasee KR, Zheng H, Shao CH, Parbhu SK, Rozanski GJ, Patel KP. 2008. Exercise training initiated after the onset of diabetes preserves myocardial function: effects on expression of beta-adrenoceptors. J Appl Physiol 105(3):907-914.

Birkenfeld AL, Schroeder C, Boschmann M, Tank J, Franke G, Luft FC, Biaggioni I, Sharma AM, Jordan J. 2002. Paradoxical effect of sibutramine on autonomic cardiovascular regulation. Circulation 106(19):2459-2465.

Blakely RD, De Felice LJ, Hartzell HC. 1994. Molecular physiology of norepinephrine and serotonin transporters. J Exp Biol 196:263-281.

Blana A, Kaese S, Fortmuller L, Laakmann S, Damke D, van Bragt K, Eckstein J, Piccini I, Kirchhefer U, Nattel S, Breithardt G, Carmeliet P, Carmeliet E, Schotten U, Verheule S, Kirchhof P, Fabritz L. 2010. Knock-in gain-of-function sodium channel mutation prolongs atrial action potentials and alters atrial vulnerability. Heart Rhythm 7(12):1862-1869.

Blanes-Mira C, Pastor MT, Valera E, Fernandez-Ballester G, Merino JM, Gutierrez LM, Perez-Paya E, Ferrer-Montiel A. 2003. Identification of SNARE complex modulators that inhibit exocytosis from an alpha-helix-constrained combinatorial library. Biochem J 375(Pt 1):159-166.

Bonisch H, Hammermann R, Bruss M. 1998. Role of protein kinase C and second messengers in regulation of the norepinephrine transporter. Adv Pharmacol 42:183-186.

Boogers MJ, Borleffs CJ, Henneman MM, van Bommel RJ, van Ramshorst J, Boersma E, Dibbets-Schneider P, Stokkel MP, van der Wall EE, Schalij MJ, Bax JJ. 2010. Cardiac sympathetic denervation assessed with 123-iodine metaiodobenzylguanidine imaging predicts ventricular arrhythmias in implantable cardioverter-defibrillator patients. J Am Coll Cardiol 55(24):2769-2777.

Borges GR, de Oliveira M, Salgado HC, Fazan R, Jr. 2006. Myocardial performance in conscious streptozotocin diabetic rats. Cardiovasc Diabetol 5:26.

Boudina S, Abel ED. 2007. Diabetic cardiomyopathy revisited. Circulation 115(25):3213-3223.

Boudina S, Bugger H, Sena S, O'Neill BT, Zaha VG, Ilkun O, Wright JJ, Mazumder PK, Palfreyman E, Tidwell TJ, Theobald H, Khalimonchuk O, Wayment B, Sheng X, Rodnick KJ, Centini R, Chen D, Litwin SE, Weimer BE, Abel ED. 2009. Contribution of impaired myocardial insulin signaling to mitochondrial dysfunction and oxidative stress in the heart. Circulation 119(9):1272-1283.

Boyle JP, Honeycutt AA, Narayan KM, Hoerger TJ, Geiss LS, Chen H, Thompson TJ. 2001. Projection of diabetes burden through 2050: impact of changing demography and disease prevalence in the U.S. Diabetes Care 24(11):1936-1940.

Bravo PE, Bengel FM. 2011. The Role of Cardiac PET in Translating Basic Science into the Clinical Arena. J Cardiovasc Transl Res 4(4):425-436.

Brede M, Wiesmann F, Jahns R, Hadamek K, Arnolt C, Neubauer S, Lohse MJ, Hein L. 2002. Feedback inhibition of catecholamine release by two different alpha2-adrenoceptor subtypes prevents progression of heart failure. Circulation 106(19):2491-2496.

Brenman JE, Temple BR. 2007. Opinion: alternative views of AMP-activated protein kinase. Cell Biochem Biophys 47(3):321-331.

Bristow MR. 1993. Changes in myocardial and vascular receptors in heart failure. J Am Coll Cardiol 22(4 Suppl A):61A-71A.

Bristow MR, Ginsburg R, Minobe W, Cubicciotti RS, Sageman WS, Lurie K, Billingham ME, Harrison DC, Stinson EB. 1982. Decreased catecholamine sensitivity and beta-adrenergic-receptor density in failing human hearts. N Engl J Med 307(4):205-211.

Bristow MR, Ginsburg R, Umans V, Fowler M, Minobe W, Rasmussen R, Zera P, Menlove R, Shah P, Jamieson S, et al. 1986. Beta 1- and beta 2-adrenergic-receptor subpopulations in nonfailing and failing human ventricular myocardium: coupling of both receptor subtypes to muscle contraction and selective beta 1-receptor down-regulation in heart failure. Circ Res 59(3):297-309.

Bristow MR, Krause-Steinrauf H, Nuzzo R, Liang CS, Lindenfeld J, Lowes BD, Hattler B, Abraham WT, Olson L, Krueger S, Thaneemit-Chen S, Hare JM, Loeb HS, Domanski MJ, Eichhorn EJ, Zelis R, Lavori P. 2004. Effect of baseline or changes in adrenergic activity on clinical outcomes in the beta-blocker evaluation of survival trial. Circulation 110(11):1437-1442.

Bristow MR, Larrabee P, Muller-Beckmann B, Minobe W, Roden R, Skerl L, Klein J, Handwerger D, Port JD. 1992. Effects of carvedilol on adrenergic receptor pharmacology in human ventricular myocardium and lymphocytes. Clin Investig 70 Suppl 1:S105-113.

Brodde OE. 1991. Beta 1- and beta 2-adrenoceptors in the human heart: properties, function, and alterations in chronic heart failure. Pharmacol Rev 43(2):203-242.

Brodde OE, Bruck H, Leineweber K. 2006. Cardiac adrenoceptors: physiological and pathophysiological relevance. J Pharmacol Sci 100(5):323-337.

Bruce CR, Hoy AJ, Turner N, Watt MJ, Allen TL, Carpenter K, Cooney GJ, Febbraio MA, Kraegen EW. 2009. Overexpression of carnitine palmitoyltransferase-1 in skeletal muscle is sufficient to enhance fatty acid oxidation and improve high-fat diet-induced insulin resistance. Diabetes 58(3):550-558.

Bruss M, Hammermann R, Brimijoin S, Bonisch H. 1995. Antipeptide antibodies confirm the topology of the human norepinephrine transporter. J Biol Chem 270(16):9197-9201.

Bryan-Lluka LJ, Paczkowski FA, Bonisch H. 2001. Effects of short- and long-term exposure to c-AMP and c-GMP on the noradrenaline transporter. Neuropharmacology 40(4):607-617.

Bugger H, Abel ED. 2009. Rodent models of diabetic cardiomyopathy. Dis Model Mech 2(9-10):454-466.

Bugger H, Riehle C, Jaishy B, Wende AR, Tuinei J, Chen D, Soto J, Pires KM, Boudina S, Theobald HA, Luptak I, Wayment B, Wang X, Litwin SE, Weimer BC, Abel ED. 2012. Genetic loss of insulin receptors worsens cardiac efficiency in diabetes. J Mol Cell Cardiol 52(5):1019-1026.

Bulow HP, Stahl F, Lauer B, Nekolla SG, Schuler G, Schwaiger M, Bengel FM. 2003. Alterations of myocardial presynaptic sympathetic innervation in patients with multi-vessel coronary artery disease but without history of myocardial infarction. Nucl Med Commun 24(3):233-239.

Burgdorf C, Richardt G, Schutte F, Dendorfer A, Kurz T. 2006. Impairment of presynaptic alpha2-adrenoceptor-regulated norepinephrine overflow in failing hearts from Zucker diabetic fatty rats. J Cardiovasc Pharmacol 47(2):256-262.

Burton LD, Kippenberger AG, Lingen B, Bruss M, Bonisch H, Christie DL. 1998. A variant of the bovine noradrenaline transporter reveals the importance of the C-terminal region for correct targeting to the membrane and functional expression. Biochem J 330 (Pt 2):909-914.

Caldwell JH, Kroll K, Li Z, Seymour K, Link JM, Krohn KA. 1998. Quantitation of presynaptic cardiac sympathetic function with carbon-11-meta-hydroxyephedrine. J Nucl Med 39(8):1327-1334.

Caldwell JH, Link JM, Levy WC, Poole JE, Stratton JR. 2008. Evidence for pre- to postsynaptic mismatch of the cardiac sympathetic nervous system in ischemic congestive heart failure. J Nucl Med 49(2):234-241.

Calera MR, Martinez C, Liu H, Jack AK, Birnbaum MJ, Pilch PF. 1998. Insulin increases the association of Akt-2 with Glut4-containing vesicles. J Biol Chem 273(13):7201-7204.

Calkins H, Lehmann MH, Allman K, Wieland D, Schwaiger M. 1993. Scintigraphic pattern of regional cardiac sympathetic innervation in patients with familial long QT syndrome using positron emission tomography. Circulation 87(5):1616-1621.

Campanucci V, Krishnaswamy A, Cooper E. 2011. Diabetes depresses synaptic transmission in sympathetic ganglia by inactivating nAChRs through a conserved intracellular cysteine residue. Neuron 66(6):827-834.

Candido R, Forbes JM, Thomas MC, Thallas V, Dean RG, Burns WC, Tikellis C, Ritchie RH, Twigg SM, Cooper ME, Burrell LM. 2003. A breaker of advanced glycation end products attenuates diabetes-induced myocardial structural changes. Circ Res 92(7):785-792.

Cantley LC. 2002. The phosphoinositide 3-kinase pathway. Science 296(5573):1655-1657.

Cao JM, Fishbein MC, Han JB, Lai WW, Lai AC, Wu TJ, Czer L, Wolf PL, Denton TA, Shintaku IP, Chen PS, Chen LS. 2000. Relationship between regional cardiac hyperinnervation and ventricular arrhythmia. Circulation 101(16):1960-1969.

Cardell SL. 2006. The natural killer T lymphocyte: a player in the complex regulation of autoimmune diabetes in non-obese diabetic mice. Clin Exp Immunol 143(2):194-202.

Carnethon MR, Golden SH, Folsom AR, Haskell W, Liao D. 2003a. Prospective investigation of autonomic nervous system function and the development of type 2 diabetes: the Atherosclerosis Risk In Communities study, 1987-1998. Circulation 107(17):2190-2195.

Carnethon MR, Jacobs DR, Jr., Sidney S, Liu K. 2003b. Influence of autonomic nervous system dysfunction on the development of type 2 diabetes: the CARDIA study. Diabetes Care 26(11):3035-3041.

Carson RP, Diedrich A, Robertson D. 2002. Autonomic control after blockade of the norepinephrine transporter: a model of orthostatic intolerance. J Appl Physiol 93(6):2192-2198.

Cefalu WT. 2007. Pharmacotherapy for the treatment of patients with type 2 diabetes mellitus: rationale and specific agents. Clin Pharmacol Ther 81(5):636-649.

Chan CB, Liu X, Jung DY, Jun JY, Luo HR, Kim JK, Ye K. 2010. Deficiency of phosphoinositide 3-kinase enhancer protects mice from diet-induced obesity and insulin resistance. Diabetes 59(4):883-893.

Chang CH, McNamara LA, Wu MS, Muise ES, Tan Y, Wood HB, Meinke PT, Thompson JR, Doebber TW, Berger JP, McCann ME. 2008. A novel selective peroxisome proliferator-activator receptor-gamma modulator-SPPARgammaM5 improves insulin sensitivity with diminished adverse cardiovascular effects. Eur J Pharmacol 584(1):192-201.

Chareonthaitawee P, Sorajja P, Rajagopalan N, Miller TD, Hodge DO, Frye RL, Gibbons RJ. 2007. Prevalence and prognosis of left ventricular systolic dysfunction in asymptomatic diabetic patients without known coronary artery disease referred for stress single-photon emission computed tomography and assessment of left ventricular function. Am Heart J 154(3):567-574.

Chen L, Wang L, Xu B, Ni G, Yu L, Han B, Yu X, Wang K, Lai Y, Zhou S, Zhu Q. 2009. Mechanisms of alpha1-adrenoceptor mediated QT prolongation in the diabetic rat heart. Life Sci 84(7-8):250-256.

Chiasson JL, Josse RG, Gomis R, Hanefeld M, Karasik A, Laakso M. 2003. Acarbose treatment and the risk of cardiovascular disease and hypertension in patients with impaired glucose tolerance: the STOP-NIDDM trial. JAMA 290(4):486-494.

Cho H, Mu J, Kim JK, Thorvaldsen JL, Chu Q, Crenshaw EB, 3rd, Kaestner KH, Bartolomei MS, Shulman GI, Birnbaum MJ. 2001. Insulin resistance and a diabetes mellitus-like syndrome in mice lacking the protein kinase Akt2 (PKB beta). Science 292(5522):1728-1731.

Choi SH, Zhao ZS, Lee YJ, Kim SK, Kim DJ, Ahn CW, Lim SK, Lee HC, Cha BS. 2007. The different mechanisms of insulin sensitizers to prevent type 2 diabetes in OLETF rats. Diabetes Metab Res Rev 23(5):411-418.

Ci X, Frisch F, Lavoie F, Germain P, Lecomte R, van Lier JE, Benard F, Carpentier AC. 2006. The effect of insulin on the intracellular distribution of 14(R,S)-[18F]Fluoro-6-thia-heptadecanoic acid in rats. Mol Imaging Biol 8(4):237-244.

Ciccarelli M, Chuprun JK, Rengo G, Gao E, Wei Z, Peroutka RJ, Gold JI, Gumpert A, Chen M, Otis NJ, Dorn GW, 2nd, Trimarco B, Iaccarino G, Koch WJ. 2011. G protein-

coupled receptor kinase 2 activity impairs cardiac glucose uptake and promotes insulin resistance after myocardial ischemia. Circulation 123(18):1953-1962.

Clark PB, Gage HD, Brown-Proctor C, Buchheimer N, Calles-Escandon J, Mach RH, Morton KA. 2004. Neurofunctional imaging of the pancreas utilizing the cholinergic PET radioligand [18F]4-fluorobenzyltrozamicol. Eur J Nucl Med Mol Imaging 31(2):258-260.

Cohade C, Osman M, Pannu HK, Wahl RL. 2003. Uptake in supraclavicular area fat ("USA-Fat"): description on 18F-FDG PET/CT. J Nucl Med 44(2):170-176.

Cohn JN, Levine TB, Olivari MT, Garberg V, Lura D, Francis GS, Simon AB, Rector T. 1984. Plasma norepinephrine as a guide to prognosis in patients with chronic congestive heart failure. N Engl J Med 311(13):819-823.

Collins S, Surwit RS. 2001. The beta-adrenergic receptors and the control of adipose tissue metabolism and thermogenesis. Recent Prog Horm Res 56:309-328.

Connelly KA, Kelly DJ, Zhang Y, Prior DL, Advani A, Cox AJ, Thai K, Krum H, Gilbert RE. 2009. Inhibition of protein kinase C-beta by ruboxistaurin preserves cardiac function and reduces extracellular matrix production in diabetic cardiomyopathy. Circ Heart Fail 2(2):129-137.

Connelly KA, Kelly DJ, Zhang Y, Prior DL, Martin J, Cox AJ, Thai K, Feneley MP, Tsoporis J, White KE, Krum H, Gilbert RE. 2007. Functional, structural and molecular aspects of diastolic heart failure in the diabetic (mRen-2)27 rat. Cardiovasc Res 76(2):280-291.

Connelly KA, Prior DL, Kelly DJ, Feneley MP, Krum H, Gilbert RE. 2006. Load-sensitive measures may overestimate global systolic function in the presence of left ventricular hypertrophy: a comparison with load-insensitive measures. Am J Physiol Heart Circ Physiol 290(4):H1699-1705.

Cooper ME. 2004. Importance of advanced glycation end products in diabetes-associated cardiovascular and renal disease. Am J Hypertens 17(12 Pt 2):31S-38S.

Crick S.J. SMN, Anderson R.H. 2000. Neural supply of the heart. In: Ter Horst GJ, editor. The nervous system and the heart: Humana Press Inc. p 3-54.

Crick SJ, Anderson RH, Ho SY, Sheppard MN. 1999. Localisation and quantitation of autonomic innervation in the porcine heart II: endocardium, myocardium and epicardium. J Anat 195 (Pt 3):359-373.

Currie GM, Iqbal B, Wheat JM, Wang L, Trifunovic M, Jelinek HF, Kiat H. 2011. Risk Stratification in Heart Failure Using 123I-MIBG. J Nucl Med Technol 39(4):295-301.

Czech MP, Corvera S. 1999. Signaling mechanisms that regulate glucose transport. J Biol Chem 274(4):1865-1868.

Dae MW, De Marco T, Botvinick EH, O'Connell JW, Hattner RS, Huberty JP, Yuen-Green MS. 1992. Scintigraphic assessment of MIBG uptake in globally denervated human and canine hearts--implications for clinical studies. J Nucl Med 33(8):1444-1450.

Daneman D. 2006. Type 1 diabetes. Lancet 367(9513):847-858.

DaSilva JN, Kilbourn MR, Mangner TJ. 1993. Synthesis of [^{11}C]tetrabenazine, a vesicular monoamine uptake inhibitor, for PET imaging studies. App Rad Isot 44(4):673-676.

DaSilva JN, Lourenco CM, Meyer JH, Hussey D, Potter WZ, Houle S. 2002. Imaging cAMP-specific phosphodiesterase-4 in human brain with (*R*)-[^{11}C]rolipram and positron emission tomography. Eur J Nucl Med Mol Imaging 29(12):1680-1683.

de Jong RM, Willemsen AT, Slart RH, Blanksma PK, van Waarde A, Cornel JH, Vaalburg W, van Veldhuisen DJ, Elsinga PH. 2005. Myocardial beta-adrenoceptor downregulation in idiopathic dilated cardiomyopathy measured in vivo with PET

using the new radioligand (S)-[11C]CGP12388. Eur J Nucl Med Mol Imaging 32(4):443-447.

DeGrado TR, Hutchins GD, Toorongian SA, Wieland DM, Schwaiger M. 1993. Myocardial kinetics of carbon-11-meta-hydroxyephedrine: retention mechanisms and effects of norepinephrine. J Nucl Med 34(8):1287-1293.

Del Rosario RB, Jung Y-W, Caraher J, Chakraborty PK, Wieland DM. 1996. Synthesis and Preliminary Evaluation of [^{11}C]-(-)-Phenylephrine as a Functional Heart Neuronal PET Agent. Nucl Med Biol 23:611-616.

Delahaye N, Le Guludec D, Dinanian S, Delforge J, Slama MS, Sarda L, Dolle F, Mzabi H, Samuel D, Adams D, Syrota A, Merlet P. 2001. Myocardial muscarinic receptor upregulation and normal response to isoproterenol in denervated hearts by familial amyloid polyneuropathy. Circulation 104(24):2911-2916.

Delaney CA, Dunger A, Di Matteo M, Cunningham JM, Green MH, Green IC. 1995. Comparison of inhibition of glucose-stimulated insulin secretion in rat islets of Langerhans by streptozotocin and methyl and ethyl nitrosoureas and methanesulphonates. Lack of correlation with nitric oxide-releasing or O6-alkylating ability. Biochem Pharmacol 50(12):2015-2020.

Delforge J, Janier M, Syrota A, Crouzel C, Vallois JM, Cayla J, Lancon JP, Mazoyer BM. 1990. Noninvasive quantification of muscarinic receptors in vivo with positron emission tomography in the dog heart. Circulation 82(4):1494-1504.

Delforge J, Mesangeau D, Dolle F, Merlet P, Loc'h C, Bottlaender M, Trebossen R, Syrota A. 2002. In vivo quantification and parametric images of the cardiac beta-adrenergic receptor density. J Nucl Med 43(2):215-226.

Dell'Italia LJ, Ardell JL. 2004. Sympathetic Nervous System in the Evolution of Heart Failure. In: Armour JA, Ardell JL, editors. Basic and Clinical Neurocardiology. New York: Oxford University Press. p 340-367.

DeMarco VG, Johnson MS, Habibi J, Pulakat L, Gul R, Hayden MR, Tilmon RD, Dellsperger KC, Winer N, Whaley-Connell AT, Sowers JR. 2011. Comparative analysis of telmisartan and olmesartan on cardiac function in the transgenic (mRen2)27 rat. Am J Physiol Heart Circ Physiol 300(1):H181-190.

Di Carli MF, Tobes MC, Mangner T, Levine AB, Muzik O, Chakroborty P, Levine TB. 1997. Effects of cardiac sympathetic innervation on coronary blood flow. N Engl J Med 336(17):1208-1215.

Diamond GA, Bax L, Kaul S. 2007. Uncertain effects of rosiglitazone on the risk for myocardial infarction and cardiovascular death. Ann Intern Med 147(8):578-581.

Dias LD, Casali KR, Leguisamo NM, Azambuja F, Souza MS, Okamoto M, Machado UF, Irigoyen MC, Schaan BD. 2011. Renal denervation in an animal model of diabetes and hypertension: Impact on the autonomic nervous system and nephropathy. Cardiovasc Diabetol 10:33.

Diggs-Andrews KA, Zhang X, Song Z, Daphna-Iken D, Routh VH, Fisher SJ. 2010. Brain insulin action regulates hypothalamic glucose sensing and the counterregulatory response to hypoglycemia. Diabetes 59(9):2271-2280.

Dincer UD, Bidasee KR, Guner S, Tay A, Ozcelikay AT, Altan VM. 2001. The effect of diabetes on expression of beta1-, beta2-, and beta3-adrenoreceptors in rat hearts. Diabetes 50(2):455-461.

Ding SY, Shen ZF, Chen YT, Sun SJ, Liu Q, Xie MZ. 2005. Pioglitazone can ameliorate insulin resistance in low-dose streptozotocin and high sucrose-fat diet induced obese rats. Acta Pharmacol Sin 26(5):575-580.

Ding YS, Lin KS, Garza V, Carter P, Alexoff D, Logan J, Shea C, Xu Y, King P. 2003. Evaluation of a new norepinephrine transporter PET ligand in baboons, both in brain and peripheral organs. Synapse 50(4):345-352.

Dluhy RG, McMahon GT. 2008. Intensive glycemic control in the ACCORD and ADVANCE trials. N Engl J Med 358(24):2630-2633.

Dormandy JA, Charbonnel B, Eckland DJ, Erdmann E, Massi-Benedetti M, Moules IK, Skene AM, Tan MH, Lefebvre PJ, Murray GD, Standl E, Wilcox RG, Wilhelmsen L, Betteridge J, Birkeland K, Golay A, Heine RJ, Koranyi L, Laakso M, Mokan M, Norkus A, Pirags V, Podar T, Scheen A, Scherbaum W, Schernthaner G, Schmitz O, Skrha J, Smith U, Taton J. 2005. Secondary prevention of macrovascular events in patients with type 2 diabetes in the PROactive Study (PROspective pioglitAzone Clinical Trial In macroVascular Events): a randomised controlled trial. Lancet 366(9493):1279-1289.

Dubois EA, Kam KL, Somsen GA, Boer GJ, de Bruin K, Batink HD, Pfaffendorf M, van Royen EA, van Zwieten PA. 1996. Cardiac iodine-123 metaiodobenzylguanidine uptake in animals with diabetes mellitus and/or hypertension. Eur J Nucl Med 23(8):901-908.

Dubois EA, Somsen GA, van den Bos JC, Janssen AG, Batink HD, Boer GJ, van Royen EA, Pfaffendorf M, van Zwieten PA. 1997. Development of radioligands for the imaging of cardiac beta-adrenoceptors using SPECT. Part II: Pharmacological characterization in vitro and in vivo of new 123I-labeled beta-adrenoceptor antagonists. Nucl Med Biol 24(1):9-13.

Dutta K, Podolin DA, Davidson MB, Davidoff AJ. 2001. Cardiomyocyte dysfunction in sucrose-fed rats is associated with insulin resistance. Diabetes 50(5):1186-1192.

Dyck JR, Barr AJ, Barr RL, Kolattukudy PE, Lopaschuk GD. 1998. Characterization of cardiac malonyl-CoA decarboxylase and its putative role in regulating fatty acid oxidation. Am J Physiol 275(6 Pt 2):H2122-2129.

Dyck JR, Cheng JF, Stanley WC, Barr R, Chandler MP, Brown S, Wallace D, Arrhenius T, Harmon C, Yang G, Nadzan AM, Lopaschuk GD. 2004. Malonyl coenzyme a decarboxylase inhibition protects the ischemic heart by inhibiting fatty acid oxidation and stimulating glucose oxidation. Circ Res 94(9):e78-84.

Eisenhofer G, Friberg P, Rundqvist B, Quyyumi AA, Lambert G, Kaye DM, Kopin IJ, Goldstein DS, Esler MD. 1996. Cardiac sympathetic nerve function in congestive heart failure. Circulation 93(9):1667-1676.

El Midaoui A, Ongali B, Petcu M, Rodi D, de Champlain J, Neugebauer W, Couture R. 2005. Increases of spinal kinin receptor binding sites in two rat models of insulin resistance. Peptides 26(8):1323-1330.

Elsinga PH, van Waarde A, Visser TJ, Vaalburg W. 1998. Visualization of beta-Adrenoceptors Using PET. Clin Positron Imaging 1(2):81-94.

Elsner M, Guldbakke B, Tiedge M, Munday R, Lenzen S. 2000. Relative importance of transport and alkylation for pancreatic beta-cell toxicity of streptozotocin. Diabetologia 43(12):1528-1533.

Enomoto H, Crawford PA, Gorodinsky A, Heuckeroth RO, Johnson EM, Jr., Milbrandt J. 2001. RET signaling is essential for migration, axonal growth and axon guidance of developing sympathetic neurons. Development 128(20):3963-3974.

Entman ML, Bornet EP, Van Winkle WB, Goldstein MA, Schwartz A. 1977. Association of glycogenolysis with cardiac sarcoplasmic reticulum: II. Effect of glycogen depletion, deoxycholate solubilization and cardiac ischemia: evidence for a phorphorylase kinase membrane complex. J Mol Cell Cardiol 9(7):515-528.

Esler M, Alvarenga M, Pier C, Richards J, El-Osta A, Barton D, Haikerwal D, Kaye D, Schlaich M, Guo L, Jennings G, Socratous F, Lambert G. 2006. The neuronal noradrenaline transporter, anxiety and cardiovascular disease. J Psychopharmacol 20(4 Suppl):60-66.

Esler M, Jennings G, Lambert G, Meredith I, Horne M, Eisenhofer G. 1990. Overflow of catecholamine neurotransmitters to the circulation: source, fate, and functions. Physiol Rev 70(4):963-985.

Esler M, Kaye D, Lambert G, Esler D, Jennings G. 1997. Adrenergic nervous system in heart failure. Am J Cardiol 80(11A):7L-14L.

Esler M, Rumantir M, Wiesner G, Kaye D, Hastings J, Lambert G. 2001. Sympathetic nervous system and insulin resistance: from obesity to diabetes. Am J Hypertens 14(11 Pt 2):304S-309S.

Esler MD, Jennings GL, Johns J, Burke F, Little PJ, Leonard P. 1984. Estimation of 'total' renal, cardiac and splanchnic sympathetic nervous tone in essential hypertension from measurements of noradrenaline release. J Hypertens Suppl 2(3):S123-125.

Etgen GJ, Oldham BA. 2000. Profiling of Zucker diabetic fatty rats in their progression to the overt diabetic state. Metabolism 49(5):684-688.

Ewing DJ, Bellavere F, Espi F, McKibben BM, Buchanan KD, Riemersma RA, Clarke BF. 1986. Correlation of cardiovascular and neuroendocrine tests of autonomic function in diabetes. Metabolism 35(4):349-353.

Ewing DJ, Campbell IW, Clarke BF. 1980. The natural history of diabetic autonomic neuropathy. Q J Med 49(193):95-108.

Facchini FS, Stoohs RA, Reaven GM. 1996. Enhanced sympathetic nervous system activity. The linchpin between insulin resistance, hyperinsulinemia, and heart rate. Am J Hypertens 9(10 Pt 1):1013-1017.

Fallavollita JA, Banas MD, Suzuki G, deKemp RA, Sajjad M, Canty JM, Jr. 2010. 11C-meta-hydroxyephedrine defects persist despite functional improvement in hibernating myocardium. J Nucl Cardiol 17(1):85-96.

Farriol M, Rosello J, Schwartz S. 1997. Body surface area in Sprague-Dawley rats. J Anim Physiol a Anim Nutr 77:61-65.

Fasshauer M, Klein J, Ueki K, Kriauciunas KM, Benito M, White MF, Kahn CR. 2000. Essential role of insulin receptor substrate-2 in insulin stimulation of Glut4 translocation and glucose uptake in brown adipocytes. J Biol Chem 275(33):25494-25501.

Fazan R, Jr., Ballejo G, Salgado MC, Moraes MF, Salgado HC. 1997. Heart rate variability and baroreceptor function in chronic diabetic rats. Hypertension 30(3 Pt 2):632-635.

Fazan R, Jr., Dias da Silva VJ, Ballejo G, Salgado HC. 1999. Power spectra of arterial pressure and heart rate in streptozotocin-induced diabetes in rats. J Hypertens 17(4):489-495.

Fein FS, Strobeck JE, Malhotra A, Scheuer J, Sonnenblick EH. 1981. Reversibility of diabetic cardiomyopathy with insulin in rats. Circ Res 49(6):1251-1261.

Felten SY, Peterson RG, Shea PA, Besch HR, Jr., Felten DL. 1982. Effects of streptozotocin diabetes on the noradrenergic innervation of the rat heart: a longitudinal histofluorescence and neurochemical study. Brain Res Bull 8(6):593-607.

Feve B, Elhadri K, Quignard-Boulange A, Pairault J. 1994. Transcriptional down-regulation by insulin of the beta 3-adrenergic receptor expression in 3T3-F442A adipocytes: a mechanism for repressing the cAMP signaling pathway. Proc Natl Acad Sci U S A 91(12):5677-5681.

Figlewicz DP, Bentson K, Ocrant I. 1993a. The effect of insulin on norepinephrine uptake by PC12 cells. Brain Res Bull 32(4):425-431.

Figlewicz DP, Szot P, Israel PA, Payne C, Dorsa DM. 1993b. Insulin reduces norepinephrine transporter mRNA in vivo in rat locus coeruleus. Brain Res 602(1):161-164.

Fillenz M, Stanford SC. 1981. Vesicular noradrenaline stores in peripheral nerves of the rat and their modification by tranylcypromine. Br J Pharmacol 73(2):401-404.

Finck BN, Lehman JJ, Leone TC, Welch MJ, Bennett MJ, Kovacs A, Han X, Gross RW, Kozak R, Lopaschuk GD, Kelly DP. 2002. The cardiac phenotype induced by PPARalpha overexpression mimics that caused by diabetes mellitus. J Clin Invest 109(1):121-130.

Finn RD, Schlyer DJ. 2002. Production of Radionuclides for PET. In: Wahl RL, editor. Principles and Practice of Positron Emission Tomography. Philadelphia, PA: Lippincott Williams & Wilkins. p 1-15.

Fischer Y, Thomas J, Rosen P, Kammermeier H. 1995. Action of metformin on glucose transport and glucose transporter GLUT1 and GLUT4 in heart muscle cells from healthy and diabetic rats. Endocrinology 136(2):412-420.

Fisher SJ, Bruning JC, Lannon S, Kahn CR. 2005. Insulin signaling in the central nervous system is critical for the normal sympathoadrenal response to hypoglycemia. Diabetes 54(5):1447-1451.

Flaa A, Aksnes TA, Kjeldsen SE, Eide I, Rostrup M. 2008. Increased sympathetic reactivity may predict insulin resistance: an 18-year follow-up study. Metabolism 57(10):1422-1427.

Florian JP, Pawelczyk JA. 2010. Sympathetic and haemodynamic responses to lipids in healthy human ageing. Exp Physiol 95(4):486-497.

Foley KF, Van Dort ME, Sievert MK, Ruoho AE, Cozzi NV. 2002. Stereospecific inhibition of monoamine uptake transporters by meta-hydroxyephedrine isomers. J Neural Transm 109(10):1229-1240.

Fonseca V, Rosenstock J, Patwardhan R, Salzman A. 2000. Effect of metformin and rosiglitazone combination therapy in patients with type 2 diabetes mellitus: a randomized controlled trial. Jama 283(13):1695-1702.

Forcheron F, Basset A, Abdallah P, Del Carmine P, Gadot N, Beylot M. 2009. Diabetic cardiomyopathy: effects of fenofibrate and metformin in an experimental model--the Zucker diabetic rat. Cardiovasc Diabetol 8:16.

Francis J, Weiss RM, Wei SG, Johnson AK, Felder RB. 2001. Progression of heart failure after myocardial infarction in the rat. Am J Physiol Regul Integr Comp Physiol 281(5):R1734-1745.

Fredersdorf S, Thumann C, Ulucan C, Griese DP, Luchner A, Riegger GA, Kromer EP, Weil J. 2004. Myocardial hypertrophy and enhanced left ventricular contractility in Zucker diabetic fatty rats. Cardiovasc Pathol 13(1):11-19.

Freeman R. 2006. Assessment of cardiovascular autonomic function. Clin Neurophysiol 117(4):716-730.

Fricke E, Eckert S, Dongas A, Fricke H, Preuss R, Lindner O, Horstkotte D, Burchert W. 2008. Myocardial sympathetic innervation in patients with symptomatic coronary artery disease: follow-up after 1 year with neurostimulation. J Nucl Med 49(9):1458-1464.

From AM, Scott CG, Chen HH. 2010. The development of heart failure in patients with diabetes mellitus and pre-clinical diastolic dysfunction a population-based study. J Am Coll Cardiol 55(4):300-305.

Fuller RW, Snoddy HD, Perry KW, Bernstein JR, Murphy PJ. 1981. Formation of alpha-methylnorepinephrine as a metabolite of metaraminol in guinea pigs. Biochem Pharmacol 30(20):2831-2836.

Gaemperli O, Liga R, Spyrou N, Rosen SD, Foale R, Kooner JS, Rimoldi OE, Camici PG. 2010. Myocardial beta-adrenoceptor down-regulation early after infarction is associated with long-term incidence of congestive heart failure. Eur Heart J 31(14):1722-1729.

Gaikwad AB, Viswanad B, Ramarao P. 2007. PPAR gamma agonists partially restores hyperglycemia induced aggravation of vascular dysfunction to angiotensin II in thoracic aorta isolated from rats with insulin resistance. Pharmacol Res 55(5):400-407.

Galderisi M. 2006. Diastolic dysfunction and diabetic cardiomyopathy: evaluation by Doppler echocardiography. J Am Coll Cardiol 48(8):1548-1551.

Gallego M, Casis O. 2001. Regulation of cardiac transient outward potassium current by norepinephrine in normal and diabetic rats. Diabetes Metab Res Rev 17(4):304-309.

Gallego M, Setien R, Izquierdo MJ, Casis O, Casis E. 2003. Diabetes-induced biochemical changes in central and peripheral catecholaminergic systems. Physiol Res 52(6):735-741.

Gando S, Hattori Y, Akaishi Y, Nishihira J, Kanno M. 1997. Impaired contractile response to beta adrenoceptor stimulation in diabetic rat hearts: alterations in beta adrenoceptors-G protein-adenylate cyclase system and phospholamban phosphorylation. J Pharmacol Exp Ther 282(1):475-484.

Ganguly PK, Beamish RE, Dhalla KS, Innes IR, Dhalla NS. 1987. Norepinephrine storage, distribution, and release in diabetic cardiomyopathy. Am J Physiol 252(6 Pt 1):E734-739.

Ganguly PK, Dhalla KS, Innes IR, Beamish RE, Dhalla NS. 1986. Altered norepinephrine turnover and metabolism in diabetic cardiomyopathy. Circ Res 59(6):684-693.

Gao L, Schultz HD, Patel KP, Zucker IH, Wang W. 2005. Augmented input from cardiac sympathetic afferents inhibits baroreflex in rats with heart failure. Hypertension 45(6):1173-1181.

Gauthier C, Tavernier G, Charpentier F, Langin D, Le Marec H. 1996. Functional beta3-adrenoceptor in the human heart. J Clin Invest 98(2):556-562.

Geerlings A, Lopez-Corcuera B, Aragon C. 2000. Characterization of the interactions between the glycine transporters GLYT1 and GLYT2 and the SNARE protein syntaxin 1A. FEBS Lett 470(1):51-54.

Gerrits CM, Bhattacharya M, Manthena S, Baran R, Perez A, Kupfer S. 2007. A comparison of pioglitazone and rosiglitazone for hospitalization for acute myocardial infarction in type 2 diabetes. Pharmacoepidemiol Drug Saf 16(10):1065-1071.

Gerson MC, Caldwell JH, Ananthasubramaniam K, Clements IP, Henzlova MJ, Amanullah A, Jacobson AF. 2011. Influence of diabetes mellitus on prognostic utility of imaging of myocardial sympathetic innervation in heart failure patients. Circ Cardiovasc Imaging 4(2):87-93.

Gerstein HC. 2002. Reduction of cardiovascular events and microvascular complications in diabetes with ACE inhibitor treatment: HOPE and MICRO-HOPE. Diabetes Metab Res Rev 18 Suppl 3:S82-85.

Gerstein HC, Yusuf S, Bosch J, Pogue J, Sheridan P, Dinccag N, Hanefeld M, Hoogwerf B, Laakso M, Mohan V, Shaw J, Zinman B, Holman RR. 2006. Effect of rosiglitazone on the frequency of diabetes in patients with impaired glucose tolerance or impaired fasting glucose: a randomised controlled trial. Lancet 368(9541):1096-1105.

Goethals LR, Weytjens CD, De Geeter F, Droogmans S, Caveliers V, Keyaerts M, Vanhove C, Van Camp G, Bossuyt A, Lahoutte T. 2009. Regional quantitative analysis of small animal myocardial sympathetic innervation and initial application in streptozotocin induced diabetes. Contrast Media Mol Imaging 4(4):174-182.

Goff DC, Jr., Gerstein HC, Ginsberg HN, Cushman WC, Margolis KL, Byington RP, Buse JB, Genuth S, Probstfield JL, Simons-Morton DG. 2007. Prevention of cardiovascular disease in persons with type 2 diabetes mellitus: current knowledge and rationale for the Action to Control Cardiovascular Risk in Diabetes (ACCORD) trial. Am J Cardiol 99(12A):4i-20i.

Golfman LS, Wilson CR, Sharma S, Burgmaier M, Young ME, Guthrie PH, Van Arsdall M, Adrogue JV, Brown KK, Taegtmeyer H. 2005. Activation of PPARgamma enhances myocardial glucose oxidation and improves contractile function in isolated working hearts of ZDF rats. Am J Physiol Endocrinol Metab 289(2):E328-336.

Goncalves AC, Tank J, Diedrich A, Hilzendeger A, Plehm R, Bader M, Luft FC, Jordan J, Gross V. 2009. Diabetic hypertensive leptin receptor-deficient db/db mice develop cardioregulatory autonomic dysfunction. Hypertension 53(2):387-392.

Goodwin GW, Taylor CS, Taegtmeyer H. 1998. Regulation of energy metabolism of the heart during acute increase in heart work. J Biol Chem 273(45):29530-29539.

Gotzsche O. 1983. The adrenergic beta-receptor adenylate cyclase system in heart and lymphocytes from streptozotocin-diabetic rats. In vivo and in vitro evidence for a desensitized myocardial beta-receptor. Diabetes 32(12):1110-1116.

Grassi G, Dell'Oro R, Quarti-Trevano F, Scopelliti F, Seravalle G, Paleari F, Gamba PL, Mancia G. 2005. Neuroadrenergic and reflex abnormalities in patients with metabolic syndrome. Diabetologia 48(7):1359-1365.

Grassi G, Seravalle G, Dell'Oro R, Facchini A, Ilardo V, Mancia G. 2004. Sympathetic and baroreflex function in hypertensive or heart failure patients with ventricular arrhythmias. J Hypertens 22(9):1747-1753.

Greene M, Thackeray JT, Kenk M, Thorn SL, Bevilacqua L, Harper M-E, Beanlands RS, DaSilva JN. 2009. Reduced *In Vivo* Phosphodiesterase-4 Response to Norepinephrine Challenge in Diet-Induced Obese Rats. Can J Physiol Pharmacol 87:196-202.

Gress TW, Nieto FJ, Shahar E, Wofford MR, Brancati FL. 2000. Hypertension and antihypertensive therapy as risk factors for type 2 diabetes mellitus. Atherosclerosis Risk in Communities Study. N Engl J Med 342(13):905-912.

Gross V, Tank J, Partke HJ, Plehm R, Diedrich A, da Costa Goncalves AC, Luft FC, Jordan J. 2008. Cardiovascular autonomic regulation in Non-Obese Diabetic (NOD) mice. Auton Neurosci 138(1-2):108-113.

Gu H, Epstein PN, Li L, Wurster RD, Cheng ZJ. 2008. Functional changes in baroreceptor afferent, central and efferent components of the baroreflex circuitry in type 1 diabetic mice (OVE26). Neuroscience 152(3):741-752.

Gundewar S, Calvert JW, Jha S, Toedt-Pingel I, Ji SY, Nunez D, Ramachandran A, Anaya-Cisneros M, Tian R, Lefer DJ. 2009. Activation of AMP-activated protein kinase by metformin improves left ventricular function and survival in heart failure. Circ Res 104(3):403-411.

Haase J, Killian AM, Magnani F, Williams C. 2001. Regulation of the serotonin transporter by interacting proteins. Biochem Soc Trans 29(Pt 6):722-728.

Habecker BA, Willison BD, Shi X, Woodward WR. 2006. Chronic depolarization stimulates norepinephrine transporter expression via catecholamines. J Neurochem 97(4):1044-1051.

Hadizad T, Kirkpatrick SA, Mason S, Burns K, Beanlands RS, Dasilva JN. 2009. Novel O-[(11)C]methylated derivatives of candesartan as angiotensin II AT(1) receptor imaging ligands: radiosynthesis and ex vivo evaluation in rats. Bioorg Med Chem 17(23):7971-7977.

Haffner SM, Morales PA, Stern MP, Gruber MK. 1992. Lp(a) concentrations in NIDDM. Diabetes 41(10):1267-1272.

Hajduch E, Turban S, Le Liepvre X, Le Lay S, Lipina C, Dimopoulos N, Dugail I, Hundal HS. 2008. Targeting of PKCzeta and PKB to caveolin-enriched microdomains represents a crucial step underpinning the disruption in PKB-directed signalling by ceramide. Biochem J 410(2):369-379.

Haka MS, Kilbourn MR. 1989. Synthesis and Regional Mouse Brain Distribution of [^{11}C]Nisoxetine, a Norepinephrine Uptake Inhibitor. Nucl Med Biol 16(8):771-774.

Harms H, de Haan S, Knaapen P, Huisman M, Schuit R, Windhorst A, Lammertsma A, Allaart C, Lubberink M. 2011. Tracer kinetic analysis of myocardial [11C]hydroxyephedrine studies. J Nucl Med 52(Suppl 1):254.

Hartmann F, Ziegler S, Nekolla S, Hadamitzky M, Seyfarth M, Richardt G, Schwaiger M. 1999a. Regional patterns of myocardial sympathetic denervation in dilated cardiomyopathy: an analysis using carbon-11 hydroxyephedrine and positron emission tomography. Heart 81(3):262-270.

He Z, Opland DM, Way KJ, Ueki K, Bodyak N, Kang PM, Izumo S, Kulkarni RN, Wang B, Liao R, Kahn CR, King GL. 2006. Regulation of vascular endothelial growth factor expression and vascularization in the myocardium by insulin receptor and PI3K/Akt pathways in insulin resistance and ischemia. Arterioscler Thromb Vasc Biol 26(4):787-793.

Hebert C, Habimana A, Elie R, Reader TA. 2001. Effects of chronic antidepressant treatments on 5-HT and NA transporters in rat brain: an autoradiographic study. Neurochem Int 38(1):63-74.

Hekimian G, Khandoudi N, Feuvray D, Beigelman PM. 1985. Abnormal cardiac rhythm in diabetic rats. Life Sci 37(6):547-551.

Hemming R, Agatep R, Badiani K, Wyant K, Arthur G, Gietz RD, Triggs-Raine B. 2001. Human growth factor receptor bound 14 binds the activated insulin receptor and alters the insulin-stimulated tyrosine phosphorylation levels of multiple proteins. Biochem Cell Biol 79(1):21-32.

Henriksen EJ. 2007. Improvement of Insulin Sensitivity by Antagonism of the Renin-Angiotensin System. Am J Physiol Regul Integr Comp Physiol.

Henriksen K, Byrjalsen I, Nielsen RH, Madsen AN, Larsen LK, Christiansen C, Beck-Nielsen H, Karsdal MA. 2009. A comparison of glycemic control, water retention, and musculoskeletal effects of balaglitazone and pioglitazone in diet-induced obese rats. Eur J Pharmacol 616(1-3):340-345.

Herrero P, Kim J, Sharp TL, Engelbach JA, Lewis JS, Gropler RJ, Welch MJ. 2006. Assessment of myocardial blood flow using 15O-water and 1-11C-acetate in rats with small-animal PET. J Nucl Med 47(3):477-485.

Heyndrickx GR, Vilaine JP, Moerman EJ, Leusen I. 1984. Role of prejunctional alpha 2-adrenergic receptors in the regulation of myocardial performance during exercise in conscious dogs. Circ Res 54(6):683-693.

Higuchi T, Fukushima K, Xia J, Mathews WB, Lautamaki R, Bravo PE, Javadi MS, Dannals RF, Szabo Z, Bengel FM. 2010. Radionuclide imaging of angiotensin II type 1 receptor upregulation after myocardial ischemia-reperfusion injury. J Nucl Med 51(12):1956-1961.

Hilton J, Yokoi F, Dannals RF, Ravert HT, Szabo Z, Wong DF. 2000. Column-switching HPLC for the analysis of plasma in PET imaging studies. Nucl Med Biol 27(6):627-630.

Himura Y, Felten SY, Kashiki M, Lewandowski TJ, Delehanty JM, Liang CS. 1993. Cardiac noradrenergic nerve terminal abnormalities in dogs with experimental congestive heart failure. Circulation 88(3):1299-1309.

Hirano Y, Tsunoda M, Funatsu T, Imai K. 2005. Rapid assay for catechol-O-methyltransferase activity by high-performance liquid chromatography-fluorescence detection. J Chromatogr B Analyt Technol Biomed Life Sci 819(1):41-46.

Hoard JL, Hoover DB, Mabe AM, Blakely RD, Feng N, Paolocci N. 2008. Cholinergic neurons of mouse intrinsic cardiac ganglia contain noradrenergic enzymes, norepinephrine transporters, and the neurotrophin receptors tropomyosin-related kinase A and p75. Neuroscience 156(1):129-142.

Hoffman BB, Lefkowitz RJ. 1995. Catecholamines, Sympathomimetic Drugs, and Adrenergic Receptor Antagonists. In: Hardman JGL, Lee E., editor. Goodman & Gilman's The Pharmacological Basis of Therapeutics. Ninth Edition ed. New York: McGraw-Hill. p 199-248.

Holton KL, Loder MK, Melikian HE. 2005. Nonclassical, distinct endocytic signals dictate constitutive and PKC-regulated neurotransmitter transporter internalization. Nat Neurosci 8(7):881-888.

Houwing H, Benthem L, Van Suylichem PT, Van der Leest J, Strubbe JH, Steffens AB. 1995. Islet transplantation in diabetic rats normalizes basal and exercise-induced energy metabolism. Diabetologia 38(8):919-926.

Howarth FC, Jacobson M, Naseer O, Adeghate E. 2005a. Short-term effects of streptozotocin-induced diabetes on the electrocardiogram, physical activity and body temperature in rats. Exp Physiol 90(2):237-245.

Howarth FC, Jacobson M, Shafiullah M, Adeghate E. 2005b. Long-term effects of streptozotocin-induced diabetes on the electrocardiogram, physical activity and body temperature in rats. Exp Physiol 90(6):827-835.

Howarth FC, Jacobson M, Shafiullah M, Adeghate E. 2006. Effects of insulin treatment on heart rhythm, body temperature and physical activity in streptozotocin-induced diabetic rat. Clin Exp Pharmacol Physiol 33(4):327-331.

Howarth FC, Jacobson M, Shafiullah M, Adeghate E. 2008. Long-term effects of type 2 diabetes mellitus on heart rhythm in the Goto-Kakizaki rat. Exp Physiol 93(3):362-369.

Hsueh W, Abel ED, Breslow JL, Maeda N, Davis RC, Fisher EA, Dansky H, McClain DA, McIndoe R, Wassef MK, Rabadan-Diehl C, Goldberg IJ. 2007. Recipes for creating animal models of diabetic cardiovascular disease. Circ Res 100(10):1415-1427.

Hu P, Zhang D, Swenson L, Chakrabarti G, Abel ED, Litwin SE. 2003. Minimally invasive aortic banding in mice: effects of altered cardiomyocyte insulin signaling during pressure overload. Am J Physiol Heart Circ Physiol 285(3):H1261-1269.

Hux JE, Ivis F, Flintoft V, Bica A. 2002. Diabetes in Ontario: determination of prevalence and incidence using a validated administrative data algorithm. Diabetes Care 25(3):512-516.

Huynh K, Kiriazis H, Du XJ, Love JE, Jandeleit-Dahm KA, Forbes JM, McMullen JR, Ritchie RH. 2012. Coenzyme Q(10) attenuates diastolic dysfunction, cardiomyocyte hypertrophy and cardiac fibrosis in the db/db mouse model of type 2 diabetes. Diabetologia.

Huynh K, McMullen JR, Julius TL, Tan JW, Love JE, Cemerlang N, Kiriazis H, Du XJ, Ritchie RH. 2010. Cardiac-specific IGF-1 receptor transgenic expression protects against cardiac fibrosis and diastolic dysfunction in a mouse model of diabetic cardiomyopathy. Diabetes 59(6):1512-1520.

Ieda M, Fukuda K. 2009. New aspects for the treatment of cardiac diseases based on the diversity of functional controls on cardiac muscles: the regulatory mechanisms of cardiac innervation and their critical roles in cardiac performance. J Pharmacol Sci 109(3):348-353.

Ieda M, Fukuda K, Hisaka Y, Kimura K, Kawaguchi H, Fujita J, Shimoda K, Takeshita E, Okano H, Kurihara Y, Kurihara H, Ishida J, Fukamizu A, Federoff HJ, Ogawa S. 2004. Endothelin-1 regulates cardiac sympathetic innervation in the rodent heart by controlling nerve growth factor expression. J Clin Invest 113(6):876-884.

Ieda M, Kanazawa H, Ieda Y, Kimura K, Matsumura K, Tomita Y, Yagi T, Onizuka T, Shimoji K, Ogawa S, Makino S, Sano M, Fukuda K. 2006. Nerve growth factor is critical for cardiac sensory innervation and rescues neuropathy in diabetic hearts. Circulation 114(22):2351-2363.

Ingebretsen CG, Hawelu-Johnson C, Ingebretsen WR, Jr. 1983. Alloxan-induced diabetes reduces beta-adrenergic receptor number without affecting adenylate cyclase in rat ventricular membranes. J Cardiovasc Pharmacol 5(3):454-461.

Iversen LL, Salt PJ, Wilson HA. 1972. Inhibition of catecholamine uptake in the isolated rat heart by haloalkylamines related to phenoxybenzamine. Br J Pharmacol 46(4):647-657.

Jacob S, Rett K, Henriksen EJ. 1998. Antihypertensive therapy and insulin sensitivity: do we have to redefine the role of beta-blocking agents? Am J Hypertens 11(10):1258-1265.

Jacobson AF, Senior R, Cerqueira MD, Wong ND, Thomas GS, Lopez VA, Agostini D, Weiland F, Chandna H, Narula J. 2010. Myocardial iodine-123 meta-iodobenzylguanidine imaging and cardiac events in heart failure. Results of the prospective ADMIRE-HF (AdreView Myocardial Imaging for Risk Evaluation in Heart Failure) study. J Am Coll Cardiol 55(20):2212-2221.

Jamerson KA, Julius S, Gudbrandsson T, Andersson O, Brant DO. 1993. Reflex sympathetic activation induces acute insulin resistance in the human forearm. Hypertension 21(5):618-623.

Jayachandran JV, Sih HJ, Winkle W, Zipes DP, Hutchins GD, Olgin JE. 2000. Atrial fibrillation produced by prolonged rapid atrial pacing is associated with heterogeneous changes in atrial sympathetic innervation. Circulation 101(10):1185-1191.

Jayanthi LD, Samuvel DJ, Ramamoorthy S. 2004. Regulated internalization and phosphorylation of the native norepinephrine transporter in response to phorbol esters. Evidence for localization in lipid rafts and lipid raft-mediated internalization. J Biol Chem 279(18):19315-19326.

Jessen N, Djurhuus CB, Jorgensen JO, Jensen LS, Moller N, Lund S, Schmitz O. 2005. Evidence against a role for insulin-signaling proteins PI 3-kinase and Akt in insulin resistance in human skeletal muscle induced by short-term GH infusion. Am J Physiol Endocrinol Metab 288(1):E194-199.

Joffe, II, Travers KE, Perreault-Micale CL, Hampton T, Katz SE, Morgan JP, Douglas PS. 1999. Abnormal cardiac function in the streptozotocin-induced non-insulin-dependent diabetic rat: noninvasive assessment with doppler echocardiography and contribution of the nitric oxide pathway. J Am Coll Cardiol 34(7):2111-2119.

John AS, Mongillo M, Depre C, Khan MT, Rimoldi OE, Pepper JR, Dreyfus GD, Pennell DJ, Camici PG. 2007. Pre- and post-synaptic sympathetic function in human hibernating myocardium. Eur J Nucl Med Mol Imaging 34(12):1973-1980.

Johnson JA, Bowker SL. 2011. Intensive glycaemic control and cancer risk in type 2 diabetes: a meta-analysis of major trials. Diabetologia 54(1):25-31.

Jung CH, Yang YS, Kim JS, Shin JI, Jin YS, Shin JY, Lee JH, Chung KM, Hwang JS, Oh JM, Shin YK, Kweon DH. 2008. A search for synthetic peptides that inhibit soluble N-ethylmaleimide sensitive-factor attachment receptor-mediated membrane fusion. FEBS J 275(12):3051-3063.

Jyotsna VP, Sahoo A, Sreenivas V, Deepak KK. 2009. Prevalence and pattern of cardiac autonomic dysfunction in newly detected type 2 diabetes mellitus. Diabetes Res Clin Pract 83(1):83-88.

Kaburagi Y, Satoh S, Tamemoto H, Yamamoto-Honda R, Tobe K, Veki K, Yamauchi T, Kono-Sugita E, Sekihara H, Aizawa S, Cushman SW, Akanuma Y, Yazaki Y, Kadowaki T. 1997. Role of insulin receptor substrate-1 and pp60 in the regulation of insulin-induced glucose transport and GLUT4 translocation in primary adipocytes. J Biol Chem 272(41):25839-25844.

Kadiiska MB, Bonini MG, Ruggiero C, Cleland E, Wicks S, Stadler K. 2012. Thiazolidinedione treatment decreases oxidative stress in spontaneously hypertensive heart failure rats through attenuation of inducible nitric oxide synthase-mediated lipid radical formation. Diabetes 61(3):586-596.

Kahn SE, Lachin JM, Zinman B, Haffner SM, Aftring RP, Paul G, Kravitz BG, Herman WH, Viberti G, Holman RR. 2011. Effects of rosiglitazone, glyburide, and metformin on beta-cell function and insulin sensitivity in ADOPT. Diabetes 60(5):1552-1560.

Kang YM, Zhang ZH, Xue B, Weiss RM, Felder RB. 2008. Inhibition of brain proinflammatory cytokine synthesis reduces hypothalamic excitation in rats with ischemia-induced heart failure. Am J Physiol Heart Circ Physiol 295(1):H227-236.

Kasama S, Toyama T, Sumino H, Kumakura H, Takayama Y, Ichikawa S, Suzuki T, Kurabayashi M. 2007. Long-term nicorandil therapy improves cardiac sympathetic nerve activity after reperfusion therapy in patients with first acute myocardial infarction. J Nucl Med 48(10):1676-1682.

Kasama S, Toyama T, Sumino H, Kumakura H, Takayama Y, Minami K, Ichikawa S, Matsumoto N, Sato Y, Kurabayashi M. 2011. Prognostic value of cardiac sympathetic nerve activity evaluated by [123I]m-iodobenzylguanidine imaging in patients with ST-segment elevation myocardial infarction. Heart 97(1):20-26.

Kashiwagi A, Nishio Y, Saeki Y, Kida Y, Kodama M, Shigeta Y. 1989. Plasma membrane-specific deficiency in cardiac beta-adrenergic receptor in streptozocin-diabetic rats. Am J Physiol 257(2 Pt 1):E127-132.

Kavak S, Ayaz L, Emre M, Inal T, Tamer L, Gunay I. 2008. The effects of rosiglitazone on oxidative stress and lipid profile in left ventricular muscles of diabetic rats. Cell Biochem Funct 26(4):478-485.

Kawai H, Mohan A, Hagen J, Dong E, Armstrong J, Stevens SY, Liang CS. 2000. Alterations in cardiac adrenergic terminal function and beta-adrenoceptor density in pacing-induced heart failure. Am J Physiol Heart Circ Physiol 278(5):H1708-1716.

Keck PE, Jr., Carter WP, Nierenberg AA, Cooper TB, Potter WZ, Rothschild AJ. 1991. Acute cardiovascular effects of tranylcypromine: correlation with plasma drug, metabolite, norepinephrine, and MHPG levels. J Clin Psychiatry 52(6):250-254.

Keller NR, Diedrich A, Appalsamy M, Tuntrakool S, Lonce S, Finney C, Caron MG, Robertson D. 2004. Norepinephrine transporter-deficient mice exhibit excessive

tachycardia and elevated blood pressure with wakefulness and activity. Circulation 110(10):1191-1196.

Kenk M, Greene M, Thackeray J, Dekemp RA, Lortie M, Thorn S, Beanlands RS, Dasilva JN. 2007. In vivo selective binding of (R)-[(11)C]rolipram to phosphodiesterase-4 provides the basis for studying intracellular cAMP signaling in the myocardium and other peripheral tissues. Nucl Med Biol 34(1):71-77.

Kenk M, Thackeray JT, Thorn SL, Dhami K, Chow BJ, Ascah KJ, Dasilva JN, Beanlands RS. 2010. Alterations of pre- and postsynaptic noradrenergic signaling in a rat model of adriamycin-induced cardiotoxicity. J Nucl Cardiol 17(2):175-176.

Kenk M, Thomas AJ, Lortie M, deKemp RA, Beanlands RS, DaSilva JN. 2011. PET Measurements of cAMP-Mediated Phosphodiesterase-4 with (*R*)-[^{11}C]Rolipram. Current Radiopharmaceuticals 4(1):44-58.

Kennedy L, Baynes JW. 1984. Non-enzymatic glycosylation and the chronic complications of diabetes: an overview. Diabetologia 26(2):93-98.

Kerbey AL, Randle PJ, Cooper RH, Whitehouse S, Pask HT, Denton RM. 1976. Regulation of pyruvate dehydrogenase in rat heart. Mechanism of regulation of proportions of dephosphorylated and phosphorylated enzyme by oxidation of fatty acids and ketone bodies and of effects of diabetes: role of coenzyme A, acetyl-coenzyme A and reduced and oxidized nicotinamide-adenine dinucleotide. Biochem J 154(2):327-348.

Kern W, Peters A, Born J, Fehm HL, Schultes B. 2005. Changes in blood pressure and plasma catecholamine levels during prolonged hyperinsulinemia. Metabolism 54(3):391-396.

Khandoudi N, Delerive P, Berrebi-Bertrand I, Buckingham RE, Staels B, Bril A. 2002. Rosiglitazone, a peroxisome proliferator-activated receptor-gamma, inhibits the Jun NH(2)-terminal kinase/activating protein 1 pathway and protects the heart from ischemia/reperfusion injury. Diabetes 51(5):1507-1514.

Kies P, Wichter T, Schafers M, Paul M, Schafers KP, Eckardt L, Stegger L, Schulze-Bahr E, Rimoldi O, Breithardt G, Schober O, Camici PG. 2004. Abnormal myocardial presynaptic norepinephrine recycling in patients with Brugada syndrome. Circulation 110(19):3017-3022.

Kim SK, Zhao ZS, Lee YJ, Lee KE, Kang SM, Choi D, Lim SK, Chung N, Lee HC, Cha BS. 2003. Left-ventricular diastolic dysfunction may be prevented by chronic treatment with PPAR-alpha or -gamma agonists in a type 2 diabetic animal model. Diabetes Metab Res Rev 19(6):487-493.

King VL, Dwoskin LP, Cassis LA. 1999. Cold exposure regulates the norepinephrine uptake transporter in rat brown adipose tissue. Am J Physiol 276(1 Pt 2):R143-151.

Kiyono Y, Iida Y, Kawashima H, Ogawa M, Tamaki N, Nishimura H, Saji H. 2002a. Norepinephrine transporter density as a causative factor in alterations in MIBG myocardial uptake in NIDDM model rats. Eur J Nucl Med Mol Imaging 29(8):999-1005.

Kiyono Y, Iida Y, Kawashima H, Tamaki N, Nishimura H, Saji H. 2001. Regional alterations of myocardial norepinephrine transporter density in streptozotocin-induced diabetic rats: implications for heterogeneous cardiac accumulation of MIBG in diabetes. Eur J Nucl Med 28(7):894-899.

Kiyono Y, Kanegawa N, Kawashima H, Iida Y, Kinoshita T, Tamaki N, Nishimura H, Ogawa M, Saji H. 2002b. Age-related changes of myocardial norepinephrine transporter density in rats: implications for differential cardiac accumulation of MIBG in aging. Nucl Med Biol 29(6):679-684.

Klein R, Beanlands RS, deKemp RA. 2010a. Quantification of myocardial blood flow and flow reserve: Technical aspects. J Nucl Cardiol 17(4):555-570.

Klein R, Renaud JM, Ziadi MC, Thorn SL, Adler A, Beanlands RS, deKemp RA. 2010b. Intra- and inter-operator repeatability of myocardial blood flow and myocardial flow reserve measurements using rubidium-82 pet and a highly automated analysis program. J Nucl Cardiol 17(4):600-616.

Koeppe RA. 2002. Data Analysis and Imaging Processing. In: Wahl RL, editor. Principles and Practice of Positron Emission Tomography. Philadelphia, PA: Lippincott Williams & Wilkins. p 65-99.

Kolwicz SC, Jr., Tian R. 2011. Glucose metabolism and cardiac hypertrophy. Cardiovasc Res 90(2):194-201.

Kopin IJ, Gordon EK. 1963. Origin of Norepinephrine in the Heart. Nature 199:1289.

Kostis JB, Sanders M. 2005. The association of heart failure with insulin resistance and the development of type 2 diabetes. Am J Hypertens 18(5 Pt 1):731-737.

Kraegen EW, James DE, Bennett SP, Chisholm DJ. 1983. In vivo insulin sensitivity in the rat determined by euglycemic clamp. Am J Physiol 245(1):E1-7.

Kreusser MM, Buss SJ, Krebs J, Kinscherf R, Metz J, Katus HA, Haass M, Backs J. 2008. Differential expression of cardiac neurotrophic factors and sympathetic nerve ending abnormalities within the failing heart. J Mol Cell Cardiol 44(2):380-387.

Kroncke KD, Fehsel K, Sommer A, Rodriguez ML, Kolb-Bachofen V. 1995. Nitric oxide generation during cellular metabolization of the diabetogenic N-methyl-N-nitroso-urea streptozotozin contributes to islet cell DNA damage. Biol Chem Hoppe Seyler 376(3):179-185.

Kusmic C, Morbelli S, Marini C, Matteucci M, Cappellini C, Pomposelli E, Marzullo P, L'Abbate A, Sambuceti G. 2008. Whole-body evaluation of MIBG tissue extraction in a mouse model of long-lasting type II diabetes and its relationship with norepinephrine transport protein concentration. J Nucl Med 49(10):1701-1706.

Kuwahara M, Yayou K, Ishii K, Hashimoto S, Tsubone H, Sugano S. 1994. Power spectral analysis of heart rate variability as a new method for assessing autonomic activity in the rat. J Electrocardiol 27(4):333-337.

Lai LP, Suematsu M, Elam H, Liang CS. 1996. Differential changes of myocardial beta-adrenoceptor subtypes and G-proteins in dogs with right-sided congestive heart failure. Eur J Pharmacol 309(2):201-208.

Lajoie C, Beliveau L, Trudeau F, Lavoie N, Massicotte G, Gagnon S, Calderone A. 2006. The rapid onset of hyperglycaemia in ZDF rats was associated with a widespread alteration of metabolic proteins implicated in glucose metabolism in the heart. Can J Physiol Pharmacol 84(11):1205-1213.

Lameris TW, de Zeeuw S, Alberts G, Boomsma F, Duncker DJ, Verdouw PD, Veld AJ, van Den Meiracker AH. 2000. Time course and mechanism of myocardial catecholamine release during transient ischemia in vivo. Circulation 101(22):2645-2650.

Landsberg L, Saville ME, Young JB. 1984. Sympathoadrenal system and regulation of thermogenesis. Am J Physiol 247(2 Pt 1):E181-189.

Langer O, Valette H, Dolle F, Halldin C, Loc'h C, Fuseau C, Coulon C, Ottaviani M, Bottlaender M, Maziere B, Crouzel C. 2000. High specific radioactivity (1R,2S)-4-[(18)F]fluorometaraminol: a PET radiotracer for mapping sympathetic nerves of the heart. Nucl Med Biol 27(3):233-238.

Latifpour J, McNeill JH. 1984. Cardiac autonomic receptors: effect of long-term experimental diabetes. J Pharmacol Exp Ther 230(1):242-249.

Lautamaki R, Tipre D, Bengel FM. 2007. Cardiac sympathetic neuronal imaging using PET. Eur J Nucl Med Mol Imaging 34 Suppl 1:S74-85.

Law MP. 1993. Demonstration of the suitability of CGP 12177 for in vivo studies of beta-adrenoceptors. Br J Pharmacol 109(4):1101-1109.

Law MP, Osman S, Davenport RJ, Cunningham VJ, Pike VW, Camici PG. 1997. Biodistribution and metabolism of [N-methyl-11C]m-hydroxyephedrine in the rat. Nucl Med Biol 24(5):417-424.

Law MP, Schafers K, Kopka K, Wagner S, Schober O, Schafers M. 2010. Molecular imaging of cardiac sympathetic innervation by 11C-mHED and PET: from man to mouse? J Nucl Med 51(8):1269-1276.

Laycock SK, Kane KA, McMurray J, Parratt JR. 1996. Captopril and norepinephrine-induced hypertrophy and haemodynamics in rats. J Cardiovasc Pharmacol 27(5):667-672.

Le Guludec D, Cohen-Solal A, Delforge J, Delahaye N, Syrota A, Merlet P. 1997. Increased myocardial muscarinic receptor density in idiopathic dilated cardiomyopathy: an in vivo PET study. Circulation 96(10):3416-3422.

Le Marchand-Brustel Y, Gautier N, Cormont M, Van Obberghen E. 1995. Wortmannin inhibits the action of insulin but not that of okadaic acid in skeletal muscle: comparison with fat cells. Endocrinology 136(8):3564-3570.

Lefkowitz RJ, Caron MG. 1985. Adrenergic receptors: molecular mechanisms of clinically relevant regulation. Clin Res 33(3):395-406.

Leonard BL, Watson RN, Loomes KM, Phillips AR, Cooper GJ. 2005. Insulin resistance in the Zucker diabetic fatty rat: a metabolic characterisation of obese and lean phenotypes. Acta Diabetol 42(4):162-170.

Levin BE, Govek EK, Dunn-Meynell AA. 1998. Reduced glucose-induced neuronal activation in the hypothalamus of diet-induced obese rats. Brain Res 808(2):317-319.

Levin BE, Hogan S, Sullivan AC. 1989. Initiation and perpetuation of obesity and obesity resistance in rats. Am J Physiol 256(3 Pt 2):R766-771.

Levin BE, Magnan C, Migrenne S, Chua SC, Jr., Dunn-Meynell AA. 2005. F-DIO obesity-prone rat is insulin resistant before obesity onset. Am J Physiol Regul Integr Comp Physiol 289(3):R704-711.

Levin BE, Sullivan AC. 1987. Glucose-induced norepinephrine levels and obesity resistance. Am J Physiol 253(3 Pt 2):R475-481.

Levin BE, Sullivan AC. 1989. Glucose-induced sympathetic activation in obesity-prone and resistant rats. Int J Obes 13(2):235-246.

Levine TB, Francis GS, Goldsmith SR, Simon AB, Cohn JN. 1982. Activity of the sympathetic nervous system and renin-angiotensin system assessed by plasma hormone levels and their relation to hemodynamic abnormalities in congestive heart failure. Am J Cardiol 49(7):1659-1666.

Li J, Zhu H, Shen E, Wan L, Arnold JM, Peng T. 2010a. Deficiency of rac1 blocks NADPH oxidase activation, inhibits endoplasmic reticulum stress, and reduces myocardial remodeling in a mouse model of type 1 diabetes. Diabetes 59(8):2033-2042.

Li W, Knowlton D, Van Winkle DM, Habecker BA. 2004. Infarction alters both the distribution and noradrenergic properties of cardiac sympathetic neurons. Am J Physiol Heart Circ Physiol 286(6):H2229-2236.

Li X, Hansen PA, Xi L, Chandraratna RA, Burant CF. 2005. Distinct mechanisms of glucose lowering by specific agonists for peroxisomal proliferator activated receptor gamma and retinoic acid X receptors. J Biol Chem 280(46):38317-38327.

Li Y, Ma J, Zhu H, Singh M, Hill D, Greer PA, Arnold JM, Abel ED, Peng T. 2011. Targeted inhibition of calpain reduces myocardial hypertrophy and fibrosis in mouse models of type 1 diabetes. Diabetes 60(11):2985-2994.

Li YJ, Wang PH, Chen C, Zou MH, Wang DW. 2010b. Improvement of mechanical heart function by trimetazidine in db/db mice. Acta Pharmacol Sin 31(5):560-569.

Liang CS, Fan TH, Sullebarger JT, Sakamoto S. 1989. Decreased adrenergic neuronal uptake activity in experimental right heart failure. A chamber-specific contributor to beta-adrenoceptor downregulation. The Journal of Clinical Investigation 84(4):1267-1275.

Lindstrom J, Louheranta A, Mannelin M, Rastas M, Salminen V, Eriksson J, Uusitupa M, Tuomilehto J. 2003. The Finnish Diabetes Prevention Study (DPS): Lifestyle intervention and 3-year results on diet and physical activity. Diabetes Care 26(12):3230-3236.

Link JM, Stratton JR, Levy W, Poole JE, Shoner SC, Stuetzle W, Caldwell JH. 2003. PET measures of pre- and post-synaptic cardiac beta adrenergic function. Nucl Med Biol 30(8):795-803.

Link JM, Synovec RE, Krohn KA, Caldwell JH. 1997. High speed liquid chromatography of phenylethanolamines for the kinetic analysis of [11C]-meta-hydroxyephedrine and metabolites in plasma. J Chromatogr B Biomed Sci Appl 693(1):31-41.

Lipscombe LL, Gomes T, Levesque LE, Hux JE, Juurlink DN, Alter DA. 2007. Thiazolidinediones and cardiovascular outcomes in older patients with diabetes. JAMA 298(22):2634-2643.

Litwin SE, Raya TE, Anderson PG, Daugherty S, Goldman S. 1990. Abnormal cardiac function in the streptozotocin-diabetic rat. Changes in active and passive properties of the left ventricle. J Clin Invest 86(2):481-488.

Logan J, Ding YS, Lin KS, Pareto D, Fowler J, Biegon A. 2005. Modeling and analysis of PET studies with norepinephrine transporter ligands: the search for a reference region. Nucl Med Biol 32(5):531-542.

Logan J, Wolf AP, Shiue CY, Fowler JS. 1987. Kinetic modeling of receptor-ligand binding applied to positron emission tomographic studies with neuroleptic tracers. J Neurochem 48(1):73-83.

Lorang D, Amara SG, Simerly RB. 1994. Cell-type-specific expression of catecholamine transporters in the rat brain. J Neurosci 14(8):4903-4914.

Lortie M, DaSilva JN, Kenk M, Thorn S, Davis D, Birnie D, Beanlands RS, deKemp RA. 2012. Analysis of (R)- and (S)-[(11)C]rolipram kinetics in canine myocardium for the evaluation of phosphodiesterase-4 with PET. Mol Imaging Biol 14(2):225-236.

Lourenco CM, Houle S, Wilson AA, DaSilva JN. 2001. Characterization of (*R*)-[^{11}C]rolipram for PET imaging of phosphodiesterase-4: in vivo binding, metabolism, and dosimetry studies in rats. Nucl Med Biol 28(4):347-358.

Lourenco CM, Kenk M, Beanlands RS, DaSilva JN. 2006. Increasing synaptic noradrenaline, serotonin and histamine enhances in vivo binding of phosphodiesterase-4 inhibitor (R)-[11C]rolipram in rat brain, lung and heart. Life Sci 79(4):356-364.

Luiken JJ, Coort SL, Koonen DP, Bonen A, Glatz JF. 2004. Signalling components involved in contraction-inducible substrate uptake into cardiac myocytes. Proc Nutr Soc 63(2):251-258.

Luiken JJ, Coort SL, Willems J, Coumans WA, Bonen A, van der Vusse GJ, Glatz JF. 2003. Contraction-induced fatty acid translocase/CD36 translocation in rat cardiac myocytes is mediated through AMP-activated protein kinase signaling. Diabetes 52(7):1627-1634.

Luiken JJ, Dyck DJ, Han XX, Tandon NN, Arumugam Y, Glatz JF, Bonen A. 2002. Insulin induces the translocation of the fatty acid transporter FAT/CD36 to the plasma membrane. Am J Physiol Endocrinol Metab 282(2):E491-495.

Luiken JJ, Ouwens DM, Habets DD, van der Zon GC, Coumans WA, Schwenk RW, Bonen A, Glatz JF. 2009. Permissive action of protein kinase C-zeta in insulin-induced CD36- and GLUT4 translocation in cardiac myocytes. J Endocrinol 201(2):199-209.

Luisi AJ, Fallavollita JA, Suzuki G, deKemp R, Haka MS, Toorongian SA, Canty JM, Jr. 2005. Regional 11C-Hydroxyephedrine Uptake in Hibernating Myocardium: Chronic Inhomogeneity of Sympathetic Innervation in the Absence of Infarction. J Nucl Med 46(8):1368-1374.

Lydell CP, Chan A, Wambolt RB, Sambandam N, Parsons H, Bondy GP, Rodrigues B, Popov KM, Harris RA, Brownsey RW, Allard MF. 2002. Pyruvate dehydrogenase and the regulation of glucose oxidation in hypertrophied rat hearts. Cardiovasc Res 53(4):841-851.

Maiese K, Chong ZZ, Shang YC. 2007. Mechanistic insights into diabetes mellitus and oxidative stress. Curr Med Chem 14(16):1729-1738.

Malfitano C, Alba Loureiro TC, Rodrigues B, Sirvente R, Salemi VM, Rabechi NB, Lacchini S, Curi R, Irigoyen MC. 2010. Hyperglycaemia protects the heart after myocardial infarction: aspects of programmed cell survival and cell death. Eur J Heart Fail 12(7):659-667.

Malizia AL, Melichar JK, Rhodes CG, Haida A, Reynolds AH, Jones T, Nutt DJ. 2000. Desipramine binding to noradrenaline reuptake sites in cardiac sympathetic neurons in man in vivo. Eur J Pharmacol 391(3):263-267.

Mandela P, Ordway GA. 2006. The norepinephrine transporter and its regulation. J Neurochem 97(2):310-333.

Manzella D, Paolisso G. 2005. Cardiac autonomic activity and Type II diabetes mellitus. Clin Sci (Lond) 108(2):93-99.

Mao W, Iwai C, Qin F, Liang CS. 2005. Norepinephrine induces endoplasmic reticulum stress and downregulation of norepinephrine transporter density in PC12 cells via oxidative stress. Am J Physiol Heart Circ Physiol 288(5):H2381-2389.

Mardon K, Montagne O, Elbaz N, Malek Z, Syrota A, Dubois-Rande JL, Meignan M, Merlet P. 2003. Uptake-1 carrier downregulates in parallel with the beta-adrenergic receptor desensitization in rat hearts chronically exposed to high levels of circulating norepinephrine: implications for cardiac neuroimaging in human cardiomyopathies. J Nucl Med 44(9):1459-1466.

Marsh SA, Dell'italia LJ, Chatham JC. 2009. Interaction of diet and diabetes on cardiovascular function in rats. Am J Physiol Heart Circ Physiol 296(2):H282-292.

Marsh SA, Powell PC, Agarwal A, Dell'Italia LJ, Chatham JC. 2007. Cardiovascular dysfunction in Zucker obese and Zucker diabetic fatty rats: role of hydronephrosis. Am J Physiol Heart Circ Physiol 293(1):H292-298.

Masuo K, Katsuya T, Fu Y, Rakugi H, Ogihara T, Tuck ML. 2005. Beta2-adrenoceptor polymorphisms relate to insulin resistance and sympathetic overactivity as early markers of metabolic disease in nonobese, normotensive individuals. Am J Hypertens 18(7):1009-1014.

Masuo K, Kawaguchi H, Mikami H, Ogihara T, Tuck ML. 2003. Serum uric acid and plasma norepinephrine concentrations predict subsequent weight gain and blood pressure elevation. Hypertension 42(4):474-480.

Matsuda N, Hattori Y, Gando S, Akaishi Y, Kemmotsu O, Kanno M. 1999. Diabetes-induced down-regulation of beta1-adrenoceptor mRNA expression in rat heart. Biochem Pharmacol 58(5):881-885.

Matsunari I, Aoki H, Nomura Y, Takeda N, Chen WP, Taki J, Nakajima K, Nekolla SG, Kinuya S, Kajinami K. 2010. Iodine-123 metaiodobenzylguanidine imaging and carbon-11 hydroxyephedrine positron emission tomography compared in patients with left ventricular dysfunction. Circ Cardiovasc Imaging 3(5):595-603.

Matsunari I, Schricke U, Bengel FM, Haase HU, Barthel P, Schmidt G, Nekolla SG, Schoemig A, Schwaiger M. 2000. Extent of cardiac sympathetic neuronal damage is determined by the area of ischemia in patients with acute coronary syndromes. Circulation 101(22):2579-2585.

Mazzadi AN, Pineau J, Costes N, Le Bars D, Bonnefoi F, Croisille P, Porcher R, Chevalier P. 2009. Muscarinic receptor upregulation in patients with myocardial infarction: a new paradigm. Circ Cardiovasc Imaging 2(5):365-372.

McAfee AT, Koro C, Landon J, Ziyadeh N, Walker AM. 2007. Coronary heart disease outcomes in patients receiving antidiabetic agents. Pharmacoepidemiol Drug Saf 16(7):711-725.

McQueen AP, Zhang D, Hu P, Swenson L, Yang Y, Zaha VG, Hoffman JL, Yun UJ, Chakrabarti G, Wang Z, Albertine KH, Abel ED, Litwin SE. 2005. Contractile dysfunction in hypertrophied hearts with deficient insulin receptor signaling: possible role of reduced capillary density. J Mol Cell Cardiol 39(6):882-892.

Meex RC, Schrauwen-Hinderling VB, Moonen-Kornips E, Schaart G, Mensink M, Phielix E, van de Weijer T, Sels JP, Schrauwen P, Hesselink MK. Restoration of muscle mitochondrial function and metabolic flexibility in type 2 diabetes by exercise training is paralleled by increased myocellular fat storage and improved insulin sensitivity. Diabetes 59(3):572-579.

Menard SL, Croteau E, Sarrhini O, Gelinas R, Brassard P, Ouellet R, Bentourkia M, van Lier JE, Des Rosiers C, Lecomte R, Carpentier AC. 2010. Abnormal in vivo myocardial energy substrate uptake in diet-induced type 2 diabetic cardiomyopathy in rats. Am J Physiol Endocrinol Metab 298(5):E1049-1057.

Mente A, Yusuf S, Islam S, McQueen MJ, Tanomsup S, Onen CL, Rangarajan S, Gerstein HC, Anand SS. 2010. Metabolic syndrome and risk of acute myocardial infarction a case-control study of 26,903 subjects from 52 countries. J Am Coll Cardiol 55(21):2390-2398.

Meredith IT, Broughton A, Jennings GL, Esler MD. 1991. Evidence of a selective increase in cardiac sympathetic activity in patients with sustained ventricular arrhythmias. N Engl J Med 325(9):618-624.

Miller TD, Rajagopalan N, Hodge DO, Frye RL, Gibbons RJ. 2004. Yield of stress single-photon emission computed tomography in asymptomatic patients with diabetes. Am Heart J 147(5):890-896.

Mills PA, Huetteman DA, Brockway BP, Zwiers LM, Gelsema AJ, Schwartz RS, Kramer K. 2000. A new method for measurement of blood pressure, heart rate, and activity in the mouse by radiotelemetry. J Appl Physiol 88(5):1537-1544.

Miner LH, Jedema HP, Moore FW, Blakely RD, Grace AA, Sesack SR. 2006. Chronic stress increases the plasmalemmal distribution of the norepinephrine transporter and the coexpression of tyrosine hydroxylase in norepinephrine axons in the prefrontal cortex. J Neurosci 26(5):1571-1578.

Mizushige K, Yao L, Noma T, Kiyomoto H, Yu Y, Hosomi N, Ohmori K, Matsuo H. 2000. Alteration in left ventricular diastolic filling and accumulation of myocardial collagen

at insulin-resistant prediabetic stage of a type II diabetic rat model. Circulation 101(8):899-907.

Mohell N, Dicker A. 1989. The beta-adrenergic radioligand [3H]CGP-12177, generally classified as an antagonist, is a thermogenic agonist in brown adipose tissue. Biochem J 261(2):401-405.

Mongillo M, John AS, Leccisotti L, Pennell DJ, Camici PG. 2007. Myocardial pre-synaptic sympathetic function correlates with glucose uptake in the failing human heart. Eur J Nucl Med Mol Imaging 34(8):1172-1177.

Moore GB, Pickavance LC, Briscoe CP, Clapham JC, Buckingham RE, Wilding JP. 2008. Energy restriction enhances therapeutic efficacy of the PPARgamma agonist, rosiglitazone, through regulation of visceral fat gene expression. Diabetes Obes Metab 10(3):251-263.

Mora A, Sakamoto K, McManus EJ, Alessi DR. 2005. Role of the PDK1-PKB-GSK3 pathway in regulating glycogen synthase and glucose uptake in the heart. FEBS Lett 579(17):3632-3638.

Morisco C, Condorelli G, Trimarco V, Bellis A, Marrone C, Sadoshima J, Trimarco B. 2005. Akt mediates the cross-talk between beta-adrenergic and insulin receptors in neonatal cardiomyocytes. Circ Res 96(2):180-188.

Muhr-Becker D, Weiss M, Tatsch K, Wolfram G, Standl E, Schnell O. 1999. Scintigraphically assessed cardiac sympathetic dysinnervation in poorly controlled type 1 diabetes mellitus: one-year follow-up with improved metabolic control. Exp Clin Endocrinol Diabetes 107(5):306-312.

Munch G, Nguyen NT, Nekolla S, Ziegler S, Muzik O, Chakraborty P, Wieland DM, Schwaiger M. 2000. Evaluation of sympathetic nerve terminals with [(11)C]epinephrine and [(11)C]hydroxyephedrine and positron emission tomography. Circulation 101(5):516-523.

Munch G, Rosport K, Bultmann A, Baumgartner C, Li Z, Laacke L, Ungerer M. 2005. Cardiac overexpression of the norepinephrine transporter uptake-1 results in marked improvement of heart failure. Circ Res 97(9):928-936.

Mustonen J, Mantysaari M, Kuikka J, Vanninen E, Vainio P, Lansimies E, Uusitupa M. 1992. Decreased myocardial 123I-metaiodobenzylguanidine uptake is associated with disturbed left ventricular diastolic filling in diabetes. Am Heart J 123(3):804-805.

Nadeau RA, de Champlain J. 1979. Plasma catecholamines in acute myocardial infarction. Am Heart J 98(5):548-554.

Nakajima-Takenaka C, Zhang GX, Obata K, Tohne K, Matsuyoshi H, Nagai Y, Nishiyama A, Takaki M. 2009. Left ventricular function of isoproterenol-induced hypertrophied rat hearts perfused with blood: mechanical work and energetics. Am J Physiol Heart Circ Physiol 297(5):H1736-1743.

Nakajo M, Shapiro B, Glowniak J, Sisson JC, Beierwaltes WH. 1983. Inverse relationship between cardiac accumulation of meta-[131I]iodobenzylguanidine (I-131 MIBG) and circulating catecholamines in suspected pheochromocytoma. J Nucl Med 24(12):1127-1134.

Nakao S, Goda A, Yuba M, Otsuka M, Matsumoto M, Yoshida C, Ohyanagi M, Naito Y, Lee M, Tsujino T, Masuyama T. 2007. Characterization of left ventricular filling abnormalities and its relation to elevated plasma brain natriuretic peptide level in acute to chronic diastolic heart failure. Circ J 71(9):1412-1417.

Narula J, Sarkar K. 2003. A conceptual paradox of MIBG uptake in heart failure: retention with incontinence! J Nucl Cardiol 10(6):700-704.

Naya M, Tsukamoto T, Morita K, Katoh C, Nishijima K, Komatsu H, Yamada S, Kuge Y, Tamaki N, Tsutsui H. 2009. Myocardial beta-adrenergic receptor density assessed by 11C-CGP12177 PET predicts improvement of cardiac function after carvedilol treatment in patients with idiopathic dilated cardiomyopathy. J Nucl Med 50(2):220-225.

Nguyen NT, DeGrado TR, Chakraborty P, Wieland DM, Schwaiger M. 1997. Myocardial kinetics of carbon-11-epinephrine in the isolated working rat heart. J Nucl Med 38(5):780-785.

Nissen SE, Wolski K. 2007. Effect of rosiglitazone on the risk of myocardial infarction and death from cardiovascular causes. N Engl J Med 356(24):2457-2471.

Noble MD, Liddle RA. 2005. Neurohormonal control of exocrine pancreatic secretion. Curr Opin Gastroenterol 21(5):531-537.

Nohara A, Okada S, Ohshima K, Pessin JE, Mori M. 2011. Cyclin-dependent kinase-5 is a key molecule in tumor necrosis factor-alpha-induced insulin resistance. J Biol Chem 286(38):33457-33465.

Norton GR, Candy G, Woodiwiss AJ. 1996. Aminoguanidine prevents the decreased myocardial compliance produced by streptozotocin-induced diabetes mellitus in rats. Circulation 93(10):1905-1912.

Nugent DA, Smith DM, Jones HB. 2008. A review of islet of Langerhans degeneration in rodent models of type 2 diabetes. Toxicol Pathol 36(4):529-551.

O'Brien IA, McFadden JP, Corrall RJ. 1991. The influence of autonomic neuropathy on mortality in insulin-dependent diabetes. Q J Med 79(290):495-502.

Odaka K, von Scheidt W, Ziegler SI, Ueberfuhr P, Nekolla SG, Reichart B, Bengel FM, Schwaiger M. 2001. Reappearance of cardiac presynaptic sympathetic nerve terminals in the transplanted heart: correlation between PET using (11)C-hydroxyephedrine and invasively measured norepinephrine release. J Nucl Med 42(7):1011-1016.

Ohinmaa A, Jacobs P, Simpson S, Johnson JA. 2004. The Projection of Prevalence and Cost of Diabetes in Canada: 2000 to 2016. Can J Diabetes 28(2):1-8.

op den Buijs J, Miklos Z, van Riel NA, Prestia CM, Szenczi O, Toth A, Van der Vusse GJ, Szabo C, Ligeti L, Ivanics T. 2005. beta-Adrenergic activation reveals impaired cardiac calcium handling at early stage of diabetes. Life Sci 76(10):1083-1098.

Otani H, Kagaya Y, Imahori Y, Yasuda S, Fujii R, Chida M, Namiuchi S, Takeda M, Sakuma M, Watanabe J, Ido T, Nonogi H, Shirato K. 2005. Myocardial 11C-diacylglycerol accumulation and left ventricular remodeling in patients after myocardial infarction. J Nucl Med 46(4):553-559.

Pan XR, Li GW, Hu YH, Wang JX, Yang WY, An ZX, Hu ZX, Lin J, Xiao JZ, Cao HB, Liu PA, Jiang XG, Jiang YY, Wang JP, Zheng H, Zhang H, Bennett PH, Howard BV. 1997. Effects of diet and exercise in preventing NIDDM in people with impaired glucose tolerance. The Da Qing IGT and Diabetes Study. Diabetes Care 20(4):537-544.

Pardini BJ, Lund DD, Schmid PG. 1989. Organization of the sympathetic postganglionic innervation of the rat heart. J Auton Nerv Syst 28(3):193-201.

Park SY, Cho YR, Kim HJ, Higashimori T, Danton C, Lee MK, Dey A, Rothermel B, Kim YB, Kalinowski A, Russell KS, Kim JK. 2005. Unraveling the temporal pattern of diet-induced insulin resistance in individual organs and cardiac dysfunction in C57BL/6 mice. Diabetes 54(12):3530-3540.

Parrish DC, Gritman K, Van Winkle DM, Woodward WR, Bader M, Habecker BA. 2008. Postinfarct sympathetic hyperactivity differentially stimulates expression of tyrosine

hydroxylase and norepinephrine transporter. Am J Physiol Heart Circ Physiol 294(1):H99-H106.

Patel A, MacMahon S, Chalmers J, Neal B, Billot L, Woodward M, Marre M, Cooper M, Glasziou P, Grobbee D, Hamet P, Harrap S, Heller S, Liu L, Mancia G, Mogensen CE, Pan C, Poulter N, Rodgers A, Williams B, Bompoint S, de Galan BE, Joshi R, Travert F. 2008. Intensive blood glucose control and vascular outcomes in patients with type 2 diabetes. N Engl J Med 358(24):2560-2572.

Patel KP, Zhang PL. 1995. Baroreflex function in streptozotocin (STZ) induced diabetic rats. Diabetes Res Clin Pract 27(1):1-9.

Paulus WJ, Tschope C, Sanderson JE, Rusconi C, Flachskampf FA, Rademakers FE, Marino P, Smiseth OA, De Keulenaer G, Leite-Moreira AF, Borbely A, Edes I, Handoko ML, Heymans S, Pezzali N, Pieske B, Dickstein K, Fraser AG, Brutsaert DL. 2007. How to diagnose diastolic heart failure: a consensus statement on the diagnosis of heart failure with normal left ventricular ejection fraction by the Heart Failure and Echocardiography Associations of the European Society of Cardiology. Eur Heart J 28(20):2539-2550.

Perez-Polo JR, Foreman PJ, Jackson GR, Shan D, Taglialatela G, Thorpe LW, Werrbach-Perez K. 1990. Nerve growth factor and neuronal cell death. Mol Neurobiol 4(1-2):57-91.

Peter R, Cox A, Evans M. 2008. Management of diabetes in cardiovascular patients: diabetic heart disease. Heart 94(3):369-375.

Phillips JK, Dubey R, Sesiashvilvi E, Takeda M, Christie DL, Lipski J. 2001a. Differential expression of the noradrenaline transporter in adrenergic chromaffin cells, ganglion cells and nerve fibres of the rat adrenal medulla. J Chem Neuroanat 21(1):95-104.

Phillips LS, Grunberger G, Miller E, Patwardhan R, Rappaport EB, Salzman A. 2001b. Once- and twice-daily dosing with rosiglitazone improves glycemic control in patients with type 2 diabetes. Diabetes Care 24(2):308-315.

Phillips MS, Liu Q, Hammond HA, Dugan V, Hey PJ, Caskey CJ, Hess JF. 1996. Leptin receptor missense mutation in the fatty Zucker rat. Nat Genet 13(1):18-19.

Poirier P, Bogaty P, Garneau C, Marois L, Dumesnil JG. 2001. Diastolic dysfunction in normotensive men with well-controlled type 2 diabetes: importance of maneuvers in echocardiographic screening for preclinical diabetic cardiomyopathy. Diabetes Care 24(1):5-10.

Pop-Busui R, Kirkwood I, Schmid H, Marinescu V, Schroeder J, Larkin D, Yamada E, Raffel DM, Stevens MJ. 2004. Sympathetic dysfunction in type 1 diabetes: association with impaired myocardial blood flow reserve and diastolic dysfunction. J Am Coll Cardiol 44(12):2368-2374.

Potenza MA, Gagliardi S, De Benedictis L, Zigrino A, Tiravanti E, Colantuono G, Federici A, Lorusso L, Benagiano V, Quon MJ, Montagnani M. 2009. Treatment of spontaneously hypertensive rats with rosiglitazone ameliorates cardiovascular pathophysiology via antioxidant mechanisms in the vasculature. Am J Physiol Endocrinol Metab 297(3):E685-694.

Raasmaja A, York DA. 1988. Alpha 1- and beta-adrenergic receptors in brown adipose tissue of lean (Fa/?) and obese (fa/fa) Zucker rats. Effects of cold-acclimation, sucrose feeding and adrenalectomy. Biochem J 249(3):831-838.

Radovits T, Korkmaz S, Loganathan S, Barnucz E, Bomicke T, Arif R, Karck M, Szabo G. 2009. Comparative investigation of the left ventricular pressure-volume relationship in rat models of type 1 and type 2 diabetes mellitus. Am J Physiol Heart Circ Physiol 297(1):H125-133.

Raffel D, Wieland D. 2001a. Assessment of cardiac sympathetic nerve integrity with positron emission tomography. Nucl Med Biol 28:541-559.

Raffel DM, Chen W. 2004. Binding of [3H]mazindol to cardiac norepinephrine transporters: kinetic and equilibrium studies. Naunyn Schmiedebergs Arch Pharmacol 370(1):9-16.

Raffel DM, Chen W, Sherman PS, Gildersleeve DL, Jung YW. 2006. Dependence of cardiac 11C-meta-hydroxyephedrine retention on norepinephrine transporter density. J Nucl Med 47(9):1490-1496.

Raffel DM, Corbett JR, del Rosario RB, Gildersleeve DL, Chiao PC, Schwaiger M, Wieland DM. 1996. Clinical evaluation of carbon-11-phenylephrine: MAO-sensitive marker of cardiac sympathetic neurons. J Nucl Med 37(12):1923-1931.

Raffel DM, Jung YW, Gildersleeve DL, Chen W. ^{11}C-Phenethylguanidines: A novel class of radiotracers for quntitative PET studies of cardiac sympathetic innervation.; 2005; Toronto, ON, Canada.

Raffel DM, Wieland DM. 2001b. Assessment of cardiac sympathetic nerve integrity with positron emission tomography. Nucl Med Biol 28(5):541-559.

Raimondi L, De Paoli P, Mannucci E, Lonardo G, Sartiani L, Banchelli G, Pirisino R, Mugelli A, Cerbai E. 2004. Restoration of cardiomyocyte functional properties by angiotensin II receptor blockade in diabetic rats. Diabetes 53(7):1927-1933.

Rajagopalan N, Miller TD, Hodge DO, Frye RL, Gibbons RJ. 2005. Identifying high-risk asymptomatic diabetic patients who are candidates for screening stress single-photon emission computed tomography imaging. J Am Coll Cardiol 45(1):43-49.

Ramachandran A, Snehalatha C, Mary S, Mukesh B, Bhaskar AD, Vijay V. 2006. The Indian Diabetes Prevention Programme shows that lifestyle modification and metformin prevent type 2 diabetes in Asian Indian subjects with impaired glucose tolerance (IDPP-1). Diabetologia 49(2):289-297.

Ramaekers D, Beckers F, Demeulemeester H, Aubert AE. 2002. Cardiovascular autonomic function in conscious rats: a novel approach to facilitate stationary conditions. Ann Noninvasive Electrocardiol 7(4):307-318.

Randle PJ, Garland PB, Hales CN, Newsholme EA. 1963. The glucose fatty-acid cycle. Its role in insulin sensitivity and the metabolic disturbances of diabetes mellitus. Lancet 1:785-789.

Raymon HK, Leslie FM. 1994. Opioid effects on [3H]norepinephrine release from dissociated embryonic locus coeruleus cell cultures. J Neurochem 62(3):1015-1024.

Reed MJ, Meszaros K, Entes LJ, Claypool MD, Pinkett JG, Gadbois TM, Reaven GM. 2000. A new rat model of type 2 diabetes: the fat-fed, streptozotocin-treated rat. Metabolism 49(11):1390-1394.

Ren J, Dominguez LJ, Sowers JR, Davidoff AJ. 1999. Metformin but not glyburide prevents high glucose-induced abnormalities in relaxation and intracellular Ca2+ transients in adult rat ventricular myocytes. Diabetes 48(10):2059-2065.

Ren ZG, Porzgen P, Zhang JM, Chen XR, Amara SG, Blakely RD, Sieber-Blum M. 2001. Autocrine regulation of norepinephrine transporter expression. Mol Cell Neurosci 17(3):539-550.

Rizk N, Dunbar JC. 2004. Insulin-mediated increase in sympathetic nerve activity is attenuated by C-peptide in diabetic rats. Exp Biol Med (Maywood) 229(1):80-84.

Rockman HA, Koch WJ, Lefkowitz RJ. 2002. Seven-transmembrane-spanning receptors and heart function. Nature 415(6868):206-212.

Rodrigues B, Rosa KT, Medeiros A, Schaan BD, Brum PC, De Angelis K, Irigoyen MC. 2011. Hyperglycemia can delay left ventricular dysfunction but not autonomic damage after myocardial infarction in rodents. Cardiovasc Diabetol 10:26.

Roselt P, Meikle S, Kassiou M. 2004. The role of positron emission tomography in the discovery and development of new drugs; as studied in laboratory animals. Eur J Drug Metab Pharmacokinet 29(1):1-6.

Rosenblatt-Velin N, Lerch R, Papageorgiou I, Montessuit C. 2004. Insulin resistance in adult cardiomyocytes undergoing dedifferentiation: role of GLUT4 expression and translocation. FASEB J 18(7):872-874.

Rosengard-Barlund M, Bernardi L, Fagerudd J, Mantysaari M, Af Bjorkesten CG, Lindholm H, Forsblom C, Waden J, Groop PH. 2009. Early autonomic dysfunction in type 1 diabetes: a reversible disorder? Diabetologia 52(6):1164-1172.

Rosenspire KC, Haka MS, Van Dort ME, Jewett DM, Gildersleeve DL, Schwaiger M, Wieland DM. 1990. Synthesis and preliminary Evaluation of Carbon-11-Meta-Hydroxyephedrine: A False Transmitter Agent for Heart Neuronal Imaging. J Nucl Med 31(8):1328-1334.

Rottman JN, Ni G, Brown M. 2007. Echocardiographic evaluation of ventricular function in mice. Echocardiography 24(1):83-89.

Routledge C, Marsden CA. 1987. Comparison of the effects of selected drugs on the release of hypothalamic adrenaline and noradrenaline measured in vivo. Brain Res 426(1):103-111.

Rufanova VA, Pozdnev VF, Kalenikova EI, Postnikov AB, Storozhilova AN, Masenko VP, Gomazkov OA, Medvedev OS, Medvedeva NA. 2009. Endothelin-converting enzyme inhibition in the rat model of acute heart failure: heart function and neurohormonal activation. Exp Biol Med (Maywood) 234(10):1201-1211.

Rundqvist B, Elam M, Bergmann-Sverrisdottir Y, Eisenhofer G, Friberg P. 1997. Increased cardiac adrenergic drive precedes generalized sympathetic activation in human heart failure. Circulation 95(1):169-175.

Rupp H, Dhalla KS, Dhalla NS. 1994. Mechanisms of cardiac cell damage due to catecholamines: significance of drugs regulating central sympathetic outflow. J Cardiovasc Pharmacol 24 Suppl 1:S16-24.

Saad MF, Khan A, Sharma A, Michael R, Riad-Gabriel MG, Boyadjian R, Jinagouda SD, Steil GM, Kamdar V. 1998. Physiological insulinemia acutely modulates plasma leptin. Diabetes 47(4):544-549.

Saad MF, Knowler WC, Pettitt DJ, Nelson RG, Mott DM, Bennett PH. 1989. Sequential changes in serum insulin concentration during development of non-insulin-dependent diabetes. Lancet 1(8651):1356-1359.

Sacre JW, Franjic B, Jellis CL, Jenkins C, Coombes JS, Marwick TH. 2010. Association of cardiac autonomic neuropathy with subclinical myocardial dysfunction in type 2 diabetes. JACC Cardiovasc Imaging 3(12):1207-1215.

Sakamoto J, Barr RL, Kavanagh KM, Lopaschuk GD. 2000. Contribution of malonyl-CoA decarboxylase to the high fatty acid oxidation rates seen in the diabetic heart. Am J Physiol Heart Circ Physiol 278(4):H1196-1204.

Sammet S, Graefe KH. 1979. Kinetic analysis of the interaction between noradrenaline and Na+ in neuronal uptake: kinetic evidence for CO-transport. Naunyn Schmiedebergs Arch Pharmacol 309(2):99-107.

Sanders JD, Happe HK, Bylund DB, Murrin LC. 2005. Development of the norepinephrine transporter in the rat CNS. Neuroscience 130(1):107-117.

Sasano T, Abraham MR, Chang KC, Ashikaga H, Mills KJ, Holt DP, Hilton J, Nekolla SG, Dong J, Lardo AC, Halperin H, Dannals RF, Marban E, Bengel FM. 2008. Abnormal sympathetic innervation of viable myocardium and the substrate of ventricular tachycardia after myocardial infarction. J Am Coll Cardiol 51(23):2266-2275.

Sasso FC, Rambaldi PF, Carbonara O, Nasti R, Torella M, Rotondo A, Torella R, Mansi L. 2010. Perspectives of nuclear diagnostic imaging in diabetic cardiomyopathy. Nutr Metab Cardiovasc Dis 20(3):208-216.

Savage DB, Petersen KF, Shulman GI. 2005. Mechanisms of insulin resistance in humans and possible links with inflammation. Hypertension 45(5):828-833.

Schafers M, Dutka D, Rhodes CG, Lammertsma AA, Hermansen F, Schober O, Camici PG. 1998. Myocardial presynaptic and postsynaptic autonomic dysfunction in hypertrophic cardiomyopathy. Circ Res 82(1):57-62.

Scheen AJ. 2004. Renin-angiotensin system inhibition prevents type 2 diabetes mellitus. Part 1. A meta-analysis of randomised clinical trials. Diabetes Metab 30(6):487-496.

Schmid H, Forman LA, Cao X, Sherman PS, Stevens MJ. 1999. Heterogeneous cardiac sympathetic denervation and decreased myocardial nerve growth factor in streptozotocin-induced diabetic rats: implications for cardiac sympathetic dysinnervation complicating diabetes. Diabetes 48(3):603-608.

Schmidt AM, Hasu M, Popov D, Zhang JH, Chen J, Yan SD, Brett J, Cao R, Kuwabara K, Costache G, et al. 1994. Receptor for advanced glycation end products (AGEs) has a central role in vessel wall interactions and gene activation in response to circulating AGE proteins. Proc Natl Acad Sci U S A 91(19):8807-8811.

Schmidt RE, Dorsey DA, Beaudet LN, Frederick KE, Parvin CA, Plurad SB, Levisetti MG. 2003a. Non-obese diabetic mice rapidly develop dramatic sympathetic neuritic dystrophy: a new experimental model of diabetic autonomic neuropathy. Am J Pathol 163(5):2077-2091.

Schmidt RE, Dorsey DA, Beaudet LN, Peterson RG. 2003b. Analysis of the Zucker Diabetic Fatty (ZDF) type 2 diabetic rat model suggests a neurotrophic role for insulin/IGF-I in diabetic autonomic neuropathy. Am J Pathol 163(1):21-28.

Schnedl WJ, Ferber S, Johnson JH, Newgard CB. 1994. STZ transport and cytotoxicity. Specific enhancement in GLUT2-expressing cells. Diabetes 43(11):1326-1333.

Scholte AJ, Schuijf JD, Delgado V, Kok JA, Bus MT, Maan AC, Stokkel MP, Kharagitsingh AV, Dibbets-Schneider P, van der Wall EE, Bax JJ. 2010. Cardiac autonomic neuropathy in patients with diabetes and no symptoms of coronary artery disease: comparison of 123I-metaiodobenzylguanidine myocardial scintigraphy and heart rate variability. Eur J Nucl Med Mol Imaging 37(9):1698-1705.

Schreihofer AM, Mandel DA, Mobley SC, Stepp DW. 2007. Impairment of sympathetic baroreceptor reflexes in obese Zucker rats. Am J Physiol Heart Circ Physiol 293(4):H2543-2549.

Schroeter S, Apparsundaram S, Wiley RG, Miner LH, Sesack SR, Blakely RD. 2000. Immunolocalization of the cocaine- and antidepressant-sensitive l-norepinephrine transporter. J Comp Neurol 420(2):211-232.

Schwaiger M, Hutchins GD, Kalff V, Rosenspire K, Haka MS, Mallette S, Deeb GM, Abrams GD, Wieland D. 1991. Evidence for regional catecholamine uptake and storage sites in the transplanted human heart by positron emission tomography. J Clin Invest 87(5):1681-1690.

Sellers DJ, Chess-Williams R. 2001. The effect of streptozotocin-induced diabetes on cardiac beta-adrenoceptor subtypes in the rat. J Auton Pharmacol 21(1):15-21.

Sethi R, Shao Q, Ren B, Saini HK, Takeda N, Dhalla NS. 2004. Changes in beta-adrenoceptors in heart failure due to myocardial infarction are attenuated by blockade of renin-angiotensin system. Mol Cell Biochem 263(1-2):11-20.

Sharma V, Dhillon P, Parsons H, Allard MF, McNeill JH. 2009. Metoprolol represses PGC1alpha-mediated carnitine palmitoyltransferase-1B expression in the diabetic heart. Eur J Pharmacol 607(1-3):156-166.

Sharma V, Dhillon P, Wambolt R, Parsons H, Brownsey R, Allard MF, McNeill JH. 2008a. Metoprolol improves cardiac function and modulates cardiac metabolism in the streptozotocin-diabetic rat. Am J Physiol Heart Circ Physiol 294(4):H1609-1620.

Sharma V, Parsons H, Allard MF, McNeill JH. 2008b. Metoprolol increases the expression of beta(3)-adrenoceptors in the diabetic heart: effects on nitric oxide signaling and forkhead transcription factor-3. Eur J Pharmacol 595(1-3):44-51.

Sharp TL, Dence CS, Engelbach JA, Herrero P, Gropler RJ, Welch MJ. 2005. Techniques necessary for multiple tracer quantitative small-animal imaging studies. Nucl Med Biol 32(8):875-884.

Shi Z, Chen AD, Xu Y, Chen Q, Gao XY, Wang W, Zhu GQ. 2009. Long-term administration of tempol attenuates postinfarct ventricular dysfunction and sympathetic activity in rats. Pflugers Arch 458(2):247-257.

Shimizu S, Akiyama T, Kawada T, Shishido T, Mizuno M, Kamiya A, Yamazaki T, Sano S, Sugimachi M. 2009. In vivo direct monitoring of interstitial norepinephrine levels at the sinoatrial node. Auton Neurosci.

Shimoni Y, Chuang M, Abel ED, Severson DL. 2004. Gender-dependent attenuation of cardiac potassium currents in type 2 diabetic db/db mice. J Physiol 555(Pt 2):345-354.

Shiomi T, Tsutsui H, Ikeuchi M, Matsusaka H, Hayashidani S, Suematsu N, Wen J, Kubota T, Takeshita A. 2003. Streptozotocin-induced hyperglycemia exacerbates left ventricular remodeling and failure after experimental myocardial infarction. J Am Coll Cardiol 42(1):165-172.

Shoghi KI, Finck BN, Schechtman KB, Sharp T, Herrero P, Gropler RJ, Welch MJ. 2009. In vivo metabolic phenotyping of myocardial substrate metabolism in rodents: differential efficacy of metformin and rosiglitazone monotherapy. Circ Cardiovasc Imaging 2(5):373-381.

Shoghi KI, Gropler RJ, Sharp T, Herrero P, Fettig N, Su Y, Mitra MS, Kovacs A, Finck BN, Welch MJ. 2008. Time course of alterations in myocardial glucose utilization in the Zucker diabetic fatty rat with correlation to gene expression of glucose transporters: a small-animal PET investigation. J Nucl Med 49(8):1320-1327.

Shulkin BL, Wieland DM, Schwaiger M, Thompson NW, Francis IR, Haka MS, Rosenspire KC, Shapiro B, Sisson JC, Kuhl DE. 1992. PET scanning with hydroxyephedrine: an approach to the localization of pheochromocytoma. J Nucl Med 33(6):1125-1131.

Shuster JJ, Jones LS, Salmon DA. 2007. Fixed vs random effects meta-analysis in rare event studies: the rosiglitazone link with myocardial infarction and cardiac death. Stat Med 26(24):4375-4385.

Sidell RJ, Cole MA, Draper NJ, Desrois M, Buckingham RE, Clarke K. 2002. Thiazolidinedione treatment normalizes insulin resistance and ischemic injury in the zucker Fatty rat heart. Diabetes 51(4):1110-1117.

Singh S, Loke YK, Furberg CD. 2007. Long-term risk of cardiovascular events with rosiglitazone: a meta-analysis. JAMA 298(10):1189-1195.

Song GY, Wu YJ, Yang YJ, Li JJ, Zhang HL, Pei HJ, Zhao ZY, Zeng ZH, Hui RT. 2009. The accelerated post-infarction progression of cardiac remodelling is associated with genetic changes in an untreated streptozotocin-induced diabetic rat model. Eur J Heart Fail 11(10):911-921.

Souza SB, Flues K, Paulini J, Mostarda C, Rodrigues B, Souza LE, Irigoyen MC, De Angelis K. 2007. Role of Exercise Training in Cardiovascular Autonomic Dysfunction and Mortality in Diabetic Ovariectomized Rats. Hypertension.

Sreenan S, Sturis J, Pugh W, Burant CF, Polonsky KS. 1996. Prevention of hyperglycemia in the Zucker diabetic fatty rat by treatment with metformin or troglitazone. Am J Physiol 271(4 Pt 1):E742-747.

Srinivasan K, Viswanad B, Asrat L, Kaul CL, Ramarao P. 2005. Combination of high-fat diet-fed and low-dose streptozotocin-treated rat: a model for type 2 diabetes and pharmacological screening. Pharmacol Res 52(4):313-320.

Steinbusch LK, Schwenk RW, Ouwens DM, Diamant M, Glatz JF, Luiken JJ. 2011. Subcellular trafficking of the substrate transporters GLUT4 and CD36 in cardiomyocytes. Cell Mol Life Sci 68(15):2525-2538.

Stevens MJ, Dayanikli F, Raffel DM, Allman KC, Sandford T, Feldman EL, Wieland DM, Corbett J, Schwaiger M. 1998a. Scintigraphic assessment of regionalized defects in myocardial sympathetic innervation and blood flow regulation in diabetic patients with autonomic neuropathy. J Am Coll Cardiol 31(7):1575-1584.

Stevens MJ, Raffel DM, Allman KC, Dayanikli F, Ficaro E, Sandford T, Wieland DM, Pfeifer MA, Schwaiger M. 1998b. Cardiac sympathetic dysinnervation in diabetes: implications for enhanced cardiovascular risk. Circulation 98(10):961-968.

Stevens MJ, Raffel DM, Allman KC, Schwaiger M, Wieland DM. 1999. Regression and progression of cardiac sympathetic dysinnervation complicating diabetes: an assessment by C-11 hydroxyephedrine and positron emission tomography. Metabolism 48(1):92-101.

Stumvoll M, Goldstein BJ, van Haeften TW. 2005. Type 2 diabetes: principles of pathogenesis and therapy. Lancet 365(9467):1333-1346.

Sung U, Apparsundaram S, Galli A, Kahlig KM, Savchenko V, Schroeter S, Quick MW, Blakely RD. 2003. A regulated interaction of syntaxin 1A with the antidepressant-sensitive norepinephrine transporter establishes catecholamine clearance capacity. J Neurosci 23(5):1697-1709.

Surwit RS, Dixon TM, Petro AE, Daniel KW, Collins S. 2000. Diazoxide restores beta3-adrenergic receptor function in diet-induced obesity and diabetes. Endocrinology 141(10):3630-3637.

Suskin N, McKelvie RS, Burns RJ, Latini R, Pericak D, Probstfield J, Rouleau JL, Sigouin C, Solymoss CB, Tsuyuki R, White M, Yusuf S. 2000. Glucose and insulin abnormalities relate to functional capacity in patients with congestive heart failure. Eur Heart J 21(16):1368-1375.

Swan JW, Anker SD, Walton C, Godsland IF, Clark AL, Leyva F, Stevenson JC, Coats AJ. 1997. Insulin resistance in chronic heart failure: relation to severity and etiology of heart failure. J Am Coll Cardiol 30(2):527-532.

Symons JD, Hu P, Yang Y, Wang X, Zhang QJ, Wende AR, Sloan CL, Sena S, Abel ED, Litwin SE. 2011. Knockout of insulin receptors in cardiomyocytes attenuates coronary arterial dysfunction induced by pressure overload. Am J Physiol Heart Circ Physiol 300(1):H374-381.

Szkudelski T. 2001. The mechanism of alloxan and streptozotocin action in B cells of the rat pancreas. Physiol Res 50(6):537-546.

Taegtmeyer H, Hems R, Krebs HA. 1980. Utilization of energy-providing substrates in the isolated working rat heart. Biochem J 186(3):701-711.

Taegtmeyer H, McNulty P, Young ME. 2002. Adaptation and maladaptation of the heart in diabetes: Part I: general concepts. Circulation 105(14):1727-1733.

Takahashi N, Nakagawa M, Saikawa T, Ooie T, Yufu K, Shigematsu S, Hara M, Sakino H, Katsuragi I, Okeda T, Yoshimatsu H, Sakata T. 2001. Effect of essential hypertension on cardiac autonomic function in type 2 diabetic patients. J Am Coll Cardiol 38(1):232-237.

Taniguchi Y, Ooie T, Takahashi N, Shinohara T, Nakagawa M, Yonemochi H, Hara M, Yoshimatsu H, Saikawa T. 2006. Pioglitazone but not glibenclamide improves cardiac expression of heat shock protein 72 and tolerance against ischemia/reperfusion injury in the heredity insulin-resistant rat. Diabetes 55(8):2371-2378.

Tank J, Schroeder C, Diedrich A, Szczech E, Haertter S, Sharma AM, Luft FC, Jordan J. 2003. Selective impairment in sympathetic vasomotor control with norepinephrine transporter inhibition. Circulation 107(23):2949-2954.

Taylor M, Wallhaus TR, Degrado TR, Russell DC, Stanko P, Nickles RJ, Stone CK. 2001. An evaluation of myocardial fatty acid and glucose uptake using PET with [18F]fluoro-6-thia-heptadecanoic acid and [18F]FDG in Patients with Congestive Heart Failure. J Nucl Med 42(1):55-62.

Thackeray JT, Beanlands RS, Dasilva JN. 2007. Presence of Specific 11C-meta-Hydroxyephedrine Retention in Heart, Lung, Pancreas, and Brown Adipose Tissue. J Nucl Med 48(10):1733-1740.

Thackeray JT, deKemp RA, Beanlands RS, DaSilva JN. 2012 (Submitted)-a. Insulin restores myocardial presynaptic sympathetic nervous integrity in insulin resistant diabetic rats. Cardiovasc Res.

Thackeray JT, Parsa-Nezhad M, Kenk M, Thorn SL, Kolajova M, Beanlands RS, Dasilva JN. 2011a. Reduced CGP12177 binding to cardiac beta-adrenoceptors in hyperglycemic high-fat-diet-fed, streptozotocin-induced diabetic rats. Nucl Med Biol 38(7):1059-1066.

Thackeray JT, Radziuk J, Harper ME, Suuronen EJ, Ascah KJ, Beanlands RS, Dasilva JN. 2011b. Sympathetic nervous dysregulation in the absence of systolic left ventricular dysfunction in a rat model of insulin resistance with hyperglycemia. Cardiovasc Diabetol 10(1):75-75.

Thackeray JT, Renaud JM, Kordos M, Klein R, deKemp RA, Beanlands RS, DaSilva JN. 2012 (Submitted)-b. Inverse Correlation of [11C]meta-Hydroxyephedrine Small Animal PET Measurements to Norepinephrine Concentration in Rats. Mol Imag Biol.

Thomas AJ, DaSilva JN, Lortie M, Renaud JM, Kenk M, Beanlands RS, deKemp RA. 2011. PET of (R)-11C-rolipram binding to phosphodiesterase-4 is reproducible and sensitive to increased norepinephrine in the rat heart. J Nucl Med 52(2):263-269.

Thompson CJ. 2002. Instrumentation. In: Wahl RL, editor. Principles and Practice of Positron Emission Tomography. Philadelphia, PA: Lippincott Williams & Wilkins. p 48-64.

Tipre DN, Fox JJ, Holt DP, Green G, Yu J, Pomper M, Dannals RF, Bengel FM. 2008. In vivo PET imaging of cardiac presynaptic sympathoneuronal mechanisms in the rat. J Nucl Med 49(7):1189-1195.

Tobaldini E, Porta A, Wei SG, Zhang ZH, Francis J, Casali KR, Weiss RM, Felder RB, Montano N. 2009. Symbolic analysis detects alterations of cardiac autonomic modulation in congestive heart failure rats. Auton Neurosci 150(1-2):21-26.

Tsai EB, Sherry NA, Palmer JP, Herold KC. 2006. The rise and fall of insulin secretion in type 1 diabetes mellitus. Diabetologia 49(2):261-270.

Tsukamoto T, Morita K, Naya M, Inubushi M, Katoh C, Nishijima K, Kuge Y, Okamoto H, Tsutsui H, Tamaki N. 2007. Decreased myocardial beta-adrenergic receptor density

in relation to increased sympathetic tone in patients with nonischemic cardiomyopathy. J Nucl Med 48(11):1777-1782.

Turk J, Corbett JA, Ramanadham S, Bohrer A, McDaniel ML. 1993. Biochemical evidence for nitric oxide formation from streptozotocin in isolated pancreatic islets. Biochem Biophys Res Commun 197(3):1458-1464.

Uberfuhr P, Frey AW, Ziegler S, Reichart B, Schwaiger M. 2000. Sympathetic reinnervation of sinus node and left ventricle after heart transplantation in humans: regional differences assessed by heart rate variability and positron emission tomography. J Heart Lung Transplant 19(4):317-323.

UKPDS Group. 1998. Intensive blood-glucose control with sulphonylureas or insulin compared with conventional treatment and risk of complications in patients with type 2 diabetes (UKPDS 33). UK Prospective Diabetes Study (UKPDS) Group. Lancet 352(9131):837-853.

Ungerer M, Bohm M, Elce JS, Erdmann E, Lohse MJ. 1993. Altered expression of beta-adrenergic receptor kinase and beta 1-adrenergic receptors in the failing human heart. Circulation 87(2):454-463.

Ungerer M, Hartmann F, Karoglan M, Chlistalla A, Ziegler S, Richardt G, Overbeck M, Meisner H, Schomig A, Schwaiger M. 1998. Regional in vivo and in vitro characterization of autonomic innervation in cardiomyopathic human heart. Circulation 97(2):174-180.

Ungerer M, Weig HJ, Kubert S, Overbeck M, Bengel F, Schomig A, Schwaiger M. 2000. Regional pre- and postsynaptic sympathetic system in the failing human heart--regulation of beta ARK-1. Eur J Heart Fail 2(1):23-31.

Valdivia AC, Estrada M, Thorn S, Sleiman L, Beanlands RS, DaSilva JN. 2011. Labeling of a c(RGDyK) peptide with [F-18]FPyKYNE via Click Chemistry for the avb3 Integrin Receptor Imaging. J Label Cpd Radiopharm 51:S469.

van den Brom CE, Huisman MC, Vlasblom R, Boontje NM, Duijst S, Lubberink M, Molthoff CF, Lammertsma AA, van der Velden J, Boer C, Ouwens DM, Diamant M. 2009. Altered myocardial substrate metabolism is associated with myocardial dysfunction in early diabetic cardiomyopathy in rats: studies using positron emission tomography. Cardiovasc Diabetol 8:39.

Van Dort ME, Tluczek L. 2000. Synthesis and Carbon-11 Labeling of the Stereoisomers of meta-Hydroxyephedrine (HED) and meta-Hydroxypseudoephedrine (HPED). Journal of Labelled Compounds and Radiopharmaceuticals 43:603-612.

van Waarde A, Anthonio RL, Visser TJ, Elsinga PH, Posthumus H, Weemaes AM, Blanksma PK, Visser GM, Paans AM, Vaalburg W. 1995a. Quantification of an 11C-labelled beta-adrenoceptor ligand, S-(-)CGP 12177, in plasma of humans and rats. J Chromatogr B Biomed Appl 663(2):361-369.

Van Waarde A, Elsinga PH, Brodde O-E, Visser GM, Vaalburg W. 1995b. Myocardial and pulmonary uptake of *S*-1'[^{18}F]fluorocarazolol in intact rats reflects radioligand binding to ß-adrenoceptors. Eur J Pharmacol 272:159-168.

van Waarde A, Vaalburg W, Doze P, Bosker FJ, Elsinga PH. 2004. PET imaging of beta-adrenoceptors in human brain: a realistic goal or a mirage? Curr Pharm Des 10(13):1519-1536.

Vanasse A, Carpentier AC, Courteau J, Asghari S. 2009. Stroke and cardiovascular morbidity and mortality associated with rosiglitazone use in elderly diabetic patients. Diab Vasc Dis Res 6(2):87-93.

Verma S, McNeill JH. 1994. Metformin improves cardiac function in isolated streptozotocin-diabetic rat hearts. Am J Physiol 266(2 Pt 2):H714-719.

Vermes E, Ducharme A, Bourassa MG, Lessard M, White M, Tardif JC. 2003. Enalapril reduces the incidence of diabetes in patients with chronic heart failure: insight from the Studies Of Left Ventricular Dysfunction (SOLVD). Circulation 107(9):1291-1296.

Vesalainen RK, Pietila M, Tahvanainen KU, Jartti T, Teras M, Nagren K, Lehikoinen P, Huupponen R, Ukkonen H, Saraste M, Knuuti J, Voipio-Pulkki LM. 1999. Cardiac positron emission tomography imaging with [11C]hydroxyephedrine, a specific tracer for sympathetic nerve endings, and its functional correlates in congestive heart failure. Am J Cardiol 84(5):568-574.

Waldhausl W. 1996. Role of sulfonylureas in non-insulin-dependent diabetes mellitus: Part I--"The pros". Horm Metab Res 28(9):517-521.

Wang G, Li W, Lu X, Zhao X. 2011. Riboflavin alleviates cardiac failure in Type I diabetic cardiomyopathy. Heart Int 6(2):e21.

Wang MY, Unger RH. 2005. Role of PP2C in cardiac lipid accumulation in obese rodents and its prevention by troglitazone. Am J Physiol Endocrinol Metab 288(1):E216-221.

Wang W, Zucker IH. 1996. Cardiac sympathetic afferent reflex in dogs with congestive heart failure. Am J Physiol 271(3 Pt 2):R751-756.

Wang Y, Fice DS, Yeung PK. 1999. A simple high-performance liquid chromatography assay for simultaneous determination of plasma norepinephrine, epinephrine, dopamine and 3,4-dihydroxyphenyl acetic acid. J Pharm Biomed Anal 21(3):519-525.

Wehrens XH, Lehnart SE, Reiken S, Vest JA, Wronska A, Marks AR. 2006. Ryanodine receptor/calcium release channel PKA phosphorylation: a critical mediator of heart failure progression. Proc Natl Acad Sci U S A 103(3):511-518.

Wehrwein EA, Parker LM, Wright AA, Spitsbergen JM, Novotny M, Babankova D, Swain GM, Habecker BA, Kreulen DL. 2008. Cardiac norepinephrine transporter protein expression is inversely correlated to chamber norepinephrine content. Am J Physiol Regul Integr Comp Physiol 295(3):R857-863.

Wieland DM, Rosenspire KC, Hutchins GD, Van Dort M, Rothley JM, Mislankar SG, Lee HT, Massin CC, Gildersleeve DL, Sherman PS, et al. 1990. Neuronal mapping of the heart with 6-[18F]fluorometaraminol. J Med Chem 33(3):956-964.

Wild S, Roglic G, Green A, Sicree R, King H. 2004. Global prevalence of diabetes: estimates for the year 2000 and projections for 2030. Diabetes Care 27(5):1047-1053.

Wong DT, Threlkeld PG, Best KL, Bymaster FP. 1982. A new inhibitor of norepinephrine uptake devoid of affinity for receptors in rat brain. J Pharmacol Exp Ther 222(1):61-65.

Wong W, Scott JD. 2004. AKAP signalling complexes: focal points in space and time. Nat Rev Mol Cell Biol 5(12):959-970.

Woolard J, Bennett T, Dunn WR, Heal DJ, Aspley S, Gardiner SM. 2004. Acute cardiovascular effects of sibutramine in conscious rats. J Pharmacol Exp Ther 308(3):1102-1110.

Wright JR, Jr., Lacy PE. 1988. Synergistic effects of adjuvants, endotoxin, and fasting on induction of diabetes with multiple low doses of streptozocin in rats. Diabetes 37(1):112-118.

Xiao L, Gao L, Lazartigues E, Zucker IH. 2011. Brain-selective overexpression of angiotensin-converting enzyme 2 attenuates sympathetic nerve activity and enhances baroreflex function in chronic heart failure. Hypertension 58(6):1057-1065.

Xu F, Gainetdinov RR, Wetsel WC, Jones SR, Bohn LM, Miller GW, Wang YM, Caron MG. 2000. Mice lacking the norepinephrine transporter are supersensitive to psychostimulants. Nat Neurosci 3(5):465-471.

Yagi K, Kim S, Wanibuchi H, Yamashita T, Yamamura Y, Iwao H. 1997. Characteristics of diabetes, blood pressure, and cardiac and renal complications in Otsuka Long-Evans Tokushima Fatty rats. Hypertension 29(3):728-735.

Yang J, Holman GD. 2006. Long-term metformin treatment stimulates cardiomyocyte glucose transport through an AMP-activated protein kinase-dependent reduction in GLUT4 endocytosis. Endocrinology 147(6):2728-2736.

Yi E, Smith TG, Baker RC, Love JA. 2004. Catecholamines and 5-hydroxytryptamine in tissues of the rabbit exocrine pancreas. Pancreas 29(3):218-224.

Yoshinaga K, Burwash IG, Leech JA, Haddad H, Johnson CB, deKemp R, Garrard L, DaSilva J, Beanlands R. 2007. The Effect of Continuous Positive Airway Pressure on Myocardial Energetics in Patients with Heart Failure and Obstructive Sleep Apnea. JACC 49(4):450-458.

Yoshinaga K, Chow BJ, deKemp R, Thorn S, Ruddy T, Davies RA, DaSilva J, Beanlands R. 2005. Application of cardiac molecular imaging using positron emission tomography in evaluation of drug and therapeutics for cardiovascular disorders. Curr Pharm Des 11:903-932.

Young LH, Wackers FJ, Chyun DA, Davey JA, Barrett EJ, Taillefer R, Heller GV, Iskandrian AE, Wittlin SD, Filipchuk N, Ratner RE, Inzucchi SE. 2009. Cardiac outcomes after screening for asymptomatic coronary artery disease in patients with type 2 diabetes: the DIAD study: a randomized controlled trial. JAMA 301(15):1547-1555.

Young ME, McNulty P, Taegtmeyer H. 2002. Adaptation and maladaptation of the heart in diabetes: Part II: potential mechanisms. Circulation 105(15):1861-1870.

Yu Y, Zhang ZH, Wei SG, Weiss RM, Felder RB. 2012. Peroxisome proliferator-activated receptor-gamma regulates inflammation and renin-angiotensin system activity in the hypothalamic paraventricular nucleus and ameliorates peripheral manifestations of heart failure. Hypertension 59(2):477-484.

Yue TL, Bao W, Gu JL, Cui J, Tao L, Ma XL, Ohlstein EH, Jucker BM. 2005. Rosiglitazone treatment in Zucker diabetic Fatty rats is associated with ameliorated cardiac insulin resistance and protection from ischemia/reperfusion-induced myocardial injury. Diabetes 54(2):554-562.

Yuill KH, Tosh D, Hancox JC. 2010. Streptozotocin-induced diabetes modulates action potentials and ion channel currents from the rat atrioventricular node. Exp Physiol 95(4):508-517.

Zhang F, Ye C, Li G, Ding W, Zhou W, Zhu H, Chen G, Luo T, Guang M, Liu Y, Zhang D, Zheng S, Yang J, Gu Y, Xie X, Luo M. 2003. The rat model of type 2 diabetic mellitus and its glycometabolism characters. Exp Anim 52(5):401-407.

Zhou G, Myers R, Li Y, Chen Y, Shen X, Fenyk-Melody J, Wu M, Ventre J, Doebber T, Fujii N, Musi N, Hirshman MF, Goodyear LJ, Moller DE. 2001. Role of AMP-activated protein kinase in mechanism of metformin action. J Clin Invest 108(8):1167-1174.

Zhou M, Xu H, Pan L, Wen J, Liao W, Chen K. 2008. Rosiglitazone promotes atherosclerotic plaque stability in fat-fed ApoE-knockout mice. Eur J Pharmacol 590(1-3):297-302.

Zhou YT, Grayburn P, Karim A, Shimabukuro M, Higa M, Baetens D, Orci L, Unger RH. 2000. Lipotoxic heart disease in obese rats: implications for human obesity. Proc Natl Acad Sci U S A 97(4):1784-1789.

Zhu MY, Kim CH, Hwang DY, Baldessarini RJ, Kim KS. 2002. Effects of desipramine treatment on norepinephrine transporter gene expression in the cultured SK-N-BE(2)M17 cells and rat brain tissue. J Neurochem 82(1):146-153.

Ziegler D, Weise F, Langen KJ, Piolot R, Boy C, Hubinger A, Muller-Gartner HW, Gries FA. 1998. Effect of glycaemic control on myocardial sympathetic innervation assessed by [123I]metaiodobenzylguanidine scintigraphy: a 4-year prospective study in IDDM patients. Diabetologia 41(4):443-451.

Zugck C, Lossnitzer D, Backs J, Kristen A, Kinscherf R, Haass M. 2003. Increased cardiac norepinephrine release in spontaneously hypertensive rats: role of presynaptic alpha-2A adrenoceptors. J Hypertens 21(7):1363-1369.